Imperial College London

Characterising A/E Pathogens' Type III Secretion System Effector Proteins

Supervised by Professor Gad Frankel

A thesis submitted by

Sabrina Loretta Slater

to the Imperial College London Department of Life Sciences in partial fulfilment of the requirements for the degree of Doctor of Philosophy

December 2019

Copyright declaration

The copyright of this thesis rests with the author. Unless otherwise indicated, its contents are licensed under a Creative Commons Attribution Non-Commercial 4.0 International Licence (CC BY-NC). Under this licence, you may copy and redistribute the material in any medium or format. You may also create and distribute modified versions of the work. This is on the condition that: you credit the author and do not use it, or any derivative works, for a commercial purpose. When reusing or sharing this work, ensure you make the licence terms clear to others by naming the licence and linking to the licence text. Where a work has been adapted, you should indicate that the work has been changed and describe those changes. Please seek permission from the copyright holder for uses of this work that are not included in this licence or permitted under UK Copyright Law.

Candidate's declaration of originality

Excepting the contributions acknowledged below or referenced in-text, I hereby confirm that this thesis constitutes my own work.

Sabrina L Slater
December 2019

Figure 3.2 | Construction of pCX340 derivatives and subsequent TEM assays were performed with the assistance of Dr Agnes Sågfors.

Figure 3.9 | Construction of pRK5-myc-NleN was performed with the assistance of Camila Acosta Lopez.

Figure 3.8 and 3.14 | Construction of pRK5-myc-$EspS_{B171}$, mutation of $EspS_{CR}^{C184A}$ and subsequent transfections and D2H assays were performed with the assistance of Krista Grimes.

Figure 3.19-21 | In the absence of a Personal Licence (PIL) as required by the Home Office, inoculation and handling of mice was performed by Dr Agnes Sågfors, Dr Valerie Crepin-Sevenou, Dr David Ruano-Gallego and Izabela Glegola-Madejska. Enumeration of bacterial CFU in stool was performed with the assistance of Dr Agnes Sågfors and Dr David Ruano-Gallego. Paraffin mounting, sectioning and H&E staining was performed by Lorraine Lawrence. Assessment of crypt hyperplasia was performed with the assistance of Dr David Ruano-Gallego.

Figure 3.23 | Shooting of MALDI-TOF samples was performed by Dr Gerald Larrouy-Maumus.

List of publications arising from this work

Slater SL, Frankel G. Working title: Pathogenic *E. coli* effector proteins in human pathology. *Frontiers in Cellular and Infection Microbiology*. Invited submission; manuscript in preparation.

Sanchez-Garrido J, **Slater SL**, Clements A, Shenoy AR, Frankel G (2020) Vying for control of the inflammasomes: the cytosolic frontier of enteric bacterial pathogen - host interactions. *Cellular Microbiology* 22:e13184. doi: 10.1111/cmi.13184.

Goddard PJ, Sanchez-Garrido J, **Slater SL,** Kalyan M, Ruano-Gallego D, Marchès O, Fernández LÁ, Frankel G, Shenoy AR (2019) Enteropathogenic *Escherichia coli* Stimulates Effector-Driven Rapid Caspase-4 Activation in Human Macrophages. *Cell Reports* 23:27(4):1008-1017. doi: 10.1016/j.celrep.2019.03.100.

Connolly JPR, **Slater SL**, O'Boyle N, Goldstone RJ, Crepin VF, Ruano-Gallego D, Herzyk P, Smith DGE, Douce GR, Frankel G, Roe AJ (2018) Host-associated niche metabolism controls enteric infection through fine-tuning the regulation of type 3 secretion. *Nature Communications* 10;9(1):4187. doi: 10.1038/s41467-018-06701-4.

Slater SL, Sågfors AM, Pollard DJ, Ruano-Gallego D, Frankel G (2018) The Type III Secretion System of Pathogenic Escherichia coli. In: Escherichia coli, a Versatile Pathogen. *Current Topics in Microbiology and Immunology* vol 416. Springer, Cham doi: 10.1007/82_2018_116

Abstract

The human diarrhoeal pathogens enteropathogenic *Escherichia coli*, enterohaemorrhagic *E. coli* and their murine analogue *Citrobacter rodentium* are a family of enteric bacteria that cause characteristic attaching and effacing lesions at the site of intestinal colonisation. Lesion formation and successful infection depends on a Type III Secretion System and its cognate effector proteins. Once translocated into the host cytosol, effectors subvert several mammalian cell processes to create and maintain an infectious niche. With the advent of high-throughput screening techniques, the rate of effector discovery has surpassed their biochemical investigation. This work therefore explores the function of seven effectors, three uncharacterised and four previously described. Through machine learning algorithms, two completely novel *C. rodentium* effectors were identified and designated NleN and NleO. While *nleN* encodes a truncation of a conserved effector, NleO disrupts the host cytoskeleton by binding and cleaving the Rho GTPase Rac1 at a unique scission site. A third *C. rodentium* effector, EspS, which has previously demonstrated to modulate intestinal pathology, binds the host mitochondrial protein TRIAP1 and contributes to the remodelling of host lipids during infection of C57Bl/6 mice. Finally, the contribution of EspZ, TccP, EspT and NleG to the recently described pyroptotic cell death pathway in human macrophages is explored. The findings presented herein contribute to the ever-growing repertoire of effector protein knowledge and underscore the importance of studying effector synergy during infection.

Acknowledgements

This work was funded by a BBSRC DTP studentship. My sincere thanks are extended to Prof. Gad Frankel, for providing both the opportunity to undertake my doctoral training and the continued professional support thereafter. Gadi, you were right: "the PhD is a journey. There are many routes to get to a last stop. Take into account some signalling and track problems on the way". After 9 years at Imperial, I am finally at the end of the line. All change.

Early work was supervised by Dr Valérie Crepin-Sevenou (LSHTM), to whom I am grateful for her extensive expertise in *C. rodentium*, the T3SS, and the contents of every Frankel lab notebook since 2004. Later work was made possible with the guidance of Dr Avinash Shenoy, to whom I am grateful for his impressive catalogue of innate immunology knowledge. Dr Xeni Miliara and Prof. Steve Matthews (ICL), and Dr Maud Dumoux and Prof. Ray Owens (Diamond Light Source/ Oxford) must be thanked for their help with recombinant EspS expression. I also thank my Progress Review Panel, Dr Gerald Larrouy-Maumus and Prof. Angelika Gründling, for their insight. To Krista Grimes and Camila Acosta-Lopez, two talented students who worked on EspS and NleN/O respectively, thank you for sharing my enthusiasm for T3 effectors.

I would also like to take this opportunity to thank Dr Morgan Beeby, Dr Vlad Pelicic, Prof. Anne Dell and Dr Stuart Haslam (ICL), Dr Matthew Golding (Queen Mary UoL) and Prof. Gipi Schiavo (UCL), Prof. Francesco Muntoni (Dubowitz Neuromuscular Centre) and Prof. Sir Magdi Yacoub (ICL/Harefield NHS Trust) for hosting me in their laboratories and ~~putting up with my annoying questions~~ satiating my curiosity for Science as a young researcher. I especially thank Dr Chris Furniss, for teaching me everything I know, and Dr Abbie Clements, for setting the benchmark for all I have yet to learn; you have both made an immeasurable contribution to my career and I am forever in your debt.

In alphabetical order, to all the members of CMBI-1 who have made my time at Imperial as enjoyable as it was: Dr Agnes Sågfors, for keeping it real; Dr Alex Byrne, for being a top lad; Dr Carrie Mullineaux-Sanders, for indulging my every whim; Dani Carson, for bringing your tenacity from the bench to the climbing wall and back again; Jasmine Clark, for providing SW

London with some East coast finesse; Dr David Ruano-Gallego, for your genomic magic; Dr Dom Pollard, for being the only person as sweaty and grumpy as me; Elli Mylona, for your constant supply of Mediterranean goodies in the form of etymology and snacks; Dr Jayne Watson, for your physical and intellectual flexibility; Dr Josh Wong, for your impeccable taste in all things science and sartorial; Dr Julia Sanchez-Garrido, for always being ready and willing to share your time and encyclopaedic knowledge; Dr Louise Kerry, for not only appreciating my DIY prowess but also for all the health and safety paperwork that inevitably followed; Dr Pippa Goddard, for your painstakingly thorough work on Tir and your commitment to the semi-colon; Dr Rachael Barry, for your expertise in cell death, and finally Wen Wen Low, for never FingTBA. Lastly, to you, future lab member trawling through this thesis: I hope you find what you're looking for in here, goodness knows I tried it all…

To my brothers, Dr Ricky Nathvani and Iain Frenkiel, thank you for supplementing my diminishing sanity with endless world-wondering, pastries, museums, and love. To the four strongest and most stubborn women I know, Lois, Nicole, Kura and Nonna: look what your girl did. Lastly, to my best friend, Tim Thomas, I hope you are as proud of me as I am of you.

Table of Contents

Copyright declaration 2
Candidate's declaration of originality 2
List of publications arising from this work 3
Abstract 4
Acknowledgements 5
Abbreviations 13
1 Introduction 17
1.1 *Escherichia coli* 17
1.1.1 Diarrhoeagenic *E. coli* 17
1.1.2 Enteropathogenic *E. coli* 18
1.1.3 Enterohaemorrhagic *E. coli* 19
1.2 Attaching and effacing pathogens 19
1.2.1 The Locus of Enterocyte Effacement 20
1.3 The type III secretion system 21
1.4 Type III effector proteins encoded by A/E pathogens 23
1.4.1 Approaches to studying effector proteins 23
1.4.2 The use of *C. rodentium* in determining effector function 24
1.5 Effector manipulation of cellular processes 25
1.5.1 Modulation of cytoskeletal dynamics 25
1.5.1.1 Tir is phosphorylated by host kinases to initiate actin pedestal formation 29
1.5.1.2 TccP/EspF$_U$ links Tir to the actin cytoskeleton 30
1.5.1.3 ADP ribosylation of non-receptor tyrosine kianses by EspJ inhibits actin remodelling 31
1.5.1.4 EspH is a Rho GEF competitor with widespread roles during infection 32
1.5.1.5 EspM and EspT are Rho GEF mimics that promote membrane perturbations 32
1.5.1.6 EspV induces morphological changes in yeast cells and human cells 33
1.5.1.7 EspW subverts Rac1 to induce unique membrane ruffling 34
1.5.1.8 EspG hijacks GTPases to inhibit protein trafficking and regulate the cytoskeleton 34
1.5.2 Prevention of NF-κB signalling 36
1.5.2.1 The Zinc metalloproteases NleC and NleD inhibit NF-κB signalling 38
1.5.2.2 NleH is a Ser/Thr kinase that subverts NF-κB 39
1.5.2.3 NleE is a Cys methyltransferase that stabilises IκB 39

1.5.3 Subversion of cell death pathways 40
1.5.3.1 Cif deamidates NEDD8 to limit cell cycle progression and aid bacterial survival 44
1.5.3.2 NleB GlcNAcylates death domains to inhibits their interaction 44
1.5.3.3 NleF binds and inhibits caspase-4/11, 8 and 9 45
1.5.3.4 The cysteine protease EspL cleaves RHIM proteins to inhibit necroptosis 45
1.5.3.5 EspZ limits cytotoxic effector translocation 46
1.5.3.6 EspY binds cell cycle related proteins 46
1.5.3.7 EspO promotes cell survival 47
1.5.4 Effectors with multiple or unique functions 48
1.5.4.1 NleG and EspX/NleL are E3-ubiquitin ligases 48
1.5.4.2 EspF subverts a variety of cellular functions 49
1.5.4.3 Map is mitochondrial-targeting Rho GEF that manipulates tight junctions 49
1.5.4.4 NleH binds Bax-1 to inhibit caspase-3 cleavage and apoptosis 50
1.5.4.5 NleA/EspI inhibits protein trafficking and prevents deubiquitylation of NLRP3 50
1.5.5 Effectors with unknown functions (EspK, NleK, NleJ, EspR, EspN, EspS/OspB) 51
1.6 Project aims 52
2 Materials and Methods 54
2.1 Bacterial culture 54
2.2 Bacterial transformation 55
2.3 Yeast culture 57
2.4 Mammalian cell culture 57
2.5 *C. rodentium* genomic manipulation 58
2.6 Oral *C. rodentium* infection of C57Bl/6 mice 61
2.7 Staining and analysis of distal colon sections 61
2.8 Transfection and immunofluorescence staining 62
2.9 Immunofluorescence staining 64
2.10 Yeast transformation 65
2.11 Yeast toxicity assay 66
2.12 Yeast 2 hybrid (Y2H) assay 67
2.13 Direct 2 hybrid (D2H) assay 67
2.14 TEM translocation assay 67
2.15 Measurement of PI uptake of infected cells 68
2.16 LDH release assay 68
2.17 Lipidomics 69

2.18 TUNEL staining assay 69
2.19 Immunoblotting 70
2.20 Bioinformatic analysis 70
2.21 Statistical analysis 70
2.22 Co-immunoprecipitation 71
3 Novel T3SS Effector proteins 73
3.1 Introduction 73
3.2 Results 76
3.2.1 TEM translocation assays reveal two novel *C. rodentium* effector proteins. 76
3.2.2 Bioinformatic analysis of uncharacterised *C. rodentium* effector proteins. 78
3.2.2.1 ORFs in GI14 contain fragments of conserved effector proteins. 78
3.2.2.2 NleO exhibits homology to a MARTX Rho GTPase inactivating effector domain. 79
3.2.2.3 Identification of EspS homologues. 81
3.2.2.4 Primary sequence analysis of EspS homologues. 82
3.2.3 Functional analysis of *C. rodentium* effectors in mammalian cells 83
3.2.3.1 Transfected $EspS_{CR}$ and $EspS_{B171}$ localise to the mitochondria. 83
3.2.3.2 NleN transfection results in diffuse cytoplasmic localisation 87
3.2.3.3 NleO transfection results in cell rounding 87
3.2.3.4 NleO catalytic residue Cys121 mediates Rac1 cleavage and cell rounding 90
3.2.4 Identifying interaction partners for $EspS_{CR}$ 92
3.2.4.1 Investigating the toxicity of EspS homologues in *S. cerevisiae*. 92
3.2.4.2 $EspS_{CR}$ binds TRIAP1 in a Y2H system. 93
3.2.5 Optimisation of recombinant $EspS_{CR}$ expression 96
3.2.5.1 Optimisation of recombinant mammalian $EspS_{CR}$ expression 98
3.2.5.2 Native EspS tagging for immunoprecipitation 99
3.2.6 Characterising $EspS_{CR}$ function *in vitro* 100
3.2.6.1 Investigating the role of $EspS_{CR}$ in apoptosis 100
3.2.7 Investigating effector function during *in vivo* infection 102
3.2.7.1 *C. rodentium* Δ*nleN*, Δ*nleO* and Δ*espS* mutants colonise C57Bl/6 mice normally 102
3.2.7.2 A *C. rodentium* Δ*espS* mutant induces exaggerated hyperplasia 104
3.2.7.3 Investigating the effect of $EspS_{CR}$ on cardiolipin synthesis *in vivo* 105
3.2.7.4 Investigating the effect of $EspS_{CR}$ on apoptosis *in vivo*. 106
3.3 Discussion 108
4 New roles for old effectors 114

4.1 Introduction 114
4.2 Results 117
4.2.1 Factors regulating Tir-induced pyroptosis 117
4.2.1.1 EPEC E69 induces cell membrane permeability in a T3- and Tir-dependent manner 117
4.2.1.2 Tir-driven stimulation of pyroptosis is modulated by EspZ 119
4.2.1.3 Investigating TccP as a modulator of pyroptosis 122
4.2.1.4 Investigating EspT as a modulator of pyroptosis 124
4.2.2 EPEC induces a second phase of necrotic cell death 125
4.3 Discussion 128
5 Conclusions and future perspectives 133
References 137

List of Schematics, Figures and Tables

Schematics

Schematic 1 | The Locus of Enterocyte Effacement (LEE)..... 20
Schematic 2 | The A/E Type III Secretion System..... 22
Schematic 3 | Simplified overview of host GTPase subversion by A/E effectors..... 28
Schematic 4 | Nck-dependent actin polymerisation by Tir..... 30
Schematic 5 | Nck-independent actin polymerisation by Tir..... 31
Schematic 6 | Manipulation of NF-κB signalling by A/E effectors..... 37
Schematic 7 | Subversion of programmed cell death pathways by A/E effectors..... 43
Schematic 8 | Principle of the Y2H assay..... 93
Schematic 9 | Actin polymerisation by EPEC Tir stimulates atypical non-canonical inflammasome activation and pyroptosis..... 116

Figures

Figure 3.1 | Candidate effector proteins in C. rodentium and their genomic context... 76
Figure 3.2 | TEM translocation assays of putative *C. rodentium* effectors..... 77
Figure 3.3 | Alignment of NleN and downstream coding regions..... 79
Figure 3.4 | Structural and sequence homology between NleO and a MARTX toxin effector domain..... 80
Figure 3.5 | Cladogram of proteins > 30% homology with $EspS_{CR}$..... 81
Figure 3.6 | Multiple sequence alignment of 12 representative EspS homologues..... 83
Figure 3.7 | Infection of HeLa cells with E69 expressing $EspS_{CR}$-HA..... 84
Figure 3.8 | Transfection of HeLa cells with $EspS_{CR}$ and $EspS_{B171}$..... 86
Figure 3.9 | Transfection of HeLa cells with NleN..... 87
Figure 3.10 | Transfection of HeLa cells with NleO..... 88
Figure 3.11 | Changes in cell area following co-transfection of NleO and Rac1..... 89
Figure 3.12 | NleO Cys121 is required for cell rounding and Rac1 cleavage..... 91
Figure 3.13 | Toxicity test of EspS homologues in *S. cerevisiae* BY4741..... 92
Figure 3.14 | Growth of auxotrophic *S. cerevisiae* expressing $EspS_{CR}$..... 95
Figure 3.15 | Protein purification of $EspS_{CR}$ under native and reducing conditions..... 97
Figure 3.16 | Transfection of HEK293T cells with the pOPIN-effector suite for mammalian effector expression..... 99
Figure 3.17 | Screening conditions to improve $EspS_{CR}$-SII solubility for immunoprecipitation..... 100
Figure 3.18 | Assessment of cell death following infection of HeLa cells with *C. rodentium*..... 101
Figure 3.19 | Colonisation of C57Bl/6 mice by *C. rodentium* Δ*nleN* and Δ*nleO*..... 103
Figure 3.20 | Colonisation of C57Bl/6 mice by *C. rodentium* Δ*espS*..... 103
Figure 3.21 | Quantification of colonic crypt hyperplasia in *C. rodentium*-infected C57Bl/7 mice at 8 d.p.i. 104
Figure 3.22 | Quantification of active proliferation in *C. rodentium* Δ*espS*-infected colons..... 105
Figure 3.23 | Lipid composition of C57Bl/6 IECs following C. rodentium Δ*espS* infection..... 106

Figure 3.24 | Enumeration of apoptotic TUNEL^{+} cells in colonic tissue of *C. rodentium*-infected C57Bl/6 mice..... 107
Figure 4.1 | Real-time PI uptake of E69-infected THP1s..... 117
Figure 4.2 | Real-time PI uptake in THP1s infected with E69 Tir mutant strains..... 118
Figure 4.3 | Contribution of Ca2+ membrane repair to GSDMD-induced damage..... 120
Figure 4.4 | Infection of THP1s with EPEC 0, 1 and 2..... 121
Figure 4.5 | Infection of pyroptotic THP1s with EspZ-expressing EPEC..... 122
Figure 4.6 | Infection of THP1s with EPEC strains with differing TccP expression..... 123
Figure 4.7 | The T3SS is required for E11-induced cell death..... 123
Figure 4.8 | NLRP3 and caspases are required for E11-induced cell death..... 124
Figure 4.9 | The effector of EspT translocation on pyroptosis..... 125
Figure 4.10 | E69 induces necroptosis at late stages of infection..... 126
Figure 4.11 | The T3SS is required for late-stage necroptosis..... 127
Figure 4.12 | Cell death following 17.5 h infection with E69 Δ*nleG*..... 127

Tables

Table 1 | Distribution and function of effector protein families across representative EPEC, EHEC and *C. rodentium* strains..... 26
Table 2 | Bacterial strains used in this study..... 54
Table 3 | Plasmids used for bacterial expression..... 56
Table 4 | Yeast strains used in this study..... 57
Table 5 | Oligos used in this study..... 58
Table 6 | Transfection plasmids used in this study..... 62
Table 7 | Antibodies used for immunofluorescence and immunoblotting..... 64
Table 8 | Plasmids used for yeast expression..... 65
Table 9 | Summary of putative interaction partners for $EspS_{CR}$ identified in a Y2H screen..... 94
Table 10 | Summary of strategies for recombinant $EspS_{CR}$ expression..... 96

Abbreviations

A
A/E: attaching and effacing
aa: amino acid
AD: Activation domain
ADF: actin-depolymerising factor
AIEC: adherent invasive *Escherichia coli*
Arf: ADP-ribosylation factor
Arp2/3: actin-related proteins 2/3

B
BD: binding domain
Bfp: bundle forming pilus
BSA: bovine serum albumin
B171: EPEC O111:NM B171

C
CARD: caspase recruitment domain
CFU: colony forming units
cIAP: cellular inhibitor of apoptosis protein
Cif: cell cycle inhibiting factor
CL: cardiolipin
cPLA2: cytosolic phospholipase A2
CR: *Citrobacter rodentium*

D
d.p.i: days post infection
D2H: direct 2 hybrid
DAEC: diffusely adherent *Escherichia coli*
DD: death domain
ddH_2O: double distilled water
DDO: double dropout
DEC: diarrhoeagenic *Escherichia coli*
DH/PH: Dbl-homology/ pleckstrin homology
DISC: death-inducing signalling complex
DMEM: Dulbecco's modified Eagle media
DAMP: damage associated molecular pattern
DMSO: dimethylsulphoxide
DRA: downregulated in adenoma
dsRNA: double stranded RNA

E
E11: EPEC O111:H9 E110019
E69: EPEC O127:H6 E2348/69
EAEC: enteroaggregative *Escherichia coli*
EAF: EPEC adherence factor
EHEC: enterohaemorrhagic *Escherichia coli*
EIEC: enteroinvasive *Escherichia coli*
EPEC: enteropathogenic *Escherichia coli*
ERK: extracellular signal-regulated kinase
Esc: *Escherichia coli* secretion component
ESCRT: endosomal sorting complexes required for transport
Esp: *Escherichia coli* secreted protein
ETEC: enterotoxigenic *Escherichia coli*
ETT2: *Escherichia coli* type III secretion system 2
ExPEC: extraintestinal pathogenic *Escherichia coli*

F
FADD: Fas-associated death domain
FAK: focal adhesion kinase

G
Gal: Galactose
GAP: GTPase-activating protein
GDI: guanosine nucleotide dissociation inhibitor
GEF: guanine nucleotide exchange factor
GFP: green fluorescent protein
GI: genomic island
Glc: Glucose
GSDMD: Gasdermin-D

H
H&E: Haematoxylin and eosin
HAX-1: HS-1 associated protein X-1
HBSS: Hank's balances salt solution
HDI: human development index
HI-FCS: heat-inactivated foetal bovine serum

I
IE: integrative element
IEC: intestinal epithelial cell
IKK: IκB kinase

IL-: interleukin-
ILK: integrin-linked kinase
IMS: inner membrane space
IRSp53: insulin receptor substrate p53/p58
IRTKS: insulin receptor tyrosine kinase substrate
IκB: inhibitor of kappa B

J
JNK: c-Jun N-terminal kinase

K
—

L
LEE: locus of enterocyte effacement
Ler: LEE-encoded regulator
LPS: lipopolysaccharide
LRR: leucine-rich repeat
LB: Luria broth

M
Map: mitochondrial associated protein
MAPK: mitogen activated protein kinase
MARTX: multifunctional-autoprocessing repeats-in-toxin
MDM: monocyte-derived macrophage
MLKL: mixed lineage kinase domain-like pseudokinase
MNEC: meningitis-associated *Escherichia coli*
MS: mass spectrometry
MSA: multiple sequence alignment
MTS: mitochondrial targeting sequence

N
Nec1: Necrostatin-1
NF-κB: nuclear factor kappa-light-chain-enhancer of activated B cells
NHERF: Na^{2+}/H^{+} exchanger regulatory factor
Nle: Non-LEE encoded
NLRC4: NLR Family CARD Domain Containing 4
NLRP3: NACHT, LRR and PYD domains-containing protein 3
NOD: nucleotide-binding oligomerisation domain
N-WASP: neural Wiskott-Aldrich syndrome protein

O
ORF: open reading frame

P
p.i.: post infection
PA: phosphatidic acid
PAK: p21-activated kinase
PAMP: pathogen-associated molecular pattern
PARP: poly (ADP-ribose) polymerase
PBS: phosphate buffered saline
PDZ: PSD95/Dlg1/ZO-1
PFA: paraformaldehyde
PI: propidium iodide
PKA: protein kinase A
PKN: Ser/Thr protein kinase N1
PMA: phorbol 12-myristate 13-acetate
PPR: pentapeptide repeat
PRR: pattern recognition receptor
PTN: pleiotrophin
PVDF: polyvinylidene difluoride
PYD: pyrin domain

Q
QDO: Quadruple dropout

R
RDEC/REPEC: rabbit diarrhoeagenic *Escherichia coli*/ rabbit EPEC
RHIM: Rip homotypic interaction motif
RID: Rho GTPase inactivation domain
RIPK: receptor-interacting protein kinase
ROCK: Rho-associate protein kinase
RTX: repeats-in-toxin

S
SD: Sabouraud dextrose
SDS: sodium dodecyl sulphate
SEC: size exclusion chromatography
SEM: standard error of the mean
SGLT1: sodium glucose linked transporter 1

SH2: Src homology 2
SIEC: synthetic injectisome *Escherichia coli*
SPATE: serine protease autotransporters of Enterobacteriaceae
STEAEC: Shiga toxin-producing enteroaggregative *Escherichia coli*
Stx: Shiga toxin

T
T3: type III
TAK1: transforming growth factor β-activated kinase 1
T_H1: T helper type 1
Tir: translocated intimin receptor
TRADD: tumour necrosis factor receptor type 1-associated death domain protein
TRAF: TNF receptor associated factor
TRAIL: TNF-related apoptosis-inducing ligand
TRIAP1: TP53-regulated inhibitor of apoptosis 1
TUNEL: terminal deoxynucleotidyl transferase dUTP nick end labelling

U
UAS: upstream activation sequence
UPEC: uropathogenic *Escherichia coli*

V
—

W
WT: wild type

X
—

Y
Y2H: yeast 2 hybrid
YPD(A): yeast extract peptone dextrose (agar)

Z
—

§: section reference

Chapter 1

Introduction

1 Introduction

1.1 *Escherichia coli*

The Gram-negative genus *Escherichia* of the Enterobacteriaceae family encompasses six species of facultative anaerobic coliform bacteria. The type species, *Escherichia coli,* can inhabit the mammalian gastrointestinal tract as both a commensal bacterium and a pathogen. Academic interest in *E. coli* stems not only from its predominance in the mammalian large intestine and its amenability to genetic manipulation for research in molecular biology (Blount, 2015), but also as one of the most prolific bacterial aetiological agents of diarrhoeal disease (WHO, 2018). Although infection of compromised intestinal barriers with commensal *E. coli* in immunosuppressed hosts is possible (Bhat et al., 2019), strains that have evolved through the acquisition of virulence factors by horizontal gene transfer are the primary causative agents of human infection (Clements et al., 2012). These acquisition events have supplemented the common *E. coli* genome of 4.1 Mb with additional elements of up to 1 Mb, giving rise to unique pathotypes (Croxen and Finlay, 2010). Each pathotype differs in its preferred site of colonisation, virulence determinants, epidemiology and clinical pathology (Gomes et al., 2016; Nataro and Kaper, 1998).

1.1.1 Diarrhoeagenic *E. coli*

Pathogenic *E. coli* strains exhibit different tissue tropisms. While diarrhoeagenic *E. coli* (DEC) are unsurprisingly gastrointestinal, extra-intestinal pathogenic *E. coli* (ExPEC) encompass uropathogenic *E. coli* (UPEC) and meningitis-associated *E. coli* (MNEC) and infect the urinary tract and nervous tissue respectively (Russo and Johnson, 2000; Terlizzi et al., 2017). Human DEC currently encompasses six pathotypes, each defined by its unique virulence factor repertoire: enteropathogenic *E. coli* (EPEC), enterohaemorrhagic *E. coli* (EHEC), enteroaggregative *E. coli* (EAEC), enterotoxigenic *E. coli* (ETEC), diffusely adherent *E. coli* (DAEC) and enteroinvasive *E. coli* (EIEC) (Clements et al., 2012). The incorporation of two further pathotypes is currently under discussion. The first, Shiga-toxin producing enteroaggregative *E. coli* (STEAEC), was proposed as a new category following the O104:H4 outbreak of 2011 in Germany (Buchholz et al., 2011), demonstrating the genomic plasticity of these pathogens. The carriage of a second pathotype, adherent invasive *E. coli* (AIEC), is associated with Crohn's

disease, but has yet to be categorically demonstrated as a causative agent of infection (Palmela et al., 2018).

1.1.2 Enteropathogenic *E. coli*

EPEC causes infantile diarrhoea, posing a significant burden to public health in countries with a low human development index (HDI). Indeed, from 2007 to 2015 the World Health Organization (WHO) reported 550 million instances of diarrhoeal disease. 230,000 cases resulted in death, of which EPEC was responsible for 16%, disproportionately affecting children under 5 years of age (WHO, 2018). EPEC infection occurs in the small intestine and is largely self-limiting if diarrhoeal symptoms are managed with oral rehydration therapy or antibiotics, although the latter is often avoided if the pathotype cannot be identified. Screening for EPEC involves PCR amplification of *bfpA* (Teixeira et al., 2015), the major subunit of the type IV bundle forming pilus (bfp) encoded on the EPEC adherence factor (EAF) plasmid, as this is one of the few virulence factors not shared by EHEC. The bfp mediate both inter-bacterial and bacteria-host interactions, creating a distinctive localised adherence pattern characteristic of EPEC infection on cultured cell monolayers (Kaper et al., 2004; Saldaña et al., 2009). While the bfp significantly contributes to EPEC virulence *in vivo*, additional surface appendages such as the flagellum (Haiko and Westerlund-Wikström, 2013), pili and fimbriae (Rendón et al., 2007; Zhou et al., 2019) and most recently the type III secretion system (T3SS) (Santos et al., 2019) can also aid adherence. Each DEC also encodes at least one Type Va secretion system-dependent serine protease autotransporter of Enterobacteriaceae (SPATE), which further aids classification (Dautin, 2010); EPEC encodes EspC (Mellies et al., 2001), while EHEC can encode EspP (Brunder et al., 1997) and EpeA (Leyton et al., 2003).

EPEC isolates can be typed in several ways: according to their serotype (O and H antigens); according to their *E. coli* phylogroup (as defined sequencing of multi-copy single-stranded DNA (Herzer et al., 1990)), or according to their allelic homology (designated lineages 1-4 (Lacher et al., 2007)). Given the variability in virulence factors among DEC isolates, research with type strains is used to represent the DEC population. The most commonly used type strain for the study of EPEC is E2348/69 (henceforth abbreviated as E69), which was isolated in the United Kingdom in 1969. E69 belongs to the B2 phylogroup, lineage 1 and its serotype is

O127:H6. It encodes among the fewest virulence factors identified in human *E. coli* isolates and is regarded as the prototype strain for EPEC biology (Iguchi et al., 2009). Two further type strains used in this study are EPEC B171 O111:NM (henceforth abbreviated as B171) from lineage 2 (Ogura et al., 2008) and EPEC E110019 O111:H9 (henceforth abbreviated as E11), an outbreak strain isolated in Finland (Viljanen et al., 1990).

1.1.3 Enterohaemorrhagic *E. coli*

EHEC's defining characteristic is its ability to produce Shiga and Shiga-like toxins (Stx) (Krause et al., 2018; Melton-Celsa, 2014). Distinguishing between EPEC and EHEC is clinically important, as treatment of EHEC with antibiotics can incite Stx expression (Zhang et al., 2000) and consequent acute kidney failure, a sequalae of haemolytic uremic syndrome (HUS) (Pacheco and Sperandio, 2012). In addition to the Shiga toxins, the extensive diversity of EHEC strains can implicate cytotoxins such as StcE, a type II secretion system-dependent metalloprotease (Abreu and Barbosa, 2017), and the haemolysins HlyA and Ehx (Schwidder et al., 2019). Together, these virulence factors contribute to outbreaks of foodborne illness and haemorrhagic colitis that are still frequently reported in countries with a high HDI. In particular, most human infections arise from the consumption of both undercooked meat and contaminated fresh produce, as ruminants are a major EHEC reservoir (Nguyen and Sperandio, 2012).

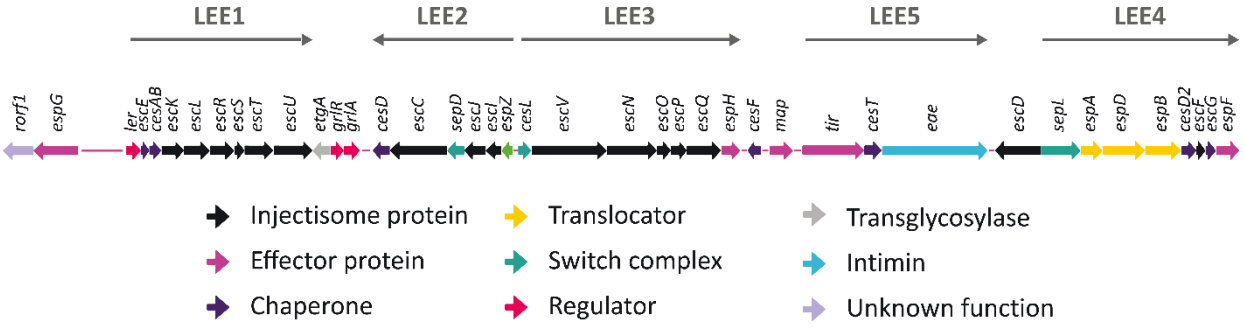
1.2 Attaching and effacing pathogens

Beyond DECs, EPEC and EHEC belong to a further classification of pathogens, along with the emerging human pathogen *E. albertii* (Ooka et al., 2015), the murine pathogen *Citrobacter rodentium* (Mullineaux-Sanders et al., 2019), and its lapine analogue rabbit diarrhoeagenic *E. coli* or rabbit-specific EPEC (RDEC/ REPEC) (Milon et al., 1999). Members of this family share a genomic region named the locus of enterocyte effacement (LEE), which confers the unique ability to induce characteristic attaching and effacing (A/E) lesions on intestinal epithelial cells (IECs). As such, LEE-encoding bacteria are commonly referred to as A/E pathogens. A/E lesions are characterised by elongation and effacement of the brush border microvilli and the archetypal accumulation of actin beneath the site of attachment, forming a so-called actin pedestal (Frankel and Phillips, 2008). These phenomena are mediated by the LEE-encoded type

III secretion system (T3SS) (Hu et al., 2020), its cognate toxins (effector proteins) and a suite of regulatory elements and proteins that coordinate effector protein translocation.

1.2.1 The Locus of Enterocyte Effacement

Spanning 35-43 kb and approximately 40 open reading frames, the LEE is divided into 5 major and 2 minor islands that facilitate localised destruction of enteric tissue, numbered *LEE1* to *LEE7* (McDaniel et al., 1995) (Schematic 1). The first 3 LEE operons encode the structural components of the T3SS in the form of *E. coli* secretion component (esc), *E. coli* secreted protein (esp) and secretion of *E. coli* proteins (sep) genes, with the filament (EspA), needle (EscF) and translocon proteins (EspB and D) in *LEE4* (further discussed in section (§) 1.3). *LEE5* encodes the adhesin intimin and the T3SS-delivered translocated intimin receptor (Tir), which interact *in situ* to physically and intimately connect the adhered bacterium and its host cell (Donnenberg et al., 1993a; Jerse and Kaper, 1991; Kenny et al., 1997) (§1.5.1.1). In addition to Tir, distributed across *LEE1-6* are the core effector proteins EspG, EspH, Map, EspF and EspZ (further discussed in §1.4).



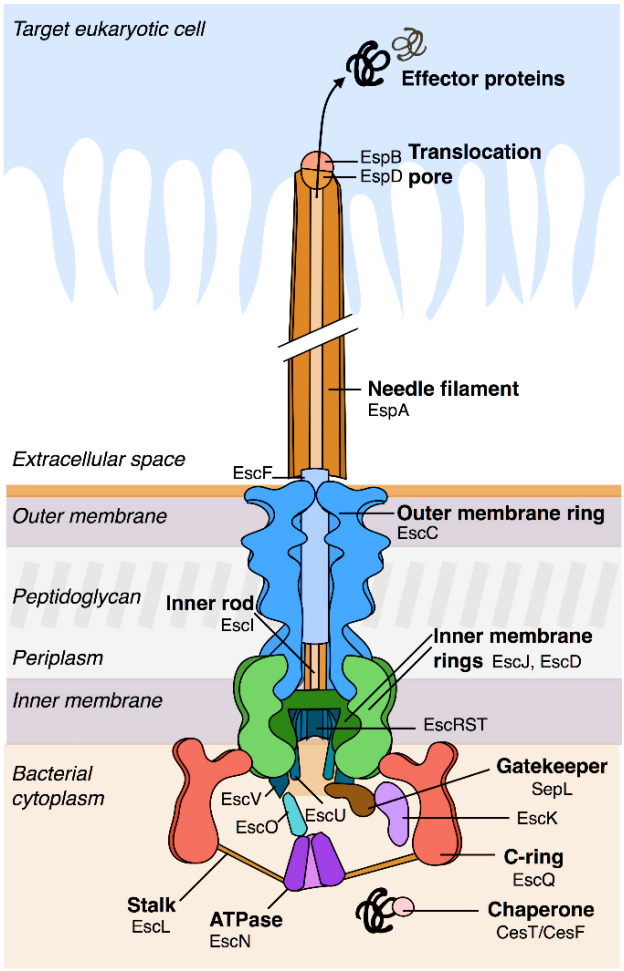
Schematic 1 | The Locus of Enterocyte Effacement (LEE)
Representative schematic of the organisation of the Locus of Enterocyte Effacement (LEE), based on EPEC E23348/69. Major operons (black arrows, above), structural components of the injectisome, core effectors, regulators of translocation and chaperones are indicated. Adapted from Slater *et al.* (2018).

Expression of the LEE is sufficient for complete T3SS formation, substrate secretion, and virulence, as demonstrated in the seminal work carried out by McDaniel and Kaper (McDaniel and Kaper, 1997) and by the laboratory-engineered synthetic injectisome *E. coli* (SIEC) (Ruano-Gallego et al., 2015). LEE expression requires intricate regulation, which is largely coordinated through the LEE-encoded regulator (Ler), a DNA-binding protein encoded on *LEE1* (Furniss and Clements, 2017), and the regulators GrlA/R (global regulator of LEE activator/repressor).

Together, these regulators are capable of integrating of numerous exogenous and endogenous signals. Additional transcriptional regulation can be imposed by non-LEE-encoded genes (such as two-component systems), small RNAs, oxygen availability, as well as host and microbiota-derived hormones, sugars and fatty acids (Carlson-Banning and Sperandio, 2018; Connolly et al., 2015; Furniss and Clements, 2017; Platenkamp and Mellies, 2018). These signals ensure the timely expression of the LEE during infection *in vivo* (Yang et al., 2010).

1.3 The type III secretion system

The T3SS is a surface-exposed macromolecular conduit that spans the bacterial inner and outer membranes of select Gram-negative pathogens and provides an aperture into the host membrane of target cells. Species with a T3SS include A/E pathogens, fellow enteric pathogens *Salmonella, Shigella* and some *Vibrio* spp., human pathogens with a broader tissue tropism such as *Burkholderia, Chlamydia, Pseudomonas* and *Yersinia*, and some species belonging to genera with a tropism for plants (e.g., *Erwinia, Ralstonia, Rhizobium* and *Xanthomonas*). The T3SS is sometimes referred to as the injectisome in order to distinguish it from the flagellar apparatus, with which it shares both primary and quaternary structural homology (Diepold and Armitage, 2015). Indeed, the recent discovery of the host nutrient extraction (HNE) machinery in *E. coli* pushes the boundary of this similarity, demonstrating that the core of these two T3-based machineries can be functionally complementary (Pal et al., 2019). The various T3SSs can vary in size, length, substrate specificity and order of assembly, though the complete *E. coli* injectisome is a 3.5 MDa complex estimated to span 8-9 nm across its membrane-bound components. An estimation for the length of the A/E injectisome is not currently available, as it presents with an additional EspA filament; the extracellular assembly of EspA subunits can extend the length of the needle in order to reach host enterocytes (Crepin et al., 2005; Sekiya et al., 2001). A complete schematic of the A/E T3SS is depicted in Schematic 2.



Schematic 2 | The A/E Type III Secretion System
The structure of the T3SS facilitates delivery of effectors from the bacterial to the host cytoplasm. It comprises several coaxial rings that form a hollow conduit. In the bacterial cytoplasm, the ATPase powers both injectisome assembly and effector translocation. Adapted from Slater *et al.* (2018).

The injectisome can be divided into five major units: its various bacterial cytoplasmic complexes, the export apparatus, the bacterial membrane-resident basal body, the extracellular needle, and the host-bound pore-forming complexes (Lara-Tejero and Galán, 2019; Slater et al., 2018). The mechanism of T3SS assembly in A/E pathogens directly correlates to the relative expression levels of *LEE* operons (Yerushalmi et al., 2014), and begins with the recruitment of the inner membrane components EscR, S, T, U and V (Diepold et al., 2011; Wagner et al., 2010). Upon autoproteolytic cleavage of EscU (Thomassin et al., 2011), the five proteins are exported via the general secretory pathway, providing a scaffold for the incorporation of the inner membrane components EscD, EscJ and EscC (Creasey et al., 2003a; Ogino et al., 2006). In the cytoplasm, formation of the sorting complex by EscQ recruits EscK, L, N and O to form the C-ring complex and ATPase (Biemans-Oldehinkel et al., 2011; Lara-Tejero et al., 2011; Romo-Castillo et al., 2014). Premature polymerisation of the inner rod and needle proteins EscI and F is prevented by their chaperones EscE and G, which release their repression to allow assembly of the needle into the periplasmic space, aided by the

peptidoglycan-degrading enzyme EtgA (García-Gómez et al., 2011). Similarly, the CesAB chaperones now allow the EspA filament to assemble (Creasey et al., 2003b; Gaytán et al., 2016; Izoré et al., 2011; Yip et al., 2005), before the translocon pore (EspD and B) complete the T3SS as it reaches the host membrane (Ide et al., 2001).

1.4 Type III effector proteins encoded by A/E pathogens

Given its distribution across pathogens with widely varying lifestyles, the T3SS must achieve host specificity through its toxin arsenal. To date, 34 different effector families have been confirmed in A/E pathogens (Table 1) to specifically manipulate mammalian gut cells. Each effector varies in size, localisation upon translocation, cellular function, distribution and homology among pathogens. While some effectors are LEE-encoded, much of an A/E pathogens effector repertoire is non-LEE encoded (Nle); distributed among integrative elements (IEs) throughout the bacterial genome. Core and non-LEE effectors are equally important for virulence *in vitro* (Cepeda-Molero et al., 2017) and in disease severity in human populations (Hazen et al., 2016). This warrants the study of effector proteins both as units of insight into fundamental cellular processes and as targets for disease intervention.

1.4.1 Approaches to studying effector proteins

Research into effector biology can be split into three phases: gene discovery; *in vitro* functional characterisation, and defining the contribution of each effector to the pathogen's infection strategy. In the first instance, several resources have been developed for the identification of new effectors. Effector-encoding genes can be predicted *in silico* (McDermott et al., 2011) or manually identified by inspecting the genomic context of existing effectors. Candidate effectors are confirmed by translocation assays, whereby tags are fused to the *C*-termini of candidates and their T3SS-dependent delivery is visualised by optical changes in the recipient cell (Charpentier and Oswald, 2004; Gawthorne et al., 2016; Mills et al., 2008; Miyake et al., 2008; O'Boyle et al., 2018). Alternatively, peptides in the secretomes of T3SS-utilising pathogens can be subjected to mass spectrometry (MS) (Deng et al., 2010; Orton et al., 2013; Tobe et al., 2006).

Characterising the role of each new effector during infection is technically more challenging. Historically, effector functionality is investigated under overexpression conditions *in vitro*, where mammalian cells are infected with bacteria translocating exaggerated quantities of a tagged effector protein, transfected for ectopic effector expression, or microinjected with purified protein. Effector–host interactions have also been studied in other eukaryotic systems, such as yeast (Popa et al., 2016; Rodríguez-Escudero et al., 2005). Although these techniques have aided in the definition of eukaryotic interaction partners, interfaces for substrate interaction and catalytic residues, they share a common flaw: effector localisation is inconsistent when not natively translocated through the injectisome, which can lead to discrepancies in the interpretation of effector function.

The field is now seeing a shift in academic practice towards more native models for infection, using mice, differentiated colonic cell lines, explants, organoids and primary tissues (Law et al., 2013), with consideration of the role of immune-associated cells. When coupled to multi-omic approaches, these models can provide an unbiased insight into effector synergy, global changes upon infection (for example on mRNA transcription, protein expression and post-translational modifications), host protein targets (Law et al., 2016) and the relationship between A/E pathogens and the microbiota (Carson et al., 2019; Hopkins et al., 2019).

1.4.2 The use of *C. rodentium* in determining effector function

C. rodentium, once classified as *C. freundii* biotype 4280 (Schauer et al., 1995), causes A/E lesions that are indistinguishable from those cause by EPEC, as well as transmissible colonic hyperplasia in mice (Barthold et al., 1976). Critically, *C. rodentium* shares 67% homology with EPEC and EHEC genomes, most notably in the LEE (Petty et al., 2010, 2011), making it an invaluable tool for the study of the A/E T3SS and its cognate effectors *in vivo* (Collins et al., 2014; Mullineaux-Sanders et al., 2019; Mundy et al., 2005). The genetic background of the mouse strain used defines the pathology of the infection: C57 mice develop a mild, self-limiting *C. rodentium* infection that is spontaneously cleared by 2–3 weeks post-infection (p.i.), while susceptible (e.g., C3H) mice develop severe disease including watery diarrhoea, succumbing to infection by day 10–14 p.i. (Carson et al., 2019). The contribution of single or multiple effectors to A/E pathogenesis can be assayed via infection with *C. rodentium* deletion

mutants (Crepin et al., 2016). To highlight some relevant examples, assessment of effector functions has historically included delineating colonisation dynamics (Mundy et al., 2004a), investigating the transcriptional regulation of host genes (Hopkins et al., 2019), proteomic and histopathological analysis of infected tissue (Berger et al., 2017), quantifying the infiltration of immune cells (Higgins et al., 1999; Vallance et al., 2002) and examining cytokine release (Berger et al., 2018).

1.5 Effector manipulation of cellular processes

In order to survive in the mammalian gut, pathogens must efficiently colonise host tissue while evading the immune system and preventing tissue damage. Effector proteins that have evolved to facilitate colonisation can also illicit local inflammation, calling for further effector proteins to offset the pathology. As such, a given A/E pathogen can encode dozens of effector proteins with intricate synergies to achieve infection (Reddick and Alto, 2014; Santos and Finlay, 2015; Shenoy et al., 2018) (Table 1).

1.5.1 Modulation of cytoskeletal dynamics

The structure of the cytoskeleton governs almost every cellular function, from cell cycle progression to morphogenesis and migration, making it an excellent target for pathogens. Unsurprisingly, such an important facet is intricately regulated by several protein families. Globular G-actin, tubulin and intermediate filament proteins polymerise into filamentous F-actin, microtubules and stabilising structures, respectively, to provide a dynamic scaffold for macrostructure formation and the transport of subcellular cargo (Hohmann and Dehghani, 2019; Rottner et al., 2017). Actin polymerisation underpins lamellipodia, filopodia, stress fibre, actin cortex and actin bleb formation. F-actin is generated when the intrinsically inactive actin related protein 2/3 (Arp2/3) complex is activated by proteins such as Wiskott-Aldrich syndrome protein (WASP) or its neural derivative (N-WASP), and the resulting F-actin bundles can be crosslinked. Polymerised actin can be quickly disassembled by the actin depolymerisation factor (ADF)/cofilin family of proteins, conferring cells adaptability in response to environmental cues.

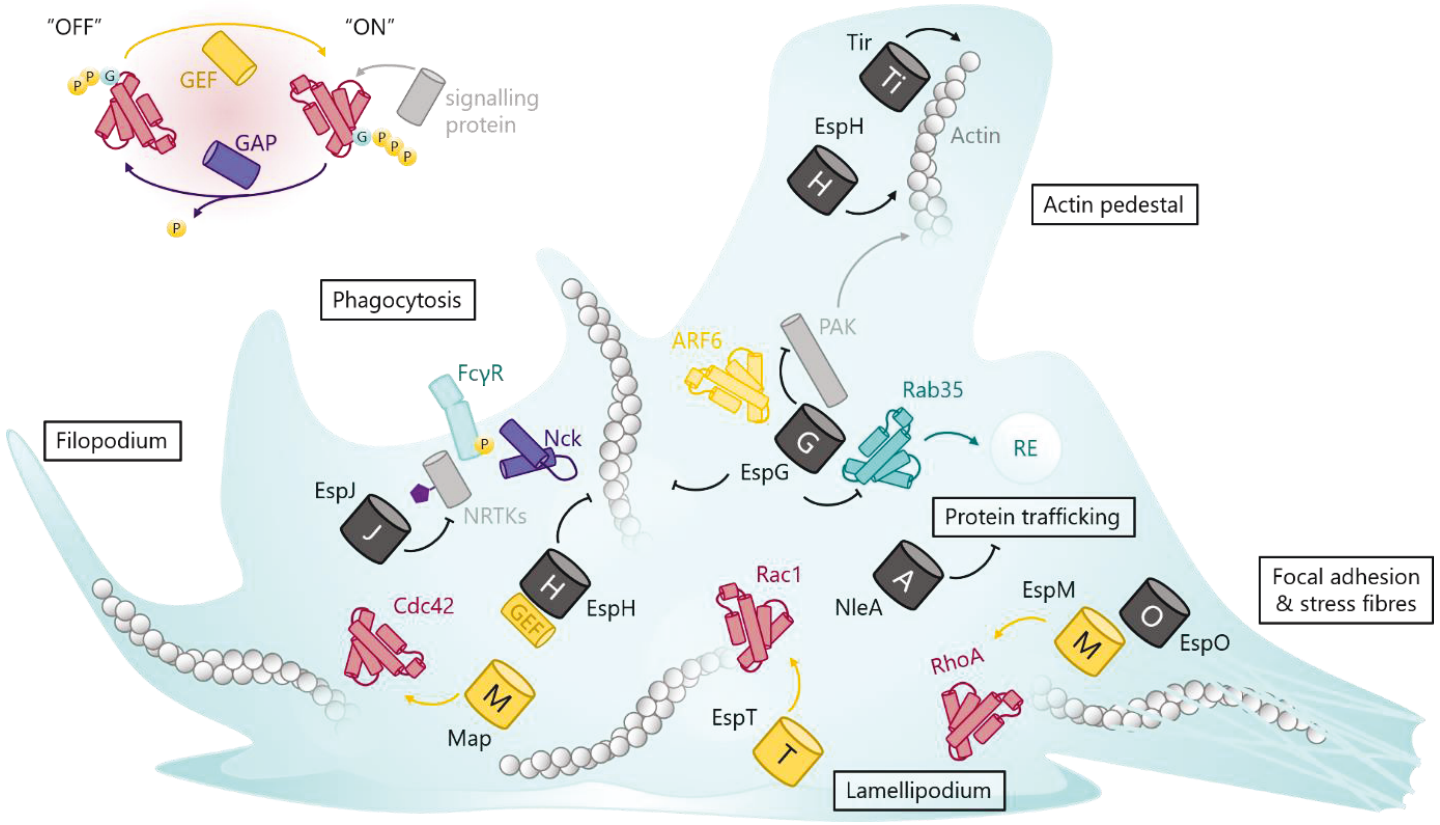
Table 1 | Distribution and function effector protein families across representative EPEC, EHEC and *C. rodentium* strains

Effector	EHEC Sakai	EPEC E2348/69	*C. rodentium* ICC169	Reported function(s)
Cif	-	1, 1*	-	Cell cycle arrest
Tir/EspE	1	1	1	Actin polymerisation and pyroptosis
EspF	1	1	1	Induction of apoptosis, cytoskeletal remodelling
EspG	1	2	1	Inhibits protein secretion, cytoskeletal remodelling
EspH	1	1	1	Cytoskeletal remodelling, inhibition of phagocytosis
EspI/NleA	1	1	1	Inhibition of inflammasome activation and protein secretion
EspJ	1	1	1	Inhibits phagocytosis
EspK	1	-	1	-
EspL	3, 1*	1, 2*	1	Inhibits necroptosis
EspM1/2	2	-	2, 1*	Cytoskeletal remodelling
EspN	1	-	1, 2*	-
EspO	2	1, 1*	1	Promotes tissue integrity
EspR	3, 1*	-	-	-
EspS/Ibe/OspB	-	-	1	-
EspT	-	-	1	Cytoskeletal remodelling, NF-κB modulation
EspW	1	-	-	Cytoskeletal remodelling
EspX/NleL	5, 1*	-	1	Ligates ubiquitin
EspY	4, 1*	-	1	Predicted cell cycle regulator
EspZ/SepZ	1	1	1	Limits effector translocation
Map	1	1	1	Cytoskeletal remodelling
NleB	2, 1*	2, 1*	1, 1*	Inhibits cell death
NleC	1	1	1	NF-κB modulation
NleD	1	1	2	MAPK signalling inhibition
NleE	1	2	1	NF-κB modulation
NleF	1	1	1	Inhibits cell death
NleG	9, 5*	1	3, 2*	Ligates ubiquitin
NleH/OspG	2	2, 1*	1	Inhibits cell death and NF-κB signalling
NleJ	-	1	-	-
NleK	-	-	1	-
NleN	-	-	1	-
NleO	-	-	1	-
TccP/EspF$_U$	1, 1*	-	-	Actin polymerisation
Total	48, 11*	23, 6*	31, 6*	

* indicates pseudogenes

The assembly of specific actin structures is largely governed by the Rho family of GTPases, among others (Singh et al., 2019a). GTPases cycle between membrane-associated GTP-bound "on" states and GDP-bound "off" states that can be sequestered in the cytosol upon association with guanosine nucleotide dissociation inhibitors (GDIs). With the aid of activating guanine nucleotide exchange factors (GEFs), GTPases bind GTP to initiate signalling through their downstream signalling effectors (Thumkeo et al., 2013), before being deactivated once more by the GTPase activating proteins (GAPs) (Cherfils and Zeghouf, 2013). Three members of the Rho GTPase family, RhoA, Rac1 and Cdc42, are responsible for stress fibre, lamellipodia and filopodia formation, respectively (Sit and Manser, 2011). RhoA promotes the activity of the formin mDia1, leading to Rho-associated protein kinase (ROCK) stimulation. ROCK in turn signals to inhibit ADF/cofilin and nucleate stress fibres (Maekawa et al., 1999). Conversely, Rac1 recruits N-WASP and Arp2/3 directly to initiate construction of the lamellipodium (Krause and Gautreau, 2014), while Cdc42 requires the formin mDia2 to recruit the N-WASP/Arp2/3 machinery for the extension of filopodia (Jacquemet et al., 2015).

While actin can serve as a mechanical guard against bacteria (Man et al., 2014), several pathogens encode T3 effector proteins that directly bind F-actin (Belyy et al., 2018; Vander Broek et al., 2017; Hiyoshi et al., 2011) or subvert the function of actin-regulating proteins (Aktories et al., 2011), and the A/E pathogens are no exception (Schematic 3).



Schematic 3 | Simplified overview of host GTPase subversion by A/E effectors

GTPases cycle between "on" and "off" states with the help of activating guanine exchange factors (GEFs), and deactivating GTPase activating proteins (GAPs). In their active state, GTP-bound GTPases interact with host effectors to mediate cytoskeletal changes and protein trafficking, among other processes. EspH enhances Tir-driven actin pedestal formation by promoting N-WASP recruitment (not depicted), but also binds Rho GEFs to prevent activation of GTPases, including those involved in phagocytosis. EspJ and EspG also prevent phagocytosis by inhibiting non-receptor tyrosine kinase signalling, and sequestering the Arf6 GTPase, respectively. Anchored to Arf6, EspG is localised to bind other proteins, such as Rab35 and p21-activated kinase (PAK), to simultaneously inhibit trafficking of protein in recycling endosomes (REs) to the cell surface and promote actin polymerisation in pedestals. Map, EspM and EspT function as GEF mimics, activating Cdc42, Rac1 and RhoA respectively to promote the formation of filopodia, lamellipodia and stress fibres. EspO can bind EspM to antagonise its effect.

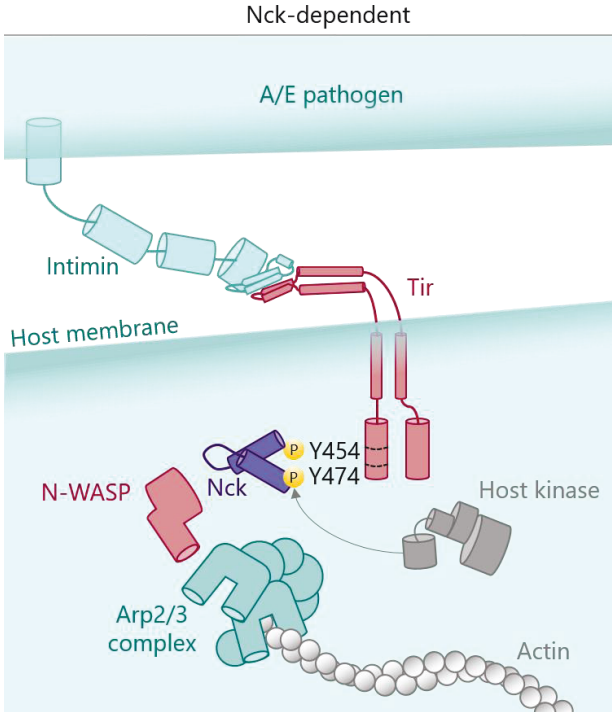
1.5.1.1 Tir is phosphorylated by host kinases to initiate actin pedestal formation

The first and arguably most important T3SS protein to be secreted is the essential *LEE5*-encoded effector, Tir (Deng et al., 2003; Kenny et al., 1997; Mills et al., 2008; Wang et al., 2008). Tir inserts into the host cell membrane in a hairpin loop confirmation, with both termini remaining membrane-embedded while an extracellular loop is exposed to the A/E bacterium's surface-exposed adhesin, intimin (Donnenberg et al., 1993a, 1993b; Luo et al., 2000; Ross and Miller, 2007). Similarly, intimin exposes its immunogenically variable 280 amino acid (aa) C-terminal domain for Tir binding (Adu-Bobie et al., 1998; Frankel et al., 1995), while its 700 aa N-terminal β-barrel autotransporter domain moors the adhesin to the bacterial outer membrane.

In the host cytosol, the C-terminus of E69, E11, B171 and *C. rodentium* Tir can be phosphorylated on a key tyrosine residue (Y474 in E69) by redundant host kinases (Rosenshine et al., 1992), such as those from the Abl, Src and Tec families (Bommarius et al., 2007; Swimm et al., 2004). This is mediated by the clustering of Tir caused by intimin binding (Campellone et al., 2004a; Hayward et al., 2009). Further C-terminal Tir residues Y483/Y511 are recognised by host inositol phosphatase SHIP2 to control pedestal morphology (Smith et al., 2010). As our understanding of the phenomenon of actin pedestal formation matures, more proteins are implicated in its formation (Law et al., 2015), however the basic outline is as follows: phosphorylated Tir recruits the adaptor protein Nck (non-catalytic region of tyrosine kinase adaptor protein 1) via its Src homology 2 (SH2) domain, to activate N-WASP and Arp2/3 (Lommel et al., 2001), resulting in localised polymerisation of actin (Schematic 4). In addition to initiating actin polymerisation, host Tir-adaptors can regulate the abundance of translocated Tir (Nieto-Pelegrin et al., 2014).

Although pedestal formation is advantageous to A/E pathogens during colonisation, it is not required for A/E lesion formation on mucosal surfaces. Therefore, a *C. rodentium* Tir mutant with abrogated Tyr471were still able to colonise murine, calf and lamb colons (Crepin et al., 2010), suggesting that Tir has additional functions during infection. Indeed, transfection of Tir into HeLa cells also facilitates the degradation of TRAF2 to inhibit TNF-induced activation of the nuclear factor κ light-chain enhancer of activated B cells (NF-κB) signalling pathway (§1.5.2).

This correlates with increased interleukin (IL)-8 production by HeLas in the absence of Tir during EPEC infection (Ruchaud-Sparagano et al., 2011). Additionally, a recent study demonstrated that Tir-mediated actin polymerisation contributes to the induction of pyroptosis in human macrophages (Goddard et al., 2019) (§4).

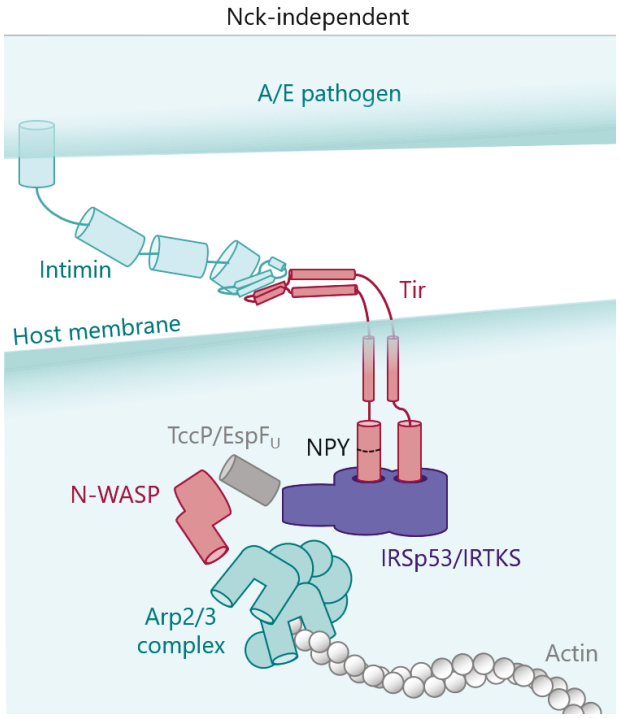


Schematic 4 | Nck-dependent actin polymerisation by Tir
Intimin, a surface-exposed adhesin, binds clusters of T3SS-translocated Tir at the host cell membrane. Clustering of Tir by intimin binding facilitates the phosphorylation of Tir at a conserved Tyr residue (474 in EPEC) by host tyrosine kinases. Phospho-Tyr is recognised by the adaptor protein Nck, which recruits N-WASP and the Arp2/3 complex to initiate actin polymerisation at the site of bacterial attachment.

1.5.1.2 TccP/EspF$_U$ links Tir to the actin cytoskeleton

Some A/E pathogens, such as strains of EHEC O157:H7, deliver a Tir variant with only a single Tyr residue (Y458), which is not tyrosine phosphorylated. Instead, these Tir variants contain an Asn-Pro-Tyr (NPY) motif that is required for pedestal formation (Allen-Vercoe et al., 2006; Kenny and Warawa, 2001). By translocating their own Tir adaptor, the Tir cytoskeleton-coupling protein (TccP, also known as EspF$_U$ owing to its homology with the effector EspF), these strains can initiate the recruitment and activation of N-WASP in a host-independent manner (Campellone et al., 2004b; Garmendia et al., 2004, 2005, 2006). TccP binds the host insulin receptor tyrosine kinase substrate (IRTKS) (or IRSp53), which recognises the Tir NPY motif to promote downstream signalling (Vingadassalom et al., 2009, 2010; Weiss et al., 2009) (Schematic 5). These Nck-dependent and Nck-independent modes of actin polymerisation can sometimes be co-opted to increase the efficiency of actin polymerisation. For example, B171 encodes a TccP-like protein (Tccp2) as well as a Tir protein containing the two conserved Tyr

residues, allowing it to recruit both host and EPEC N-WASP adaptor proteins (Martins et al., 2017; Ogura et al., 2007; Ooka et al., 2007; Whale et al., 2007).



Schematic 5 | Nck-independent actin polymerisation by Tir
Tir variants with an NPY motif are recognised by host adaptor proteins IRSp53 or IRTKS following T3SS-dependent translocation. A further effector protein, TccP (also called EspF$_U$) serves as a signalling mediator, associating Tir:IRTKS with N-WASP. Downstream recruitment of Arp2/3 facilitates actin polymerisation and subsequent pedestal formation.

1.5.1.3 ADP ribosylation of non-receptor tyrosine kianses by EspJ inhibits actin remodelling

EspJ is a 24.6 kDa non-LEE encoded effector, identified by transcriptomics analysis in an operon with TccP in EHEC O157:H7 and on genomic island (GI) 14 in *C. rodentium* (Dahan et al., 2004, 2005; Garmendia and Frankel, 2005; Petty et al., 2010). As with many effectors, early research pointed towards mitochondrial localisation (Kurushima et al., 2010) and a role for EspJ in colonisation of C57Bl/6 mice (Dahan et al., 2005), though reports on the importance of EspJ in human infection are conflicting (Donnenberg et al., 2015; Hazen et al., 2016). EspJ, and its *S. enterica* subsp. *salamae* and *arizonae* homologue SeoC, are ADP ribosyl-transferases that specifically modify a conserved residue (E310) in the Src family of kinases (Pollard et al., 2016, 2018). ADP ribosylation prevents Src adopting an active conformation, inhibiting both FcγR- and CR3-mediated phagocytosis (Marchès et al., 2008; Young et al., 2014). Given the role of non-receptor tyrosine kinases in actin pedestal formation, overexpression of EspJ can modulate pedestal length (Young et al., 2014), as well as reduce the pyroptosis driven by Tir actin polymerisation (Goddard et al., 2019).

1.5.1.4 EspH is a Rho GEF competitor with widespread roles during infection

EspH is a core LEE-encoded effector that supports enteric colonisation (Ritchie and Waldor, 2005; Shaw et al., 2005). This is suggested to entail EspH's ability to augment pedestal formation (Tu et al., 2003), as EPEC EspH enhances recruitment of N-WASP to the C-terminal of Tir beneath the site of attachment (Wong et al., 2012a). Tethering of EspH could be mediated by its interaction with CD81 microdomains in the plasma membrane (Ramachandran et al., 2018). Independently of this, EspH also inhibits host Rho GTPases; downstream Rho signalling to incite stress fibre, filopodia and lamellipodia formation, as well as the activity of bacterial Rho GEFs, are unaffected by EspH (Dong et al., 2010; Wong et al., 2012b). Instead, EspH maintains RhoGTPases in their inactive state by competitively binding to the Dbl-homology/pleckstrin-homology (DH-PH) domain of select RhoGEFs, such as p115. This prevents their interaction with Rho and results in cell rounding (Dong et al., 2010). As Rho GTPase function underpins several cellular pathways (Narumiya and Thumkeo, 2018), the consequences of EspH-mediated inactivation are widespread. For example, EspH is reported to repress EPEC phagocytosis by macrophages (Dong et al., 2010) and perturb protein trafficking networks that define cell polarity (Roxas et al., 2018).

1.5.1.5 EspM and EspT are Rho GEF mimics that promote membrane perturbations

The discovery of a bacterial protein family with a common Trp-xxx-Glu motif defined a new category of Rho GTPase subverting effectors: the WxxxE effectors (Alto et al., 2006). These effectors are represented in *Salmonella* (SifA and B), *Shigella* (IpgB1 and 2) and the A/E pathogens (Map, EspT and the bfpT-regulated chaperone-like protein TrcA) (Bulgin et al., 2010; Orchard and Alto, 2012). Despite minimal homology to mammalian Rho GTPases, Map, IpgB1 and IpgB2 use the WxxxE motif to functionally mimic Cdc42, Rac1 and RhoA GEFs, respectively, leading to Rho activation (Alto et al., 2006). Analysis of the EHEC Sakai secretome identified EspM1 and 2 as further WxxxE members (Tobe et al., 2006), and later screens revealed EspM-like proteins are present in over 96% of tested O157-like EHEC strains (Arbeloa et al., 2009), as well as EPEC B171 and E11, while *C. rodentium* encodes EspM2 and EspM3 (Arbeloa et al., 2008). Although each of the three A/E EspM-like effectors share up to 86% identity, EspM2 and EspM3 stimulate the Rho-ROCK pathway by structurally mimicking a RhoA GEF (Arbeloa et al., 2010) to produce cytoskeletal structures distinct from both one another and EspM1

(Arbeloa et al., 2008). These actin rearrangements dysregulate pedestal formation and tight junctions in polarised cells (Simovitch et al., 2010).

Using the WxxxE family members IpgB2 (*Shigella*) and Map as queries, a BLAST search revealed the presence of EspT in *C. rodentium* neighbouring EspO, NleG8 and fellow WxxxE family member EspM2 (Bulgin et al., 2009b). Analysis of EspT distribution also uncovered homologues in E11 and other EPEC isolates (Arbeloa et al., 2009). The recent sequencing of the E11 genome demonstrated that *espT* is found on several unique plasmids, yet only 65 of the 12,253 sequenced *E. coli* genomes encode EspT (Hazen and Rasko, 2019). Like its *Shigella* homologue IpgB2 (Alto et al., 2006), EspT localises to the mitochondrial network, despite lacking a mitochondrial targeting sequence, and induces the formation of lamellipodia in Swiss 3T3 fibroblasts and membrane ruffles in HeLa cells (Bulgin et al., 2009b). These morphological perturbations involve both Rac1 and Cdc42, for which EspT behaves as a GEF mimic. When EspT was non-natively delivered to the human macrophage line U937 by E69, EspT facilitated invasion and induced IL-8 and IL-1β secretion through activation of NF-κB and Erk/JNK pathways. As IL-8 production was abolished by mutation of EspT's active loop residue (Q117), this signalling is linked to EspT's Rac1-activating activity (Raymond et al., 2011). A direct interaction with either GTPase has yet to be demonstrated, as neither Rac1 nor Cdc42 were identified as EspT interactors; instead the mitochondrial Heat Shock Protein family D1 (HSPD1) was identified, which could potentially tether EspT to its location (Sontag et al., 2016). Membrane remodelling itself is fulfilled downstream of Rac1 and Cdc42 by the host GTPase effectors Wave2, Abi1 and, in some cases, IRSp53 (Bulgin et al., 2009a). Pathogen-induced membrane ruffling is usually associated with bacterial invasion (Hume et al., 2017; Patel and Galán, 2005), and indeed EspT expression by E11, or non-natively by the EPEC strain JPN15 (but not E69), induces membrane ruffling-dependent EPEC uptake in non-phagocytic cells (Bulgin et al., 2009a, 2009b). Internalised EPEC remains vacuolar and retains the ability to produce actin pedestals, challenging the paradigm of EPEC's extracellular infection strategy.

1.5.1.6 EspV induces morphological changes in yeast cells and human cells

EspV, although small (60 aa) and present as a pseudogene in EHEC O157:H7 Sakai (Tobe et al., 2006), is an intact and functional effector in *C. rodentium*, E11 and EPEC E22. It has been shown

to inhibit yeast cell growth, and can lead to cell rounding, dendrite-like projections and nuclear condensation in transfected HeLa cells (Arbeloa et al., 2011). The mechanism by which EspV subverts these processes is currently unknown.

1.5.1.7 EspW subverts Rac1 to induce unique membrane ruffling

EspW was first identified in EHEC O157:H7 Sakai as a homologue of the uncharacterised *Pseudomonas syringae* effector HopW (Tobe et al., 2006), but is also represented in other intestinal pathogens, including EPEC B171 and *Shigella boydii* (Sandu et al., 2017). EspW binds the host microtubule protein Kinesin-12 (Kif15) in a yeast 2 hybrid system (Y2H), and the two proteins independently localised to the base of actin pedestals, signifying an unconfirmed role for Kif15 as an EspW recruitment factor. Although EspW is not a WxxxE effector, its transfection results in membrane ruffling and the formation of 'flower-shaped' structures on the membrane that are achieved through activation of Rac1. Indeed, EHEC infection in the absence of EspW results in cell shrinkage that can be rescued with the Rac1 activator S1P, leading to the hypothesis that fine-tuning of Rac1 dynamics during infection is achieved by co-expression of EspM, EspT and EspW (Sandu et al., 2017).

1.5.1.8 EspG hijacks GTPases to inhibit protein trafficking and regulate the cytoskeleton

EspG is a 43.8 kDa *Shigella* VirA homologue encoded at the 5' end of the LEE upstream *LEE1*, and is one of the most extensively studied, well-conserved and wide-acting core effectors (Elliott et al., 2001; Hazen et al., 2013). VirA is an α-tubulin-specific cysteine protease-like effector that is required by *Shigella* for cell-to-cell spread (Yoshida et al., 2002, 2006), and early EspG research sought to confirm the conservation of this function (Tomson et al., 2005). More recent structural studies revealed that neither EHEC EspG nor VirA are true proteases and do not directly destabilise microtubules (Germane and Spiller, 2011; Germane et al., 2008), as intact microtubule networks are observed following microinjection of EspG (Selyunin et al., 2011).

More recent literature has established EspG as a GTPase hijacker. EspG is capable of binding ADP-ribosylation factors (Arfs) — a five-member family of Ras superfamily GTPases (Furniss et al., 2016; Humphreys et al., 2016; Selyunin et al., 2014). In macrophages, EspG:Arf6 binding

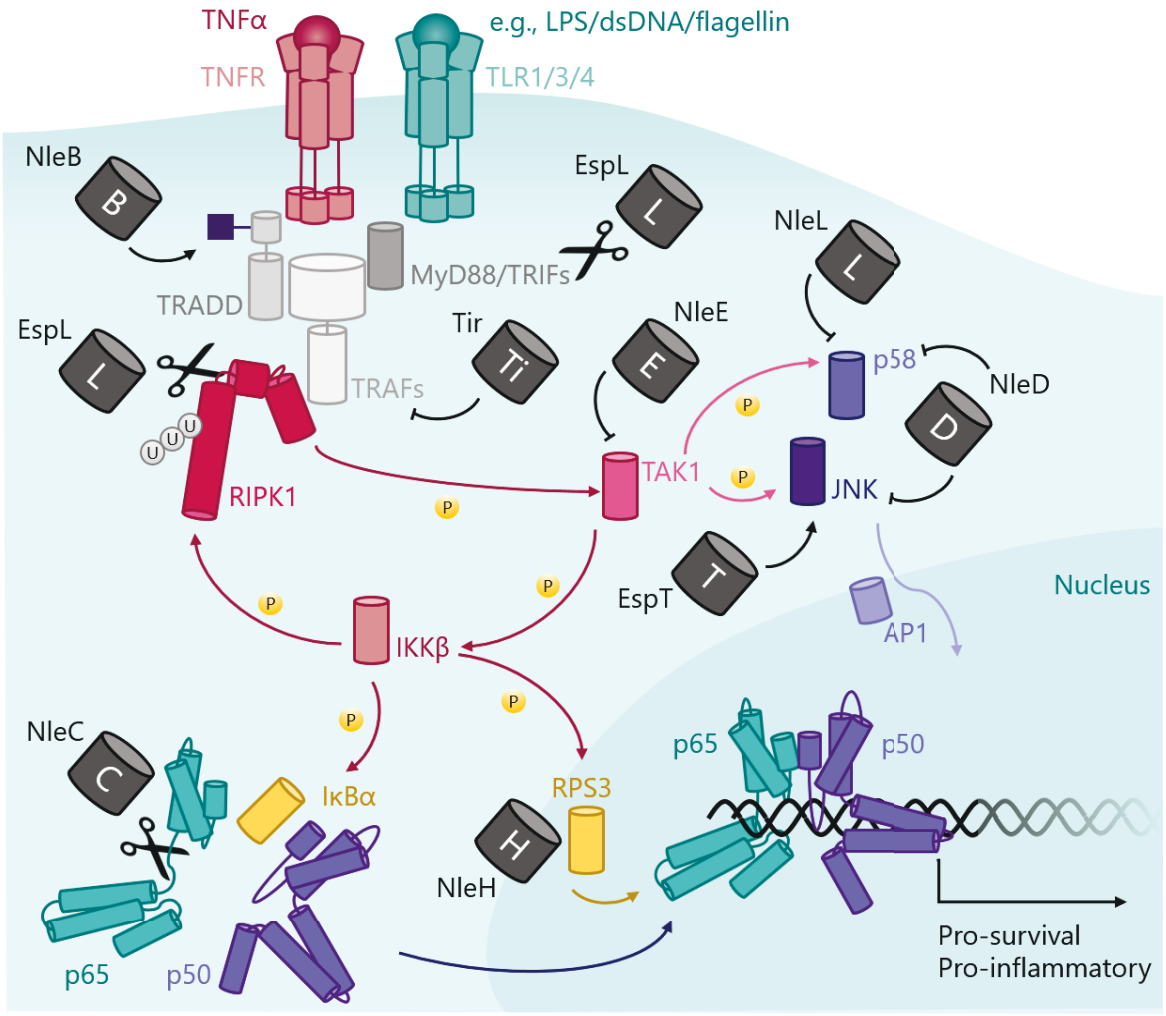
impedes Arf6 binding to its cognate effector ARNO, disrupting the localised manipulation of actin for phagocytosis (Humphreys et al., 2016). EspG also harbours a Tre-2/Bub2/Cdc16 (TBC) catalytic domain that mimicks Rab GAPs, exhibiting *in vitro* GAP activity on eight Rab GTPases (Dong et al., 2012). During infection, this Rab binding is used to manipulate protein trafficking to the cell surface, which was first demonstrated with the epidermal growth factor receptor, β1 integrin and the transferrin receptor (Clements et al., 2011). Mechanistically, this is mediated by EspG forming a tripartite complex with Arf6 and Rab35 during infection to prevent Rab35-mediated recycling of cargo to the plasma membrane (Furniss et al., 2016). In support of this, trafficking of the Downregulated in Adenoma (DRA) Cl^-/OH^- anion exchanger to the apical plasma membrane in intestinal cells is attenuated in wild type (WT) EPEC infection, and re-established when EspG/EspG2 is deleted (Gill et al., 2007). Consistently, recycling of β1 integrin and the transferrin receptor are both Arf6-dependent (Powelka et al., 2004; Souza-Schorey and Chavrier, 2006). To potentiate this activity, T3SS-translocated EspG localises to recycling endosomes (Furniss et al., 2016); EspG introduced independently of the T3SS results in disruption of Golgi architecture (Clements et al., 2011; Selyunin et al., 2014). Ectopic EspG expression is additionally described to promote paracellular enterocyte permeability (Matsuzawa et al., 2005) and perturb tight junctions (Glotfelty et al., 2014; Morampudi et al., 2017).

In addition to the Arf and Rab GTPases, EspG has also been implicated in Rho GTPase subversion. For example, like EspM2, EspG is reported to trigger the release of GEF-1 and the downstream activation of the RhoA-ROCK pathway (Matsuzawa et al., 2004). Additionally, a pocket between EspG helices a4 and a9 facilitates binding to the Rac/Cdc42-binding domain of p21-activated kinase (PAK1), a Rho GTPase effector (Germane and Spiller, 2011; Sells et al., 1997). Independent studies confirm this interaction with PAK1, PAK2 and PAK3, but suggest that EspG binds to the Ia3 helix of the PAK2 autoinhibitory domain, promoting PAK activation (Selyunin and Alto, 2011). Most recently, EspG binding to PAK was demonstrated to be critical for efficient pedestal formation. These actin perturbations are underpinned by the localisation of PAK and its Rho family GTPase complex to EspG by Arf6 (Singh et al., 2019b).

1.5.2 Prevention of NF-κB signalling

The NF-κB signalling pathway transcriptionally regulates the expression of genes involved in cell survival, immunity and inflammation (Liu et al., 2017b; Napetschnig and Wu, 2013; Zhang et al., 2017), all of which can be targeted during infection. NF-κB regulates expression of the pro-inflammatory cytokines IL-8 and IL-1β and inflammasome components (§1.5.3), among other proteins (Liu et al., 2017b). The NF-κB complexes comprise five transcription factors that assemble into homo- and heterodimers and translocate to the nucleus to bind the major groove of target DNA via their N-terminal Rel homology domain. Three of the five, RelA (p65), c-Rel and RelB, are transcriptional activators with a C-terminal transactivation domain, whereas the remaining two, p50 (p105/NF-κB1) and p52 (p100/NF-κB2), lack this domain and serve as repressors.

NF-κB signalling is activated by the recognition of microbial and danger signals by pattern recognition receptors (PRRs), which are widely expressed in immune and epithelial cells. An important family of PRRs are the Toll-like receptors (TLRs), which can detect pathogen-associated molecular patterns (PAMPs) such as double-stranded RNA (dsRNA; TLR3), lipopolysaccharide (LPS) (TLR4), flagellin (TLR5), lipoproteins (TLR1/2/6) and CpG DNA (TLR9) (Kawasaki and Kawai, 2014). TLR signalling, similarly to tumour necrosis factor receptor (TNFR) signalling, proceeds via a complex cascade that requires the recruitment of members of the TNFR-associated factor (TRAF) family of intracellular proteins to the receptor complex. These proteins can then form signalling hubs through the recruitment of kinases, such as the TAK1 (Transforming growth factor beta-activated kinase 1)-TAB2/3 complex — a central regulator of canonical NF-κB signalling. Under normal physiological conditions, p65 is held in a cytoplasmic complex with p50 bound to the inhibitor of NF-κB inhibitory proteins (IκB); only when IκB is ubiquitinated for proteosomal degradation can the p65/p50 enter the nucleus. The purpose of TAK1, therefore, is to phosphorylate IκB kinases (IKKs), which themselves phosphorylate and deactivate IκB to induce nuclear translocation of p65/p50 and transcription of pro-inflammatory genes. Notably, TAK1 can also phosphorylate and activate mitogen activated protein kinase (MAPK) family members such as Jun N-terminal Kinase (JNK), Extracellular Signal-Regulated Kinase (ERK) and p38 to mediate expression of genes involved in inflammatory responses and cell survival (Plotnikov et al., 2011). Unsurprisingly, several A/E effectors work in concert to subvert these inflammatory signalling pathways (Schematic 6).



Schematic 6 | Manipulation of NF-κB signalling by A/E effectors
Stimulation of the Toll-like receptors (TLRs) or tumour necrosis factor receptor (TNFR) by their cognate ligands triggers NF-κB signalling, and transcription of pro-inflammatory and pro-survival genes. This requires recruitment of signalling complexes to engaged receptors, and the downstream mobilisation of ubiquitylated receptor interacting protein kinase 1 (RIPK1). RIPK1 association with TNFR-associated factors (TRAFs), as well as the association of the TRIF family of TLR-adaptors, is precluded by EspL cleavage. Tir also targets select TRAFs for degradation. Recruitment of the membrane complex is further inhibited by NleB, which GlcNAcylates the TNF-receptor associated death domain protein (TRADD), rendering it unable to associate with TNFR. Under physiological conditions, RIPK1 phosphorylates transforming growth factor β-activated kinase 1 (TAK1) to promote prosurvival signalling through phosphorylation of JNK and p58. NleD and NleL work in concert to inhibit JNK and p58 signalling, preventing activator protein 1 (AP1) translocation into the nucleus. NleE also indirectly inhibits pro-inflammatory signalling by binding and inhibiting TAK1-associated proteins (not shown). Conversely, EspT activates JNK signalling to promote inflammation. TAK1 also phosphorylates IκB kinase β (IKKβ), which in turn phosphorylates and deactivates the inhibitor of NF-κB inhibitor proteins (IκB). When IκB releases its inhibition on p65 and p50, they can translocate to the nucleus for transcription of NF-κB target genes. Transcription is also promoted by ribosomal protein S3 (RPS3), which is differentially regulated by host IKKβ and bacterial NleH-family proteins.

1.5.2.1 The Zinc metalloproteases NleC and NleD inhibit NF-κB signalling

NleC is a 37 kDa member of the Zinc metalloprotease family of effectors (Marchès et al., 2005), that, together with its *S. enterica* homologues GtgA, GogA and PipA, cleave NF-κB subunits (Jennings et al., 2018; Mühlen et al., 2011). NleC exhibits the widest substrate specificity and is able to cleave all five subunits (Hodgson et al., 2015), whereas the *S. enterica* homologues cannot cleave p50 or p52 (Jennings et al., 2018). This disparity is explained by the biochemistry of the substrate pocket in each effector and therefore its preferred cleavage sites in each NF-κB subunit: NleC cleaves p65 between Cys38 and Glu39, which are conserved in all five subunits, whereas GtgA, GogA and PipA preferentially cleave two non-conserved amino acids present downstream. NleC's anti-NF-κB activity is extended by its ability to cleave p300, an acetyltransferase that positively regulates NF-κB-driven IL-8 production (Shames et al., 2011a), its cleavage of IκB when overexpressed and its prevention of p38 phosphorylation (Sham et al., 2011). NleC achieves its catalytic activity with a strip of acidic, negatively charged residues in its active site that mimic the major groove of DNA phosphate backbone (Jennings et al., 2018; Turco and Sousa, 2014), as well as an HExxH motif that coordinates its Zn^{2+} cofactor (Li et al., 2014). Befitting of its role in infection, NleC is observed in the nucleus, despite its large size and lack of nuclear localisation signal (Yen et al., 2010), and the resulting NF-κB proteolysis minimises intestinal pathology in a *C. rodentium* model (Baruch et al., 2011; Sham et al., 2011) and suppresses IL-8 secretion *in vitro* (Sham et al., 2011; Shames et al., 2011a).

NleD was identified through signature-tagged mutagenesis as an important factor for colonisation of the bovine (Dziva et al., 2004) and murine gut (Deng et al., 2004), though this could not be recapitulated with the genomic disruption of *nleD* with an *aphT* resistance cassette (Marchès et al., 2005), or in an independent *C. rodentium* infection model (Kelly et al., 2006). Like NleC, NleD is a Zinc metalloprotease with a HExxH motif, but NleD instead targets JNK and p38. Co-operatively targeting of both NF-κB (NleC) and MAPK (NleD) pro-inflammatory signalling inhibits IL-8 production (Baruch et al., 2011). As JNK signalling can also promote apoptosis (Dhanasekaran and Premkumar Reddy, 2017), the activity of NleD also functionally complements other anti-apoptotic effectors.

1.5.2.2 NleH is a Ser/Thr kinase that subverts NF-κB

NleH was discovered in the *C. rodentium* genome upstream of *nleF* (García-Angulo et al., 2008), and was noted for its 49% similarity to the *Shigella* NF-κB modulator OspG (Hemrajani et al., 2008), a kinase that prevents degradation of phospho-IκBα (Kim et al., 2005). Two independent ORFs with 83% identity to *C. rodentium* NleH (NleH1 and 2) were henceforth identified in both EPEC and EHEC (García-Angulo et al., 2008). NleH1 and 2 themselves share 84% identity (Pham et al., 2012), differing by a 10 aa stretch that in NleH2 encodes an SH2 domain and a protein kinase A (PKA) interaction domain (Gao et al., 2009). Deletion of *C. rodentium nleH* delays colonisation of C57Bl/6 mice (Feuerbacher and Hardwidge, 2014; García-Angulo et al., 2008; Hemrajani et al., 2008) and reduces mortality of susceptible C3H/HeJ mice (Pham et al., 2012), and an EHEC O157:H7 Δ*nleH1/2* double mutant exhibits a comparable delay in shedding and quicker clearance in a calve and lamb model, respectively (Hemrajani et al., 2008).

There is considerable disparity among the functions of each NleH family members (Pham et al., 2012). In accord with NleH's homology to OspG, NF-κB-RE-luc reporter mice exhibit 2.5-fold less luminescence when infected *C. rodentium* Δ*nleH* compared with WT (Hemrajani et al., 2008). In EHEC, this may be mediated by the N-terminus of NleH1 and NleH2, which bind the p65-associated ribosomal protein, RPS3 (Gao et al., 2009). Conversely, phosphorylation of RPS3 by IKKβ promotes nuclear translocation to interact with p65; this is inhibited exclusively by NleH1 binding (Pham et al., 2012; Wan et al., 2011), although NleH1 and 2 heterodimerise *in vivo* (Martinez et al., 2010), and both effectors can prevent IκBα degradation when overexpressed through an RPS3-independent mechanism (Royan et al., 2010). Like OspG, A/E NleH effectors are auto-phosphorylating serine threonine kinases with a minimal kinase core (Grishin et al., 2014; Halavaty et al., 2014). Although they do not specifically phosphorylate any of their known binding partners (Grishin et al., 2014; Hemrajani et al., 2010), their kinase activity is essential for their subversion of NF-κB signalling (Gao et al., 2009; Pham et al., 2012).

1.5.2.3 NleE is a Cys methyltransferase that stabilises IκB

NleE is a 27 kDa effector that inhibits IκB degradation, leading to sequestration of p65 in the cytosol. Though the NleE mechanism of NF-κB inhibition is unique, it is functionally redundant

with NleB (§1.5.3.2) and NleC (§1.5.2.1). It is therefore less commonly found in pathogenic *E. coli* isolates: only approximately half of EPEC genomes encode an NleE homologue (Santos and Finlay, 2015), with greater representation in non-O157 EHEC-like strains (Wickham et al., 2006). In EPEC, NleE is encoded in IE6 together with NleB (Iguchi et al., 2009). Some genomes also encode a shorter NleE variant in IE2 with a deletion of an internal 56 aa region, rendering it a cryptic, untranslocated effector (Nadler et al., 2010). Despite these observations, *C. rodentium* NleE is required for full colonisation several mouse strains (Wickham et al., 2007), indicating the utility of NleE to A/E pathogens. A/E NleEs differ from their *Shigella* homologue OspZ in their C-termini, which contain an IDSYMK motif that is necessary for the inhibition of p65 nuclear translocation (Newton et al., 2010). Structural studies revealed NleE facilitates S-adenosyl-L-methionine-dependent methylation of TAB2/3 on a Zn^{2+}-coordinating Cys residue (Yao et al., 2014). This is mediated by an independent N-terminal binding region in NleE that is necessary for TAB2/3 binding and subsequent inhibition of IL-8 production (Zhang et al., 2016).

1.5.3 Subversion of cell death pathways

Cell death is the physiological response to stress. As our understanding of cellular signalling broadens, many forms of programmed cell death have been defined, each differing in their molecular triggers and subsequent pathology (reviewed by Tang et al., 2019). These include intrinsic and extrinsic apoptosis (Kerr et al., 1972), NETosis (Brinkmann, 2004), entosis (Overholtzer et al., 2007), parthanatos (Wang et al., 2009), autophagy-dependent cell death or autosis (Liu et al., 2013), ferroptosis (Stockwell et al., 2017), oxeiptosis (Holze et al., 2018), and the programmed necrotic forms of cell death, necroptosis and pyroptosis (Cookson and Brennan, 2001; Degterev et al., 2005; Schroder and Tschopp, 2010). In the context of A/E pathogenesis, only apoptosis and necrotic cell death pathways have historically been considered.

Many forms of programmed cell death are mediated by cysteine-aspartic proteases (caspases). These can be broadly divided into traditionally apoptotic caspases, including initiator caspases (-2, -8, -9 and -10), which serve to cleave and activate executioner caspases (-3, and -7), and the inflammatory caspases (-4/-11/-5 and -1). Initiator caspases are proximity-activated via

their pro-domains, which facilitate assembly of the death-type specific complexes: the apoptosome, the DISC complex, and the inflammasome (detailed below).

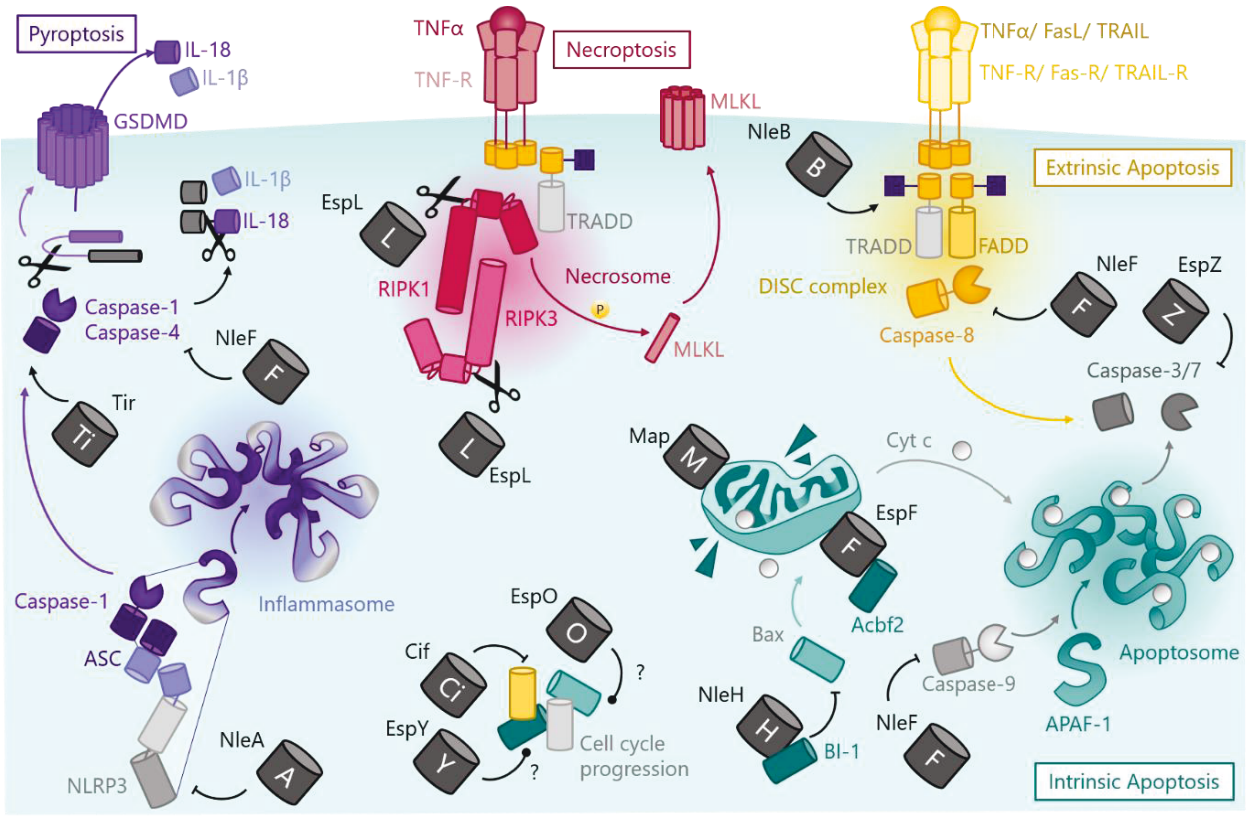
Intrinsic apoptosis results in apoptosome formation. This occurs when cytochrome c is released from the inner mitochondrial membrane into the cell cytoplasm as result of cellular stress. Forms of stress can include DNA damage and mitochondrial outer membrane permeabilisation. Liberated cytochrome c can join apoptotic protease activating factor-1 (APAF-1) and caspase-9 to complete the apoptosome complex. Downstream signalling then results in the activation of executioner caspases-3, -6 and -7 (Julien and Wells, 2017; Reubold and Eschenburg, 2012). Conversely, extrinsic apoptosis requires the activation of TNF family death ligands including TNF, Fas ligand (FasL) and TRAIL, which bind to their respective extracellular receptors to mediate the localised assembly of the death-inducing signalling complex (DISC). The DISC complex, having recruited the appropriate adaptor proteins for the stimulated death receptor (i.e., Fas-associated death domain protein (FADD) or TNF-receptor associated death domain protein (TRADD)), promotes the self-oligomerisation and activation of caspase-8 via its death-inducing domain (Park et al., 2007; Strasser et al., 2009). Caspase-8 can subsequently cleave the executioner caspases to initiate apoptotic death. The result of apoptosis, whether intrinsic or extrinsically triggered, is DNA fragmentation, cytoskeletal condensation and characteristic cell blebbing (Galluzzi et al., 2018).

Cells have adapted a further, caspase-independent programmed cell death pathway in response to TNF, Fas and TRAIL receptor engagement in the absence of caspase-8: necroptosis (Dhuriya and Sharma, 2018; Peltzer and Walczak, 2019). Necroptotic cell death results in membrane fragmentation, which allows the release of pro-inflammatory cell contents through cell lysis. Necrosome assembly is mediated by receptor interacting protein kinases 1 and 3 (RIPK1 and 3), which hetero-oligomerise via their RIP homotypic interaction motif (RHIM) domains. This is normally inhibited by extensive ubiquitination, inhibitory phosphorylation or caspase-8 dependent cleavage of RIPK1/3 (Dondelinger et al., 2019; Lin et al., 1999). The subsequent autophosphorylation and activation of RIPK3 allows it to phosphorylate mixed lineage kinase domain-like protein (MLKL) (Rodriguez et al., 2016; Wang et al., 2014a). Phosphorylated MLKL next binds to highly negatively charged inositolhexakisphosphate moieties, relieving the MLKL autoinhibitory N-terminal domain (Dondelinger et al., 2014; Quarato et al., 2016) and inciting spontaneous MLKL assembly into octameric pores in the

plasma membrane. This facilitates ion influx that results in cell lysis and necroptotic cell death (Cai et al., 2014; Chen et al., 2014; Huang et al., 2016).

A third mode of cell death that also results in cell lysis is pyroptosis. Similar to necroptosis, pyroptosis is executed by the formation of pores in the cell membrane, in this case by the N-terminus of Gasdermin-D (GSDMD). Uniquely, pyroptosis involves the inflammatory caspases-4, (-11 in mice) and -1, that cleave GSDMD to remove of the autoinhibitory C-terminal of GSDMD (Ding et al., 2016; Kayagaki et al., 2015; Shi et al., 2015). Thus, GSDMD cleavage can occur downstream of both canonical (caspase-1) and non-canonical (caspase-4) pathways. In the non-canonical pathway, caspase-4 directly senses bacterial LPS, leading to caspase-4 activation and cleavage of GSDMD (Kayagaki et al., 2011; Shi et al., 2014). Conversely, in the canonical pathway, nucleotide-binding oligomerization domain (NOD)-like receptors such as NACHT, LRR and PYD domains-containing protein 3 (NLRP3) and NLR family CARD domain-containing protein 4 (NLRC4) oligomerise in response to pathogen- or damage-associated molecular patterns (PAMPs/DAMPs). In A/E pathogenesis, each NOD-like receptor responds to a unique repertoire of stimuli (Yen et al., 2016; Sanchez-Garrido et al., under revision), resulting in their oligomerisation and recruitment of caspase-1. Proximity-dependent autoproteolytic cleavage and activation of caspase-1 precedes the maturation of pro-inflammatory cytokines (IL-18 and IL-1β) (Lieberman et al., 2019), which are released through the GSDMD pore.

Responding to pathogens by undergoing cell death is an important facet of bacterial clearance *in vivo* (Liu et al., 2012; Miao et al., 2010a; Nordlander et al., 2014). Although the A/E pathogens translocate several cytotoxic effectors, it is therefore unclear whether induction of cell death is an A/E infection strategy or a pathological by-product. Given that there is little evidence of late-stage apoptosis in infected tissue, such as nuclear fragmentation, cell shrinkage and membrane blebbing (Galluzzi et al., 2018), the A/E pathogens must encode cytoprotective effectors to balance tissue damage. Indeed, several effectors are reported to prevent different aspects and modes of cell death (Lacey and Miao, 2019; Wong Fok Lung et al., 2014) (Schematic 7).



Schematic 7 | Subversion of programmed cell death pathways by A/E effectors

Pyroptosis and necroptosis result from GSDMD or MLKL pores forming in the plasma membrane. Pyroptosis proceeds after inflammasome activation, such as the NACHT, LRR and PYD domains-containing protein 3 (NLRP3) inflammasome (depicted). Caspase-4-mediated LPS recognition stimulates non-canonical inflammasome activation, while caspase-1 activation results from several exogenous stimuli, including actin polymerisation by Tir, and results in the cleavage of pro-inflammatory cytokines IL-18/1β. NleA inhibits pyroptosis by preventing caspase-1 recruitment to the inflammasome. Both pro-inflammatory caspases (-1 and -4) can process GSDMD, although caspase-4 activity is inhibited by NleF. NleF also inhibits initiator caspases-8 and 9, which act upstream of the executioner caspases-3/-7. Upon stimulation of TNF/Fas or TRAIL receptors, caspase-8 is recruited to the death-inducing signalling complex (DISC) by Fas-associated death domain protein (FADD), and TNF-receptor associated death domain protein (TRADD). FADD and TRADD can both be inhibited by NleB's GlcNAcylation activity. TRADD is additionally implicated in necroptosis, where it recruits RIPK1/3 to phosphorylate MLKL; EspL cleaves RIPK1/3 to inhibit this. Finally, intrinsic apoptosis can be triggered by loss of mitochondrial outer membrane potential in the presence of Map and EspF, releasing cytochrome c. This is countered by NleH, which binds Bax inhibitor 1 (BI-1). Cytosolic cytochrome c joins APAF-1 and caspase-9 to form the apoptosome, resulting in caspase-3/7 activation and intrinsic apoptosis. Cell death also stimulated by Cif, which inhibits cell cycle progression. EspO and EspY may also contribute to this.

1.5.3.1 Cif deamidates NEDD8 to limit cell cycle progression and aid bacterial survival

Cell cycle inhibiting factor (Cif) is a member of the cyclomodulins: a family of papain-like hydrolases that inhibit cell cycle progression. Cif is encoded by a lambdoid prophage in EPEC, EHEC, and other T3SS-wielding pathogens, including *Yersinia*, *Burkholderia* and *Photorhabdus* (Loukiadis et al., 2008; Yao et al., 2009), although Sakai and E69 encode truncations (Marchès et al., 2003). Upon Cif translocation, cells accumulate focal adhesion plaques and stress fibres before cell cycle arrest at the G1 or G_2/M phase transition (Marchès et al., 2003; Nougayrède et al., 2001; Samba-louaka et al., 2008; Taieb et al., 2006). Although Cif structurally resembles a cysteine protease (Hsu et al., 2008), its true catalytic function is to deamidate the Gln40 residue on NEDD8 (Cui et al., 2010), a ubiquitin family moiety that is added prior to protein ubiquitylation and degradation. This leads to the accumulation of the cell cycle progression inhibitors p21 and p27 (Morikawa et al., 2010; Samba-louaka et al., 2008), eventually resulting in apoptosis (Samba-Louaka et al., 2009). It was initially proposed that the inhibition of cell turnover enables enteric colonisation (Samba-Louaka et al., 2009), although Cif also blocks ubiquitylation and distribution of the bactericidal protein Perforin-2 (McCormack et al., 2015a, 2015b), suggesting that Cif also directly enhances bacterial survival.

1.5.3.2 NleB GlcNAcylates death domains to inhibits their interaction

NleB is a 38 kDa effector homologous to the SseK effectors in *S. enterica* (El Qaidi et al., 2017). NleB represents a family of GT-A-type glycosyltransferases that mediate the presumably irreversible addition of an N-linked GlcNAc onto Arg residues. In A/E infection, NleB targets the death domain (DD) of TRADD/FADD and RIPK1 to disrupt their interaction with other DD-containing proteins and therefore inhibit RIPK1-dependent pro-inflammatory signalling and apoptotic or necroptotic cell death (Li et al., 2013; Pearson et al., 2013). Specifically, NleB GlcNAcylates TRADD-DD at Arg235, FADD-DD at the equivalent R117 and RIPK1 at Arg602 (Ding et al., 2019; Li et al., 2013; Pearson et al., 2013; Scott et al., 2017). NleB is additionally able GlcNAcylate GAPDH, binding of which to TRAF2 enhances ubiquitylation and degradation, leading to impaired TNF-induced NF-κB activation in the presence of NleB (Gao et al., 2013). The importance of these pathways during infection is highlighted by the requirement for NleB and its catalytic residues in murine infection models (Gao et al., 2013; Kelly et al., 2006; Pearson

et al., 2013; Pollock et al., 2017). The recent discovery of NleB/SseK-specific glycosyltransferase inhibitors is therefore an attractive anti-virulence agent (El Qaidi et al., 2018).

1.5.3.3 NleF binds and inhibits caspase-4/11, 8 and 9

NleF is a highly conserved 21–22 kDa effector in EPEC and EHEC with a homologous counterpart in *C. rodentium* (85% identity). Co-crystallisation of NleF with human caspase-9 reveals a similar mode of binding in the caspase-9 catalytic pocket to the synthetic peptide inhibitor z-EVD-Dcbmk (Blasche et al., 2013), albeit with less efficient salt-bridging. This lack of fine specificity despite convincing functional inhibition may explain why NleF is also able to bind and inhibit the activity of human caspase-8 and human and mouse caspase-4/11. With targets like caspase-8 and 9, NleF was initially regarded as an anti-apoptotic and subsequently pro-necroptotic effector and was demonstrated as such (Pollock et al., 2017). As the role of caspase-4 in non-canonical inflammasome activation was elucidated (Kayagaki et al., 2011; Shi et al., 2014), NleF biology was reconsidered in the light of LPS-driven pyroptosis. This led to the discovery that NleF reduces caspase-11-dependent IL-18 secretion during *C. rodentium* infection *in vivo* (Pallett et al., 2017).

1.5.3.4 The cysteine protease EspL cleaves RHIM proteins to inhibit necroptosis

EspL-like effectors have only recently been characterised, although they have been identified in several A/E strains since their discovery in 2006 (Iguchi et al., 2009; Soledad-Cadona et al., 2018; Tobe et al., 2006), as well as in other T3SS-utilising pathogens such as *Edwardsiella, Ralstonia, Yersinia* and *S. enterica* subsp. *houtenae* (Pearson et al., 2017). EspL1–4 were first identified in EHEC Sakai as *Shigella* OspD2/3 homologues, presenting with N-terminal ShET enteroxin domains and C-terminal ankyrin-like repeats (Farfán et al., 2011; Tobe et al., 2006), of which EspL2 was implicated in supporting actin aggregation at pedestals via annexin 2 binding (Miyahara et al., 2009). More recently, the EPEC EspL2-like effector, located upstream of NleB1 and NleE on IE6, was identified as a cysteine protease (Pearson et al., 2017). Its conserved catalytic triad (Cys47/His131/Asp153) and the secondary structure of its catalytic N-terminal domain resembles the papain-like proteases, similar to the unrelated *Yersinia* effector YopT (Shao et al., 2003). EPEC and *C. rodentium* EspL cleave RHIM domains to inhibit necroptosis; RIPK1 and RIPK3, TRIF and ZBP1/DAI are confirmed targets in mouse dermal

fibroblasts, although RIPK1 is EspL's preferred substrate. In support of this, EspL inhibits necroptotic signalling and MLKL phosphorylation during EPEC infection of the human colorectal cancer cell line HT-29. Consistent with fellow necroptosis inhibitor NleB, deletion of *espL* from *C. rodentium* results in faster pathogen clearance (Pearson et al., 2017), highlighting the involvement of necroptosis during A/E infection.

1.5.3.5 EspZ limits cytotoxic effector translocation

EspZ, once called SepZ, immediately follows the delivery of Tir (Mills et al., 2008). It is one of the few effectors that are critical for A/E pathogenesis: *C. rodentium* ΔespZ is deficient in colonisation of NIH Swiss mice, therefore it does not cause mortality in the susceptible C3H/HeJ mouse model (Deng et al., 2004) and the analogous REPEC ΔespZ strain fails to induce symptoms of pathology in a rabbit infection model (Wilbur et al., 2015). EspZ appears to accumulate at the site of bacterial attachment (Kanack et al., 2005), together with one of its interacting partners CD98 (Shames et al., 2010), where it inserts into the host plasma and mitochondrial membranes via two transmembrane helices and hampers effector translocation, rendering cells refractory to further waves of infection (Berger et al., 2012; Kanack et al., 2005; Wilbur et al., 2015). EspZ was first implicated in cell death when an E69 Δ*espZ* mutant induced increased HeLa cell rounding, loss of adherence and release of cytoplasmic contents (Roxas et al., 2012; Shames et al., 2010). Consistently, REPEC EspZ limits apoptotic cell death in the rabbit colon (Wilbur et al., 2015). EspZ achieves its protective role through several mechanisms. Firstly, its interaction with CD98 modestly upregulates focal adhesion kinase (FAK) and AKT signalling (Shames et al., 2010), which mediate cell survival (Brunet et al., 1999). Additionally, EspZ localises to the mitochondrial membrane by interacting with TIM17b, inhibiting the loss of mitochondrial membrane potential during EPEC infection (Shames et al., 2011b). Therefore, EspZ both directly and indirectly modulates cell survival by limiting the translocation of cytotoxic effectors.

1.5.3.6 EspY binds cell cycle related proteins

The least characterised manipulator of cell survival is the 28 kDa effector EspY1, first identified by Tobe et al. in EHEC Sakai as a family of five *Salmonella* SPI-1 SopD-like effectors with an N-terminal WEX5F motif (Tobe et al., 2006). EspY1–4 are confirmed effectors in EHEC, while EspY5

is a pseudogene (Abe et al., 2008). In a large-scale Y2H screening protocol, Blasche et al. reported 31 novel interactions between EHEC effectors and human proteins, eight of which were EspY1-specific interactors (Blasche et al., 2014). Of note, three of these are implicated in cell cycle regulation (calpain-3, 26S protease regulatory subunit 4 and PCI domain-containing protein 2), although the functional role of these interactions during infection has yet to be investigated. A further member of the EspY family, EspY3, was recently reported to show additional homology to the Salmonella SPI-2 effector PipB2 as well as SopD, as they share a region of pentapeptide repeats (PPR) of unknown significance (Larzábal et al., 2018). Though not noted by the authors, this PPR is shared with EspY1, which has also been automatically annotated as a UDP pyrophosphate phosphatase through protein homology. Like many effectors, EspY3 localises beneath the pedestal at the site of translocation, though this offers little insight into its function. It also remains to be seen whether the other EspY family members are also implicated in apoptosis and cell cycle regulation.

1.5.3.7 EspO promotes cell survival

The final effector associated with cell survival is EspO, though a definitive link between EspO and apoptotic pathways has yet to be demonstrated. EHEC O157:H7 type strains EDL933 and Sakai encode two EspO family members (EspO1-1 and EspO1-2) (Tobe et al., 2006) on different genomic loci. The EHEC EspO paralogues share 60.9% identity with one another and 52.2%/56.% similarity with *C. rodentium* EspO, respectively. The foremost accepted function of the EspO effectors is inferred from their *Shigella* orthologues OspE1 and OspE2; all EspO homologues were demonstrated to bind integrin-linked kinase ILK (Kim et al., 2009). In *Shigella* infection, this interaction supresses the turnover of focal adhesions to promote adherence of infected cells to the basement membrane and prevent sloughing. At focal adhesion loci in EHEC infected cells, EspO1 has similarly been demonstrated to bind ILK as well as EspM2, inhibiting EspM2's stress fibre formation (Morita-Ishihara et al., 2013). While the most recent report of EspO function *in vivo* implicates it in the modulation of IL-22 secretion and mucosal damage, the presence of EspO promotes significantly more cell division associated with colonic crypt hyperplasia (Berger et al., 2018). Additionally, unpublished data from the Frankel lab demonstrates binding of EspO to HS-1-associated-protein-X-1 (HAX-1) in a yeast 2 hybrid screen, co-elution of purified recombinant proteins and identification of HAX-1 as a prey

protein for EspO during colonic cell line infection and peptide discovery mass spectrometry (N. Constantinou, S. Lekmeechai, S. Chatterjee, unpublished). Although HAX-1 is an anti-apoptotic protein (Yap et al., 2011), the function of EspO-HAX1 binding *in vivo* has yet to be delineated.

1.5.4 Effectors with multiple or unique functions

1.5.4.1 NleG and EspX/NleL are E3-ubiquitin ligases

The NleG effector family is widely represented, with over 20 known homologues in A/E pathogens alone (Wu et al., 2010). The EPEC NleG homologue, then dubbed NleI, was the first to be discovered in 2006 (Li et al., 2006; Tobe et al., 2006). The NleGs harbour a conserved ~100 aa C-terminal region that structurally resembles the RING/U-box domain of eukaryotic E3 ubiquitin ligases (Wu et al., 2010), while it is speculated that the variable NleG N-terminus defines substrate specificity. Some A/E NleGs, namely EHEC NleG7, 8.1 and *C. rodentium* NleG8, also encode a PSD-95/Disc Large/ZO-1 (PDZ) domain (A. Sagfors, unpublished), that mediates host protein binding in several fellow effectors (such as Map, NleH and NleA). To date, the only known interactors of A/E NleGs are protein hexokinase 2 and MED15, which bind the N-terminus of EHEC NleGs 2.3 and 5.1, respectively (Valleau et al., 2018), however the functional relevance of these interactions during infection is unclear.

Like the NleGs, an A/E pathogen can encode several EspX-like effectors. Seven EspX family members were identified in EHEC O157:H7, one of which is a pseudogene, but all of which harbour PPR motifs (Tobe et al., 2006). Like EspY, these are further homologues of PipB, as well as SopA, the latter being a structural and functional HECT-type E3 ligase mimic (Zhang et al., 2006). In *C. rodentium*, EspX7 (equivalent to ECs1560 in EHEC) is weakly translocated; this is hypothesised to reflect its large size (87.35 kDa). Despite this, EspX7 is also an E3 ubiquitin ligase that downregulates pedestal formation during infection, leading to its renaming as NleL (non-LEE-encoded ligase) (Piscatelli et al., 2011). This was confirmed when NleL was co-crystallised with human E2 enzymes, which catalyse the conjugation of ubiquitin moieties (Lin et al., 2012). Most recently, NleL was reported to ubiquitylate JNK, although this modification was demonstrated to favour pedestal formation (Sheng et al., 2017), rather than repress it.

1.5.4.2 EspF subverts a variety of cellular functions

EspF, known as the A/E pathogen's Swiss Army Knife (Holmes et al., 2010), is a versatile core effector encoded in *LEE4* (McNamara and Donnenberg, 1998), one operon away from its exclusive chaperone CesF in *LEE3* (Elliott et al., 2002; Mills et al., 2008). EspF is cytotoxic in its many roles. Firstly, it disrupts mitochondrial membrane potential, resulting in cytochrome c release and intrinsic apoptosis (Nougayrède and Donnenberg, 2004). This is mediated by the N-terminus of EspF, which corresponds to a mitochondrial targeting sequence (MTS; residues 1–24, of which Leu16 is essential) (Nagai et al., 2005; Wang et al., 2017; Zhao et al., 2013). Immediately following the MTS is a nucleolus targeting motif (residues 21–74), which facilitates nuclear entry of EPEC EspF after dissipation of the mitochondrial membrane (Dean et al., 2010), although the purpose of this during infection is unknown. The C-terminus of EspF underpins its multifunctionality; it can contain between three and five SH3 domains (McNamara and Donnenberg, 1998), as well as an actin/ N-WASP binding motif domain, that mediate binding to sorting nexin 9 (SNX9) and N-WASP, respectively (Alto et al., 2007; Weflen et al., 2010). These interactions, among other actin-associated target proteins, are thought to mediate EspF-dependent reorganisation of cell membrane components, resulting in tight junction disruption (Peralta-Ramírez et al., 2008; Singh et al., 2018), which could lead to disruption of water reabsorption. Indeed, other EspF targets, such as the sodium-glucose transporter 1 (SGLT1), sodium-hydrogen exchanger (NHE3) and aquaporins 2 and 3, may facilitate this (Dean et al., 2006; Guttman et al., 2007; Hodges et al., 2008). Additionally, EspF interacts with the caspase-inhibiting factor Abcf2, causing Abcf2 degradation and therefore increased activation of caspases-3 and -9 (Nougayrède et al., 2007). The ability of EspF to subvert mitochondrial and cytoskeletal signalling through distinct host proteins underscores its utility as a multifunctional effector.

1.5.4.3 Map is mitochondrial-targeting Rho GEF that manipulates tight junctions

The mitochondrial associated protein (Map) is a core LEE-encoded effector that shares 75% identity throughout the A/E pathogens (Simpson 2006). Named for its ability to associate with the mitochondria, it contains an N-terminal MTS, a WxxxE motif and a five-residue-spanning catalytic loop. Its C-terminus comprises a PDZ domain to mediate host protein targeting. Specifically, the PDZ of Map is used to bind Na^+/H^+ exchanger regulatory factor (NHERF1 and

2) (Martinez et al., 2010), tethering Map to the host membrane and enhancing its catalytic activity locally. Similar to EspM and EspT, the WxxxE motif of Map mimics a GEF, in this case for Cdc42, to promote filopodia formation (Berger et al., 2009; Huang et al., 2009). Early reports of Map demonstrated its role in cell invasion *in vitro* (Jepson et al., 2003), although this has since been overshadowed by the observation that, like EspF, Map is imported into the mitochondria where it disrupts membrane integrity, independently of its GEF activity (Kenny and Jepson, 2000; Kenny et al., 2002; Ma et al., 2006; Papatheodorou et al., 2006). Conflicting reports exist regarding Map's involvement in barrier function, tight junction assembly and transepithelial resistance (Dean and Kenny, 2004; Simpson et al., 2006; Singh et al., 2018; Tapia et al., 2017) and the subsequent development of diarrhoea in mouse disease models (Simpson et al., 2006). What is clear is that the synergism between Map, EspM, EspT, NleH and EspF serves to maintain tissue homeostasis during infection.

1.5.4.4 NleH binds Bax-1 to inhibit caspase-3 cleavage and apoptosis

In addition to their role in NF-κB signalling, EPEC NleH1 and NleH2 (but not *C. rodentium* NleH or OspG) have a further role in inhibiting apoptosis (Robinson et al., 2010) through binding of Bl-1 (Bax-inhibitor 1) to inhibit pro-caspase-3 cleavage *in vitro* (Hemrajani et al., 2010) and *in vivo* (Kralicek et al., 2018). Like Map and NleA, NleH-like effectors also possess a C-terminal PDZ domain, which is not only important for NF-κB pathway regulation (Pham et al., 2012), but also mediates binding to NHERF2 to modulate NleH's anti-apoptotic activity (Martinez et al., 2010).

1.5.4.5 NleA/EspI inhibits protein trafficking and prevents deubiquitylation of NLRP3

Z6024 type III secreted protein P54 (Z6024) was the first non-LEE-encoded effector to be discovered (Kresse et al., 2000), although its expression is co-regulated with the LEE (García-Angulo et al., 2012; Roe et al., 2007). It was simultaneously reported following an *in vivo* signature-tagged mutagenesis screen of *C. rodentium* (Mundy et al., 2004a) and after two-dimensional gel electrophoresis of EHEC secreted proteins (Gruenheid et al., 2004), and named EspI or NleA, respectively. NleA/EspI is one of the few effectors that are necessary for efficient *C. rodentium* colonisation (Mundy et al., 2004a; Runte et al., 2018), and is more prevalent in outbreak strains and strains associated with severe disease (Coombes et al., 2008; Mundy et

al., 2004b), demonstrating its importance in A/E pathogenesis. Unbiased screens consistently reveal that NleA/EspI interacts with protein sorting complex proteins Sec23A (Sontag et al., 2016) and Sec24 (Kim et al., 2007; Lee et al., 2008; Thanabalasuriar et al., 2012) via its PDZ domain (Lee et al., 2008), which is concordant with its localisation to the protein secretory pathway *in vitro* (Clements et al., 2011; Gruenheid et al., 2004; Lee et al., 2008; Thanabalasuriar et al., 2010). Indeed, its PDZ domain is required for colonic colonisation (Lee et al., 2008; Thanabalasuriar et al., 2012). NleA/EspI binding to the Sec23/24 complex inhibits COPII-coated vesicle-mediated transport of proteins from the endoplasmic reticulum to the Golgi, ultimately restricting protein secretion at the plasma membrane (Kim et al., 2007; Thanabalasuriar et al., 2012). Most recently, NleA/EspI was identified in a screen for inhibitors of IL-1β secretion during EPEC infection. Mechanistically, NleA/EspI prevents association of caspase-1 with the nascent inflammasome by binding directly to NLRP3, preventing its deubiquitylation and halting inflammasome activation (Yen et al., 2015).

1.5.5 Effectors with unknown functions (EspK, NleK, NleJ, EspR, EspN, EspS/OspB)

With the advent of high-throughput bioinformatic and biochemical techniques, the rate of effector discovery has surpassed the rate of biological characterisation, creating a list of effectors with no assigned function. EspK (previously named z1829) was first identified in EHEC EDL933 as an important factor for calf colonisation (Vlisidou et al., 2006). Like many effectors, the EspK family was also identified by Tobe et al. in EHEC Sakai as an effector with leucine-rich repeats (LRRs) (Tobe et al., 2006), and was dubbed as a homologue to the *S.* Typhimurium effector GogB (Coombes et al., 2005) and the *Y. enterolitica* effector YopM (Vlisidou et al., 2006), possibly pointing towards an immunosuppressive role during infection. Two novel effectors, NleK (ROD_09131 in *C. rodentium*) and NleJ (C_0814 in EPEC), were identified by mass spectrometry in the secretome of *C. rodentium* and E69 (Deng et al., 2010, 2012). The *C. rodentium nleK* gene encodes a 12.3 kDa protein that does not resemble any known effector family, but exhibits 88% similarity to proteins in EPEC and *S. enterica* serovar Typhi isolates (Deng et al., 2010). NleK is poorly transcribed (Petty et al., 2010) and its genetic deletion from *C. rodentium* does not affect colonisation or disease severity of C57BL/6 or C3H/HeJ mice (Deng et al., 2010). More recently, NleK was demonstrated to interact with the host factor heterogeneous nuclear ribonucleoprotein M (hnRNP M) by affinity purification from HeLa lysates, although the functional relevance of this interaction remains untested

(Sontag et al., 2016). NleJ lacks functional characterisation altogether; with no *C. rodentium* or EHEC homologues, it is encoded on the E69 PP3 island and can be found in a similar genomic context in *S.* Typhimurium (Deng et al., 2012).

Two further effectors lacking functional characterisation are EspR and EspN. EspR resembles the uncharacterised *S. flexneri* protein SF1757; its prevalence is scarcely reported, though there are four *espR*-like genes and one pseudogene in O157:H7 Sakai (Stevens and Frankel, 2014; Tobe et al., 2006). On the other hand, EspN is documented in 13.3% of EPEC strains and 86.5% of EHEC strains (Delannoy et al., 2013). In EHEC EDL933, EspN is carried on the O1-50 prophage locus together with EspK. *C. rodentium* encodes 3 *espN*-like genes, all with instances of mutational attrition (Deng et al., 2010; Petty et al., 2010). Analysis of the *C. rodentium* secretome and genome also revealed *espS* (Deng et al., 2010; Petty et al., 2010)*:* an 876 bp ORF encoding a homologue of *Shigella* OspB, which is regarded as an immunomodulator (Ambrosi et al., 2015). In a more recent screen, this time of the relative abundance of effector mRNA, *C. rodentium* EspS is one of the most highly transcribed effectors under T3SS-expression conditions (Connolly et al., 2018), and is therefore discussed in detail in §3.

1.6 Project aims

The A/E pathogens encode an impressive repertoire of effector proteins with wide-ranging functions. Historically, the study of effectors has been governed by their distribution among the type strains. While this simplifies research, it does not reflect the expanding genomic diversity of the A/E pathogens. This study therefore seeks to identify and characterise effector novelty via three primary objectives:

1. Systematic identification of new effectors
2. Assign function to recently acknowledged effectors
3. Investigate synergistic roles for existing effectors in light of the latest research.

Chapter 2

Materials and Methods

2 Materials and Methods

2.1 Bacterial culture

Bacterial strains were routinely grown at 37 °C in Luria broth (LB) (*E. coli*), LB Lennox broth (*C. rodentium*) or on LB agar supplemented with the appropriate antibiotic (Table 2).

Table 2 | Bacterial strains used in this study

Strain	Description	Selection	Source
C. rodentium ICC169	Wild type with spontaneous nalidixic acid resistance	Nal^{50}	Frankel lab
C. rodentium + pACBSR	Triparental mating receiver strain	Nal^{50}, Cm^{30}	This study
C. rodentium ΔespS	*espS* deletion mutant	Nal^{50}	This study
C. rodentium ΔespS + espS	*espS* deletion mutant complemented with espS at the original locus of deletion	Nal^{50}	This study
C. rodentium espS-SII	Wild type-like with SII tag inserted C-terminally to *espS*	Nal^{50}	This study
C. rodentium tir-SII	Wild type-like with SII tag inserted C-terminally to *tir*	Nal^{50}	E. So, Frankel lab
C. rodentium ΔespA	*espA* deletion mutant	Nal^{50}, Kan^{50}	Petty et al., 2010
C. rodentium ΔespF	*espF* deletion mutant	Nal^{50}, Kan^{50}	Mundy et al., 2004b
C. rodentium ΔespZ	*espZ* deletion mutant	Nal^{50}, Kan^{50}	V. Crepin, ICC1340
C. rodentium ΔnleF	*nleF* deletion mutant	Nal^{50}, Kan^{50}	Pallett et al., 2017
E. coli TOP10	F- mcrA Δ(mrr-hsdRMS-mcrBC) φ80lacZΔM15 ΔlacX74 nupG recA1 araD139 Δ(ara-leu)7697 galE15 galK16 rpsL(Str^R) endA1 λ^-	None	ThermoFisher Scientific CA, USA
E. coli cc118λpir	Triparental mating donor strain	None	Herrero et al., 1990
E. coli 1047 + pRK2013	Triparental mating helper strain	Kan^{50}	Filloux lab, Imperial College London
EPEC E2348/69 (E69)	WT strain	None	Levine *et al.*, 1978
E69 Δ*tir*	*tir* replaced with *aphT*	Kan^{50}	Berger *et al.*, 2009
E69 Δ*escF*	*escF* replaced with *aphT*	Kan^{50}	Wilson *et al.*, 2001
E69 Δ*eae*	*eae* replaced with *aphT*	Kan^{50}	Marchès *et al.*, 2008

E69 Tir^{AA}	*tir* replaced with *tir$^{Y454A/Y474A}$ and aphT*	Kan^{50}	Wong *et al*., 2012
E69 Δ*espF*	*espF* replaced with *aphT*	Kan^{50}	O. Marchès, ICC211
E69 Δ*espG1/2*	*espG1 and espG2* replaced with *aphT* and *cat* respectively	Kan^{50}/Cm^{30}	O. Marchès, ICC243
E69 Δ*espH*	*espH* replaced with *aphT*	Kan^{50}	O. Marchès, ICC312
E69 Δ*espI/nleA*	*espI/nleA* replaced with *aphT*	Kan^{50}	O. Marchès, ICC248
E69 Δ*espJ*	*espJ* replaced with *aphT*	Kan^{50}	Dahan et al., 2005
E69 Δ*espL2*	*espL2* replaced with *aphT*	Kan^{50}	A. Wong, Frankel lab
E69 Δ*espZ*	Deletion of *espZ*	None	L. Ángel-Fernandez, ICC1115
E69 Δ*nleB1*	*nleB1* replaced with *cat*	Cm^{30}	O. Marchès, ICC250
E69 Δ*nleC*	*nleC* replaced with *aphT*	Kan^{50}	O. Marchès, ICC193
E69 ΔnleD	*nleD* replaced with *aphT*	Kan^{50}	O. Marchès, ICC194
E69 Δ*nleE*	*nleE* replaced with *cat*	Cm^{30}	Newton et al., 2010
E69 Δ*nleF*	*nleF* replaced with *aphT*	Kan^{50}	Pallett et al., 2014
E69 Δ*nleG*	*nleG* replaced with *aphT*	Kan^{50}	B. McGeever, Frankel lab
E69 Δ*nleH1/2*	*nleH1* and *nleH2* replaced with *aphT* and *cat* respectively	Kan^{50}/Cm^{30}	Frankel lab
E69 Δ*map*	*map* replaced with *aphT*	Kan^{50}	O. Marchès, ICC193
E69 ΔPP4ΔIE6	*PP4* and *IE6 (*containing *nleG, nleB2, nleC, nleD, nleE1, nleB1* and *espL)* replaced with *cat*	Cm^{30}	O. Marchès, ICC1063
EPEC E11019 (E11)	WT isolate	None	Viljanen *et al*., 1990
E11 Δ*escN*	*escN* replaced with *aphT*	Kan^{50}	O. Marchès, ICC937
E11 Δ*espT*	*espT* replaced with *aphT*	Kan^{50}	A. Sågfors, Frankel lab
EPEC B171	Wild type isolate	Cm^{30}	Riley *et al*., 1987

2.2 Bacterial transformation

Bacteria were made competent according to standard protocols. Briefly, for preparation of electrically competent *C. rodentium*, log-phase cultures were washed thrice and resuspended

in electrocompetence buffer (15% (v/v) glycerol, 20 mM sucrose). For preparation of chemically competent bacteria EPEC and *E. coli*, log-phase cultures were washed once in ice-cold buffer RF1 (100 mM rubidium chloride, 50 mM manganese chloride, 30 mM potassium acetate, 10 mM calcium chloride, 15% (w/v) glycerol, pH 5.8) then once in buffer RF2 (10 mM MOPS, 20 mM rubidium chloride, 75 mM calcium chloride, 15% (w/v) glycerol, pH 6.5) and resuspended in buffer RF2. All buffers were kept ice-cold throughout. Plasmids listed in Table 3 were incubated with competent bacteria on ice before shocking. Chemically competent bacteria were heat shocked at 42 °C for 1 min; a 2.5 kV pulse (300 Ω resistance; 25 µF capacitance) was applied to electrically competent bacteria through a BioRad Gene Pulser® II.

Table 3 | Plasmids used for bacterial expression

Plasmid	Description	Selection	Source
pCX340-ROD_48841	Encodes NleN with C-terminal TEM-1 fusion (*blaM*) under LacI^q/P*trc* control	Tet$^{12.5}$	This study
pCX340-ROD_48831	Encodes ROD_48831 with C-terminal TEM-1 fusion (*blaM*) under LacI^q/P*trc* control	Tet$^{12.5}$	This study
pCX340-ROD_40941	Encodes ROD_40941 with C-terminal TEM-1 fusion (*blaM*) under LacI^q/P*trc* control	Tet$^{12.5}$	This study
pCX340-ROD_40981	Encodes ROD_40981 with C-terminal TEM-1 fusion (*blaM*) under LacI^q/P*trc* control	Tet$^{12.5}$	This study
pCX340-ROD_48821	Encodes ROD_48821 with C-terminal TEM-1 fusion (*blaM*) under LacI^q/P*trc* control	Tet$^{12.5}$	This study
pCX340-EspH	Encodes EspH with C-terminal TEM-1 fusion (*blaM*) under LacI^q/P*trc* control	Tet$^{12.5}$	Petty et al., 2010
pACBSR	Receiver plasmid. Encodes endonuclease I-SceI under *ara* promoter	Cm^{25}	Herring et al., 2003
pRK2013	Helper plasmid. *RK2* replicon.	Kan^{50}	Figurski and Helinski, 1979
pSEVA612S-EspSHR	pSEVA612S (oriT) backbone carrying homology regions 300 bp upstream and downstream of $espS_{CR}$	Gent^{10}	This study
pSA10-Tir$_{E69}$	Encodes Tir$_{E69}$ under Lac	Amp^{100}	Wong et al., 2012a
pSA10-EspZ$_{E69}$	Encodes EspZ$_{E69}$ under Lac	Amp^{100}	Berger et al., 2012
pSA10-NleG$_{E69}$-HA	Encodes C-terminally HA-tagged NleG$_{E69}$ under Lac	Amp^{100}	B. McGeever, Frankel lab

pSA10-$EspT_{E11}$	Encodes $EspT_{E11}$ under Lac	Amp^{100}	Bulgin et al., 2009a
pSA10-$EspS_{CR}$-4xHA	Encodes C-terminally 4xHA-tagged $EspS_{CR}$ under Lac	Amp^{100}	This study
pET28a-$EspS_{CR}$-6His	Encodes C-terminally 6His-tagged $EspS_{CR}$ under T7*lac* promoter.	Kan^{50}	This study

2.3 Yeast culture

Yeast strains were grown in yeast extract peptone dextrose (YPD) broth supplemented with adenine (YPDA) or Sabouraud Dextrose (SD) broth supplemented with appropriate amino acids for selection (Table 4).

Table 4 | Yeast strains used in this study

Yeast strains	Description	Selection	Source
S. cerevisiae BY4741	MATa, his3Δ1, leu2Δ0, met15Δ0, ura3Δ0	Uracil-deficient media	Brachmann et al., 1998
S. cerevisiae AH109	MATa, trp1-901, leu2-3,112, ura3-52, his3-200, gal4Δ, gal80Δ, LYS2::GAL1UAS-GAL1TATA-HIS3,GAL2UAS-GAL2TATA-ADE2, URA3::MEL1UAS MEL1TATA-lacZ		Takara Clontech, Japan

2.4 Mammalian cell culture

HeLa cells were maintained at 37 °C in a 5% CO_2 atmosphere in low glucose Dulbecco's modified Eagle medium (DMEM) (1000 mg/L glucose; Sigma-Aldrich, MA, USA), supplemented with 1% (vol/vol) GlutaMAX (Gibco, MA, USA), 1% non-essential amino acids (Sigma-Aldrich) and 10% heat-inactivated foetal calf serum (HI-FCS) (Gibco). THP1 monocyte-like cells were maintained at 37 °C in a 5% CO_2 atmosphere in Roswell Park Memorial Institute (RPMI) 1640 supplemented with 1 mM sodium pyruvate, 10 mM HEPES pH 7.4 with 10U penicillin, 0.1 mg/mL streptomycin and 10% HI-FCS. THP1s with pMX-CMV-YFP encoding miRNA30E-bsaed targeting of GSDMD (TACACATTCATTGAGGTGCTGG) or LacZ (TCACGACGTTGTAATACGACGT) were maintained with an additional 2 µg/mL puromycin.

2.5 *C. rodentium* genomic manipulation

C. rodentium chromosomal manipulation was performed using a triparental mating method as follows. Electrocompetent *C. rodentium* were transformed with the receiver plasmid pACBSR (Table 3) to create the receiver strain (Table 2). Donor strains were created by transforming *E. coli* cc118λpir with pSEVA612S containing homology regions 300 bp upstream and 300 bp downstream of the site to be mutated outside I-SceI cut sites. The receiver strain, donor and helper (Table 2) were grown for 16 h in LB supplemented with the indicated antibiotics (200 rpm). 20 µL of the helper and donor were spotted atop one another on LB agar and incubated for 4 h at 37°C. 40 µL of the receiver strain was spotted atop the donor and helper, and incubated for a further 6 h. Bacteria were resuspended in 1 ml LB and plated on LB agar supplemented with chloramphenicol and gentamicin to select for colonies with pSEVA612S integrated into *C. rodentium* genome. Resulting colonies were cultured in LB supplemented with chloramphenicol and 0.4% arabinose to induce expression of the pACBSR-encoded endonuclease I-SceI to excise the pSEVA612S backbone. After 8 h, the culture was streaked on chloramphenicol and grown for 16 h. Colonies were re-streaked on LB-chloramphenicol and LB-chloramphenicol + gentamicin agar to select for co-integrants no longer harbouring the donor plasmid. Colonies that grew on LB-chloramphenicol alone were analysed by colony PCR using primers flanking the *espS* homology regions (Table 5). Positive colonies were passaged several times to remove the pACBSR plasmid.

Table 5 | Oligos used in this study

Oligo identifier	Oligo sequence (5'-3')
ROD_48821_Lstart_pCX340_F	gcggtaccttgctaatacaggcattatttttta
ROD_48821_Mstart_pCX340_F	gcggtaccatgctaatacaggcattatttttta
ROD_48821_pCX340_R	cgccggaattccgacggtcaacacaaagagctattg
ROD_48831_Lstart_pCX340_F	cgccatatggtggcaattgatatcaattccc
ROD_48831_Mstart_pCX340_F	cgccatatgatggcaattgatatcaattccc
ROD_48831_pCX340_R	cgccggaattccgatgccgcctccagatctgaa
ROD_48841_Lstart_pCX340_F	cgccatatgatgttgactccaaattcaatttcaa
ROD_48841_Mstart_pCX340_F	cgccatatgatgttgactccaaattcaatttcaa
ROD_48841_pCX340_R	cgccggaattccgtgttgtcaaaaaatcgtttaatgtta
40941_pCX340_F	gtccatatgatggggtatttgcttgcacc
40941_pCX340_R	gacgaattcggacgttccgaaaaatgctgag
40951_pCX340_F	gtccatatgatggggattcatcatacag

40951_pCX340_R	gacgaattcggcatcgtccgcgctatcc
40891_pCX340_F	gtccatatgatgaacggtataagtggaag
40891_pCX340_R	gacgaattcggacgcattttcaggcacac
pCX340_check_F	atcgcatataatagattttgcgg
pCX340_check_R	ctttgtccattgaatgcatagg
NleN_pRK5-myc_F	gtcggatccttgactccaaattcaatttcaaac
NleN_pRK5-myc_R	gacgaattcttatgttgtcaaaaaatcgtttaatg
NleO_pRK5-myc_F	gtcggatccatgaacggtataagtggaagtg
NleO_pRK5-myc_R	gacgaattcttaacgcattttcaggcacac
pcDNA3.1_F	gaaaatgcgttaagtcgacgcggccgcgagc
pcDNA3.1_R	cacttataccgttcacgaattcgctggcggtggtagg
NleO_pCDNA_F	agcgaattcgtgaacggtataagtggaagtg
NleO_pCDNA_R	ggccgcgtcgacttaacgcattttcaggcac
iPCR_NleO_C121A_F	cgggaaaaacgcggcggatattgtcg
iPCR_NleO_C121A_R	atcatacgataatgaggattg
EspSCR_pRK5-myc_N_F	gtcggatccatgtttagtataaaagg
EspSCR_pRK5-myc_N_R	caggaattcttagtcaatatctgttg
EspSCR_pRK5-myc_C_R	gacaagcttttacaggtcctcctcggagatcagcttctgctcgtcaatatctg ttggttgtgtccttcc
EspSCR_pSA10:4xHA_F	gtcgaattcatgtttagtataaaagg
EspSCR_pSA10:4xHA_R	cagggtaccgtcaatatctgttgg
EspSCR_pGBKT7_F	gtcgaattcatgtttagtataaaagg
EspSCR_pGBKT7_R	cagggatccttagtcaatatctgttg
iPCR_EspSCR_C184A_F	gctcattcagcggacatttatgcaaac
iPCR_EspSCR_C184A_R	gcttgttaatctgatgtcttttatttatg
mTRIAP1_pGADT7_F	gtcgaattcatgaacagcgtcggggagg
mTRIAP1_pGADT7_R	gacggatcctcatcaagaggagttttcaggc
mTRIAP1_PRK5-myc_F	gtcggatccaacagcgtcggggaggct
mTRIAP1_PRK5-myc_R	gacaagcttcatcaagaggagttttcaggc
EspSEPEC_pGADT7_F	gtcgaattcatgtttagcataagaaccctac
EspSEPEC_pGADT7_R	gacggatccttactcaatatctatgggttgag
EspSEPEC_pRK5myc_C_R	gacaagcttttacaggtcctcctcggagatcagcttctgctcctcaatatctat gggttgag
EspSEPEC_pYES2_F	gtcggatccatgtttagcataagaaccctac
EspSEPEC_pYES2_R	gacgaattcttactcaatatctatgggttgag
VPA1380_pYES2_F	gtcggatccttggttgtgtgtttttggcc
VPA1380_pYES2_R	gacgaattcttaatctaaatcagattctaagg
OspBM90T_pYES_F	gtcggatccatgaatttagatggtgttagacc
OspBM90T_pYES_R	gacgaattcctaatccagttctttgttgatga
EspSCR_HR_pSEVA612S_F	gtcaagcttatgtttagtataaaaggatacc

EspSCR_HR_pSEVA612S_R	caggaattccctgtaacatcatcatgaatcc
EspS-StrepII_pSEVA612S_F	gtcaagcttaaggatttctctcctgaagag
EspS-StrepII_pSEVA612S_R	gacgaattcaatgggtaaaataatattagcatta
EspS_StrepII_check_F	cctggaataggtttatctgg
EspS_StrepII_check_R	ggtacgcattgctaaactgc
pET-28a-EspSCR-His_F	gtccatatgggcagtataaaaggatacc
pET-28a-EspSCR-His_R	gacgcggccgcgtcaatatctgttgg
EspOCR_FL_SII_popinE_3C_F	aggagatataccatgccattttcaatcaaaaacagattttc
EspOCR_FL_SII_popinE_3C_R	cagaacttccagtttttcttttgtgttgtgtatctctg
SII_EspOCR_FL_popinE_3C_F	aagttctgtttcagggcccgccattttcaatcaaaaacagattttc
SII_EspOCR_FL_popinE_3C_R	atggtctagaaagctttattcttttgtgttgtgtatctctg
GFP_EspOCR_FL_popinF_3C_F	aagttctgtttcagggcccgccattttcaatcaaaaacagattttc
GFP_EspOCR_FL_popinF_3C_R	atggtctagaaagctttattcttttgtgttgtgtatctctg
NleG1CR_C_SII_popinE_3C_F	aggagatataccatggaaaatgcaccctcatcattac
NleG1CR_C_SII_popinE_3C_R	cagaacttccagtttactatttttttataacgaagttaccc
NleG1CR_C_GFP_popinE_3C_F	aggagatataccatggaaaatgcaccctcatcattac
NleG1CR_C_GFP_popinE_3C_R	cagaacttccagtttactatttttttataacgaagttaccc
SII_NleG1CR_C_popinF_3C_F	aagttctgtttcagggcccggaaaatgcaccctcatcattac
SII_NleG1CR_C_popinF_3C_R	atggtctagaaagctttaactatttttttataacgaagttaccc
NleG1CR_FL_SII_popinE_3C_F	aggagatataccatgcagcctgtaggactatctaatac
NleG1CR_FL_SII_popinE_3C_R	cagaacttccagtttaccaggaaacaggatatcccc
NleG1CR_FL_GFP_popinE_3C_F	aggagatataccatgcagcctgtaggactatctaatac
NleG1CR_FL_GFP_popinE_3C_R	cagaacttccagtttaccaggaaacaggatatcccc
SII_NleG1CR_N_popinF_3C_F	aagttctgtttcagggcccgcagcctgtaggactatctaatac
SII_NleG1CR_N_popinF_3C_R	atggtctagaaagctttaaccaggaaacaggatatcccc
GFP_NleG1CR_N_popinF_3C_F	aagttctgtttcagggcccgcagcctgtaggactatctaatac
GFP_NleG1CR_N_popinF_3C_R	atggtctagaaagctttaaccaggaaacaggatatcccc
NleG1CR_FL_SII_popinE_3C_F	aggagatataccatgcagcctgtaggactatctaatac
NleG1CR_FL_SII_popinE_3C_R	cagaacttccagtttactatttttttataacgaagttaccc
NleG1CR_FL_GFP_popinE_3C_F	aggagatataccatgcagcctgtaggactatctaatac
NleG1CR_FL_GFP_popinE_3C_R	cagaacttccagtttactatttttttataacgaagttaccc
SII_NleG1CR_FL_popinF_3C_F	aagttctgtttcagggcccgcagcctgtaggactatctaatac
SII_NleG1CR_FL_popinF_3C_R	atggtctagaaagctttaactatttttttataacgaagttaccc
NleACR_FL_SII_popinE_3C_F	aggagatataccatgaacattcaaccgaacatacattcc
NleACR_FL_SII_popinE_3C_R	cagaacttccagtttgacccttgtttcttggattatttc
NleACR_FL_GFP_popinE_3C_F	aggagatataccatgaacattcaaccgaacatacattcc
NleACR_FL_GFP_popinE_3C_R	cagaacttccagtttgacccttgtttcttggattatttc
GFP_NleACR_FL_popinF_3C_F	aagttctgtttcagggcccgaacattcaaccgaacatacattcc
GFP_NleACR_FL_popinF_3C_R	atggtctagaaagctttagacccttgtttcttggattatttc
EspSCR_FL_SII_popinE_3C_F	aggagatataccatgtttagtataaaaggatacctacc

EspSCR_FL_SII_popinE_3C_R	cagaacttccagtttgtcaatatctgttggttgtgtc
EspSCR_FL_GFP_popinE_3C_F	aggagatataccatgtttagtataaaaggatacctacc
EspSCR_FL_GFP_popinE_3C_R	cagaacttccagtttgtcaatatctgttggttgtgtc
SII_EspSCR_FL_popinF_3C_F	aagttctgtttcagggcccgtttagtataaaaggatacctacc
SII_EspSCR_FL_popinF_3C_R	atggtctagaaagctttagtcaatatctgttggttgtgtc
GFP_EspSCR_FL_popinF_3C_F	aagttctgtttcagggcccgtttagtataaaaggatacctacc
GFP_EspSCR_FL_popinF_3C_R	atggtctagaaagctttagtcaatatctgttggttgtgtc

2.6 Oral *C. rodentium* infection of C57Bl/6 mice

Infection of mice was performed as previously described (Crepin et al., 2016). Briefly, *C. rodentium* cultures inoculated from a single bead were grown to saturation for 16 h at 37 °C in 15 ml LB supplemented with Nalidixic acid. Bacteria were pelleted and resuspended in 1.5 ml sterile PBS (inoculum). Animal experiments were performed in accordance with the Animals Scientific Procedures Act (1986) and were approved by the local Ethical Review Committee. Female C57Bl/6 mice between 18-20 g were inoculated as described (Crepin et al., 2016) with 3 x 10^9 colony forming units (CFU) by oral gavage. Inoculum CFU were confirmed by retrospective plating. Colonisation was monitored during infection by plating serial dilutions of faecal bacteria.

2.7 Staining and analysis of distal colon sections

0.5 cm of distal murine colon was embedded in paraffin, sectioned and mounted on glass coverslips. For crypt length measurements, sections were haematoxylin and eosin (H&E) stained to visualise tissue architecture. For immunofluorescence, sections were unwaxed and rehydrated with sequential washes in Histo-Clear™ (National Diagnostics, GA, USA), 100%, 95% and 85% ethanol, and PBS with 0.1% Tween-20 and 0.1% saponin (PBS-TS). Sections were boiled in 11.5 mM trisodium citrate with 0.05% Tween-20 for 20 mins, blocked in 10% normal donkey serum in PBS-TS (PBS-TS-NDS) for 20 mins and incubated with primary antibody solution for 1 h (anti-Ki67 and anti-Int280β in PBS-TS-NDS). Slides were rinsed twice in PBS-TS for 10 mins before secondary antibody solution (DAPI, goat anti-chicken Cy3, donkey anti-rabbit Alexa488 in PBS-TS-NDS) was applied for a further hour. Crypt length measurements were recorded using the ruler tool on Zeiss ZEN blue v2.3.

2.8 Transfection and immunofluorescence staining

HeLa or HEK293T cells were seeded on glass coverslips and grown to approximately 60% confluency. Cells were transfected with a maximum of 0.125 µg (24-well plate) or 0.75 µg (6-well plate) of mammalian expression vectors (Table 6) using GeneJuice (Merck, Germany) according to the manufacturer's instructions. Transfected cells were incubated for 24 h–72 h before washing 3 times in warmed PBS and fixing in 4% paraformaldehyde (PFA) for 20 mins at 25°C. PFA was quenched in 50 mM NH_4Cl before immunofluorescence.

Table 6 | Transfection plasmids used in this study

Plasmid	Description	Selection	Source
pRK5-myc-NleN	Transfection plasmid encoding NleN with an N-terminal myc tag under *CMV* promoter.	Amp^{100}	This study
pRK5-myc-NleO	Transfection plasmid encoding NleO with an N-terminal myc tag under *CMV* promoter.	Amp^{100}	This study
pRK5-$EspS_{CR}$-myc	Transfection plasmid encoding $EspS_{CR}$ with a C-terminal myc tag under *CMV* promoter.	Amp^{100}	This study
pRK5-myc-$EspS_{CR}$	Transfection plasmid encoding $EspS_{CR}$ with an N-terminal myc tag under *CMV* promoter.	Amp^{100}	This study
pRK5-$EspS_{B171}$-myc	Transfection plasmid encoding $EspS_{B171}$ with a C-terminal myc tag under *CMV* promoter.	Amp^{100}	This study
pRK5-myc-Rac1	Transfection plasmid encoding Rac1 with an N-terminal myc tag under *CMV* promoter.	Amp^{100}	G. Bokoch (Addgene #12985)
pRK5-myc-$Rac1^{Q61L}$	Transfection plasmid encoding dominant positive $Rac1^{Q61L}$ with an N-terminal myc tag under *CMV* promoter.	Amp^{100}	G. Bokoch (Addgene #12983)
pRK5-myc-GFP	Transfection plasmid encoding GFP with an N-terminal myc tag under *CMV* promoter.	Amp^{100}	This study
pcDNA3-FLAG-NleO	Transfection plasmid encoding NleO with an N-terminal FLAG tag under *CMV* promoter.	Amp^{100}	This study
pcDNA3-FLAG-$NleO^{C121A}$	Transfection plasmid encoding $NleO^{C121A}$ with an N-terminal FLAG tag under *CMV* promoter.	Amp^{100}	This study

pOPINE-3C-eGFP-6His $EspS_{CR}$	Transfection plasmid encoding N-terminally GFP-6His-tagged $EspS_{CR}$ under chicken β-actin promoter	Amp^{100}	This study
pOPINE-3C-$EspS_{CR}$-eGFP-6His	Transfection plasmid encoding C-terminally GFP-6His-tagged $EspS_{CR}$ under chicken β-actin promoter	Amp^{100}	This study
pOPINE-3C-eGFP-6His $EspS_{CR}$	Transfection plasmid encoding N-terminally GFP-6His-tagged $EspO1_{CR}$ under chicken β-actin promoter	Amp^{100}	This study
pOPINE-3C-$EspS_{CR}$-eGFP-6His	Transfection plasmid encoding C-terminally GFP-6His-tagged $EspO1_{CR}$ under chicken β-actin promoter	Amp^{100}	This study
pOPINE-3C-eGFP-6His-$NleG1_{CR}^{191-194}$	Transfection plasmid encoding N-terminally GFP-6His-tagged $NleG1_{CR}^{191-194}$ under chicken β-actin promoter	Amp^{100}	This study
pOPINE-3C-$NleG1_{CR}^{191-194}$ -eGFP-6His	Transfection plasmid encoding C-terminally GFP-6His-tagged $NleG1_{CR}^{191-194}$ under chicken β-actin promoter	Amp^{100}	This study
pOPINE-3C-eGFP-6His-$NleG1_{CR}^{2-67}$	Transfection plasmid encoding N-terminally GFP-6His-tagged $NleG1_{CR}^{2-67}$ under chicken β-actin promoter	Amp^{100}	This study
pOPINE-3C-$NleG1_{CR}^{2-67}$-eGFP-6His	Transfection plasmid encoding C-terminally GFP-6His-tagged $NleG1_{CR}^{2-67}$ under chicken β-actin promoter	Amp^{100}	This study
pOPINE-3C-eGFP-6His-$NleG1_{CR}^{2-194}$	Transfection plasmid encoding N-terminally GFP-6His-tagged $NleG1_{CR}^{2-194}$ under chicken β-actin promoter	Amp^{100}	This study
pOPINE-3C-$NleG1_{CR}^{2-194}$-eGFP-6His	Transfection plasmid encoding C-terminally GFP-6His- $NleG1_{CR}^{2-194}$ under chicken β-actin promoter	Amp^{100}	This study
pOPINE-3C-eGFP-6His-$NleA_{CR}$	Transfection plasmid encoding N-terminally GFP-6His-tagged $NleA_{CR}$ under chicken β-actin promoter	Amp^{100}	This study
pOPINE-3C- $NleA_{CR}$ -eGFP-6His	Transfection plasmid encoding C-terminally GFP-6His- $NleA_{CR}$ under chicken β-actin promoter	Amp^{100}	This study

2.9 Immunofluorescence staining

Cells were permeabilised for 8 mins in 0.1% Triton X-100 in PBS and blocked in 3% bovine serum album (BSA) in PBS. Primary and secondary antibodies (Table 7) were consecutively applied in 1% BSA in PBS for 30 mins in a humid chamber with 3 PBS washes in between. Coverslips were mounted on ProLong Gold antifade (Molecular Probes, OR, USA) or VECTASHIELD® with DAPI (Vector Laboratories, UK) and images were obtained at consistent exposure times on a Zeiss Axiovision Z3. Where appropriate, cell area was measured by manually tracing the cell periphery as defined by phalloidin staining using the polygon tool on Zeiss ZEN blue v2.3.

Table 7 | Antibodies used for immunofluorescence and immunoblotting

Antibody/Reagent	Origin	Application	Dilution	Supplier
Human/mouse Ki67	Rabbit	Colon sections	1:50	ThermoFisher Scientific
Int280β	Chicken	Colon sections	1:50	Frankel lab
Chicken IgY-Cy3	Goat	Colon sections	1:100	Jackson Immunoresearch
Rabbit IgG-Alexa488	Donkey	Colon sections	1:100	Jackson Immunoresearch
DAPI	-	Colon sections, transfection, infection	1:1000	Invitrogen
Human c-Myc	Rabbit	Transfection	1:200	Sigma
Human myc clone 4A6	Mouse	Transfection	1:200	Merck Millipore
Human/mouse TOMM-22	Mouse	Transfection	1:200	Abcam
FLAG®M2	Mouse	Transfection	1:500	Sigma
HA.11 clone 16B12	Mouse	Infection	1:200	Cambridge Bioscience
Phalloidin iFluor647	-	Transfection, infection	1:100	Stratech
Int280α 2346	Rabbit	Western blot	1:1000	Frankel lab
Strep-II	Mouse	Western blot	1:1000	Genscript
Human/mouse caspase-9	Rabbit	Western blot	1:10000	Abcam
Human/mouse PARP	Rabbit	Western blot	1:1000	Cell Signalling Technologies
FLAG	Rabbit	Western blot	1:1000	Cell Signalling Technologies
Human c-Myc	Chicken	Western blot	1:2000	Bethyl
Rabbit IgG Fc fragment-HRP	Goat	Western blot	1:50000	Jackson Immunoresearch
Mouse IgG Fc fragment-HRP	Goat	Western blot	1:10000	Jackson Immunoresearch

β-actin-HRP	Mouse	Western blot	1:50000	Sigma

2.10 Yeast transformation

Yeast strains (Table 4) were transformed with plasmids listed in Table 8 using the lithium acetate method (adapted from Agatep et al., 1998). Briefly, yeast extract peptone dextrose (YPD) was inoculated and growth for 16 h at 30 °C (200 rpm), sub-cultured 1:10 and allowed to grow for a further 4 h. Cultures were pelleted at 4,000 x g for 5 mins, washed in deionised water, 100 mM lithium acetate and resuspended in yeast transformation solution (30% w/v PEG, 100 mM lithium acetate, 50 ng herring sperm DNA, 1 µg plasmid DNA). Cells were incubated at 30 °C for 30 mins before a 42 °C heat shock for 25 mins. Cells were pelleted and resuspended in 100 µL deionised water. Transformants were recovered for 3 days at 30 °C on selective SD agar.

Table 8 | Plasmids used for yeast expression

Plasmid	Description	Selection	Source
pYES2	Inducible yeast expression plasmid with *GAL1* promoter.	Amp^{100}, ura-deficient media	Thermo Fisher
pYES2-$EspS_{CR}$	Expresses $EspS_{CR}$ upon induction with galactose. Repressed by glucose.	Amp^{100}, ura-deficient media	This study
pYES2-$EspS_{B171}$	Expresses $EspS_{B171}$ upon induction with galactose. Repressed by glucose.	Amp^{100}, ura-deficient media	This study
pYES2-$EspS_{E11}$	Expresses $EspS_{E11}$ upon induction with galactose. Repressed by glucose.	Amp^{100}, ura-deficient media	This study
pYES2-OspB	Expresses OspB upon induction with galactose. Repressed by glucose.	Amp^{100}, ura-deficient media	This study
pYES2-VPA1380	Expresses VPA1380 upon induction with galactose. Repressed by glucose.	Amp^{100}, ura-deficient media	This study
pGBKT7	Yeast expression plasmid with GAL4 DNA binding domain aa1-147 and SV40 nuclear localisation signal under *ADH1* promoter	Kan^{50}, trp-deficient media	Takara Clontech
pGBKT7-$EspS_{CR}$	Expresses bait protein $EspS_{CR}$ as an N-terminal fusion with	Kan^{50}, trp-deficient media	This study

pGBKT7	GAL4 DNA binding domain under *ADH1* promoter		
pGBKT7-TRIAP1	Expresses bait protein mouse TRIAP1 as an N-terminal fusion with GAL4 DNA binding domain under *ADH1* promoter	Kan^{50}, trp-deficient media	This study
pGBKT7-StoD	Expresses internal control bait protein *S.* Typhimurium StoD as an N-terminal fusion with GAL4 DNA binding domain under *ADH1* promoter	Kan^{50}, trp-deficient media	McDowell et al., 2019
pGADT7	Yeast expression plasmid encoding GAL4 activation domain under *ADH1* promoter	Amp^{100}, leu-deficient media	Takara Clontech
pGADT7-TRIAP1	Expresses prey protein mouse TRIAP1 as an N-terminal fusion with GAL4 activation domain under *ADH1* promoter	Amp^{100}, leu-deficient media	This study
pGADT7-$EspS_{CR}$	Expresses prey protein $EspS_{CR}$ as an N-terminal fusion with GAL4 activation domain under *ADH1* promoter	Amp^{100}, leu-deficient media	This study
pGADT7-$EspS_{CR}^{C184A}$	Expresses prey protein $EspS_{CR}^{C184A}$ as an N-terminal fusion with GAL4 activation domain under *ADH1* promoter	Amp^{100}, leu-deficient media	This study
pGADT7-ubiquitin	Expresses internal control prey peptide ubiquitin as an N-terminal fusion with GAL4 activation domain under *ADH1* promoter	Amp^{100}, leu-deficient media	McDowell et al., 2019

2.11 Yeast toxicity assay

pYES2 constructs were cloned using conventional restriction digest using genomic DNA templates and the primers listed in Table 5. *Vibrio parahaemolyticus* RIMD2210633 and *Shigella flexneri* M90T genomic DNA were kind gifts from Dr Jennifer Ritchie (University of Surrey, UK), and Dr Abigail Clements (Imperial College London, UK) respectively. S. *cerevisiae* BY4741 were transformed with pYES2 constructs (Table 8) and were grown in SD broth lacking uracil (-ura) supplemented with kanamycin (50 µg/ ml) for 24 h at 30 °C (200 rpm). 1 ml samples were pelleted for 1 min at 14,000 rpm, washed and resuspended in 1 ml deionised

water. Serial dilutions from 10^{-1} to 10^{-7} were plated on SD -ura plates supplemented with either 1% glucose or galactose and incubated for 2 days at 30°C.

2.12 Yeast 2 hybrid (Y2H) assay

50 ml *S. cerevisiae* AH109 harbouring bait plasmid pGBKT7-$EspS_{CR}$ (Table 8) was grown for 16 h at 30 °C in SD lacking tryptophan (-trp) broth supplemented with 1% glucose. Cells were harvested by centrifugation at 1000 rpm for 10 mins and resuspended in 5 ml of fresh media. 1 ml *S. cerevisiae* Y187 prey strains containing clones of the Mate & Plate Library – universal mouse (normalised; library strain; Takara Clontech) was mixed with the bait strain and subcultured into 45 ml 2x YPDA broth. The cultures were mated for 25 h at 30 °C (30 rpm). Mated cells were harvested by centrifugation at 4,000 rpm for 10 mins, resuspended in 0.5x YPDA and plated on SD -trp -leu -ade -his agar (quadruple drop out, QDO) supplemented with 0.2 mg/ml x-α-gal for selection of cells carrying both a bait and prey plasmid. Colonies were restreaked 3 times on QDO plates before plasmids were extracted using the peqGOLD plasmid miniprep kit I (VWR, PA, USA) according to modified manufacturer's instructions, wherein glass beads are added to samples in solution I and vigorously shaken for 10 mins. To reveal prey identity plasmid inserts were sequenced using the pGADT7-sqn-F primer (Table 5).

2.13 Direct 2 hybrid (D2H) assay

S. cerevisiae AH109 was co-transformed with bait and prey plasmids. Transformed colonies were diluted in sterile deionised H_2O and spotted on SD-double dropout (-leu, -trp, DDO) to confirm uptake of plasmids or SD-QDO plates to confirm bait-prey interactions. Plates were incubated at 30 °C until growth of the positive control was observed.

2.14 TEM translocation assay

Swiss 3T3 cells were seeded in triplicate in a black-walled 96-well plate at 7 x 10^4 cells/well in DMEM with 4500 mg/L glucose, L-glutamine and 10% FBS and incubated overnight at 37 °C with 5% (v/v) CO_2. *C. rodentium* was grown to saturation at 37 °C with 200 rpm agitation for 8 h before subculturing 1:500 for 16 h in DMEM with 1000 mg/L glucose at 37 °C, 5% (v/v) CO_2, static to induce expression of the T3SS. Cells were infected with the induced culture at an MOI

of 100 confirmed by retrospective plating. The plate was centrifuged at 1000 rpm for 5 mins to synchronise infection. Cells were cultured at 37 °C with 5% (v/v) CO_2 for 2 h before effector-TEM-1 expression was induced with 1 mM IPTG and incubated for a further 1.5 h. Cells were washed thrice in HBSS and incubated with freshly prepared 6 mM probenecid (in HBSS), 20 mM HEPES and 1 x CCF2/AM (Invitrogen) in the dark for 1.5 h. Cells were further washed in HBSS and fluorescence resulting from 410 nm excitation was measured on a Fluostar Optima (BMG Labtech, UK) at 450 nm and 540 nm. Response ratio is expressed as the 450/520 nm emission ratio, adjusted for background fluorescence from uninfected cells.

2.15 Measurement of PI uptake of infected cells

1.5 x 10^5 THP1 cells (for EPEC infection) or 7.5 x 10^4 HeLa cells (for *C. rodentium* infection) were seeded in black-walled 96-well plates. THP1s were differentiated into macrophage-like cells with the addition of 100 ng/ml phorbol 12-myristate 13-acetate (PMA) 72 h prior to infection. Puromycin, streptomycin, and penicillin were removed 24 h prior to infection. Immediately before infection, culture media was replaced with phenol-red-free media supplemented with 5 µg/ml propidium iodide (PI); 10% well volume of bacterial culture corresponding to an MOI of 10 (EPEC) or 50 (*C. rodentium*) was then added to each well. The plate was spun for 10 mins at 700 x g to synchronise infection. At 2 h p.i. all wells were treated with 150 µg/ml gentamicin to kill extracellular bacteria. Emission at 620 nm was monitored every 10 mins at 37 °C and 5% (v/v) CO2. Experimental values are blanked against uninfected cells and expressed as a percentage of the maximal as defined by cells treated with 0.05% Triton-X-100. Colony-forming units (CFU) present in the inoculum were confirmed by retrospective plating.

2.16 LDH release assay

Quantification of released lactose dehydrogenase (LDH) was performed on 25% well volume of cell supernatant using the CytoTox 96® Non-Radioactive Cytotoxicity Assay (Promega, UK) according to the manufacturer's instructions. Absorbance was measured at 490 nm on a Fluostar Optima, blanked to untreated cell supernatants. Cell lysis values are expressed as a percentage of the maximal as defined by cells treated with 1% (v/v) Triton-X-100.

2.17 Lipidomics

Enterocytes were purified from C56Bl/6 mice at 8 and 21 d.p.i. as previously published (Berger et al., 2017), with the following modifications: 4 cm section of distal colon was cut longitudinally and placed in 4 ml enterocyte dissociation buffer (Hank's Balanced Salt Solution without Mg2+ or Ca2+, 1 mM EDTA, 10 mM HEPES, 5 µL/ml β-mercaptoethanol) for 45 mins at 37 °C with 200 rpm agitation. Enterocytes were spun at 2000 x g for 10 min and washed twice in PBS. In preparation for mass spectrometry, cells were further washed three times in double-distilled water (ddH_2O) with 15000 x g spins and resuspended 1:1 (w/v) in ddH_2O. A 2,5-dihydroxybenzoic acid matrix was used at a concentration of 10 mg/ml in 90:10 (v/v) chloroform/methanol. 0.4 µL of biological sample and 0.6 µL of the matrix solution were deposited on the target, mixed and allowed to dry before MALTI-TOF MS analysis using the reflectron mode on a 4800 Proteomics Analyzer with TOF-TOF Optics (Applied Biosystems) operating at 20 kV in the negative ion mode using a 20 ns extraction delay time. The final spectra are a sum of 500–2000 laser shots and were analysed using Data Explorer v4.9 (Applied Biosystems).

2.18 TUNEL staining assay

TUNEL staining was performed with the DeadEnd™ fluorometric TUNEL kit (Promega) according to manufacturer's instructions with the following modifications. PFA-fixed distal colonic crypt sections were paraffin-mounted and dewaxed in Histo-Clear™ for 5 mins before sequential rehydration in 100%, 95%, 85%, 70% and 50% ethanol series for 3 mins per solution with a final 5 min immersion in 0.85% (w/v) NaCl. Slides were washed for 5 mins in PBS, fixed in 4% PFA for 15 mins, then washed thrice further in PBS. Tissue was permeabilised in a 20 µg/ml Proteinase K solution for 8 mins then washed in PBS for 5 mins and fixed once more in 4% PFA for 5 mins. PFA was removed for 5 mins in PBS before sections were bathed in Equilibration Buffer for 7 mins. A positive control slide was simultaneously prepared by flooding tissue with 10U/ml DNase I in DNase I buffer. Nucleotide mix (containing fluorescein-12-dUTP), recombinant terminal deoxynucleotidyl transferase and equilibration buffer were added to sections in a 5:1:45 ratio and incubated at 37 °C for 1 h in a dark humid chamber to facilitate incorporation of labelled dUTP to 3'OH nicked ends of apoptotic cell DNA. The reaction was terminated in 2X SSC buffer for 15 mins and washed three times in PBS to remove

unincorporated dUTP. Slides were mounted with VECTASHIELD® with DAPI and immediately imaged as described in §2.8.

2.19 Immunoblotting

Samples were diluted in 5x Laemmli sample buffer (10% sodium dodecyl sulphate (SDS), 50% Glycerol, 0.05% Bromophenol Blue, 0.3125 M Tris pH 6.8, 0.5 M DTT) and boiled for 5 mins before loading on tris-glycine SDS gels made with an appropriate percentage of acrylamide for the desired separation. Proteins were transferred to methanol-activated polyvinylidene fluoride (PVDF) membranes and blocked for 1 h in 5% skimmed milk powder in PBS with 0.05% Tween-20 (PBS-T). Antibodies were applied at the dilutions listed in Table 7 with three 7 min PBS-T washes between applications. Membranes were incubated with ECL™ Prime (GE-healthcare) according to manufacturer's instructions and chemiluminescence was detected using a BioRad ChemiDoc XRS^{+}.

2.20 Bioinformatic analysis

Full length effector protein queries were submitted to NCBI BLAST, the Phyre2 intensive mode server (Kelley et al., 2015), or I-TASSER (Roy et al., 2011) with default settings selected. Primary sequences were aligned using Clustal Omega (Sievers et al., 2014) for MSA or EMBOSS Water (Madeira et al., 2019). Predicted structures were aligned using TM-align (Zhang and Skolnick, 2005). Figures were generated with PyMOL v.2.3.2 for structural prediction or JalView (Waterhouse et al., 2009) for sequence alignments.

2.21 Statistical analysis

All experiments subject to statistical testing were independently, but not randomly or blindly, performed a minimum of thrice or as indicated in figure legends. Data were consistently analysed for normal distribution using D'Agostino & Pearson or Shapiro Wilk normality tests, and log2 transformed where appropriate to meet criteria for parametric testing. All analyses with three or more comparisons were subjected to multiple comparison correction as indicated in figure legends. All data were also tested for outliers using the ROUT method (FDR; Q= 5%)

and removed from comparisons where indicated. Unless otherwise stated, mean ± standard error of the mean (SEM) is plotted. Testing was applied with GraphPad Prism v8.3.0 (538).

2.22 Co-immunoprecipitation

The supernatant from 3 x 10^6 transfected HeLa cells was removed and pelleted, while adhered cells were lysed in 450 µL FLAG Co-IP buffer (50 mM Tris pH 7.4, 150 mM NaCl, 1 mM EDTA, 1% Triton X-100 with cOmplete™ mini protease inhibitor cocktail (Roche)). Pelleted and adherent cells were combined, and the insoluble fraction was separated by centrifugation. 10% of the lysate was retained as the input fraction. 40 µL ANTI-FLAG M2 affinity agarose gel (Sigma) was pre-equilibrated with two washes in lysis buffer then incubated with cell lysate at 4 °C with 20 rpm rotation. After 2 h, the supernatant was discarded, beads were washed twice in Tris-buffered saline (50 mM Tris pH 7.4, 150 mM NaCl), and bound proteins were eluted by boiling in 20 µL 4x Laemmli sample buffer (BioRad) for 5 mins.

Chapter 3

Novel T3SS effector proteins

3 Novel T3SS Effector proteins

3.1 Introduction

With the advent of bioinformatic approaches for predicting type III (T3) effector proteins, the number of putative T3 substrates is continually expanding. Indeed, many novel effector proteins have been identified and validated in a range of secretion system-encoding pathogens, including *Pseudomonas syringae* (Samudrala et al., 2009; Vinatzer et al., 2005), *P. fluorescens* (Vinatzer et al., 2005), *S.* Typhimurium (Samudrala et al., 2009), *Chlamydia trachomatis* and *C. psittaci* (Hovis et al., 2013), *Legionella pneumophila* (Burstein et al., 2009), *Xanthomonas euvesicatoria* (Teper et al., 2016) and *Pantoea agglomerans* (Nissan et al., 2018). Through genome-scale computational screens, typical features of T3 effectors can be defined: an N-terminal enrichment of small polar amino acids such as serine and threonine (Arnold et al., 2009), conservation of regulatory motifs upstream of the gene, a differing GC content to the rest of the genome, lack of gene homology to non-T3SS-encoding strains, and gene proximity to known effectors (Teper et al., 2016). Prior to this work, machine learning-aided identification of putative effectors from A/E genomes had yet to be performed. A genus-optimised bioinformatic approach was therefore developed for *C. rodentium* by our collaborator Tal Pupko at the University of Tel Aviv, Israel, who provided a shortlist of candidate effector proteins. These proteins are investigated herein.

Unlike the *in silico*-based approach described above, the uncharacterised type III effector EspS was reported during the sequencing of the *C. rodentium* genome in 2010 (Petty et al., 2010); it was manually identified through homology to the *Shigella* spp. T3 effector OspB. The T3-dependent secretion of EspS was demonstrated and independently confirmed by mass spectrometry (Deng et al., 2010). In *C. rodentium*, EspS is encoded by an 876 bp ORF to create a 32.3 kDa effector, hereafter referred to as $EspS_{CR}$. In a recent screen of bacterial mRNA isolated from LB, DMEM and the murine caecum, *C. rodentium espS* mRNA was relatively more abundant than other non-LEE encoded effectors, with the exception of its neighbour *nleA/espI,* with which *espS* is co-transcribed (Connolly et al., 2018). Conversely, as *espS* is acquired through phage transmission, the gene is present at different loci in human *E. coli* isolates, neighbouring *espG*, *nleG* or prophage tail elements. Consistently, EspS homologues have also been identified on the Stx2x-carrying phage 2851 next to tail assembly genes (Strauch et al.,

2008), and various *nleA/espI*-encoding phages along with *nleG* and tail fibre genes (Creuzburg et al., 2011).

EspS homologues are conserved to differing degrees in several enteric pathogens, including all four *Shigella* species, *Salmonella enterica* serovar Paratyphi A, *S.* Typhi, *S. bongori, Vibrio cholerae*, *V. parahaemolyticus* and a multitude of pathogenic *E. coli* isolates. To date, the only EspS homologues biochemically investigated are OspB (*Shigella spp.*), VPA1380 (V. parahaemolyticus) and Ibe (atypical enteropathogenic *E. coli* (ATEC)).

VPA1380, the EspS homologue encoded by *V. parahaemolyticus,* is a 33.2 kDa protein secreted by the T3SS-2 (Hiyoshi et al., 2011). When locally aligned, VPA1380 shares 34% identity and 58% similarity with $EspS_{CR}$. Sequence alignment and secondary structural predictions show that the C-terminus of VPA1380 is homologous to cysteine protease domains of several large bacterial toxins, including the multifunctional-autoprocessing repeats-in-toxin (RTX; MARTX) toxin of *V. cholerae*, as well as glucosylating toxins TcdA and TcdB from Clostridium difficile. These toxins have a conserved catalytic dyad (Cys and His) and further conserved inositol hexakiphosphate (IP6) binding residues that are both required for their activity and toxicity in the experimental *Saccharomyces cerevisiae* system (Calder et al., 2014).

In *Shigella spp.* genomes, the large virulence plasmid harbours the *ospB* gene, upstream of the T3SS apparatus (Buchrieser et al., 2000). OspB is regarded as an immunomodulator, as its expression in HEK293 cells activates NF-κB signalling, while infection with the *S. flexneri* Δ*ospB* strain resulted in reduced NF-κB activation (Fukazawa et al., 2008). The subcellular localisation of OspB upon transfection is cell-type and tag-dependent; in MDCK cells, transfected GFP-tagged OspB appears to be punctate and perinuclear (Fukazawa et al., 2008), while in HeLa cells transfected OspB-FLAG exhibits diffuse cytoplasmic and nuclear staining (Ambrosi et al., 2015). It was proposed that these differing localisations reflect different stages of infection, culminating with OspB nuclear translocation and subsequent phosphorylation of the mitogen-activated protein kinases (MAPK) ERK1/2 and p38, and activation of cytosolic phospholipase A2 ($cPLA_2$). This MAPK-phosphorylating function is also shared by the *S.* Typhi homologue STY1360 (Hannemann and Galán, 2017). In turn, $cPLA_2$ releases the eicosanoid precursor arachidonic acid from phospholipid membranes, allowing eicosanoid synthesis and secretion,

consequent transepithelial migration of polymorphonuclear leukocytes (Ambrosi et al., 2015); a hallmark of *S. flexneri* infection.

In addition to its role in immunomodulation, OspB is proposed to form a scaffolding complex with IQGAP1 and mTORC1 to promote cell proliferation during *Shigella* cell-to-cell spread, likely via ERK1 (Lu et al., 2015). Interestingly, the ATEC-encoded homologue Ibe also binds IQGAP1 where it is localised beneath pedestals (Buss et al., 2009). The function of Ibe during infection remains unexplored, however as A/E pathogens are extracellular and do not disseminate from the cytoplasm like *Shigella*, it is likely that Ibe-IQGAP binding plays a role distinct from that of OspB during infection.

The above considered, this chapter addresses the following experimental aims:

1. Test the T3SS-dependent secretion of candidate effector proteins identified in *C. rodentium* by machine learning.
2. Bioinformatic characterisation of uncharacterised *C. rodentium* effectors.
3. Exploration of uncharacterised *C. rodentium* effector protein functions in a mammalian cell model.
4. Biochemical identification of interacting partners for uncharacterised *C. rodentium* effectors.
5. Investigate effector protein function in an *in vivo* murine model.

3.2 Results

3.2.1 TEM translocation assays reveal two novel *C. rodentium* effector proteins.

In order to identify novel effector proteins encoded by *C. rodentium*, a machine-learning approach was employed by Tal Pupko et al. (Univ. Tel Aviv, Israel), who provided a ranked list of genes in the *C. rodentium* genome (Figure 3.1A). As the smallest known *C. rodentium* effector is EspO (92 aa), each gene was assessed for length; hypothetical proteins more than 10% smaller than EspO were excluded from testing. The remaining loci (ROD_48841, ROD_48831, ROD_40941, ROD_40891, and ROD_48821) were cloned into pCX340 with a C-terminal TEM-1 fusion to generate strains for assaying T3SS-dependent translocation. Swiss

A

Identifier	Weighted vote	Size (aa)	Genomic context	Testing status	Translocation status
ROD_48841	**0.990059294**	**85**	**GI14**	**Tested**	**Translocated**
ROD_48831	0.973129001	113	GI14	Tested	Not translocated
ROD_40951	0.969299483	69	GI11	Untested	-
ROD_40871	0.967504774	42	GI11	Untested	-
ROD_19131	0.965747006	38	Neighbours *espV*	Untested	-
ROD_40941	0.964946341	130	GI11	Tested	Not translocated
ROD_40891	**0.964550062**	**192**	**GI11**	**Tested**	**Translocated**
ROD_40811	0.963595389	56	GI11	Untested	-
ROD_41111	0.960802007	40	Isolated	Untested	-
ROD_48821	0.958762882	253	GI14	Tested	Not translocated
ROD_40801	0.958510844	36	GI11	Untested	-

B

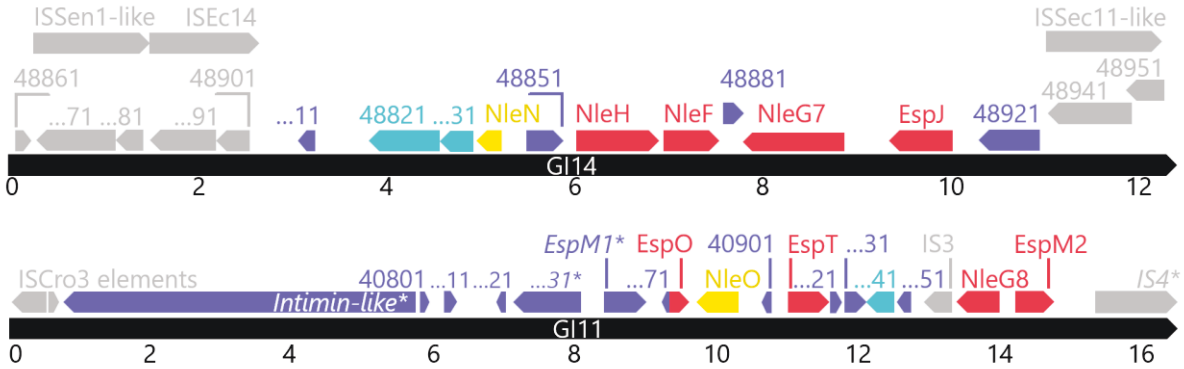


Figure 3.1 | Candidate effector proteins in *C. rodentium* and their genomic context **A** Summary of candidate effector proteins, ranked by Pupko *et al.* (unpublished data). **B** Genomic location of NleN and NleO (yellow) on GI14 and GI11 respectively, which are both flanked by insertion elements (grey). Also indicated are experimentally validated effectors (red), other candidates tested (teal) and uncharacterised genes and pseudogenes (purple). Pseudogenes are indicated with an asterisk. Scale provided in kb.

3T3 murine fibroblasts are provided with the passively diffusing TEM substrate CCF2/AM: a coumarin moiety that provides fluorescence energy transfer (FRET) to a linked fluorescein moiety, emitting fluorescence at 520 nm. In the presence of the translocated TEM β-lactamase, the substrate is cleaved and emission from the coumarin moiety alone can be detected at 409 nm (Charpentier and Oswald, 2004). ROD_48841 (L), ROD_44831 (V) and ROD_44821, which are all present in the same operon on the GI14 genomic island (Figure 3.1), present with an 5' GTG (Val) or TTG (Leu) start codon, and as such were cloned as both V/L-start and M-start to assess the effect of the start codon on translocation efficiency. The remaining two candidates, ROD_40941 and ROD_40891 are present on the GI11 genomic island.

ROD_48841 and ROD_40891 were consistently translocated by WT *C. rodentium* but not *C. rodentium* Δ*espA* in similar manner to the known effector EspH (Figure 3.2), irrespective of the ROD_48841 start codon. *C. rodentium* Δ*espA* is used as a negative control as it lacks the T3SS filament protein necessary for host attachment and therefore cannot translocate effectors. Emission from ROD_48831, ROD_48821 and ROD_40941-infected cells was indistinguishable between WT and Δ*espA* infection conditions, indicating these are not translocated. ROD_48841 and ROD_40941 will henceforth be referred to as NleN and NleO, respectively.

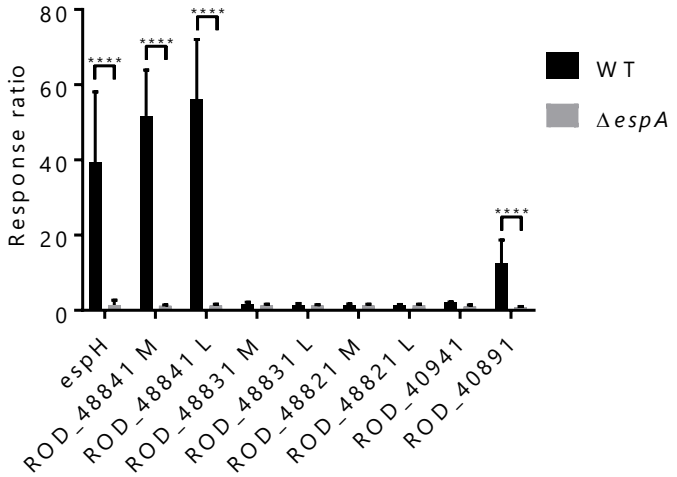


Figure 3.2 | TEM translocation assay of putative *C. rodentium* effectors
ROD_48841 (NleN) and ROD_40891 (NleO)-TEM-1 fusion proteins are translocated by WT but not Δ*espA C. rodentium* into Swiss 3T3 cells. Results are means from 4 biological repeats, analysed by multiple t tests corrected with the two-stage step-up method of Benjamini, Krieger and Yekutieli approach for False Discovery Rate (FDR) (**** = $p < 0.0001$). Error bars represent SEM.

3.2.2 Bioinformatic analysis of uncharacterised *C. rodentium* effector proteins.

3.2.2.1 ORFs in GI14 contain fragments of conserved effector proteins.

C. rodentium nleN is a 258 bp gene encoding a 9.48 kDa protein positioned in GI14, neighbouring NleH, NleF, NleG7 and EspJ. BLASTp searching indicates NleN-like sequences are present at the N-terminus of several hypothetical proteins sequenced from human and cattle isolates of pathogenic *E. coli*, including O26:H11, O177:25 and O45:H2, *E. albertii*, *S. enterica* subsp. salamae and *Shigella boydii* and *S. dysenteriae*, but not *S. flexneri* or *S. sonnei*. Hits were also obtained against Stx1 converting phage AU6Stx1 and Escherichia phage SH2026Stx1, likely indicating the *nleN* gene and longer variations thereof have been acquired multiple times by phage transmission. The top 100 hits vary in protein sequence length, with *C. rodentium* NleN representing the shortest peptide and the largest protein comprising 613 aa. Detailed analysis of the *C. rodentium* DNA sequence reveals it differs to the 613 aa hypothetical protein hit by 5 stop codons, starting at an upstream Met and reading over the ROD_48831 and ROD_48821 ORFs (Figure 3.3), although the predicted ORF for ROD_48831 has a -1 frameshift relative to *nleN*. Consistent with the short length of NleN, no functional motifs or domains were detected, and the tertiary structure could not be predicted. Taken together, NleN could represent the N-terminal fragment of a longer protein, but unlike ROD_48831 and ROD_48821, it has retained the ability to be recognised by the T3SS for secretion and is a *bona fide* T3SS effector.

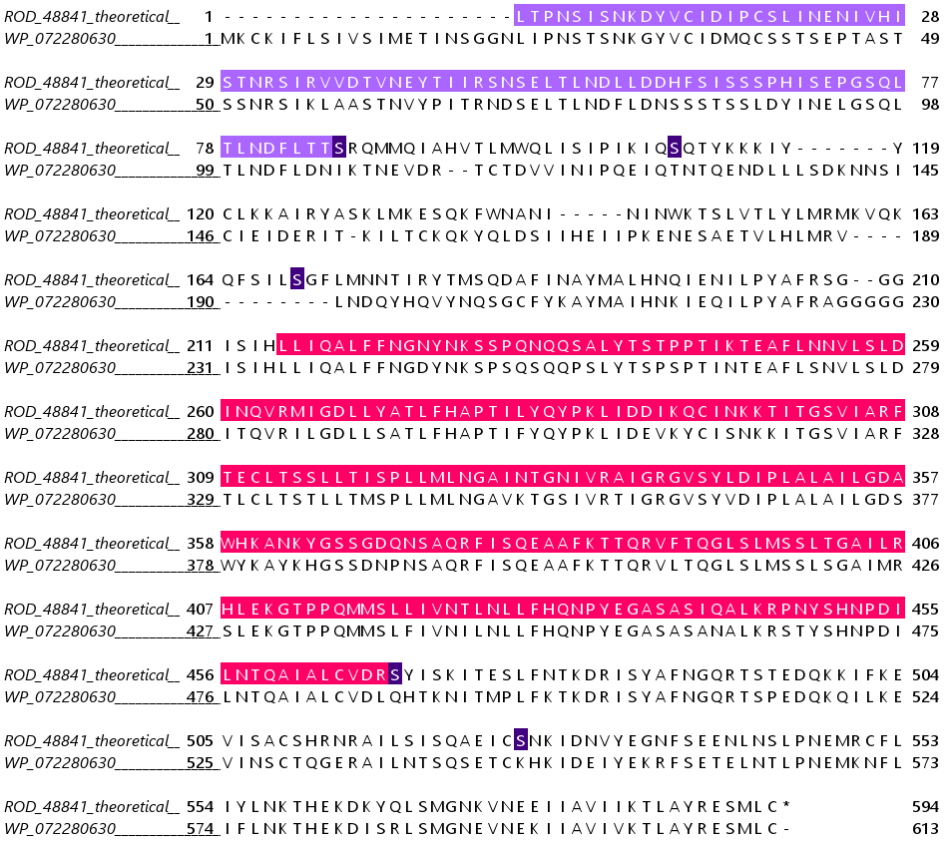


Figure 3.3 | Alignment of NleN and downstream coding regions
ClustalW alignment of a hypothetical NleN protein with stop codons replaced with TCA (Ser, blue) to WP_072280630 (an *E. coli* homologue identified by BLASTp). The translation of NleN as it appears in the *C. rodentium* genome (lilac), the hypothetical product for ROD_48821 (magenta) are highlighted. Formatted with JalView.

3.2.2.2 NleO exhibits homology to a MARTX Rho GTPase inactivating effector domain.

Like *nleN*, *nleO* neighbours other known effectors: *espO*, *espT*, *espM2* and *nleG8* on GI11. The *nleO* gene encodes a protein of 21.91 kDa with high similarity (<94%) and identity (<89%) to uncharacterised proteins in human isolates of *E. coli*, as well as less conserved homologues in *S. boydii* (44% identity, 56% similarity). A more sensitive PSI-BLAST search protocol also returned hits to RTX-like toxins, despite having no functional domains identified by ExPASy PROSITE. Unlike NleN, the tertiary structure of NleO can be readily predicted by both Phyre2 and I-TASSER (Figure 3.4A). TMalign scored the prediction alignment 0.834/1, deviating only in a 30 aa stretch that presents as a loop-helix-loop formation in the Phyre2 prediction, but an uninterrupted, high B-factor α-helix according to I-TASSER. Consistent with PSI-BLAST hits, the Phyre2 structure is based on an effector domain of the RTX toxin of *Vibrio vulnificus*, with 100% confidence over 88% of the alignment; the remaining 12% is represented by the extreme

termini. Manually mapping the predicted structures back to the primary sequence of *V. vulnificus* MARTX ($MARTX_{VV}$) reveals overlap with the C-terminus of the Rho GTPase inactivating domain (RID) effector portion (*V. vulnificus* residues 2578-2884) (Figure 3.4B). The highlighted residues C2835 (conserved in NleO at C121) together with H2895 (not conserved) mediate fatty acylation of Rho GTPases such as Rac1 to induce cell rounding (Zhou et al., 2017).

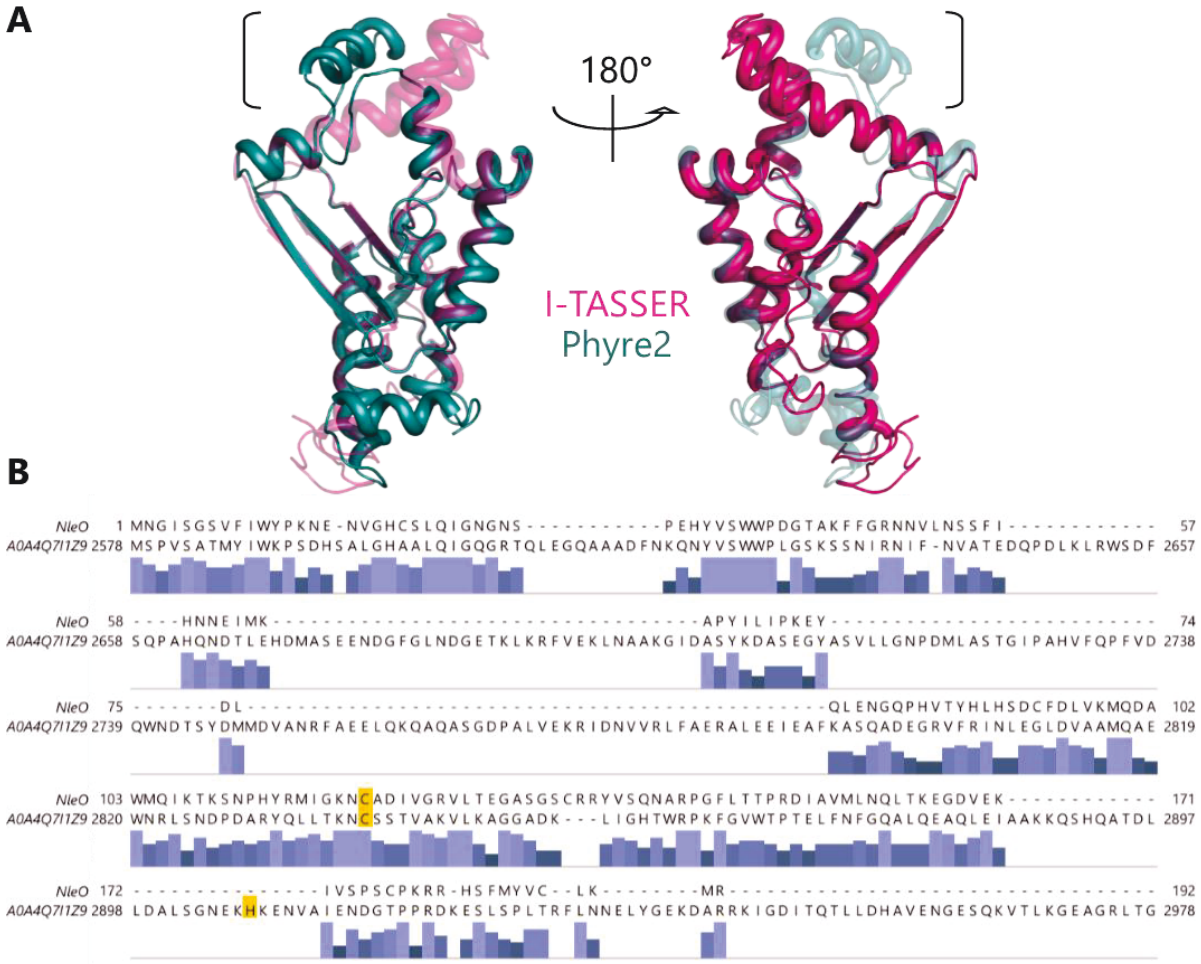


Figure 3.4 | Structural and sequence homology between NleO and a MARTX toxin effector domain

A Phyre2 (teal) and I-TASSER (magenta) predictions of NleO structure are highly homologous. **B** NleO maps to the C-terminal Rho GTPase inactivating (RID) domain of the *V. vulnificus* MARTX toxin (A0A4Q7I1Z9; $MARTX_{VV}$). $MARTX_{VV}$ catalytic residues are highlighted in yellow.

3.2.2.3 Identification of EspS homologues.

Identification of effector homologues can offer insight into shared functions. To identify EspS homologues, a BLASTp search was conducted using $EspS_{CR}$ as a query against the NCBI database. 34 proteins were identified with over 30% sequence similarity, all encoded by Gammaproteobacteria; a cladogram was generated using Phylogeny.fr to visualise their relationship (Figure 3.5) (Dereeper et al., 2008). With the exception of the Vibrionaciae *Grimontia hollisae*, *Vibrio ichthyoenteri* and *Vibrio parahaemolyticus*, all homologues identified are encoded by *Enterobacteriaciae*. $EspS_{CR}$ homologues encoded by *Escherichia spp*. share the most sequence identity (63.9% - 66.6%), while the most distantly related EspS homologue was traced in *Serratia odorifera* (21.4%). The *Shigella spp*. homologues OspB are identical to one another; homologues from *S. enterica* isolates share a minimum of 97.5% identity, while the percentage identity shared by *E. coli* homologues is 80.7%. No EspS homologue was detected in EPEC E2348/69, EHEC EDL933 or Sakai type strains.

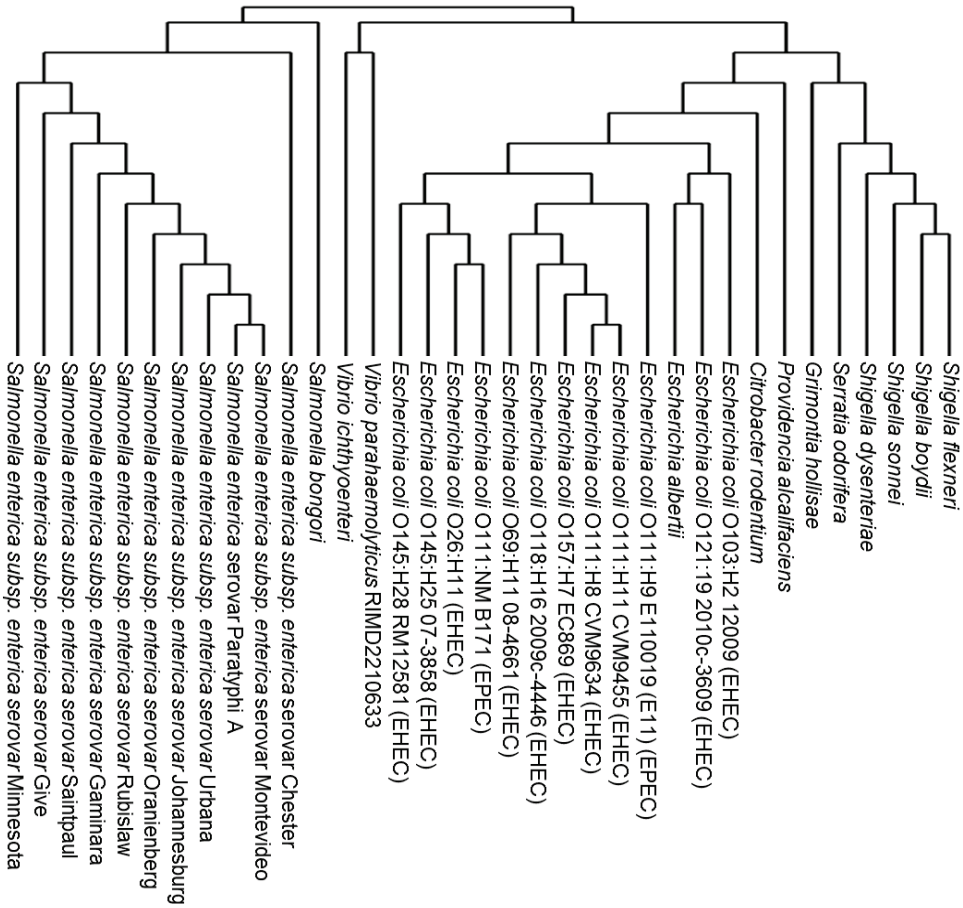


Figure 3.5 | Cladogram of proteins with >30% homology with $EspS_{CR}$
Cladogram of proteins with >30% homology with Esp_{CR}. Tree generated using phylogeny.fr using default settings.

3.2.2.4 Primary sequence analysis of EspS homologues.

To identify areas of sequence homology, EspS proteins representing 12 different branches of the cladogram in Figure 3.5 were selected and aligned using the Clustal Omega multiple sequence alignment (MSA) tool (Sievers et al., 2014) and formatted using JalView (Waterhouse et al., 2009) (Figure 3.6). Expectedly, the N-terminus of each homologue is the least conserved, as it contains the species-specific secretion signal necessary for T3SS translocation. The MSA highlights three areas of notable sequence conservation: a KΦYΦxGxGxπG motif, a DΦRΦxxCxSπζ motif and a πYζGxGV motif at the C-terminus (where Φ represents a hydrophobic residue, π represents a small-chain residue, ζ represents a hydrophilic residue and x represents any amino acid (Aasland et al., 2002)). With reference to Calder *et al*. (2014), the KΦYΦxGxGxπG and DΦRΦxxCxSπζ motifs overlap with the putative cysteine protease catalytic dyad (Cys195 and His154) identified in VPA1380, through its sequence homology to large bacterial toxins. While Cys195 is completely conserved across the 12 EspS homologues, His154 is replaced with Asp in *E. coli* B171 and *E. albertii*, and an Ile in *C. rodentium*.

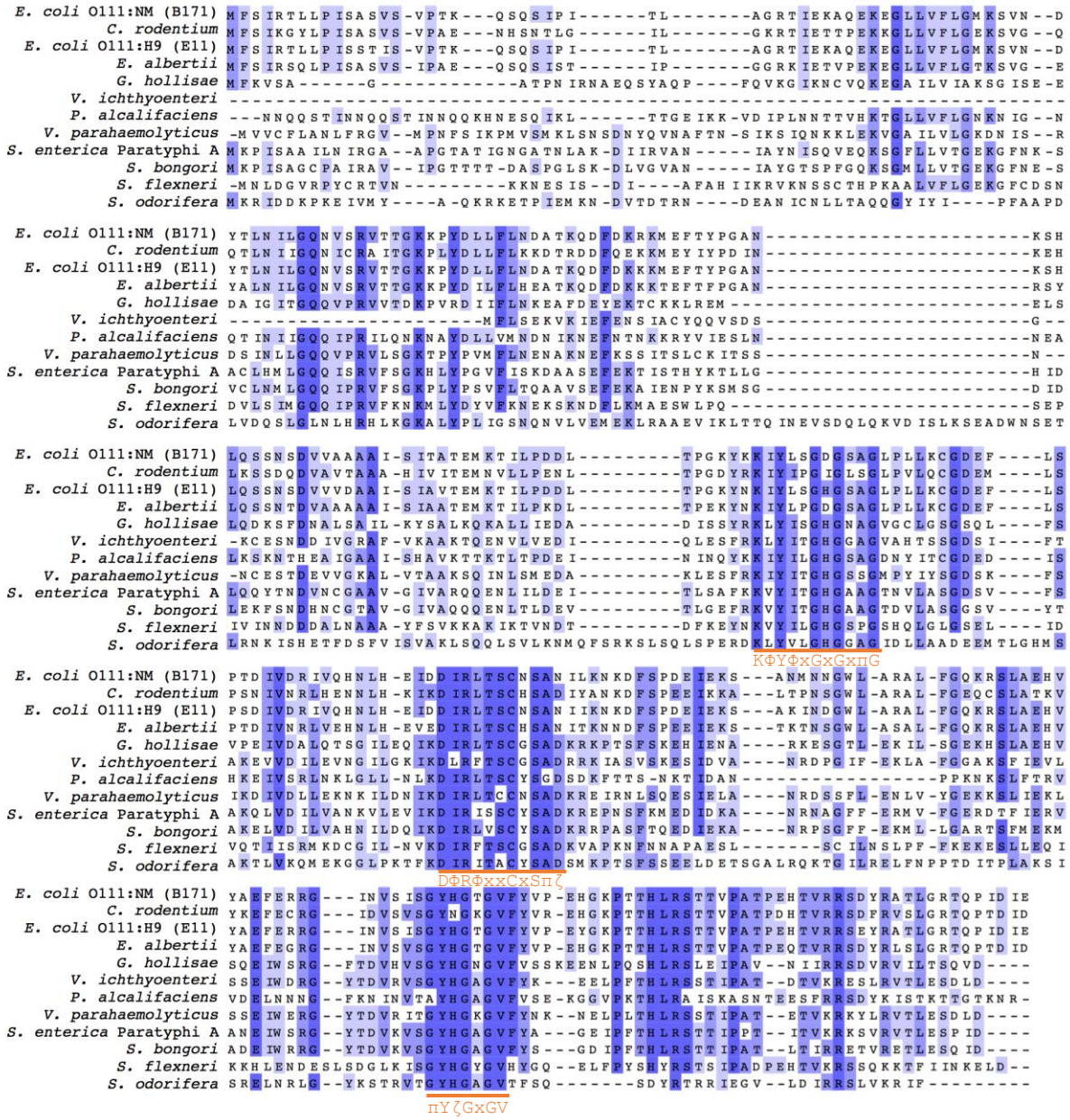


Figure 3.6 | Multiple sequence alignment of 12 representative EspS homologues
Globally aligned primary sequences of 12 representative EspS homologues with >30% homology to $EspS_{CR}$. Darker shading represents greater residue conservation. Highlighted in orange are motifs identified through alignment.

3.2.3 Functional analysis of *C. rodentium* effectors in mammalian cells

3.2.3.1 Transfected $EspS_{CR}$ and $EspS_{B171}$ localise to the mitochondria.

Effector localisation is an important indicator of its cellular function. As effector translocation relies on the recognition of an N-terminal secretion signal by the T3 apparatus, attempts were made to tag $EspS_{CR}$ on its C-terminus. A C-terminal chromosomal strep II (SII) tag was introduced onto *$espS_{CR}$* for infection of HeLa cells. Immunofluorescence staining against SII

strain produced no signal (not shown). Equally, no staining was observed when $EspS_{CR}$ was C-terminally tagged with 4xHA and introduced into *C. rodentium* on an IPTG-inducible plasmid, despite attempts to optimise IPTG concentration and infection duration (not shown).

In a final attempt to visualise EspS localisation following T3SS translocation, plasmids $EspS_{CR}$-4xHA, $EspS_{B171}$-4xHA or $EspS_{E11}$-4xHA under the control of the LacI promoter were introduced into EPEC E2348/69 (E69), which does not encode an EspS homologue. No HA-specific staining could be observed when infected HeLa cells were visualised by immunofluorescence, however induction of EspS homologue expression in E69 either from the naturally "leaky" promoter or with 0.1 mM IPTG resulted in markedly elongated E69 bacteria with a low rate of bacterial attachment (Figure 3.7). This could not be observed in E69 carrying the empty pSA10-HA plasmid, suggesting the phenomenon is EspS homologue-specific. Importantly, although all E69 strains were able to form pedestals, anti-HA staining was observed exclusively inside the bacterium or at the top of the pedestal, suggesting E69 cannot translocate overexpressed $EspS_{CR}$.

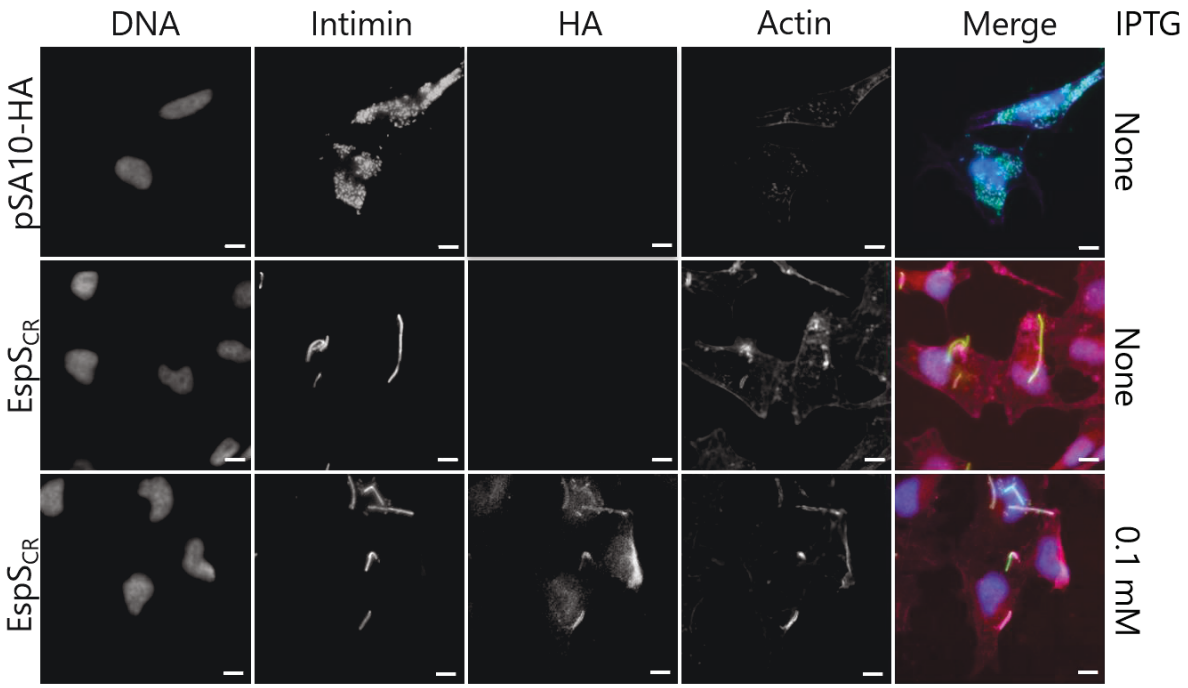


Figure 3.7 | Infection of HeLa cells with E69 expressing $EspS_{CR}$-HA
HeLa cells infected with EPEC E2348/69 carrying pSA10-HA or pSA10-$EspS_{CR}$-4xHA were induced for 3 h in DMEM ± 0.1 mM IPTG. Nucleic acids (DAPI; blue), EPEC E2348/69 intimin (green), the HA tag (red) and actin (phalloidin; magenta) were visualised by immunofluorescence staining. Scale bars: 10 µm. Representative images from 3 independent biological repeats.

To bypass the issues described, localisation of $EspS_{CR}$ was assayed by transfection. This was initially avoided as introducing effectors to mammalian cells without the T3SS can result in incorrect localisation. Nevertheless, a myc tag was cloned onto the N- and C-termini of $EspS_{CR}$ to be constitutively expressed by HeLa cells (Figure 3.8A). The transfection of myc-$EspS_{CR}$ resulted in diffuse, cytoplasmic localisation, whereas $EspS_{CR}$-myc transfection resulted in a more specific staining pattern. This indicates the N-terminal myc tag impedes recognition of an N-terminal signal sequence on $EspS_{CR}$ that is required for localisation. In order to determine the location of transfected $EspS_{CR}$-myc and $EspS_{B171}$-myc, transfected cells were probed with a panel of antibodies representing distinct subcellular compartments, including TOMM22 (mitochondria), Giantin (Golgi), Clathrin (post-Golgi vesicles), Snx-1 (pre-Golgi vesicles). Calnexin (ER), Eea1 (Early endosomes) or Rab7 (late endosomes). Of these, $EspS_{CR}$ and $EspS_{B171}$ exhibited the same localisation pattern as the mitochondrial marker TOMM22 (Figure 3.8B).

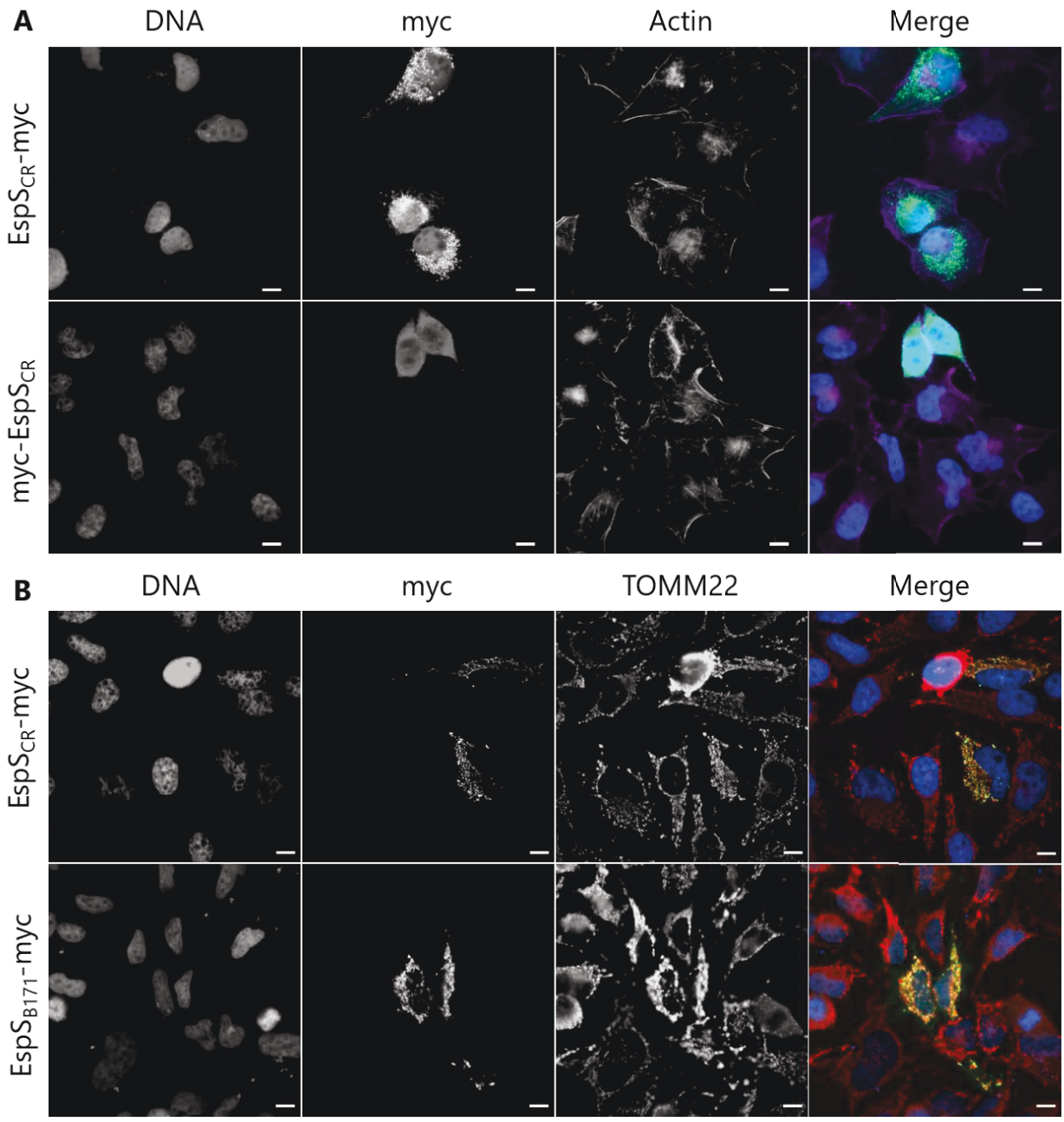


Figure 3.8 | Transfection of HeLa cells with EspS$_{CR}$ and EspS$_{B171}$

A HeLa cells transfected with pRK5-EspS$_{CR}$ with C- and N-terminal myc tags. Immunofluorescence staining used to visualise nucleic acids (DAPI; blue), myc (green), and actin (phalloidin; magenta).

B HeLa cells transfected with pRK5-EspS$_{CR}$-myc or pRK5-EspS$_{B171}$-myc. Immunofluorescence staining used to visualise nucleic acids (DAPI; blue), myc (green), and TOMM22 (mitochondria; red). Scale bars: 10 µm. Representative images from a minimum of 3 independent biological repeats.

3.2.3.2 NleN transfection results in diffuse cytoplasmic localisation

C. rodentium translocates NleN into host cells in a T3SS-dependent manner (Figure 3.2). To determine the subcellular localisation of NleN following translocation, *nleN* was subcloned with a C-terminal HA tag for bacterial translocation or a C-terminal myc tag for transfection, in a similar manner to EspS. As with EspS, no staining was observed following bacterial infection and probing for HA (not shown). Myc-NleN can be transfected with around 3% efficiency and exhibits a diffuse cytoplasmic localisation with no obvious impact on cell morphology (Figure 3.9). Staining is denser in perinuclear regions, and often assumes the shape of an unknown subcellular structure, which is not observed with the parent vector containing green fluorescent protein (GFP) (Figure 3.10 – bottom panel).

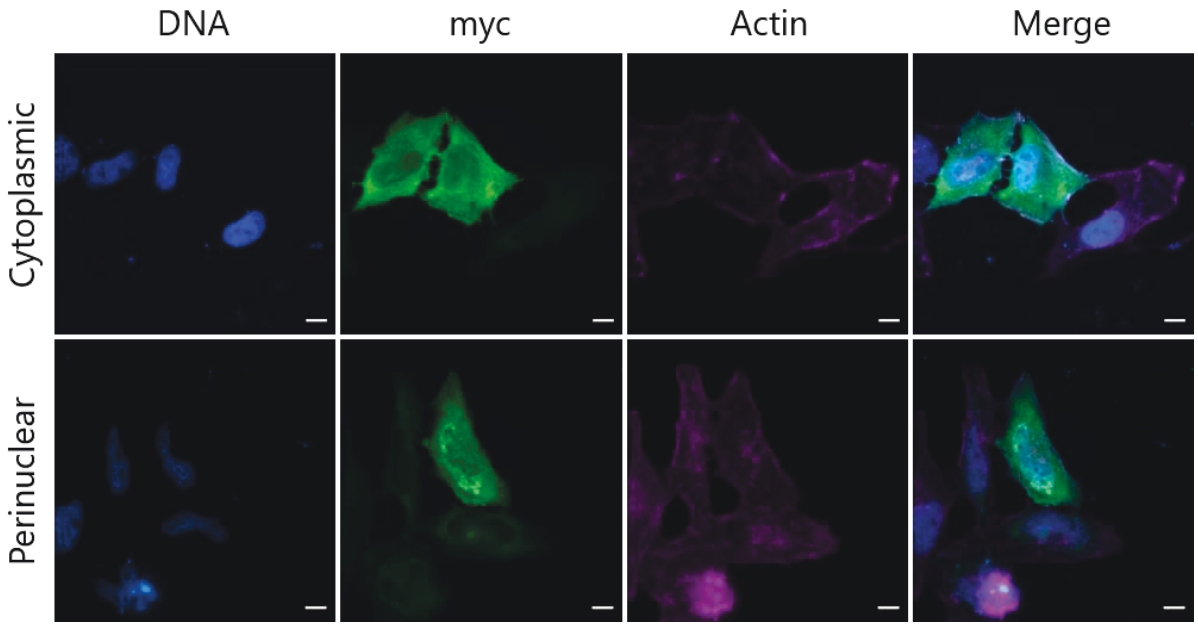


Figure 3.9 | Transfection of HeLa cells with NleN
HeLa cells transfected with pRK5-myc-NleN for 24 h and probed for the myc tag (green), DNA (DAPI; blue) actin (phalloidin; magenta) gives cytoplasmic and perinuclear staining patterns. Scale bars: 10 μm. Representative images from 5 independent biological repeats.

3.2.3.3 NleO transfection results in cell rounding

Bioinformatic analysis of the NleO peptide sequence revealed that NleO structural homologues interact with and subvert Rho GTPases (Figure 3.4) (Zhou et al., 2017). To test whether NleO fulfils a similar function, NleO was subcloned with an N-terminal FLAG tag and its localisation was assessed by transfection, as it could not be detected by immunofluorescence following C-terminal tagging and injectisome translocation. Regardless of the tag or plasmid use for transfection, ectopic NleO expression results in pronounced cell

rounding, shrinkage and gross loss of cytoskeletal structures (Figure 3.10). NleO transfection also induces apoptosis-like membrane blebbing as well as loss of nuclear integrity and displacement of nuclear contents, whereas GFP expression from the same plasmid does not induce any notable morphological changes.

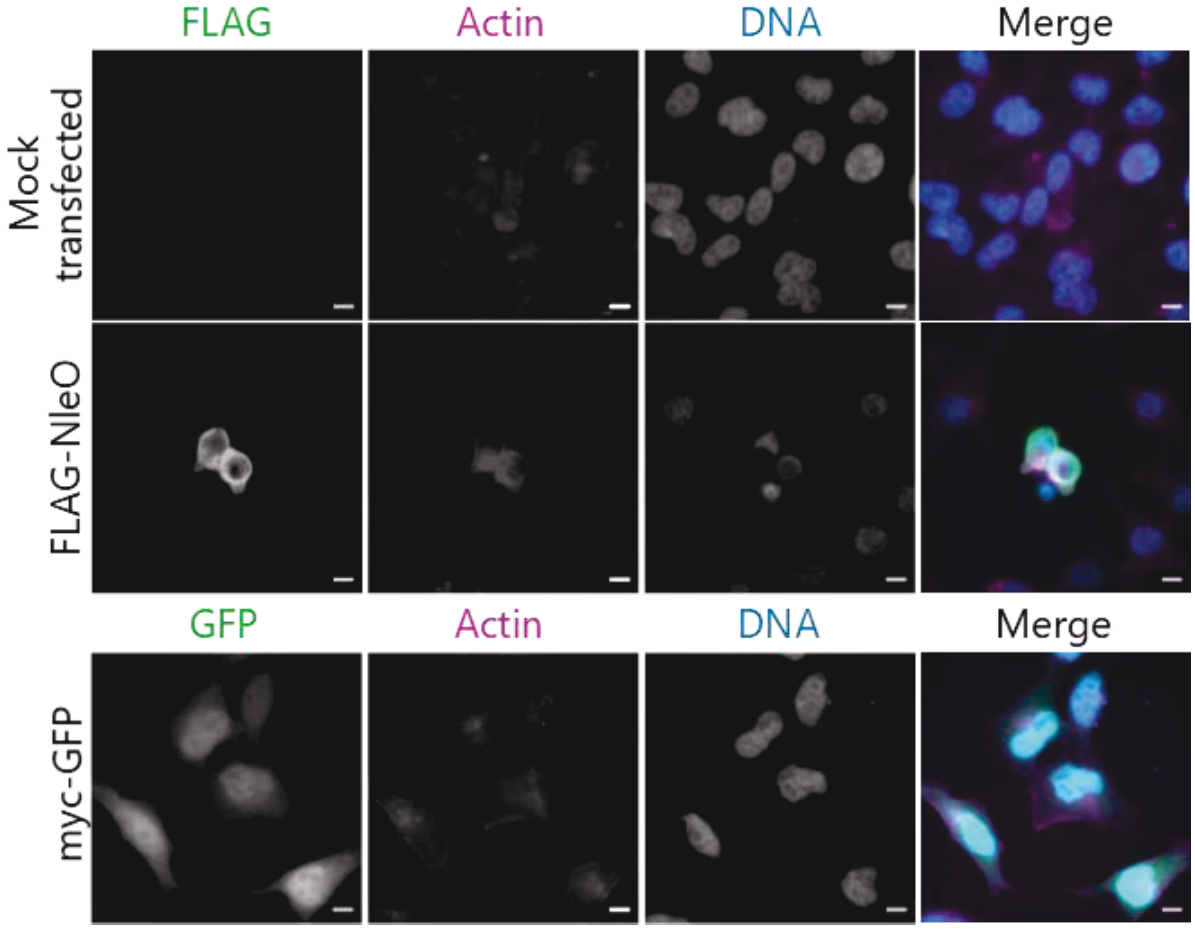


Figure 3.10 | Transfection of HeLa cells with NleO
HeLa cells transfected with pCDNA3-FLAG-NleO for 24 h and probed for the FLAG tag (green), actin (phalloidin; magenta) or nucleic acids (DAPI; blue). Scale bars: 10 µm. Representative images from 5 independent biological repeats.

As preliminary immunofluorescence staining suggested co-localisation of NleO and endogenous Rac1 (not shown), and the NleO structural prediction resembles the $MARTX_{vv}$ Rac1-inhibiting domain (Figure 3.4), the functional consequence of NleO and Rac1 overexpression was investigated. FLAG-NleO was co-transfected with myc-$Rac1^{WT}$ or its dominant positive synthetic variant $Rac1^{Q61L}$, which significantly enlarges the cell diameter and incites lamellipodia formation. Epifluorescence signals suggest NleO and Rac1 occupy the same location in the cytoplasm and cell cortex, but neither $Rac1^{WT}$ overexpression nor introduction of the dominant-positive myc-$Rac1^{Q61L}$ rescues NleO-induced cell rounding. These observations suggest an NleO:Rac1 interaction that could destabilise Rac1 (Figure 3.11).

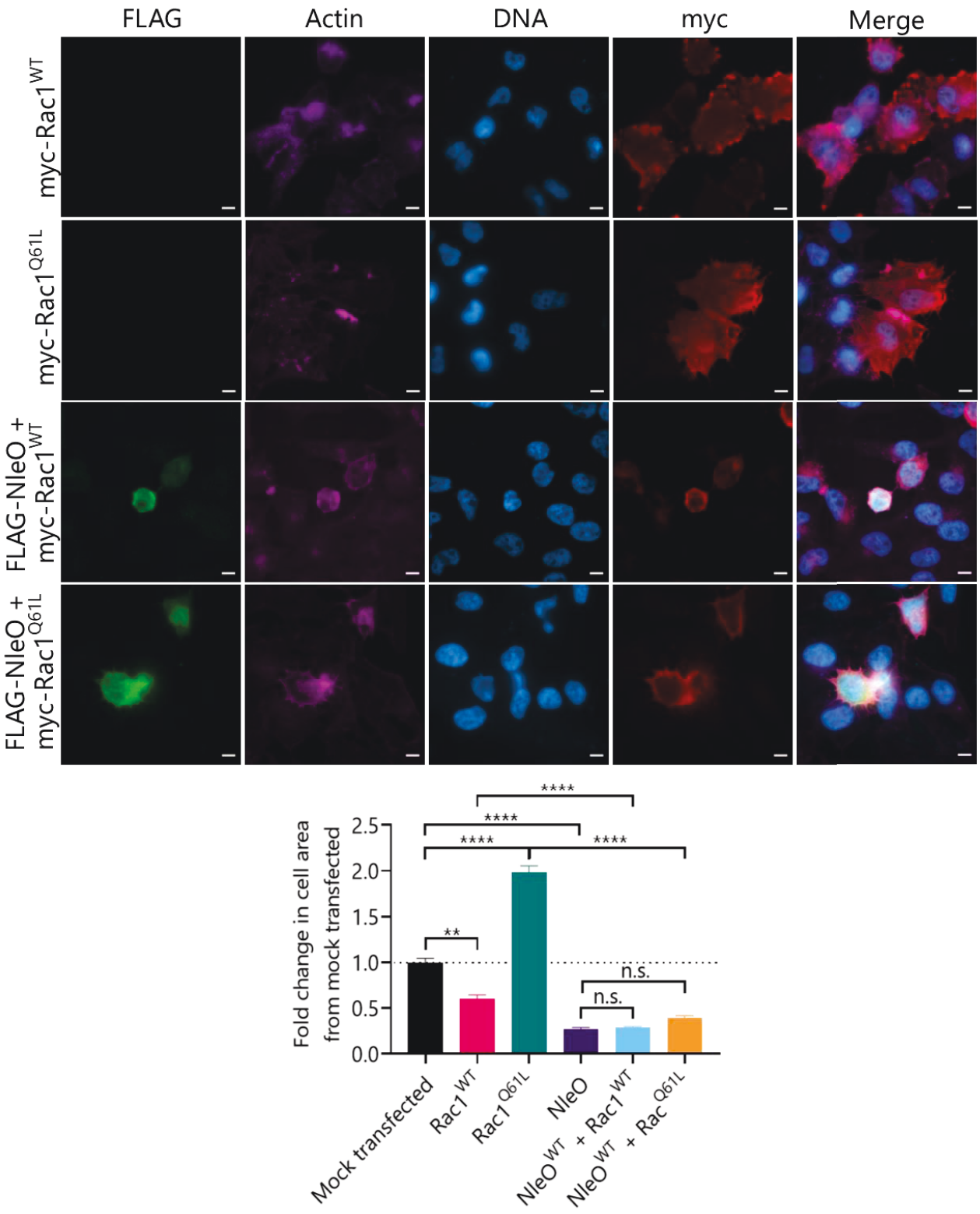


Figure 3.11 | Changes in cell area following co-transfection of NleO and Rac1
HeLa cells transfected with WT Rac1, dominant positive myc-Rac1^{Q61L}, FLAG-NleO, or both. Total area of transfected cells quantified by tracing the cell periphery in ZEN blue v2.3 is plotted below. Bars represent mean cell area expressed as a fold change from mock transfected cells across 4 biological repeats. Data analysed by Kruskal-Wallis test with Dunn's multiple comparison test. **= $p < 0.0021$; ****= $p < 0.0001$. Error bars represent SEM.

3.2.3.4 NleO catalytic residue Cys121 mediates Rac1 cleavage and cell rounding

As mentioned in §3.2.2.2, the conserved catalytic residue Cys2835 is present in NleO (Cys121), but NleO lacks the partner His residue. Closer inspection of the Phyre2 structure of NleO reveals Cys121 is ~6.6Å away from His20 (Figure 3.12A), which could serve as a surrogate proton donor. To investigate whether Cys121 mediates catalytic activity, an NleO^{C121A} point mutant was transfected into HeLa cells and cell rounding was assessed once more. Mutation of Cys121 abrogates NleO's cell rounding activity and results in mock-transfected-like cells that retain the ability to form lamellipodia and filopodia (Figure 3.12B). To independently confirm the NleO:Rac1 interaction, myc-Rac1 was co-immunoprecipitated (co-IP) from co-transfected HeLa cells lysates against a FLAG column (Figure 3.12C). Interestingly, co-transfection of FLAG-NleO and myc-Rac1, but not FLAG-NleO^{C121A} and myc-Rac1, results in the appearance of two myc-Rac1 products corresponding to the full-length protein and an ~11–12 kDa fragment. This indicates that NleO exhibits cysteine protease activity that facilitates the cleavage and inactivation of Rac1.

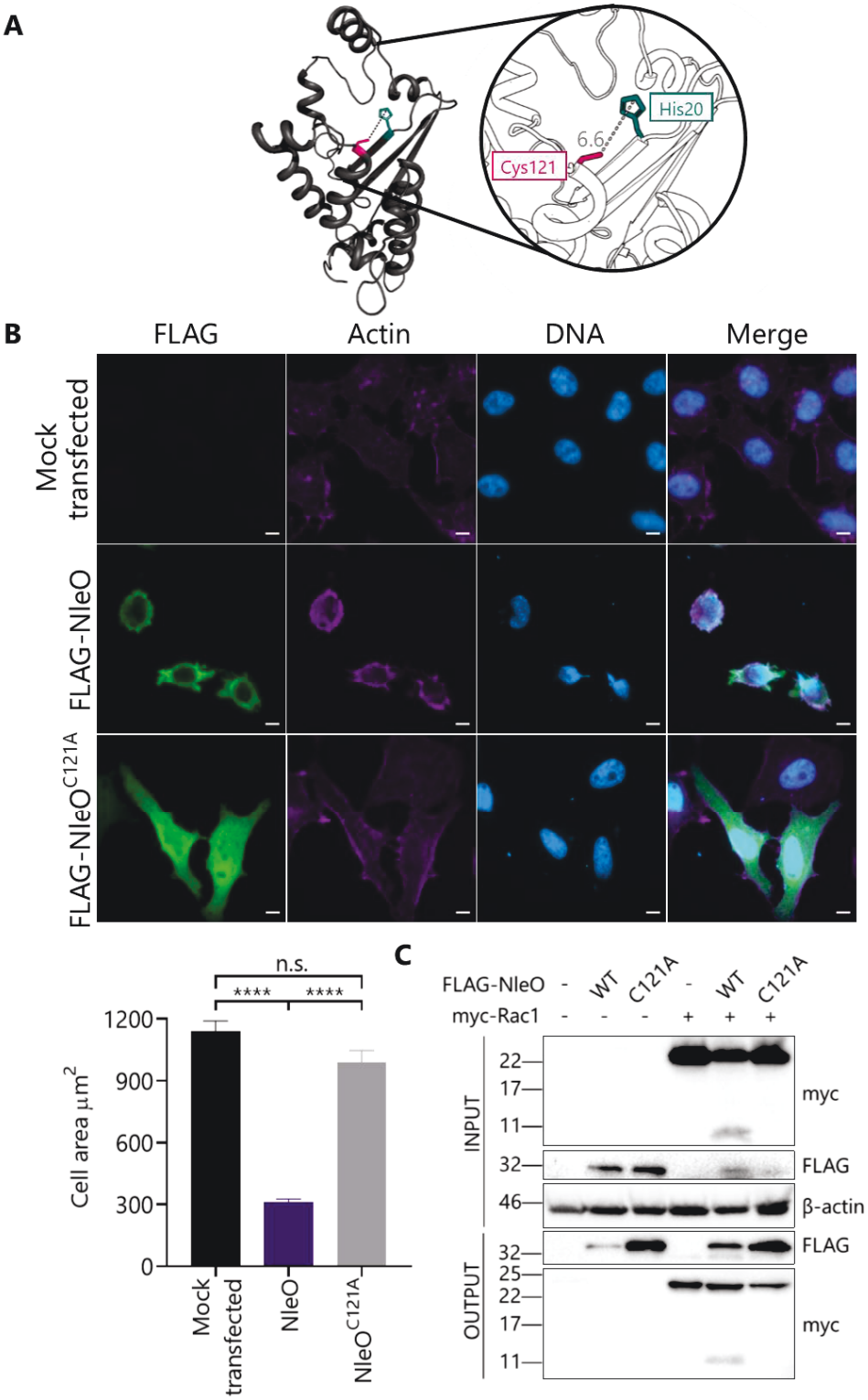


Figure 3.12 | NleO Cys121 is required for cell rounding and Rac1 cleavage

A Annotated Phyre2 structure of NleO highlighting the conserved catalytic residue Cys121 and a nearby His residue. **B** Immunofluorescence staining of HeLa cells transfected with FLAG-NleO or FLAG-NleO^{C121A}. Total area of transfected cells quantified are plotted below. Bars represent mean cell area across 3 biological repeats. Data analysed by Kruskal-Wallis test with Dunn's multiple comparison test. **** = $p < 0.0001$. Error bars represent SEM. **C** Co-IP of myc-Rac1 from HeLa cells co-transfected with FLAG-NleO or FLAG-NleO^{C121A}. Input samples were taken before incubating lysates with anti-FLAG beads. β-actin is used as a loading control.

3.2.4 Identifying interaction partners for $EspS_{CR}$

3.2.4.1 Investigating the toxicity of EspS homologues in *S. cerevisiae*.

Historically yeast 2 hybrid (Y2H) have been successfully employed to screen binding partners for T3 effector proteins (Allen-Vercoe et al., 2005; Pallett et al., 2014; Simpson et al., 2006). These assays rely on the expression of the effector protein by *Saccharomyces cerevisiae*. As $EspS_{CR}$ exhibited the most interesting subcellular localisation by transfection, this effector was carried forward. It has been demonstrated that expression of the EspS homologue VPA1380 is detrimental to yeast growth (Calder et al., 2014). This growth impediment is dependent on the putative catalytic dyad Cys^{195} and His^{154}. The toxicity of EspS homologues from *C. rodentium, V. parahaemolyticus, S. flexneri*, EPECs B171 and E11 was therefore assayed in *S. cerevisiae,* both to assess the feasibility of a Y2H screen and the possibility that VPA1380 and EspS from A/E pathogens share a catalytic function. Effectors were cloned under the glucose-repressible *GAL1* promoter in the pYES2 vector, which contains the selective marker *URA3* for uracil biosynthesis. The resulting constructs were transformed into the *URA3*-deficient *S. cerevisiae* strain BY4741 and grown on glucose (glc)- or galactose (gal)-supplemented SD agar. *S. cerevisiae* growth on SD-gal agar indicate that $EspS_{E11}$ and $EspS_{B171}$ inhibit yeast growth in a similar manner to VPA1380, while $EspS_{CR}$ and OspB are not toxic (Figure 3.13).

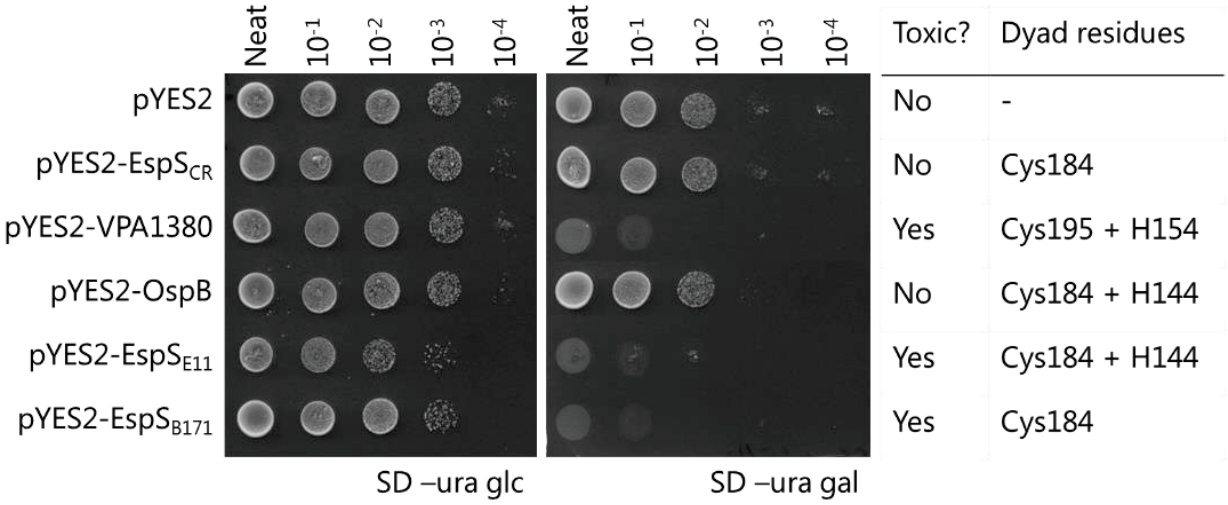
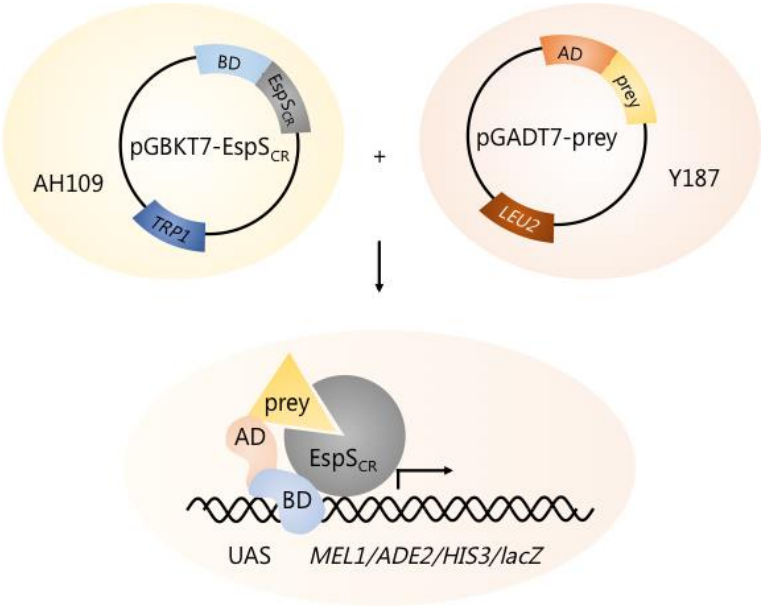


Figure 3.13 | Toxicity test of EspS homologues in *S. cerevisiae* BY4741
Serial dilutions of *S. cerevisiae* BY4741 on selective plates that suppress (SD –ura glc) or induce (SD –ura gal) transcription of the effector gene cloned into pYES2. The presence of the putative catalytic dyad in each effector is indicated on the right.

Additionally, contrary to what is known about VPA1380, the toxicity of the effectors is not correlated to the presence of the putative catalytic dyad.

3.2.4.2 $EspS_{CR}$ binds TRIAP1 in a Y2H system.

As $EspS_{CR}$ can be expressed in *S. cerevisiae* without any detriment to growth, a Y2H was conducted using $EspS_{CR}$ as bait against a mouse library. Identification of interacting partners is achieved through mating of the haploid bait strain (*S. cerevisiae* AH109 carrying pGBKT7-$EspS_{CR}$) and the haploid prey strains (*S. cerevisiae* Y187 carrying pGADT7-prey) resulting in diploid mated cells containing both plasmids. $EspS_{CR}$ was cloned with an N-terminal GAL4 DNA binding domain (BD), while prey proteins were cloned with an N-terminal GAL4 activation domain (AD). Contact of bait and prey proteins unites the BD and AD of GAL4 to allow the transcription of reporter genes under the control of the GAL4 upstream activation sequence (UAS): *MEL1*, *HIS3*, *ADE2* and *lacZ* (Schematic 8) (Fields and Song, 1989). *MEL1* and *lacZ* transcription results in secreted α-galactosidase and β-galactosidase, respectively, while HIS3 and ADE3 encode the enzymes required for histidine and adenine synthesis, respectively. Transcription of the reporter genes allows *S. cerevisiae* to grow on -His, -Ade agar supplemented with X-gal as a blue colony. Successful mating can be confirmed by plating on SD DDO (-Leu, -Trp) agar; mated cells that facilitate a bait-prey interaction will also grow as a blue colony on SD QDO (-Ade, -His, -Leu, -Trp) agar. Mating occurred between the bait and



Schematic 8 | Principle of the Y2H assay
Mating of the bait strain (*S. cerevisiae* AH109, left) and the prey strain (*S. cerevisiae* Y187, right) results in inheritance of both plasmids. Intracellular interaction of bait (BD-$EspS_{CR}$) and prey (AD-prey) fusion proteins allows the transcription of reporter genes under the control of the GAL4-UAS (*MEL1*, *ADE2*, *HIS3*/ and *lacZ*)

prey strains at 2.27% efficiency, resulting in 51 clones on QDO agar. After re-streaking three times, 47 colonies remained, 40 of which were blue. 39 plasmids were successfully extracted from yeast and sequenced to reveal the identity of 9 unique pGADT7-encoded prey proteins (Table 9).

Table 9 | Summary of putative interaction partners for $EspS_{CR}$ identified in a Y2H screen

Hit protein	Sequencing notes	Appearance frequency	Colony colour
PTN/Pleiotrophin/ HBNF/ NEGF1/ HB-GAM	24–58.6% sequence coverage of 18.8 kDa	12 total 5 unique	10 blue 2 Pink
TRIAP1/TP53-regulated inhibitor of apoptosis/ P53csv/ p53-inducible cell survival factor	88.5–90.4% sequence coverage of 8.8 kDa	7 total 5 unique	Blue
MED8/ Mediator of RNA pol II subunit 8/ Arc32	96–100% sequence coverage of 29 kDa	2 unique	Blue
TRAP1/TNF receptor associated protein/ Hsp75	46% sequence coverage of 80.1 kDa	1 unique	Blue
Karyopherin subunit alpha 5	18.7% sequence coverage of 37.3 kDa	1 unique	Blue
CALD1/Caldsemon	21.3% sequence coverage of 61.7 kDa	1 unique	Pink
GOLGA5/ Golgi subfamily a5/ Sumiko	35.8% sequence coverage of 82.2 kDa	1 unique	Pink
SLC4A7/ $NaHCO_3$ member 3	11.2% sequence coverage of 127 kDa	1 unique	Pink
SLC4A4/ $NaHCO_3$ cotransporter member 4	8.84% sequence coverage of 121.3 kDa	1 unique	Pink

Both pleiotrophin (PTN) and the TP53-regulated inhibitor of apoptosis (TRIAP1) appeared five unique times. 2 of 12 PTN-encoding colonies appeared pink, indicating weak activation of the reporter genes *ADE3* and *lacZ*. Additionally, PTN is a secreted growth factor; as $EspS_{CR}$ should only exist inside *C. rodentium* or inside the host cell, it is unlikely to encounter PTN during infection. As such, investigation of $EspS_{CR}$:PTN was not carried out. Instead, to confirm the interaction between $EspS_{CR}$ and TRIAP1, the full-length mouse cDNA was re-cloned into pGADT7 or pGBKT7, co-transformed into *S. cerevisiae* AH109 with pGADT7-$EspS_{CR}$/pGBKT7-$EspS_{CR}$ and plated on SD DDO or QDO (Figure 3.14A). All co-transformants were able to grow on SD DDO, confirming the carriage of both D2H plasmids. Expression of the *S. enterica* serovar

Typhi effector StoD, which is known to interact with ubiquitin (McDowell et al., 2019), was used as a positive control with pGADT7-ubiquitin. Co-transformation of empty plasmids or a single protein and an empty plasmid did not permit growth on QDO, whereas co-expression of both $EspS_{CR}$ and TRIAP1, irrespective of their vector backbone, facilitated growth. Further, the $EspS_{CR}$:TRIAP1 interaction was somewhat affected but not abolished by mutation of the putative catalytic residue Cys184 to alanine (Figure 3.14B). Together these results confirm that $EspS_{CR}$ interacts with TRIAP1 independently of the putative catalytic residue Cys184.

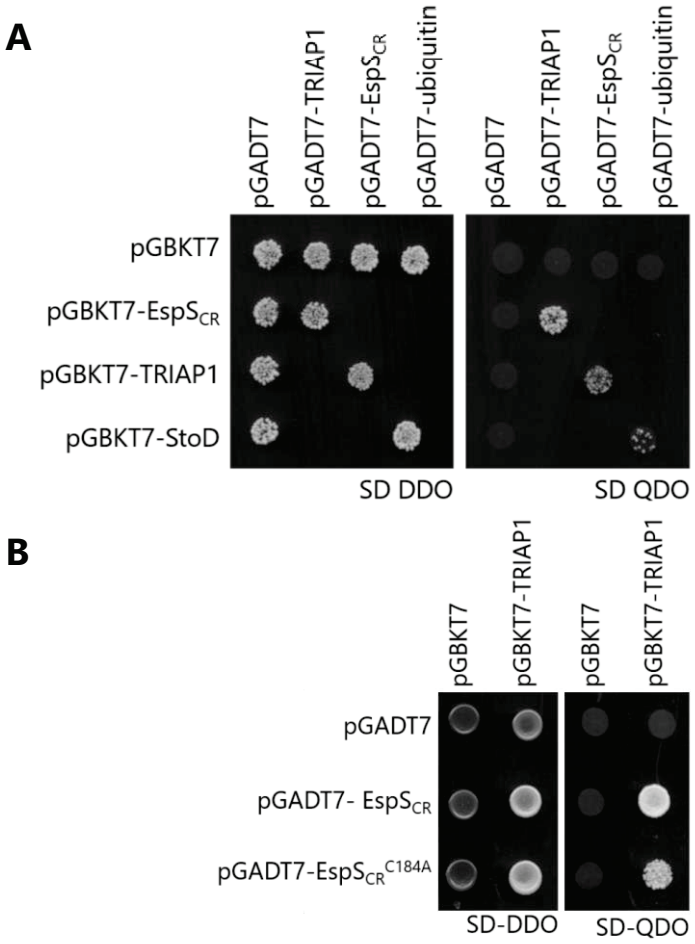


Figure 3.14 | Growth of auxotrophic *S. cerevisiae* expressing $EspS_{CR}$
S. cerevisiae AH109, which cannot synthesise Trp, Leu, Ade or His was co-transformed with a combination of bait and prey plasmids and plated on SD agar. pGBKT7 and pGADT7 confer Trp and Leu biosynthesis necessary for growth on SD DDO. A BD-bait and AD-prey fusion protein interaction allows transcription of Ade and His synthesis genes necessary for growth on SD QDO. Yeast co-transformed with WT $EspS_{CR}$ and TRIAP1 (**A**) or $EspS_{CR}^{C184A}$ and TRIAP1 (**B**) exhibit different growth kinetics.

3.2.5 Optimisation of recombinant $EspS_{CR}$ expression

To independently confirm the $EspS_{CR}$:TRIAP1 interaction, several *in vitro* approaches to recombinantly express $EspS_{CR}$ were tested. These are summarised in Table 10. Bacterial expression offers high protein yield and simpler optimisation protocols and was therefore undertaken first. $EspS_{CR}$ contains 5 Cys residues that may be disulphide bonded, therefore *E. coli* SHuffle cells were chosen for expression as they constitutively cytosolically express the disulphide bond isomerase and protein chaperone DsbC (Lobstein et al., 2012).

Table 10 | Summary of strategies for recombinant $EspS_{CR}$ expression

Expression system	Expression conditions	Conclusion
Bacterial		
E. coli BL21 pLysS *E. coli* BL21* *E. coli* SHuffle	Sequence modifications: • Truncated unstructured flexible N-terminal signal sequence (ΔN20) • Point mutation (C184A)	Full length and ΔN20 $EspS_{CR}$ constructs were more highly expressed than C184A.
	Plasmid construction • N-terminal or C-terminal 6His tag (pET28a) • N-terminal MBP tag (pMALX(E)) • N-terminal or C-terminal SII-6His tag (pOPINFS) • N-terminal or C-terminal GFP-6His tag (pOPINE-3C-eGFP)	
	Co-transformation and expression of pMALX(E)-MBP-TRIAP1	Co-transfection of TRIAP1-MBP did not improve $EspS_{CR}$ expression.
	Growth conditions, post-induction • 37°C, 2 h • 30°C, 4 h • 18°C, 16 h	More prominent SDS-PAGE band at 37°C for 2 h.
	Induction conditions (pET28a plasmids only) • Low 0.1 and 0.3 mM IPTG • Mid 0.5 mM IPTG • High 0.7, 0.8 and 1 mM IPTG	No dose-dependent increase in protein production with higher IPTG concentration at 37°C.
	Purification conditions • Neutral lysis buffer (Tris pH 7.9, 150 mM NaCl) • Reducing lysis buffer (8 M urea, 100 mM HEPES pH 8.5, 200 mM NaCl, 5 mM β-mercaptoethanol)	More protein could be retrieved under reducing conditions.
Yeast		
Pichia pastoris GS115	Strain construction • Genomic integration of $EspS_{CR}$ at *AOX1* locus using pPICZα-A system	No genomic integration despite success with another effector (EspO).
Mammalian		
HEK293T	Plasmid construction • N-terminal or C-terminal SII-6His tag (pOPINFS) • N-terminal or C-terminal GFP-6His tag (pOPINE-3C-eGFP)	N-terminal SII-6His tag expression only visible by Western blot; scaling up not financially justified.

Expression of full length, C-terminally His-tagged $EspS_{CR}$ in *E. coli* SHuffle cells with 0.7 mM IPTG induction and 2 h of growth at 37°C post-induction offered the most prominent band by Coomassie-stained SDS-PAGE. Despite this, the majority of $EspS_{CR}$ was present in the insoluble fraction after sonication and exhibited slower SDS-PAGE migration (Figure 3.15). SHuffle cells were therefore lysed under reducing conditions and $EspS_{CR}$ was allowed to refold on a Nickel-resin column for 2 h at 4°C. Presence of large quantities of slow-migrating protein in the flowthrough further supports the notion of an unfolded protein aggregate that is unable to form 6His-Ni^{2+} interactions with the column. The eluate content was separated by size exclusion chromatography (SEC) on a Superdex 200 10/300 GL column. According to column calibration data, a 32.3 kDa protein should elute around 16 ml, which corresponds to 80 mins at a flow-rate of 0.2 ml/min with 1 ml fraction collection, suggesting this proportion of recombinant $EspS_{CR}$ was monomeric. SDS-PAGE analysis of fractions confirmed presence of a protein with similar SDS-PAGE migration to $EspS_{CR}$ (25-40, Figure 3.15), however this band still migrates slower than its expected 32 kDa weight. Protein-containing fractions were

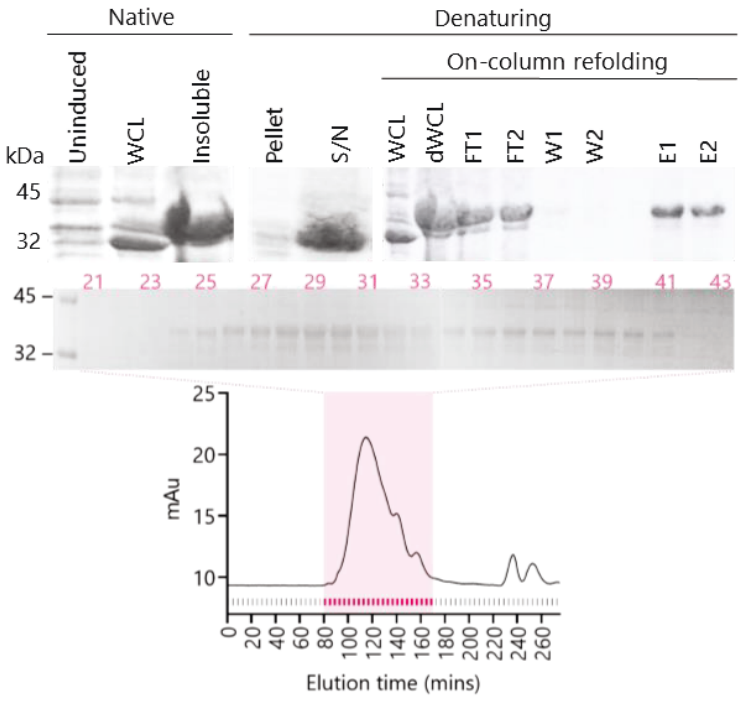


Figure 3.15 | Protein purification of $EspS_{CR}$ under native and reducing conditions
Coomassie blue-stained SDS-PAGE gel of purification of $EspS_{CR}$-6His expressed in *E. coli* SHuffle cells (top). (d)WCL: (denatured) whole cell lysate; FT: flowthrough; W: wash; E: elution. Pooled eluates from $EspS_{CR}$-6His extracted under reducing conditions were separated on a Superdex 200 10/300 GL column by size exclusion chromatography (bottom); fractions 21 to 43 were collected and analysed by SDS-PAGE (middle).

concentrated to around 0.1 mg/ml in an approximated 500 µL volume, which was of insufficient quantity and quality for NMR studies and bacterial expression was not pursued further.

3.2.5.1 Optimisation of recombinant mammalian $EspS_{CR}$ expression

Among the 30 T3SS components and effectors studied in the Frankel lab until 2017, only 8 proteins have been recombinantly purified from bacteria. We reasoned that as effectors are translocated as unfolded polypeptides through the T3SS filament (Radics et al., 2014), perhaps not all effectors are able to refold correctly without a eukaryotic host cell. A proposal was therefore accepted by the Diamond-based Instruct consortium (Oxford, UK) to design and test a vector suite for mammalian expression for EspS and three other *C. rodentium* effectors of interest (NleA, NleG and EspO). Vectors were built and transfected into HEK293T cells to screen for transfection efficiency, toxicity and solubility over 24 and 72 h (Figure 3.16). Consistent with bacterial expression attempts and transfection of HeLa cells with myc-tagged EspS, $EspS_{CR}$ expression efficiency was among the lowest of all effector fragments tested, regardless of the incubation time following transfection. While an N-terminal GFP tag did improve transfection efficiency at 24 h compared to a C-terminal tag, by 72 h aggregated GFP-EspS was observed, precluding the utility of this expression system (Figure 3.16A).This is reflected in HEK293T cell lysates, wherein expression of N-terminally Strep-II-tagged (SII) EspS is higher than EspS-SII after 24 h of transfection, but not enough to proceed to protein purification (Figure 3.16B). Additionally, it is unclear whether mammalian systems improved $EspS_{CR}$ folding, therefore scaling up this system was not financially or scientifically justified.

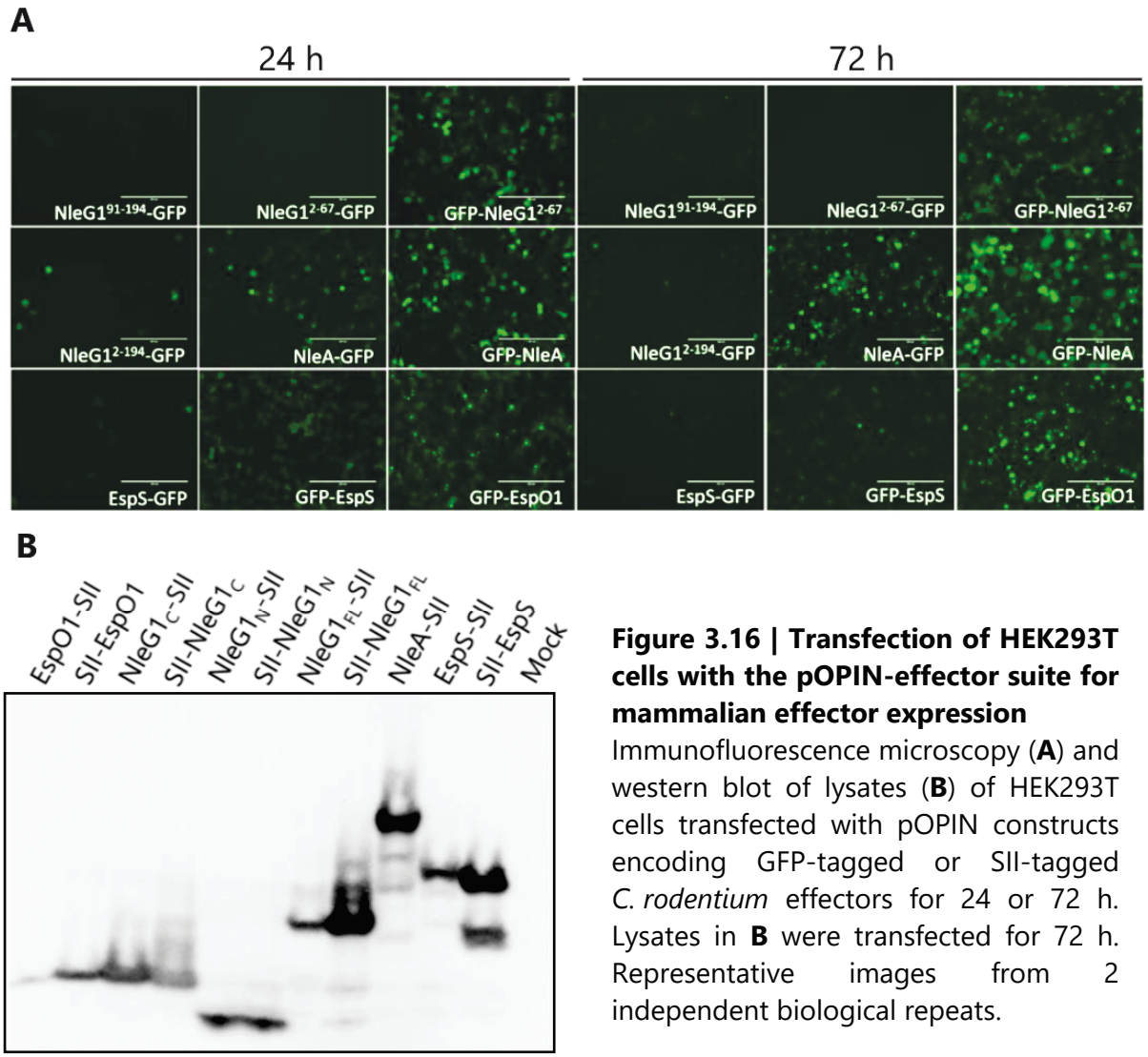


Figure 3.16 | Transfection of HEK293T cells with the pOPIN-effector suite for mammalian effector expression
Immunofluorescence microscopy (**A**) and western blot of lysates (**B**) of HEK293T cells transfected with pOPIN constructs encoding GFP-tagged or SII-tagged *C. rodentium* effectors for 24 or 72 h. Lysates in **B** were transfected for 72 h. Representative images from 2 independent biological repeats.

3.2.5.2 Native EspS tagging for immunoprecipitation

In a final attempt to confirm the EspS$_{CR}$-TRIAP1 interaction *in vitro*, a C-terminal SII-tag was introduced onto EspS in the *C. rodentium* chromosome to use as prey for immunoprecipitation. This approach had previously been employed for other effectors to confirm their interactors by peptide discovery MS (Ernest So, Frankel group, unpublished). As the resultant *C. rodentium* EspS-SII strain could be used to infect HeLa cells, EspS should be correctly folded upon translocation and able to localise correctly. Trial infections carried out to ascertain the efficiency of EspS pulldown indicated that EspS was largely present in the insoluble fraction (Figure 3.17A). Tir-SII, which is also membrane-associated, is also largely insoluble but could

be eluted with appreciable efficiency, unlike EspS-SII. A lysis buffer panel was therefore screened to improve $EspS_{CR}$ solubility for elution (Figure 3.17B). Consistent with the prediction that EspS is membrane-associated, buffers with high detergent content offered the most improved solubility, but not appreciably enough to warrant further processing for MS.

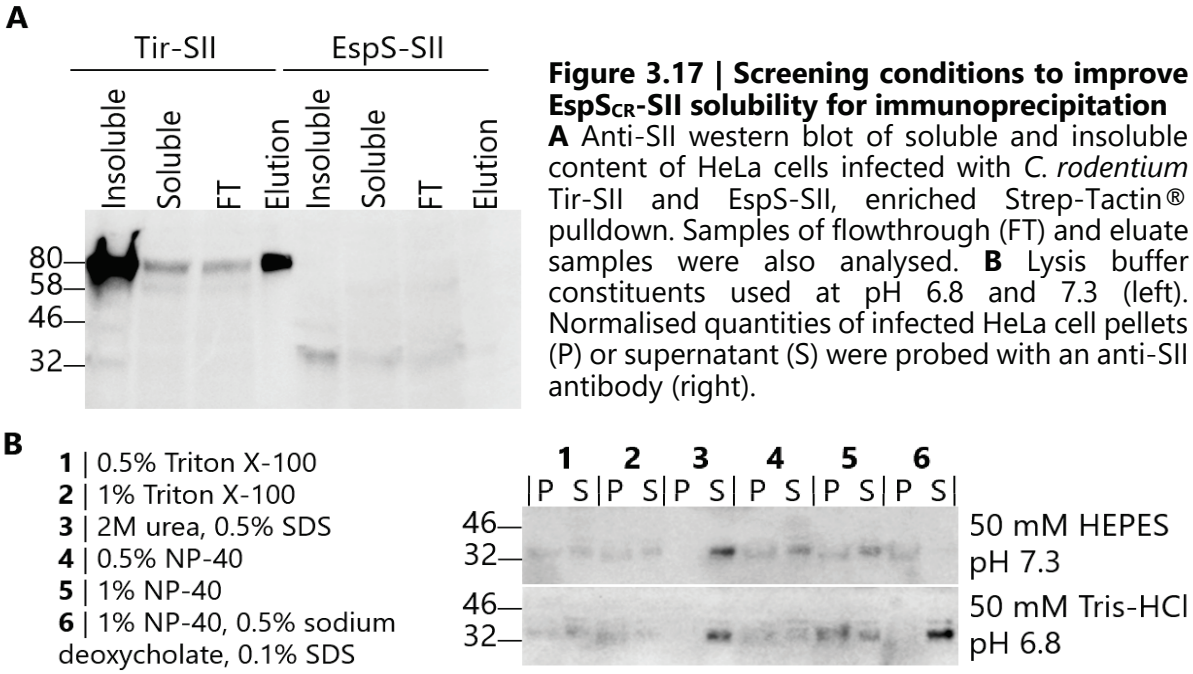


Figure 3.17 | Screening conditions to improve $EspS_{CR}$-SII solubility for immunoprecipitation
A Anti-SII western blot of soluble and insoluble content of HeLa cells infected with *C. rodentium* Tir-SII and EspS-SII, enriched Strep-Tactin® pulldown. Samples of flowthrough (FT) and eluate samples were also analysed. **B** Lysis buffer constituents used at pH 6.8 and 7.3 (left). Normalised quantities of infected HeLa cell pellets (P) or supernatant (S) were probed with an anti-SII antibody (right).

3.2.6 Characterising $EspS_{CR}$ function *in vitro*

3.2.6.1 Investigating the role of $EspS_{CR}$ in apoptosis

$EspS_{CR}$ is not permissive to recombinant purification, therefore its function was next assessed during infection of mammalian cells. Several effectors are coined pro- or anti-apoptotic based on their effect on mammalian cells, sometimes under overexpression conditions (Wong Fok Lung et al., 2014). As $EspS_{CR}$ binds the anti-apoptotic protein TRIAP1, it may have a role in apoptosis. To test this hypothesis, HeLa cells were infected with *C. rodentium* or treated with the pro-apoptotic compound staurosporine or the anti-apoptotic pan-caspase inhibitor zVAD, and apoptotic cell death markers were visualised by western blot. Additionally, HeLas were incubated with propidium iodide (PI), a fluorescing DNA intercalating dye that only emits light when cell membrane integrity is compromised, and fluorescence was monitored at 610 nm. PI uptake is commonly used to quantify cell death during necrotic forms of cell death such as pyroptosis and necroptosis, and in late stages of apoptosis, during which the membrane is

damaged. Consistent with unpublished observations of *C. rodentium* infection, no cell death was visually observed during early timepoints but membrane permeability increases following 8 h of infection (Figure 3.18A), suggesting a non-apoptotic form of death.

Probing lysates for cleavage and activation of the caspase-9, involved in intrinsic apoptosis, and poly (ADP-ribose) polymerase (PARP), a classical late apoptotic caspase substrate, confirms infection with *C. rodentium* does not induce classical intrinsic apoptosis *in vitro* (Figure 3.18B). To explore whether apoptosis was being inhibited by previously identified effectors with putative anti- (EspZ and NleF) or pro-apoptotic (EspF) roles, HeLa cells were infected with single-effector deletion mutants of the above, alongside the EspS-deficient strain. All of the mutants tested failed to induce caspase-9 or PARP cleavage. Together with PI uptake assays (Figure 3.18C), these data rule out the involvement of EspS in apoptosis or the described form of cell death observed in late-stage *C. rodentium* infection.

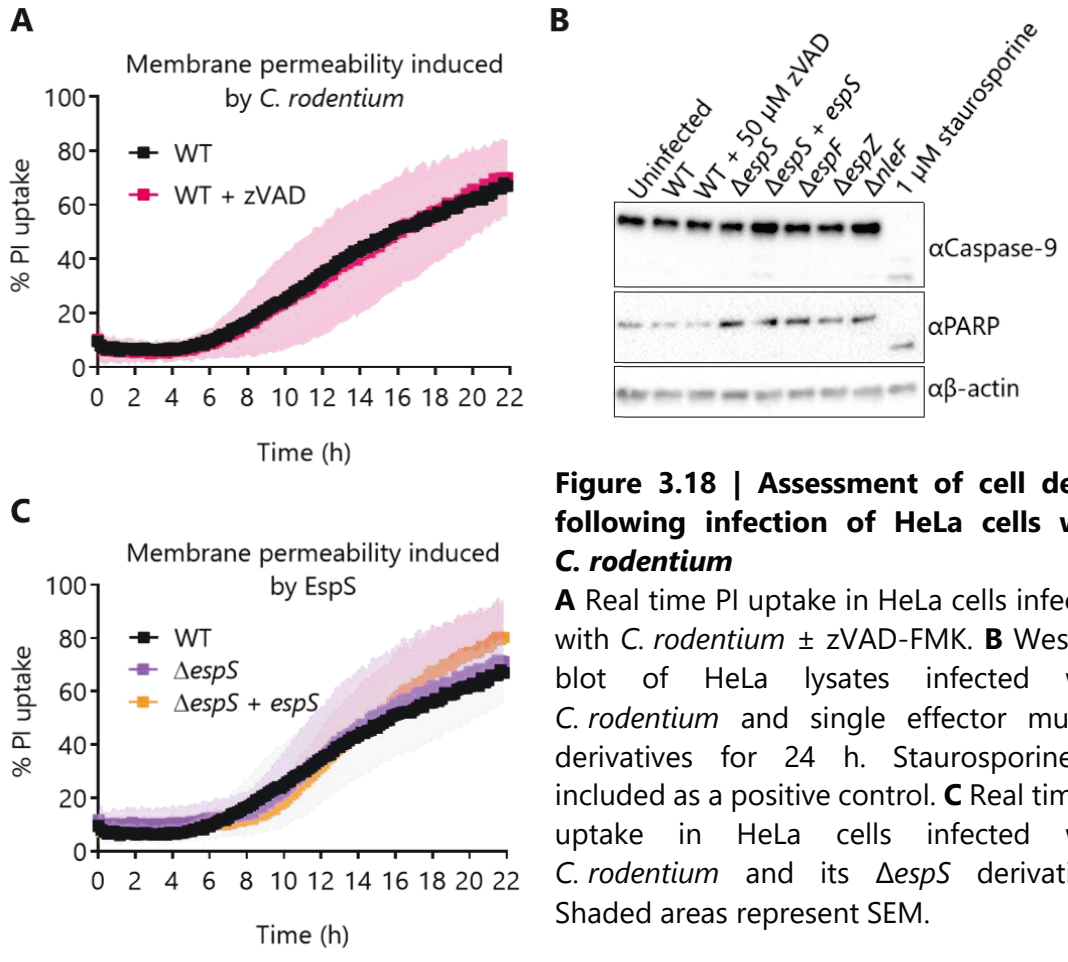


Figure 3.18 | Assessment of cell death following infection of HeLa cells with *C. rodentium*

A Real time PI uptake in HeLa cells infected with *C. rodentium* ± zVAD-FMK. **B** Western blot of HeLa lysates infected with *C. rodentium* and single effector mutant derivatives for 24 h. Staurosporine is included as a positive control. **C** Real time PI uptake in HeLa cells infected with *C. rodentium* and its Δ*espS* derivatives. Shaded areas represent SEM.

3.2.7 Investigating effector function during *in vivo* infection

3.2.7.1 *C. rodentium* Δ*nleN*, Δ*nleO* and Δ*espS* mutants colonise C57Bl/6 mice normally

Several effector proteins, such as Tir, NleA and EspZ, are required for efficient *C. rodentium* colonisation in mouse infection models (Deng et al., 2003; Mundy et al., 2004a). To ascertain whether deletion of NleN, NleO or EspS attenuates virulence, *C. rodentium*-resistant C57Bl/6 mice were inoculated with single deletion mutants and bacterial load was enumerated from faecal pellets until the peak of *C. rodentium* infection. Each mutant demonstrated comparable colonisation compared to their WT-infected cagemates (Figure 3.19–20). However, in contrast to NleN and NleO deletion mutants, there is a delay in *C. rodentium* Δ*espS* clearance at 8 days post-infection (d.p.i.), but this did not reach statistical significance (Figure 3.). To determine whether EspS is directly involved in clearance of *C. rodentium*, mice were observed until bacterial counts reached the limit of detection at 21 d.p.i.. *C. rodentium* Δ*espS* clearance is faster compared to WT, but this is not statistically significant. This denotes no direct involvement for these effectors in colonisation.

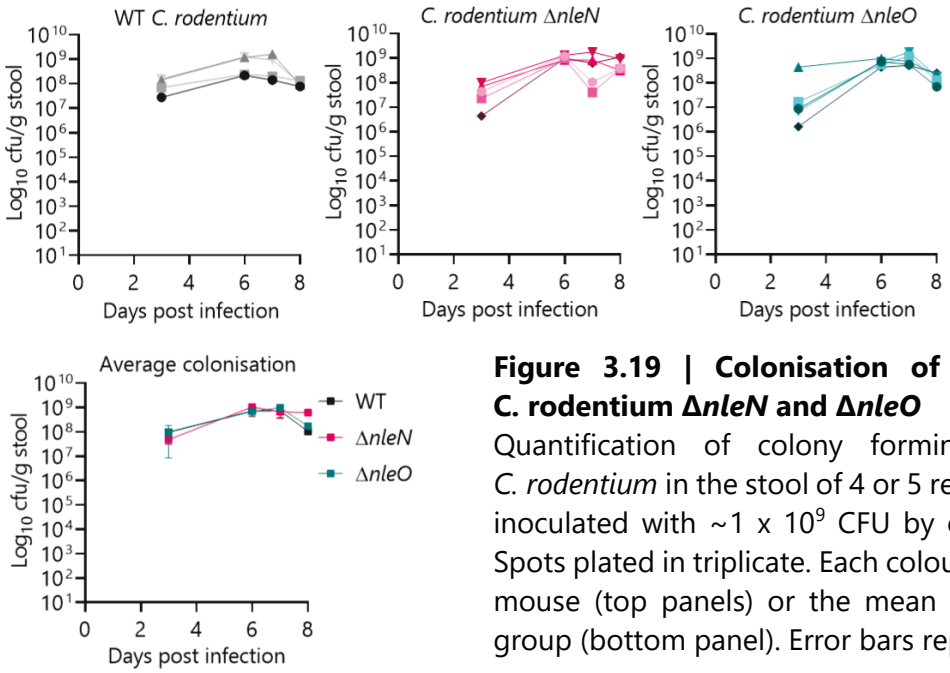


Figure 3.19 | Colonisation of C57Bl/6 mice by C. rodentium Δ*nleN* and Δ*nleO*

Quantification of colony forming units (CFU) of *C. rodentium* in the stool of 4 or 5 resistant C57Bl/6 mice inoculated with ~1 x 10^9 CFU by oral gavage (day 0). Spots plated in triplicate. Each colour represents a single mouse (top panels) or the mean of the experimental group (bottom panel). Error bars represent SEM.

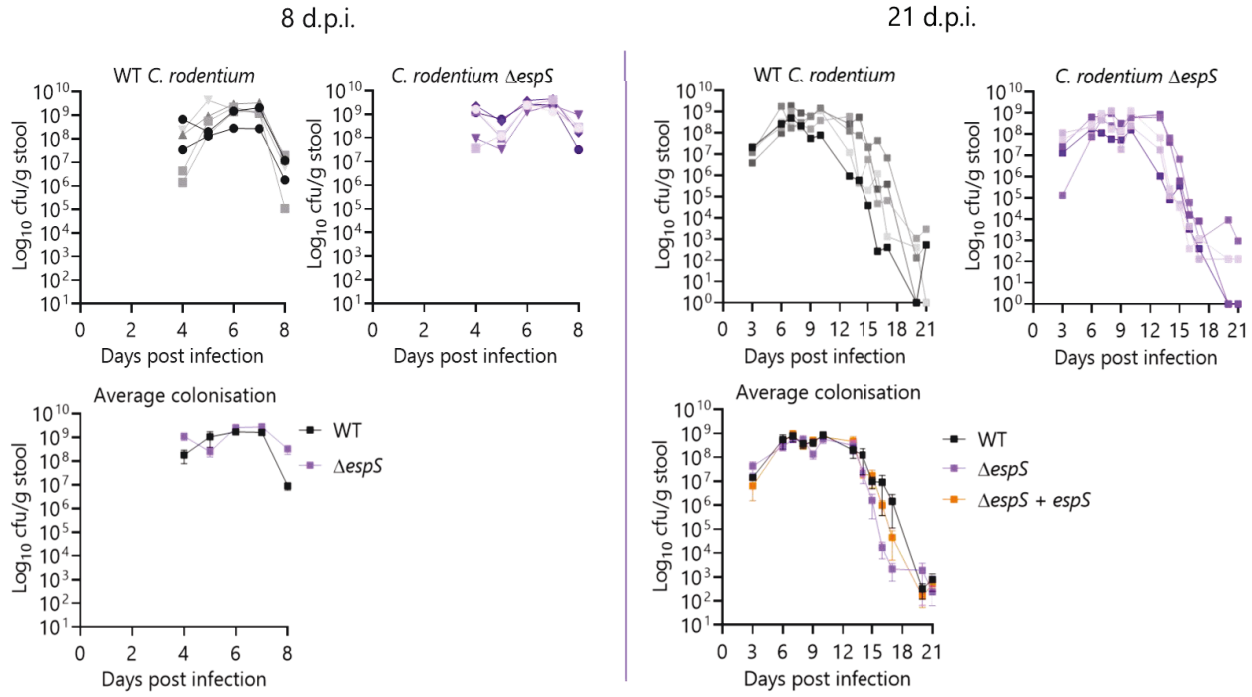


Figure 3.20 | Colonisation of C56Bl/6 mice with *C. rodentium* Δ*espS*

Quantification of CFU of *C. rodentium* in the stool of 5 C57Bl/6 mice inoculated with ~1 x 10^9 CFU by oral gavage at 8 and 21 days post infection (d.p.i.). Each colour represents a single mouse (top panels) or an average of the experimental group (bottom panels). Error bars represent SEM.

3.2.7.2 A *C. rodentium* Δ*espS* mutant induces exaggerated hyperplasia

A hallmark of *C. rodentium* infection is colonic crypt hyperplasia, characterised by an increased proportion of dividing enterocytes at the base of the crypt and subsequent crypt elongation (Luperchio *et al.*, 2000). To determine whether NleN, NleO or $EspS_{CR}$ have any effect on hyperplasia, 5 mm-long distal colon sections were removed from PBS-treated, WT-infected or *C. rodentium* single effector mutant-infected mice at 8 d.p.i. and subjected to haematoxylin and eosin (H&E) staining. As expected, crypts from WT-infected mice were consistently and significantly longer than PBS-treated mice (Figure 3.21A), while mice infected with either *C. rodentium* Δ*nleN* or Δ*nleO* exhibit reduced but not statistically significant intestinal hyperplasia (Figure 3.A). Interestingly, the average crypt lengths of *C. rodentium ΔespS*-treated mice were longer than WT-treated mice (Figure 3.21B), but this could not be complemented by chromosomal reintroduction of espS. These observations implicate $EspS_{CR}$ in the modulation of colonic crypt hyperplasia.

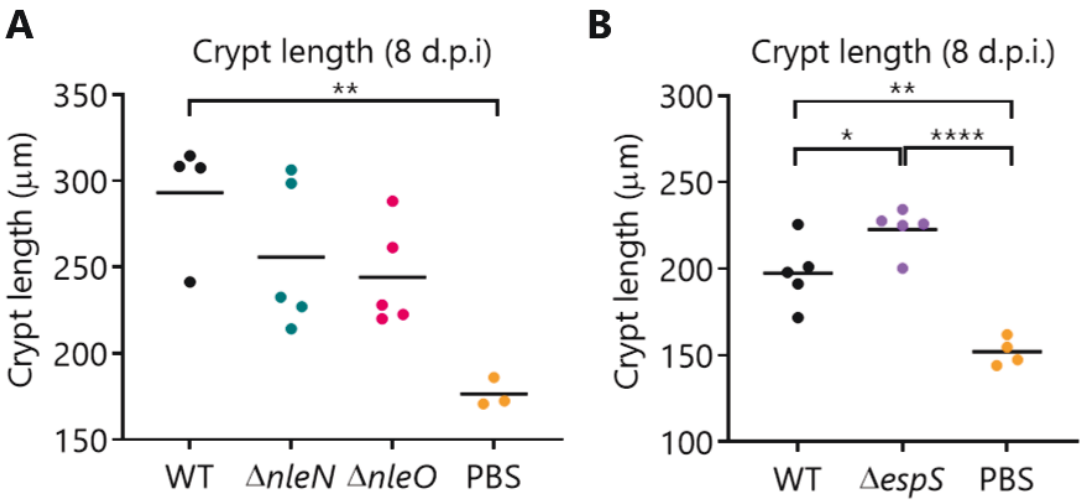


Figure 3.21 | Quantification of colonic crypt hyperplasia in *C. rodentium*-infected C56Bl/6 mice at 8 d.p.i.

Measurement of crypt lengths in sections obtained from C56Bl/6 mice inoculated with ~ 1 x 10^9 CFU *C. rodentium* at 8 d.p.i.. Each point represents average crypt length of an individual mouse. Bars represent group mean. Brown Forsythe and Welch ANOVA with Benjamini, Krieger and Yekutieli correction for multiple comparisons is applied. *= $p < 0.05$; **= $p < 0.002$; ****= $p < 0.0001$.

To assess whether the increased hyperplasia induced by *C. rodentium ΔespS* at 8 d.p.i. was due to increased mitotic activity at the base of the crypt, 5 mm distal colon sections were stained with anti-Ki67, a widely-used marker for cell division (Scholzen and Gerdes, 2000). 62% of *C. rodentium ΔespS*-infected crypts comprised actively dividing cells, compared to 55% in WT and 39% in the PBS-treated group (mean values) (Figure 3.22), indicating increased cell division in the absence of $EspS_{CR}$.

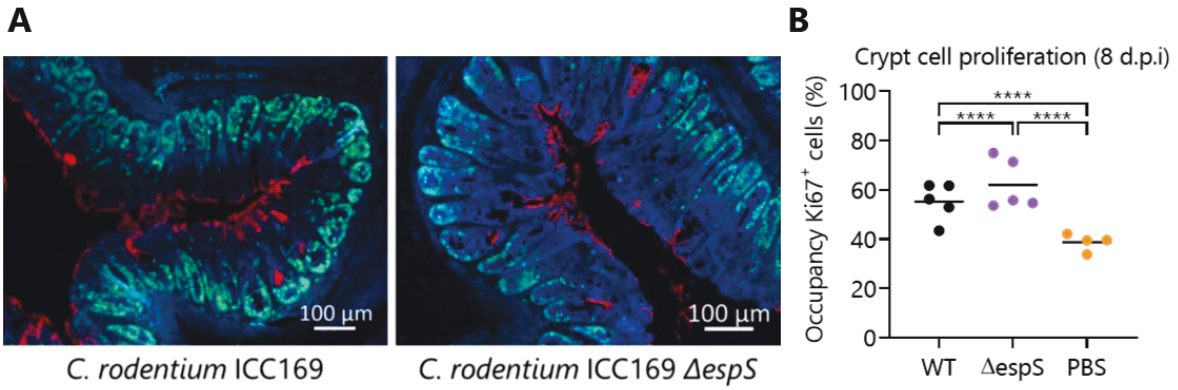


Figure 3.22 | Quantification of active proliferation in *C. rodentium* Δ*espS*-infected colons
A Immunofluorescence staining of actively dividing Ki67-positive cells (green) in distal colon sections obtained from C56Bl/6 mice inoculated with ~ 1 x 10^9 CFU *C. rodentium* at 8 d.p.i.. Nucleic acid (DAPI; blue) and *C. rodentium* (red) are also indicated. **B** Quantification of the percentage occupancy of each crypt with Ki67+ cells. Each point represents average crypt length of an individual mouse. Bars represent group mean. Brown Forsythe and Welch ANOVA with Benjamini, Krieger and Yekutieli correction for multiple comparisons is applied. ****= $p < 0.0001$.

3.2.7.3 Investigating the effect of $EspS_{CR}$ on cardiolipin synthesis *in vivo*.

TRIAP1 is essential for the import of phosphatidic acid (PA) across the mitochondrial outer membrane (Miliara et al., 2015; Watanabe et al., 2015). Through a series of enzymatic modifications, PA is converted into cardiolipin (CL) (Tatsuta and Langer, 2017). In order to probe whether $EspS_{CR}$ inhibits the TRIAP1-dependent PA transport, the relative abundance of CL was determined in IECs purified from C57Bl/6 mice infected with WT *C. rodentium* or an *ΔespS* mutant. IEC lipid fingerprints were obtained by MALDI-TOF MS and the relative abundance of a representative CL species was analysed. WT *C. rodentium* infection significantly increases CL abundance (Figure 3.23A) by 21 d.p.i. (Figure 3.23B). CL abundance is also consistently increased by the deletion of *espS* and reduced again in a complemented *C. rodentium* strain, but this does not reach statistical significance owing to high standard

deviations. As such, $EspS_{CR}$ has a subtle and long-lasting impact on TRIAP1-dependent CL synthesis *in vivo* that is not statistically significant.

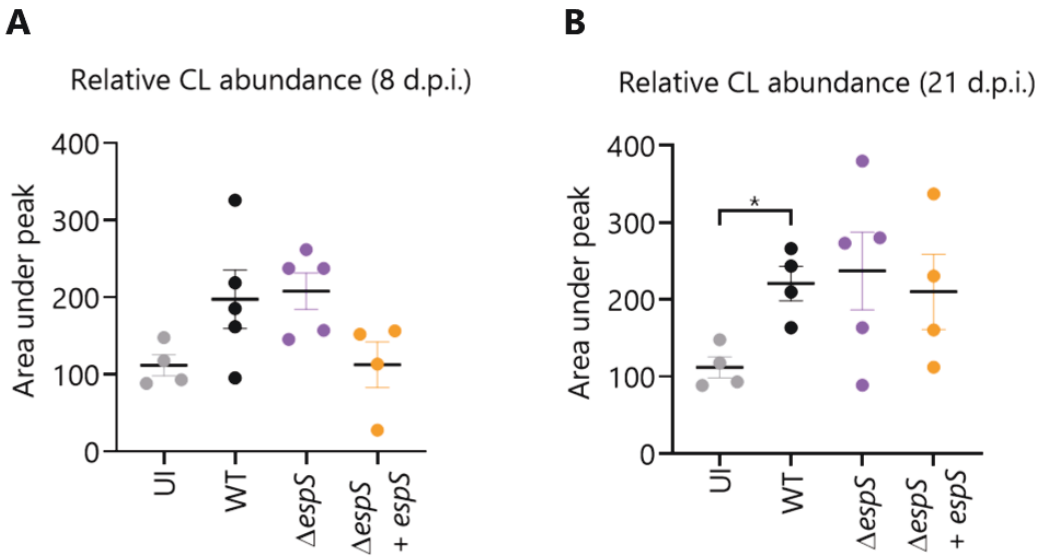
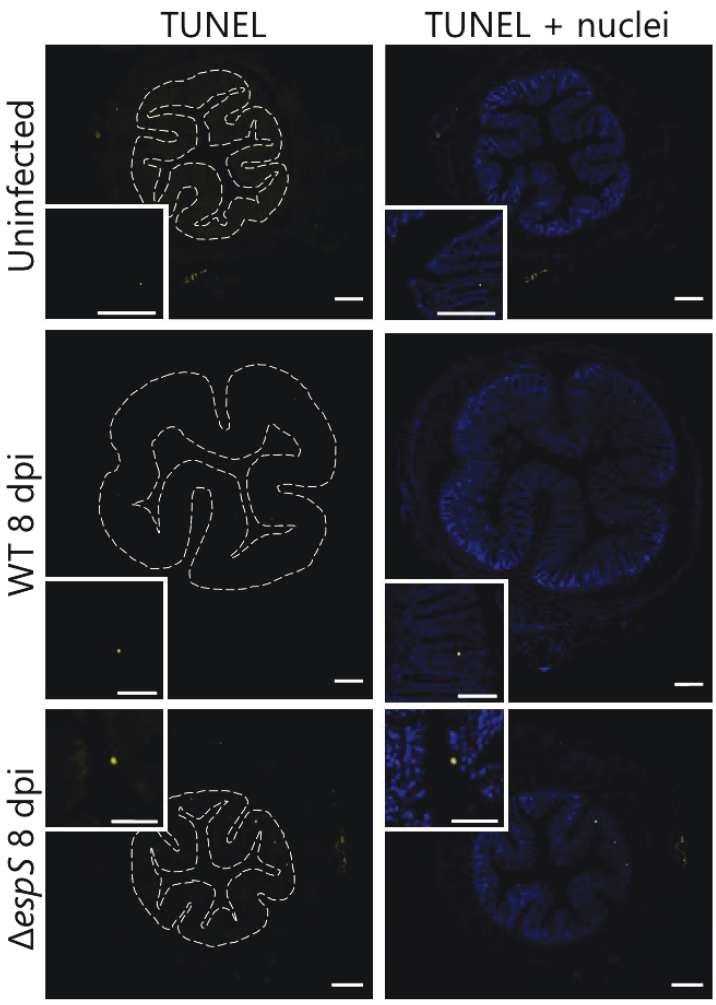


Figure 3.23 | Lipid composition of C57Bl/6 IECs following *C. rodentium* Δ*espS* infection
Quantification of the relative abundance of cardiolipin (CL) relative to lipids extracted from the purified intestinal epithelial cells (IECs) of *C. rodentium*-infected C57Bl/6 mice at 8 (**A**) and 21 (**B**) d.p.i.. Points represent individual mice with group mean indicated as a horizontal line; error bars represent SEM. Brown Forsythe and Welch ANOVA with Benjamini, Krieger and Yekutieli correction for multiple comparisons is applied. *= $p < 0.05$.

3.2.7.4 Investigating the effect of $EspS_{CR}$ on apoptosis *in vivo*.

CL accumulation prohibits release of cytochrome c and is therefore protective against intrinsic apoptosis (Potting et al., 2013; Zhang, 2019). To assess whether $EspS_{CR}$'s subtle modulation of lipid composition impacts apoptosis *in vivo*, sections of infected colon were probed for apoptotic cells using terminal deoxynucleotidyl transferase dUTP nick end labelling (TUNEL), wherein fluorescein-12-dUTP is incorporated at the 3′ hydroxyl group of fragmented DNA in apoptotic cells. The number of apoptotic $TUNEL^+$ cells were enumerated and normalised to crypt area to account for the increased cell number following *C. rodentium*-induced hyperplasia. As a positive control, sections were treated with DNase I to ensure the efficacy of TUNEL labelling (not shown). At both 8 and 21 d.p.i., neither WT nor *C. rodentium* Δ*espS*-infected colons had significantly more $TUNEL^+$ cells than uninfected sections (Figure 3.24), indicating C. rodentium infection does not trigger apoptotic death in the C57Bl/6 colon, independently of the presence of $EspS_{CR}$.



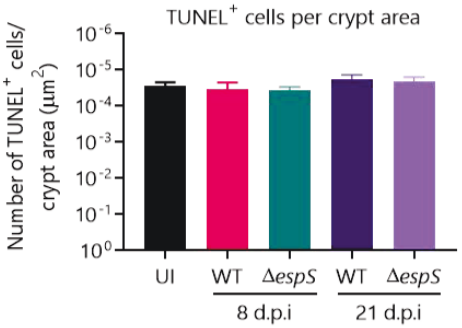


Figure 3.24 | Enumeration of apoptotic TUNEL⁺ cells in colonic tissue of *C. rodentium*-infected C57Bl/6 mice.
Visualisation and quantification of the mean number of apoptotic TUNEL-positive cells in distal colon sections from 5 *C. rodentium* infected C57Bl/6 mice (per group) at 8 and 21 d.p.i.. Nuclei (DAPI; blue) and TUNEL⁺ labelled cells (yellow) are indicated in magnified sections. Total section and magnified section scale bars: 500 µm (total section) and 20 µm (magnified section).

3.3 Discussion

Effector proteins manipulate an array of mammalian cell pathways to potentiate T3SS-mediated infection (Shenoy et al., 2018). As such, the merit in researching novel effectors is twofold: it offers both insight into bacterial infection biology, and exploration of novel protein functions. Presented here are two completely uncharacterised effectors, NleN and NleO, and one known effector, EspS, with no assigned function prior to this study (Petty et al., 2010).

The identification of novel effectors through machine learning techniques is well established (Arnold et al., 2009; Burstein et al., 2009, 2015; Hobbs et al., 2016; Lifshitz et al., 2014; Xue et al., 2019). Prior to this study, A/E effectors were identified manually through inspection of pathogenicity island genes, mutagenesis screening (Kanack et al., 2005; Mundy et al., 2004a), homology searches to other T3SS effectors in different species (Bulgin et al., 2009a; Petty et al., 2010), mRNA profiling during infection (Dahan et al., 2005), and through peptide discovery MS analysis of secreted proteins (Deng et al., 2010), among other techniques. However, machine learning algorithms had yet to be applied to A/E genomes. By ranking genes in the *C. rodentium* genome according to their likelihood of T3 secretion, manually curating hits by sequence length and biologically validating their translocation, we have confirmed two new *C. rodentium* effectors: NleN and NleO.

Identifying homology to known proteins is a common method of assigning function to uncharacterised effectors (Tobe et al., 2006). While NleO exhibits homology to the Rho-inactivation domain of MARTX toxins, the NleN ORF has suffered considerable mutational attrition, which can suggest a lack of evolutionary pressure on the *C. rodentium* genome to maintain a functional NleN. This is reflected by the lack of effect of *nleN* deletion in archetypal markers of *C. rodentium* intestinal pathology. On the other hand, while NleO has a negligible role in the development of crypt hyperplasia or the rate of intestinal colonisation, it has a pronounced effect on cell morphology that is consistent with its predicted function as an inactivator of Rho GTPases. Several A/E effectors activate Rho GTPases (i.e., Map, EspM, EspT, EspW) (Arbeloa et al., 2009; Bulgin et al., 2010, 2009b; Kenny and Jepson, 2000; Sandu et al., 2017) but *in vitro* infection with WT *C. rodentium* does not induce the same morphological changes as seen with dominant positive GTPase transfection. This is likely a result of the

antagonistic translocation Rho GTPase inactivating effectors, such as EspH (Dong et al., 2010) and now NleO.

To date, there are several reported methods of GTPase inactivation by bacterial virulence factors (Aktories, 2011): cleavage of the lipidation motifs to preclude membrane association (Burnaevskiy et al., 2013; Shao et al., 2003); GAP mimicry to stimulate GTPase activity (Wang et al., 2014b); competitive binding to impede of GEF association (Dong et al., 2010), and post-translational modification to impede GEF recognition (Chardin et al., 1989; Herrmann et al., 1998; Xu et al., 2014). Further to these mechanisms, the $MARTX_{VV}$ RID effector domain can inactivate Rho, Rac and Cdc42 by covalently acylating lysine residues in Rac1 to impede its correct localisation (Sheahan and Fullner Satchell, 2007; Zhou et al., 2017). Acylation is mediated by C2835 and H2895, which mirror C121 and His20 in the predicted tertiary structure of NleO, yet NleO's mechanism of action appears to be distinct from that of $MARTX_{VV}$; the dominant positive $Rac1^{Q61L}$ is not refractory to NleO, as NleO uses C121 to directly inactivate Rac1 through cleavage. Although NleO bares no sequence or structural resemblance to YopT, this Rac1 cleavage could also liberate Rac1 from plasma membranes to preclude its function. However, overexpression of Cdc42 was able to rescue YopT-induced toxicity in an *S. cerevisiae* system (Shao et al., 2002), but neither $Rac1^{WT}$ nor ^{Q61L} overexpression compensate for NleO-induced cell rounding. Additionally, YopT cleaves Rac1 immediately upstream of the extreme C-terminal prenylation site (Shao et al., 2003), but myc-Rac1 releases a ~ 12 kDa fragment from its 21 kDa entirety when exposed to NleO, suggesting the Rac1 cleavage site targeted by NleO is nearer to the N-terminus. Together, these two observations denote that NleO could represent a novel class of Rho GTPase modifying enzymes. Follow up experiments should therefore address the cleavage site of Rac1 and its prenylation state, in addition to investigating whether NleO can also target all three Rho GTPase family proteins, and whether His20 indeed completes the catalytic dyad.

Unlike NleO homologues, EspS homologues did not immediately reveal any potential interaction partners for EspS. EspS homologues from enteric pathogens have differing levels of toxicity in yeast expression systems. Additionally, these differences are not accounted for by the presence of the toxicity-inducing catalytic dyad identified in VPA1380 identified through homology to another MARTX from *V. cholerae* (Calder et al., 2014). This could indicate

that either these effectors do not function as cysteine proteases, and as such the presence of the dyad is not important for toxicity, or that each homologue has a different binding mammalian partner, as is the case with other A/E effector proteins of the same family (El Qaidi et al., 2017). Of note, while the KΦYΦxGxGxπG and DΦRΦxxCxSπζ motifs identified in EspS homologues correspond to the residues surrounding the putative catalytic dyad, there is no indication of the function of the C-terminal πYζGxGV motif. This could represent a host protein binding domain that directs any putative enzymatic function of EspS, or a stabilisation interface in the tertiary structure of mature EspS.

The conservation of EspS homologues among human isolates of EPEC and EHEC reveals several aspects of EspS biology. First, further to the E11 and B171 *espS* genes identified in this study, Buss et al., note that *espS* is present in 34 of the 68 (47%) human pathogenic *E. coli* tested (Buss et al., 2009). The *Shigella spp*. EspS homologues (OspBs) are identical to one another and other EspS homologues from *S*. enterica isolates share a minimum of 97.5% identity, while the percentage identity shared by *E. coli* homologues is 80.7%. Together with the sporadic prevalence of the *espS* among isolates, this could reflect the genomic instability of clinical EPEC and EHEC isolates, as well as the importance of EspS to the pathogenicity of these strains. Indeed, $EspS_{EPEC}$ is significantly more associated with asymptomatic or non-lethal infections in humans (Donnenberg et al., 2015). Conversely, while deletion of *espS* from the *C. rodentium* genome does not impact colonisation or clearance of the pathogen in a resistant C56Bl/6 mouse model, in a susceptible C3H/HeJ mouse model EspS is required for full lethality (Deng et al., 2010), and is highly transcribed during *C. rodentium* infection to modulate colonic crypt hyperplasia (Connolly et al., 2018). While $EspS_{EPEC}$ has integrated into human *E. coli* genomes at inconsistent loci, it shares an operon with the critical effector NleA in *C. rodentium* (Deng et al., 2010; Petty et al., 2010). It is plausible that its genomic location and therefore its transcriptional regulation is linked to its importance during infection.

The localisation of effector proteins reflects both the subcellular compartment they manipulate and the host proteins they interact with. The cytoplasmic localisation of NleN is unsurprising given that it represents a truncated A/E effector with no recognisable localisation sequences or binding motifs, but the observation that NleN is frequently perinuclear is not readily explicable. Confocal microscopy may resolve whether NleN is also excluded from the nucleus,

or whether it is able to colocalise with a host factor in the nuclear envelope. Conversely, the diffuse and mitochondrial localisations of NleO and EspS respectively are unsurprising given their putative interaction partners. Notably, this is the first report of an EspS family effectors localising to the mitochondria; it joins several other mitochondrial-associated effectors, including Map (Kenny and Jepson, 2000; Papatheodorou et al., 2006), EspJ (Kurushima et al., 2010), EspZ (Shames et al., 2011b), EspF (Nagai et al., 2005; Nougayrède and Donnenberg, 2004), and NleF (Pallett et al., 2014), although of these only Map and EspF have a biochemically confirmed N-terminal mitochondrial localisation signal. Previously the aEPEC EspS homologue Ibe was observed at the base of pedestals and is membrane-associated (Buss et al., 2009). The persistent insolubility of $EspS_{CR}$ may indicate that $EspS_{CR}$ is also membrane-associated, but with mitochondrial membranes where it can interact with TRIAP1.

TRIAP1 is a 67 aa cell survival factor with several functions for $EspS_{CR}$ to exploit. In the inner mitochondrial space, TRIAP1 associates with PRELI and PRELID3b to transport phosphatidic acid (PA) and phosphatidylserine, respectively, across the outer mitochondrial membrane (Miliara et al., 2019). PA is a precursor for CL synthesis, which in turn prevents the release of cytochrome c from the inner membrane space to the cytosol (Potting et al., 2013). TRIAP1 also interacts with APAF1 via HSP70, precluding apoptosome complex formation with cytochrome c and pro-caspase-9 to incite intrinsic apoptosis (Park and Nakamura, 2005). Lastly, TRIAP1 suppresses p21 expression, resulting in increased cell cycle progression (Andrysik et al., 2013). TRIAP1 is proposed to interact with its binding partners via a conserved hydrophobic strip of aromatic residues (Miliara et al., 2015, 2019); it is unknown if the $EspS_{CR}$:TRIAP1 interaction also occurs via this surface and therefore prevents TRIAP1 from interacting with its native partners.

Colonic crypt hyperplasia is significantly exaggerated in the absence of $EspS_{CR}$ (Connolly et al., 2018). It is conceivable that during WT *C. rodentium* infection, the $EspS_{CR}$:TRIAP1 interaction prohibits TRIAP1-dependent p21 expression and therefore supresses augmented hyperplasia. This is comparable to the incidence of TRIAP1 overexpression in cancers through loss of inhibitory miRNAs (Felix et al., 2009; Fook-Alves et al., 2016; Ketteler et al., 2019; Li et al., 2016; Liu et al., 2017a; Luo et al., 2019; Ming et al., 2019; Shen et al., 2018; Siu et al., 2014; Zhang et al., 2019), making TRIAP1 a desirable drug target (Adams et al., 2015; Luo et al., 2019; Zhang, 2019). Conversely, as there is no significant difference in the relative abundance of CL between

C. rodentium WT and Δ*espS*-infected enterocytes, the $EspS_{CR}$:TRIAP1 interaction may not preclude TRIAP1:PRELI interacting, and therefore PA import is unaffected. The final scenario is one in which EspS does not affect TRIAP1 function at all, but EspS simply binds TRIAP1 to anchor itself in the mitochondrial network and exert its activity on another target protein.

Chapter 4

New roles for old effectors

4 New roles for old effectors

4.1 Introduction

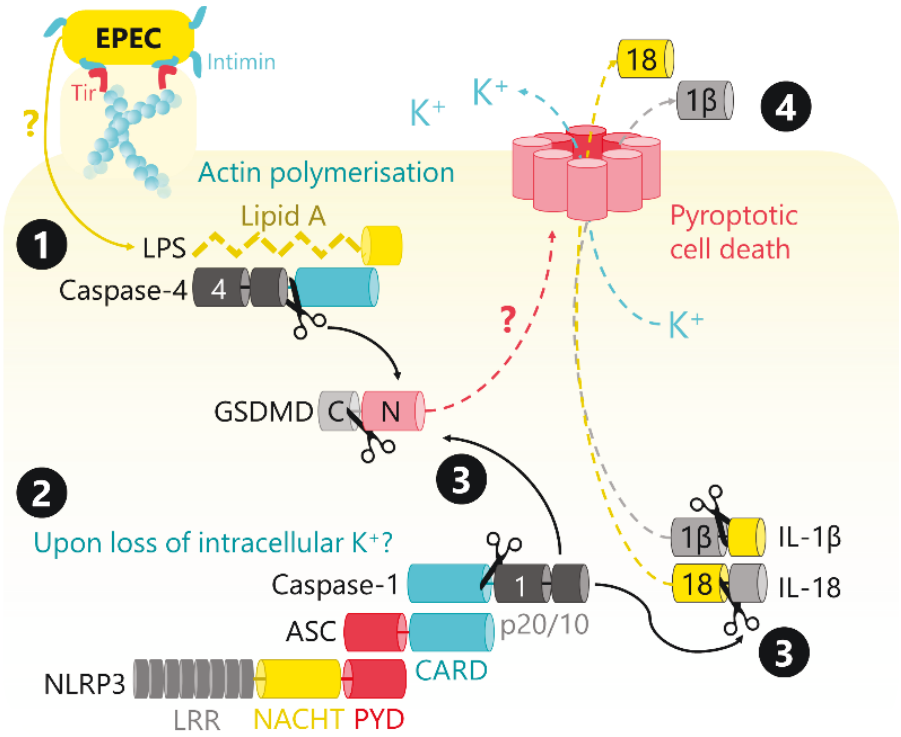
T3 effector biology is typically conducted in a 'bottom-up' fashion as exemplified in §3, where research begins with a DNA or protein sequence and ends with a validated phenotype. However, a 'top-down' approach offers the promise of a validated phenotype from the outset. As such, the scope of this work was broadened to investigate alternative functions for characterised effectors in established paradigms of EPEC infection. Recently, the use of various inhibitors facilitated the identification two distinct phases of EPEC-induced cell death in human macrophages: pyroptosis, followed by necroptosis (P. Goddard, unpublished).

The interaction between EPEC and macrophages *in vivo* is poorly understood. In murine models of septic EPEC infection, peritoneal macrophages are responsible for the production of anti-O127 antibodies that facilitate capture by liver-resident Kuppfer cells (Zeng et al., 2018), indicating that macrophages can interact with bloodborne EPEC. This is not the usual route of EPEC infection, but is clinically relevant in patients with post-operative sepsis (Sampaio et al., 2014). From a more fundamental standpoint, EPEC is extensively documented to inhibit several modes of phagocytosis (Celli et al., 2001; Goosney et al., 1999), which could represent a mechanism to counteract its exposure to macrophages during infection. Indeed, several effectors are implicated in the inhibition of phagocytosis: EspF in its capacity as an inhibitor of PI3 kinase signalling (Quitard et al., 2006); EspG, an Arf scaffolding protein (Humphreys et al., 2016); EspH, a Rho GEF inhibitor (Dong et al., 2010), and EspJ, an ADP-ribosyl transferase (Marchès et al., 2008; Pollard et al., 2016). These T3SS-dependent roles in macrophages are further exemplified by the ability of the T3SS pore component EspB to induce cell lysis through an unknown mechanism in THP1 macrophages but not in HeLa, T84 or undifferentiated U-937 cells (Baumann et al., 2018), as well as by the EspB-dependent resistance of phagocytosis via its binding to myosin family proteins recruited to the phagocytic cup (Iizumi et al., 2007).

Macrophages and other immune cells are recruited to the cite of infection where they recognise PAMPs via their PRRs (Broz and Monack, 2013; Takeuchi and Akira, 2010). PAMPs from A/E pathogens can activate several PRRs; for example, NLRP3 via EHEC enterohaemolysin

and Stx (Cheng et al., 2015; Lee et al., 2015; Platnich et al., 2018) as well as via bacteria-derived RNA:DNA hybrids (Kailasan Vanaja et al., 2014), and NLRC4 via recognition of the T3SS inner rod protein EscI and the non-LEE T3SS (ETT2) inner rod and needle proteins EprI and EprJ (Miao et al., 2010b; Wu et al., 2019; Yang et al., 2015; Zhao et al., 2011). Indeed, mice lacking NLRP3 or NLRC4 suffer increased bacterial burden and exaggerated pathology in response to *C. rodentium* (Liu et al., 2012; Nordlander et al., 2014). As such, the A/E pathogens have evolved mechanisms to mitigate PRR signalling leading to inflammasome activation including diversification of the T3SS needle protein EscF to evade NLRC4 recognition (Yang et al., 2015), translocation of effectors such as NleA/EspI to impair deubiquitylation of NLRP3 and inhibit inflammasome assembly (Yen et al., 2015), and NleF expression to inhibit caspase-4 activation and block the secretion of IL-18 that would promote further immune cell recruitment (Pallett et al., 2017; Song et al., 2017).

It was recently reported that infection with EPEC E2348/69 (E69) causes rapid NLRP3-dependent pyroptosis in THP1 macrophages and human monocyte-derived macrophages (MDMs), but only when primed in DMEM to incite T3SS expression (Goddard et al., 2019). E69 Δ*escF*, Δ*tir* and $Tir^{Y454A/Y474A}$ (TirAA) fail to induce pyroptosis, implicating the ability of translocated Tir to polymerise actin in this mode of cell death. A further requirement for pyroptosis was the concurrent recognition of *E. coli*-derived LPS by caspase-4. The resultant host signalling began with caspase-4 activation and initial GSDMD cleavage, followed by activation of the ASC-NLRP3 inflammasome triggered by GSDMD-mediated pore formation and potassium efflux. NLRP3 stimulation led to caspase-1 activation, further GSDMD cleavage and rapid pyroptotic cell death release of mature inflammatory cytokines IL-18 and IL-1β (Schematic 9).



Schematic 9 | Actin polymerisation by EPEC Tir stimulates atypical non-canonical inflammasome activation and pyroptosis

1 EPEC forms pedestals on human macrophages as they are phagocytosed. EPEC LPS is liberated and recognised by cytoplasmic caspase-4. **2** Caspase-4 activation leads to gasdermin D (GSDMD) cleavage and NLRP3 stimulation, likely via formation of GSDMD pores in the cell membrane and subsequent loss of intracellular potassium ions. **3** NLRP3 and ASC association via PYRIN domain (PYD)-PYD interactions. ASC binding to caspase-1 via their respective caspase recruitment domains (CARDs) completes inflammasome assembly, promoting autoproteolytic cleavage of caspase-1 in a proximity-dependent manner. Liberation of active caspase-1 facilitates further cleavage of GSDMD, as well as pro-inflammatory cytokines pro-IL-18 and pro-IL-1β. **4** The mature cytokines are released to the extracellular space via the GSDMD pore.

Additionally, unpublished research by Goddard *et al.* revealed a second stage of T3SS-dependent cell death. Through knockdown and inhibition of mammalian cell death machinery expressed by THP1s (i.e., MLKL, RIPK1), Goddard *et al.* demonstrated this late-stage death was necroptosis, but had yet to define which effector protein, if any, was responsible for this phenotype. Several aims were therefore formulated:

1. Investigate the conservation of the mechanism of Tir-driven pyroptosis among EPEC isolates.
2. Identify host- and bacterial-driven regulation of Tir-induced pyroptosis.
3. Identify candidate effectors for necroptotic cell death.

4.2 Results

4.2.1 Factors regulating Tir-induced pyroptosis

4.2.1.1 EPEC E69 induces cell membrane permeability in a T3- and Tir-dependent manner

Following infection of human macrophages, Goddard *et al.* report rapid and atypical activation of the non-canonical inflammasome mediated by Tir-driven actin polymerisation (Goddard et al., 2019); §4.2.1.1 aimed to reproduce the phenomena reported. 'Priming' of A/E pathogens by subculturing in DMEM is known to induces expression of the T3SS and related proteins (Abe et al., 2002). While it is reported that *E. coli* K12, unprimed pathogenic *E. coli* and unprimed *C. rodentium* induce LPS-driven death at 16 h p.i. (Rathinam et al., 2012), the contribution of the T3SS to macrophage cell death remained unexplored. During pyroptosis, membrane permeabilisation occurs as a result of the insertion of the oligomerised N-terminal domain of GSDMD into the host cell membrane to form a pore (Mulvihill et al., 2018), facilitating the uptake of PI and the release of LDH. Therefore, to confirm the contribution of the T3SS to cell death, THP1 macrophages were infected with E69 and the uptake of PI was monitored over time. PI uptake is significantly increased beyond 1 h 20 mins of WT E69 infection, reaching 41.24% PI uptake at 16 h p.i. compared to 29.16% for uninfected (UI) cells. Conversely, DMEM-primed E69 induces marked PI uptake within the first 4 h of infection (Figure 4.1A). As an appreciable level of background signal is emitted by untreated THP1s over time, all further data is normalised to uninfected control cells. The T3SS-dependence of increased PI uptake was verified with the E69 T3SS-deficient mutant Δ*escF*, which lacks the

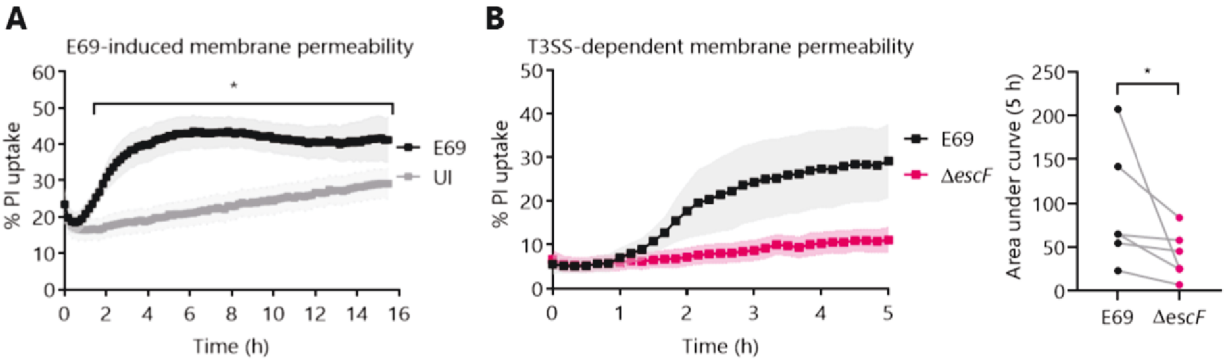


Figure 4.1 | Real-time PI uptake of E69-infected THP1s
PI uptake measured in THP1 macrophages infected with **A** E69 (n=10) or **B** E69 and the T3SS-deficient Δ*escF* (n=5). * = $p < 0.05$. Significance was calculated by 2-way ANOVA with two-stage linear step-up procedure of Benjamini, Krieger and Yekutieli correction for multiple comparisons by controlling the false discovery rate (FDR) in **A** and a ratio paired t-test in **B**. Shaded area represents SEM (n=5).

T3SS needle protein and is unable to secrete effectors or incite PI uptake; comparison of the area under the curve after 5 h of infection with E69 or E69 Δ*escF* reveals a significant difference in PI uptake (Figure 4.1B).

E69 secretes 23 known effectors via the T3SS, beginning with Tir (Wang et al., 2008). In agreement with Goddard *et al*., a Δ*tir* deletion mutant fails to induce pyroptosis as measured by PI uptake, while complementation of E69 *Δtir* with IPTG-inducible Tir^{E69} stimulated an exaggerated phenotype due to excessive Tir production (Figure 4.2A). Upon insertion into the host membrane and interaction with intimin on the surface of E69, Tir clusters undergo phosphorylation by host kinases, recruiting the adaptor protein N-WASP to facilitate localised actin polymerisation (Lai *et al*., 2013). To confirm that the Tir:intimin interaction and subsequent actin polymerisation is required for membrane pore formation as reported, THP1 cells were infected with an E69 intimin-deficient strain (E69 Δ*eae*) and E69 in which Tir Tyr454 and Tyr474 are replaced with Ala and are therefore unable to initiate actin polymerisation (TirAA) (Wong et al., 2012a). As expected, WT E69 induces significantly more membrane damage than any mutant strain (Figure 4.2B and C). Notably, both E69 Δ*eae* and E69 TirAA are significantly less attenuated than E69 Δ*tir*, indicating a subtle Tir toxicity that is independent

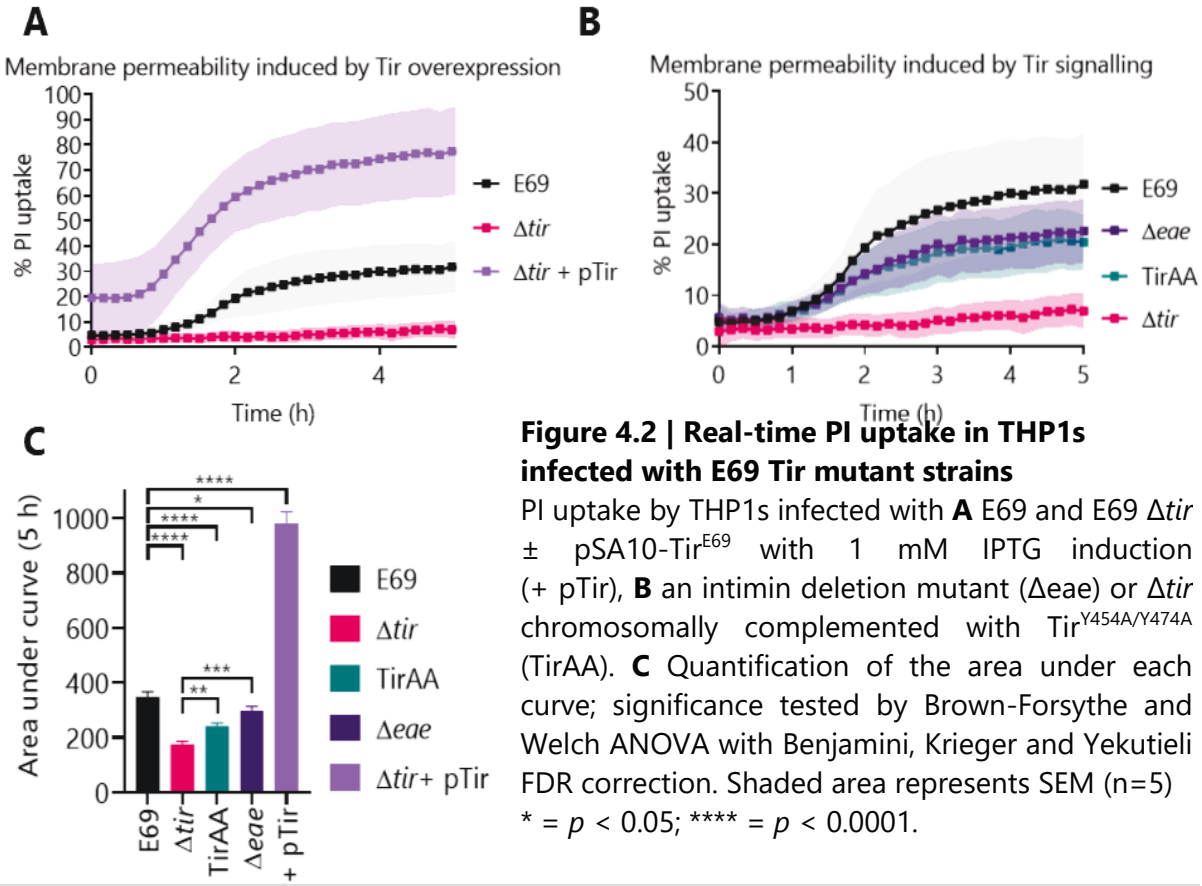


Figure 4.2 | Real-time PI uptake in THP1s infected with E69 Tir mutant strains
PI uptake by THP1s infected with **A** E69 and E69 Δ*tir* ± pSA10-Tir^{E69} with 1 mM IPTG induction (+ pTir), **B** an intimin deletion mutant (Δeae) or Δ*tir* chromosomally complemented with $Tir^{Y454A/Y474A}$ (TirAA). **C** Quantification of the area under each curve; significance tested by Brown-Forsythe and Welch ANOVA with Benjamini, Krieger and Yekutieli FDR correction. Shaded area represents SEM (n=5) * = $p < 0.05$; **** = $p < 0.0001$.

of its signalling role. Together, these observations confirm both the toxicity of Tir and the necessity for the Tir:intimin interaction and subsequent actin polymerisation in inducing membrane damage.

4.2.1.2 Tir-driven stimulation of pyroptosis is modulated by EspZ

Overstimulation of the inflammasome promotes excessive release of pro-inflammatory cytokines, which is not beneficial to the pathogen. Paradoxically, atypical NLRP3 activation by E69 effectively amplifies the non-canonical inflammasome pathway, requiring both caspase-4 and caspase-1 activation for pyroptosis (Goddard et al., 2019). It is not clear why LPS-driven activation of caspase-4 alone is insufficient for pyroptosis during E69 infection, therefore factors governing Tir-induced pyroptosis were next sought. Recently, Rühl *et al*. demonstrated mouse BMDMs are able to repair around 10% of GSDMD-damaged membranes by recruiting the Ca^{2+}-dependent endosomal sorting complex required for transport (ESCRT) ESCRT-0 and -III (Rühl et al., 2018), and that this repair can be abolished by chelating Ca^{2+}. To ascertain whether THP1s are also capable of repairing GSDMD-damaged membranes upon EPEC infection, EPEC-infected THP1s were supplemented with increasing concentrations of the Ca^{2+} chelator EDTA and monitored for membrane damage. Pre-treatment of THP1s with EDTA had no significant effect on E69 infection, as demonstrated by their statistically indistinguishable PI uptake (Figure 4.3A, upper panel). Although Rühl *et al.* report a similar trend in LDH release at the tested EDTA concentrations, this did not reach statistical significance in a human macrophage system (Figure 4.3A, lower panel). To ascertain whether THP1s were indeed capable of Ca^{2+}-dependent repair of GSDMD-induced membrane damage, LPS was transfected to activate the non-canonical inflammasome and EDTA was supplemented. Like during E69 infection, LPS-driven GSDMD pore formation was unaffected by the addition of EDTA (Figure 4.3B). Altogether, host driven Ca^{2+}-dependent membrane repair does not significantly regulate E69-induced pyroptosis.

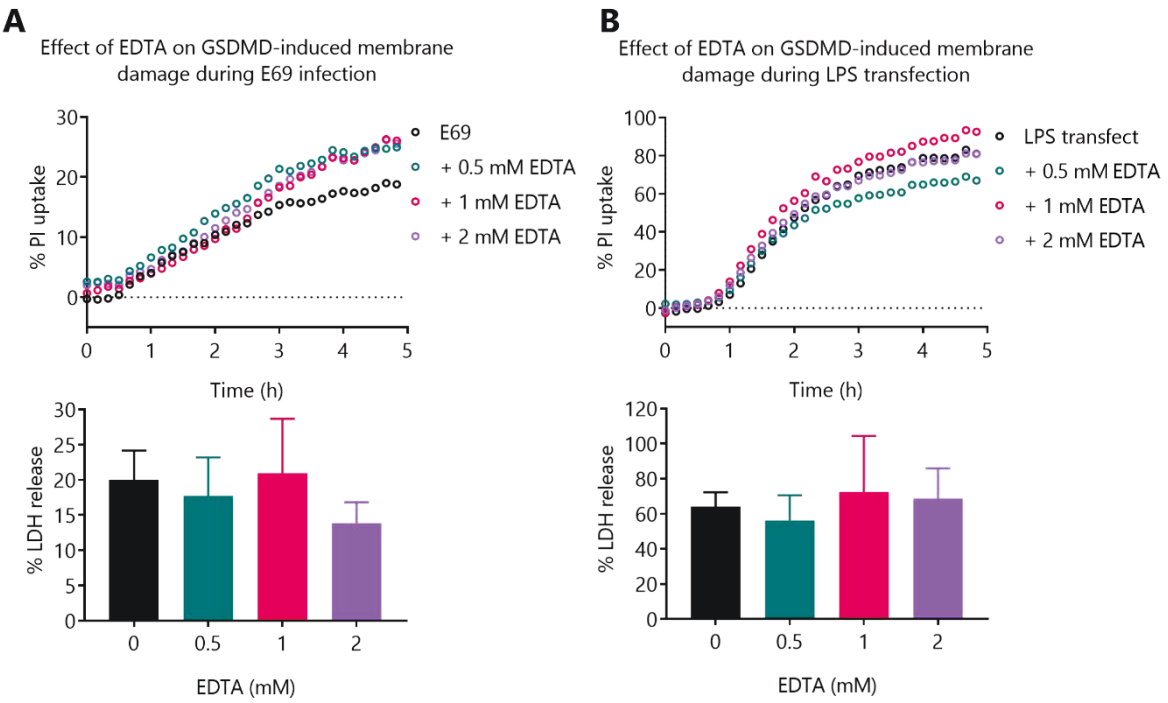


Figure 4.3 | Contribution of Ca^{2+} membrane repair to GSDMD-induced damage
Real time PI uptake (top) and LDH release (bottom) of **A** THP1s infected with E69 or **B** THP1s transfected with 5 µg/ml LPS under increasing concentrations of EDTA. For clarity, error bars are omitted on upper panels; error bars on bottom panels represent SEM (n=4).

If not host-driven, limitation of pyroptosis could be conferred by E69 itself. We and others have previously demonstrated the LEE-encoded effector EspZ limits EPEC/EHEC effector-induced cytotoxicity by restricting T3-dependent translocation (Berger et al., 2012; Deng et al., 2015). To test whether Tir-induced cell death is modulated by EspZ, THP1 macrophages were infected with the following modified E69 strains (Cepeda-Molero et al., 2017): EPEC 0 (an engineered E69 derivative devoid of all known effectors), EPEC 1 (only expressing Tir) and EPEC 2 (only expressing Tir and EspZ). To demonstrate the presence of Tir in these strains and confirm that the presence of EspZ does not affect Tir expression, EPEC 0 and 1 were transformed with empty plasmid (pSA10) or a plasmid encoding IPTG-inducible EspZ (pSA10-EspZ), and bacterial lysates were probed with an anti-Tir antibody (Figure 4.4A). Upon THP1 infection, EPEC 0 causes significantly less cell death than its parent strain E69 at 5 h p.i. owing to its lack of Tir (Figure 4.4B). EPEC 1, which can translocate unregulated quantities of Tir, affects membrane integrity to a similar degree than that of positive control THP1s treated with the detergent Triton-X-100. EPEC 2 reduces Tir-induced death to significantly below WT levels (Figure 4.4C). Together, these observations implicate the translocation of EspZ in regulating cell permeability.

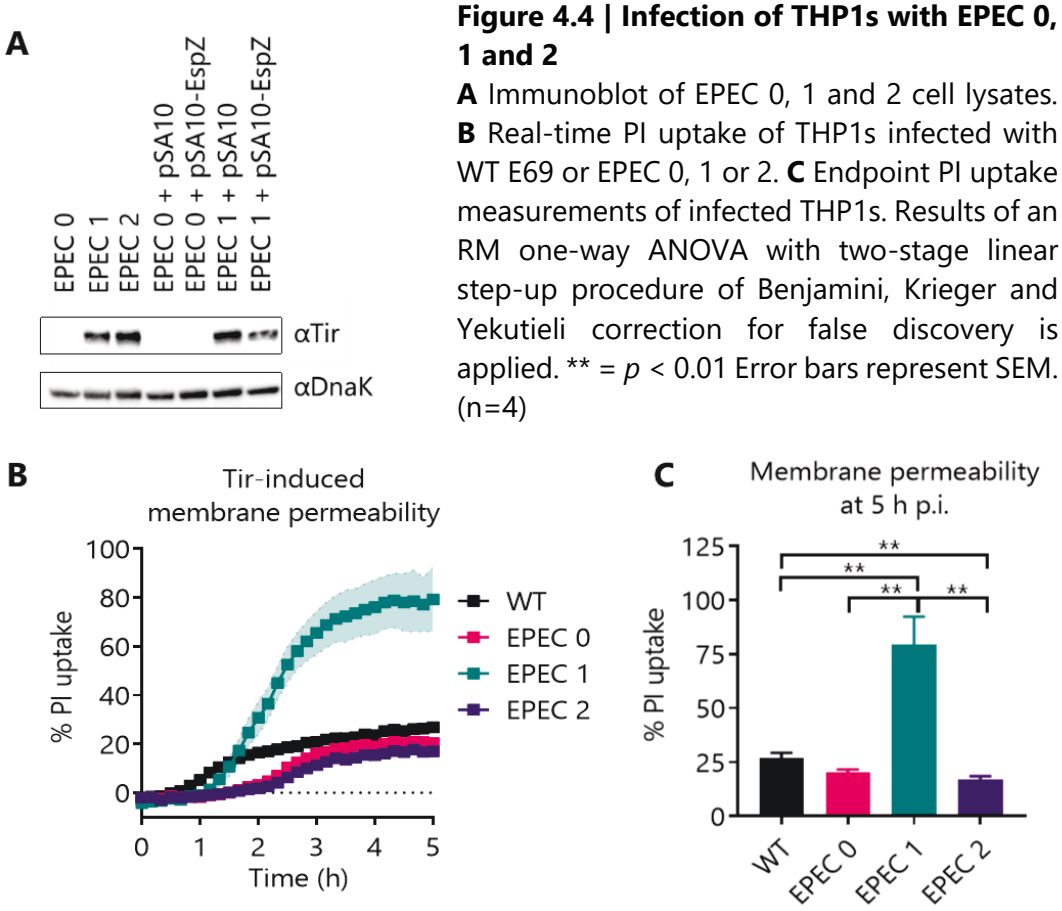


Figure 4.4 | Infection of THP1s with EPEC 0, 1 and 2
A Immunoblot of EPEC 0, 1 and 2 cell lysates. **B** Real-time PI uptake of THP1s infected with WT E69 or EPEC 0, 1 or 2. **C** Endpoint PI uptake measurements of infected THP1s. Results of an RM one-way ANOVA with two-stage linear step-up procedure of Benjamini, Krieger and Yekutieli correction for false discovery is applied. ** = $p < 0.01$ Error bars represent SEM. (n=4)

Berger et al. demonstrate that upon transfection, EspZ localises to the plasma membrane, where it further blocks multiple waves of infection (Berger et al., 2012). To ascertain whether EspZ insertion into the host membrane prevents an aspect of GSDMD pore formation, THP1 cells were pre-incubated with LPS to induce expression of pyroptotic cell machinery infected with EPEC 2 for 4 h to allow EspZ insertion, and treated with nigericin to induce pyroptosis. Total LDH release was quantified at 5 h p.i. as a measure of cell lysis. As before, EPEC 2 prevents Tir-induced cell lysis, but pre-infection with EPEC 2 does not protect cells from nigericin-induced pyroptosis (Figure 4.5). As such, EspZ modulates Tir-driven cell death by downregulating Tir translocation.

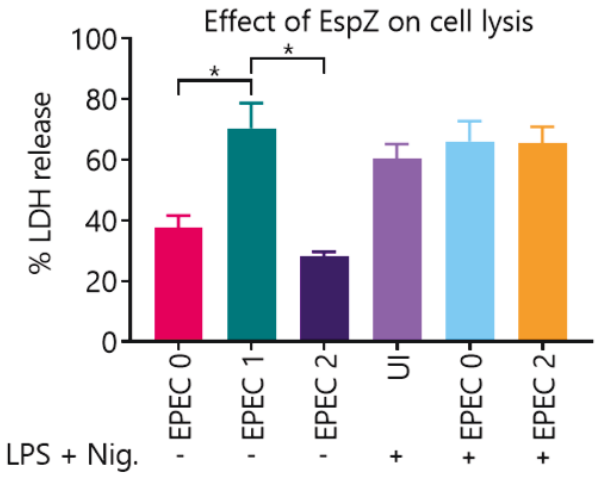


Figure 4.5 | Infection of pyroptotic THP1s with EspZ-expressing EPEC
Quantification of THP1 cell lysis following infection with EPEC 0, 1 or 2 ± LPS and nigericin treatment via LDH release. Cells were infected with EPEC strains 30 mins prior to nigericin challenge to allow EspZ delivery. Significance tested by Brown-Forsythe and Welch ANOVA with two-stage linear step-up procedure of Benjamini, Krieger and Yekutieli correction for false discovery.
* = p > 0.05. Error bars represent SEM. (n=4)

4.2.1.3 Investigating TccP as a modulator of pyroptosis.

EPEC isolates encode different combinations of host-targeted Tir tyrosine residues and TccP to mediate actin polymerisation in host cells (Figure 4.6A). Goddard *et al.* demonstrate that the NLRP3 inflammasome assembles in response to both Nck-dependent and Nck-independent modes of actin-polymerisation by Tir. Additionally, while Tir^{EHEC} alone is unable to complement E69 *Δtir*, full non-canonical inflammasome activation is restored when E69 *Δtir* is provided with Tir^{EHEC} and $TccP^{EHEC}$ (Goddard et al., 2019), suggesting the activation signal for inflammasome assembly lies downstream of N-WASP/ARP2/3. However, as EPEC and EHEC isolates express different combinations of TccP and intimin, further assessment the contribution of unique intimin:effector repertoires to polymerise actin and induce membrane permeability was undertaken. THP1 cells were therefore infected with E69 as well as B171 and E11 and assayed for PI uptake as before. Despite equivalent MOIs, E11 induced significantly more membrane permeability than E69 (Figure 4.6B). Surprisingly, PI uptake in B171-infected THP1s, which is theoretically able to induce actin polymerisation via host machinery and TccP2, was reduced compared to E69, which lacks TccP altogether. These findings suggest that although EPEC strains differ significantly in their ability to induce membrane damage, the presence of TccP is not the determining factor for this disparity.

A

Strain	Tyr	TccP
E69	454 474	-
E11	464 474	TccP + TccP2
B171	442 462	TccP2

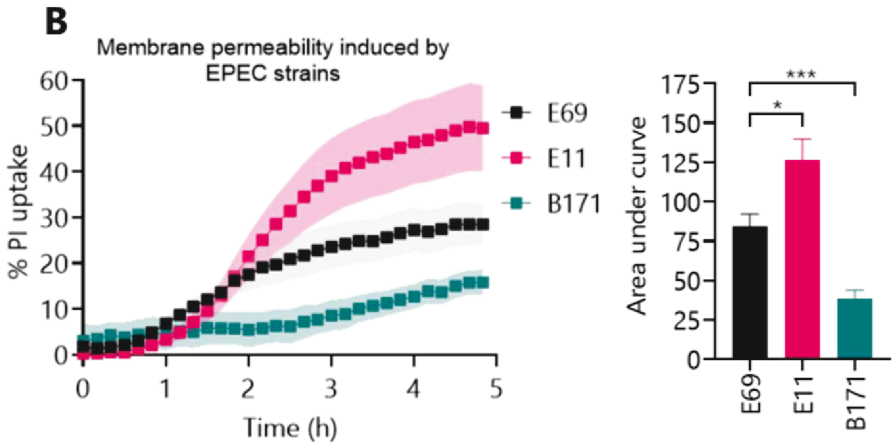


Figure 4.6 | Infection of THP1s with EPEC strains with differing TccP expression
Real time PI uptake by THP1 cells following infection with EPEC E69, E11 or B171. Total area under the curve is quantified on the right. significance tested by Brown-Forsythe and Welch ANOVA with Benjamini, Krieger and Yekutieli FDR correction. Shaded area and error bars represent SEM. * = $p < 0.05$; *** = $p < 0.0002$. (n=6).

Given the rapid and exaggerated E11-induced membrane permeability, we next sought to confirm whether this was also pyroptotic and T3SS-dependent, like E69. To this end, THP1s were infected with E11 and E11 Δ*escN*, which does not encode the T3SS ATPase and therefore does not assemble the T3SS fully or secrete effectors. Like E69, E11 without a functional secretion system is attenuated in its ability to induce membrane permeability (Figure 4.7), confirming the importance of the T3SS across strains.

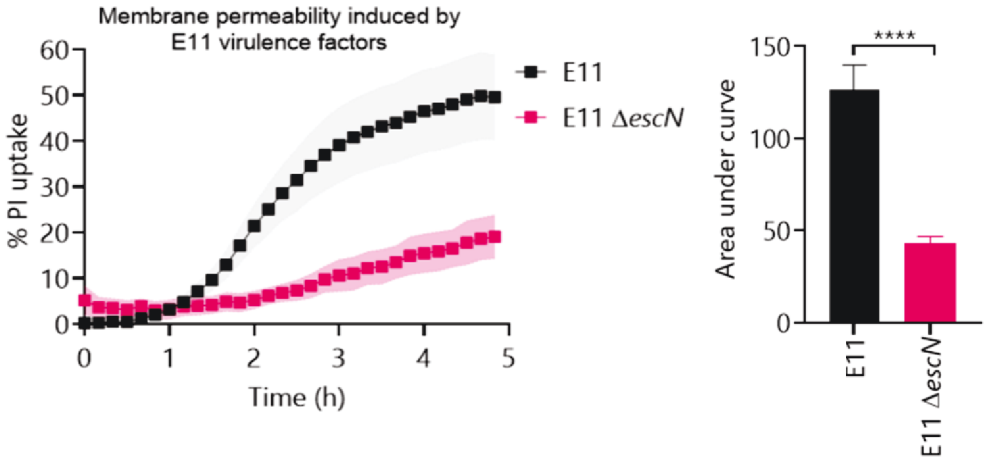


Figure 4.7 | The T3SS is required for E11-induced cell death
Real time PI uptake by THP1 cells following infection with EPEC E11 or its T3SS-null Δ*escN* derivative. Total area under the curve is quantified on the right. Significance tested by Welch's unpaired t-test. ****= $p < 0.0001$. Shaded area and error bars represent SEM (n=4).

To ascertain whether E11-induced death is NLRP3 and caspase-dependent, THP1 cells were pre-treated with MCC950 to prevent NLRP3 inflammasome formation, the irreversible pan-caspase inhibitor zVAD to prevent caspase activation, or dimethylsulphoxide (DMSO) as a vehicle control and infected with E11 for 5 h as before. Cells pre-treated with either inhibitor maintained significantly more membrane integrity than DMSO infected cells (Figure 4.8) although surprisingly DMSO itself exhibits a significant protective effect. This demonstrates that E11, like E69, induces cell death that proceeds via NLRP3 and caspase activation.

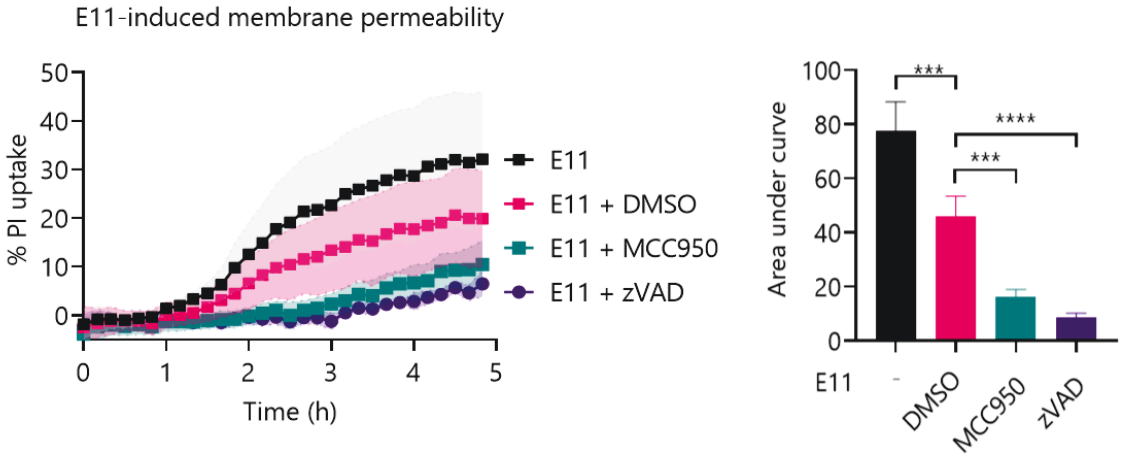


Figure 4.8 | NLRP3 and caspases are required for E11-induced cell death
Real-time PI uptake by THP1 cells following pre-treatment with the NLRP3-specific inhibitor MCC950 or the pan-caspase inhibitor zVAD-FMK and infection with EPEC E11. Total area under the curve is quantified on the right. Significance tested by one-way ANOVA with Benjamini, Krieger and Yekutieli FDR correction. *** = $p < 0.001$; **** = $p < 0.0001$. Shaded area and error bars represent SEM (n=3).

4.2.1.4 Investigating EspT as a modulator of pyroptosis

E11 induces significantly more T3SS-dependent inflammasome activation and subsequent cell death than E69 during 5 h of infection. E69 encodes 21 effector proteins, 19 fewer than E11 (Iguchi et al., 2009), leading to the hypothesis that an effector present in E11 but not E69 could be responsible for increased cell death. EspT is a rare Rho GEF present in 0.54% of pathogenic *E. coli* strains and around 1.8% of EPEC strains, most notably in E11 (Arbeloa et al., 2009; Hazen and Rasko, 2019). Previous research demonstrated EspT-dependent invasion of non-phagocytic cells through membrane ruffling and the subsequent formation of intracellular actin pedestals (Bulgin et al., 2009a, 2009b). To investigate whether EspT is responsible for the increased pyroptotic death observed with E11, THP1s were infected with E11 or an E11 Δ*espT* strain and assayed for PI uptake. While the absence of EspT during E11 infection does reduce

PI uptake, this did not reach statistical significance under these conditions (Figure 4.9A). Additionally, PI uptake in THP1s infected with E69 non-natively expressing EspT was not significantly different to cells infected with E69 carrying an empty plasmid (Figure 4.9B). Together, these data do not support a role for EspT in the exaggerated pyroptosis observed in E11 infection.

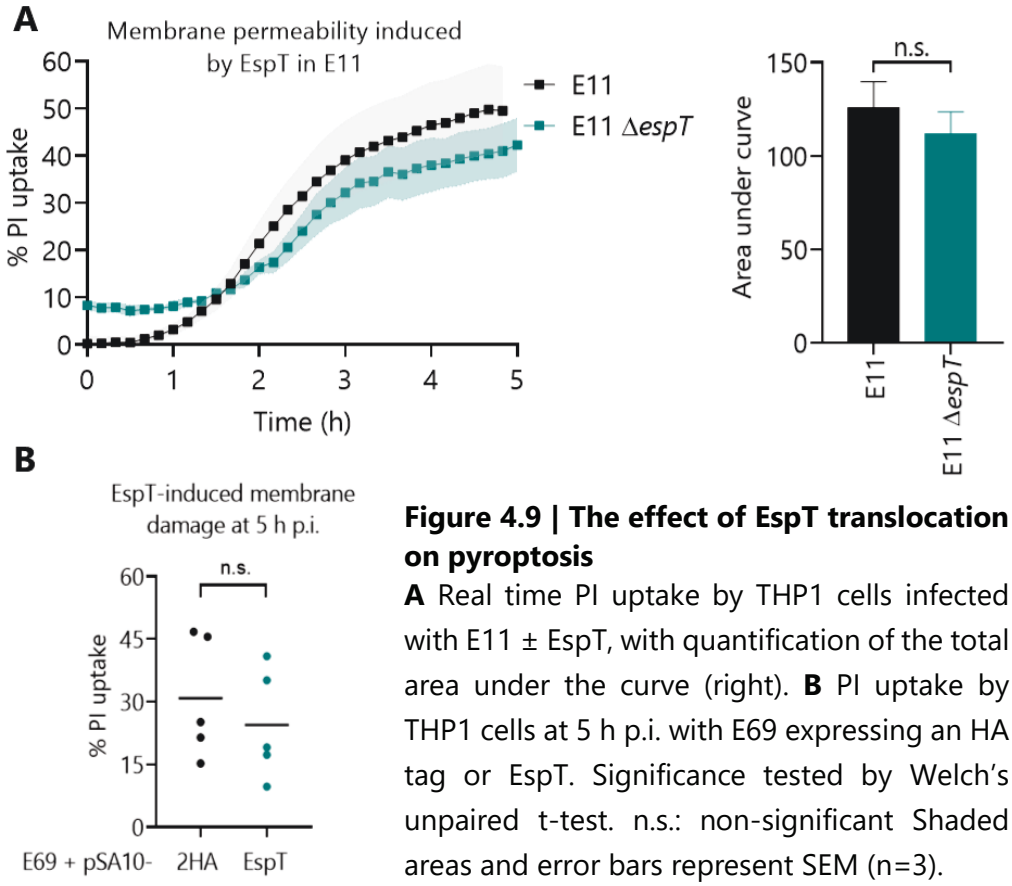


Figure 4.9 | The effect of EspT translocation on pyroptosis

A Real time PI uptake by THP1 cells infected with E11 ± EspT, with quantification of the total area under the curve (right). **B** PI uptake by THP1 cells at 5 h p.i. with E69 expressing an HA tag or EspT. Significance tested by Welch's unpaired t-test. n.s.: non-significant Shaded areas and error bars represent SEM (n=3).

4.2.2 EPEC induces a second phase of necrotic cell death

Further to the pyroptotic cell death pathway described by Goddard et al., a second phase of GSDMD-independent cell death can be observed in EPEC-infected macrophages (P. Goddard, unpublished). In addition to pyroptosis, macrophages are also capable of undergoing necroptosis, a GSDMD-independent, caspase-independent inflammatory form of lytic cell death. To ascertain whether EPEC induces necroptosis, macrophages were infected with EPEC treated with Nec1, which inhibits RIPK1 (Degterev et al., 2005), or Nec1 in combination with zVAD, which additionally inhibits caspases. This was performed in a THP1^{GSDMDmiR} line, wherein GSDMD is silenced with a specific miRNA. GSDMD silencing removes the contribution of earlier pyroptotic death signalling. Both Nec1 and Nec1 + zVAD treatment significantly reduced E69-

induced PI uptake (Figure 4.10A), indicating that the lytic cell death observed is necroptosis. Several effectors are documented to target the necroptotic machinery (§1.5.3). GSDMD-deficient macrophages were therefore infected with our in-house library of E69 T3SS and effector mutants to ascertain which, if any, effectors were implicated in necroptosis. Although clear differences in the level of PI can be observed with each infection condition (Figure 4.10B), no condition reached statistical significance by 1-way ANOVA with FDR correction due to the high variation between biological repeats.

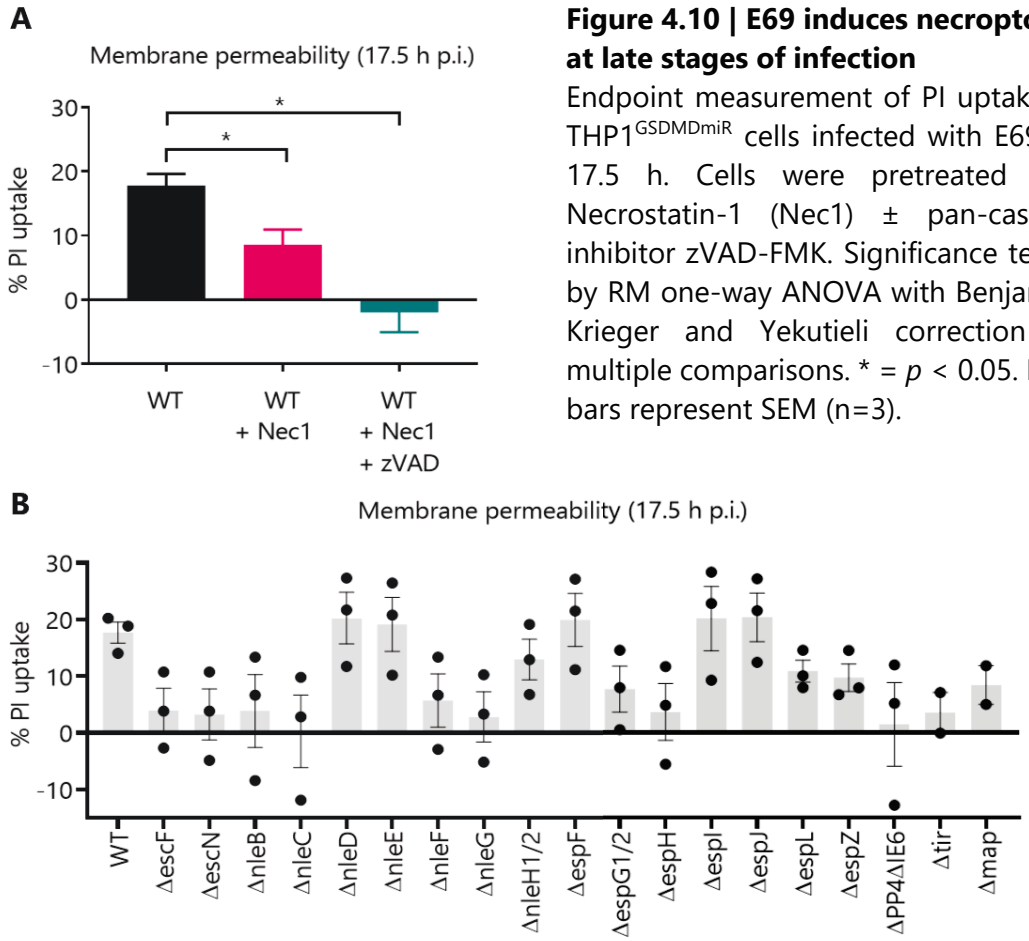


Figure 4.10 | E69 induces necroptosis at late stages of infection
Endpoint measurement of PI uptake by THP1^{GSDMDmiR} cells infected with E69 for 17.5 h. Cells were pretreated with Necrostatin-1 (Nec1) ± pan-caspase inhibitor zVAD-FMK. Significance tested by RM one-way ANOVA with Benjamini, Krieger and Yekutieli correction for multiple comparisons. * = $p < 0.05$. Error bars represent SEM (n=3).

As this is a preliminary screen with clear biological implications of removing T3 virulence proteins, the stringency of statistical testing was reduced. Using unpaired t-tests, at 17.5 h post-treatment, the addition of Necrostatin-1 (Nec1) ± zVAD maintained its statistical significance, and both T3SS mutants E69 Δ*escN* and E69 Δ*escF* induced significantly less necroptosis than WT at the end of the infection (Figure 4.11A), exhibiting a clear defect throughout the infection timecourse (Figure 4.11B).

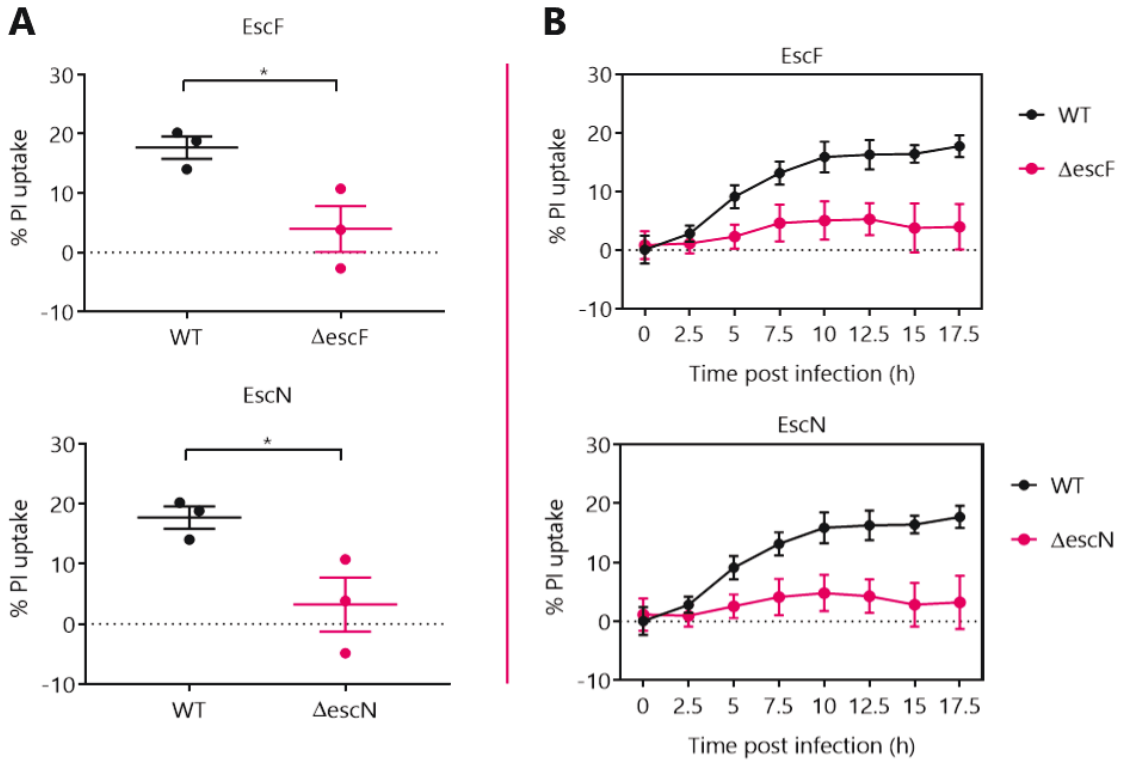


Figure 4.11 | The T3SS is required for late-stage necroptosis
Endpoint (**A**) and real-time (**B**) PI uptake by THP1^{GSDMDmiR} cells infected with E69 and two independent T3SS-null mutant derivatives, Δ*escN* and Δ*escF*. Significance tested by unpaired two-tailed t-test. * = $p < 0.05$. (n=3)

Expanding this analysis to the remaining E69 effector deletion mutants, only one effector was significantly defective for the induction of necroptosis, though three other effectors (NleC, EspH and EspZ) were borderline. Deletion of NleG reduces the mean PI uptake of E69-induced necroptosis from 18.3% to 3.3% (Figure 4.12). However, when this was repeated using LDH release as a monitor of lytic cell death, neither E69 Δ*nleG* nor its complementation induced significantly different lysis to WT E69 (not shown). Together, these results indicate E69 uses the T3SS to induce necroptosis in human macrophages, but crucially, this process is probably mediated by more than one effector, or an uncharacterised effector.

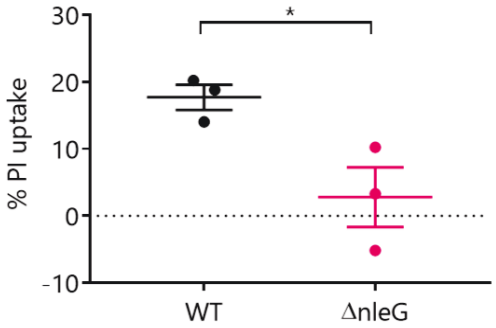


Figure 4.12 | Cell death following 17.5 h infection with E69 Δ*nleG*
Endpoint PI uptake by THP1^{GSDMDmiR} cells infected with E69 and its Δ*nleG* derivative. Significance tested by unpaired two-tailed t-test. * = $p < 0.05$ (n=3).

4.3 Discussion

With advances in our understanding of cell biology and its subversion upon infection, previously characterised effectors are newly implicated in novel processes. It was recently demonstrated that the key LEE-encoded effector Tir is responsible for inducing rapid actin polymerisation dependent NLRP3-driven pyroptosis (Goddard et al., 2019), in addition to its other roles in the intimate attachment between pathogen and host (Kenny et al., 1997), colonisation (Deng et al., 2003), providing a signalling platform for actin rearrangement (Crepin et al., 2010), and inhibition of pro-inflammatory signalling (Ruchaud-Sparagano et al., 2011; Yan et al., 2012). As the interplay between effectors determines the success of A/E pathogenesis, this chapter sought to identify other effectors implicated in pyroptotic and necroptotic cell death.

Consistent with Goddard et al., EPEC induces rapid lytic cell death in THP1 macrophages that is diminished by the genetic manipulation of EPEC's actin-polymerisation factors: the deletion of Tir or intimin, and replacement of the phosphorylated Tyr residues in Tir with Ala (Wong et al., 2012a). Interestingly, removal of intimin and mutagenesis of Tir's phosphorylation sites reduces, but did not completely abolish, EPEC-induced cell death. This could indicate more subtle Tir toxicity that is uncorrelated to its role in actin polymerisation, and that can also be observed during infection of colonic epithelial cancer cell lines (Qiyun Zhong, unpublished data). Deletion of intimin also affects EPEC's ability to associate closely with the target cell, but this does not play a major role in macrophage infection as the intimin deletion mutant induces significantly more death than deletion of Tir alone. This could indicate that the rate-limiting step in EPEC-driven pyroptosis is the access of caspase-4 to EPEC LPS upon phagocytosis, and that the activity of Tir amplifies and accelerates this pyroptotic signalling.

Actin polymerisation is clearly necessary for efficient activation of the rapid pyroptotic cell death. It is conceivable that cytoskeletal remodelling itself is recognised by the host. For example, manipulation of Rho family GTPases by *Shigella* spp. and *S.* Typhimurium effectors is recognised by NOD1, and other toxin-based perturbations of RhoA, B and C are recognised by the Pyrin inflammasome (Mostowy and Shenoy, 2015). Indeed, there are many reports of co-regulation between actin and NLRP3 inflammasome components. Both NLRP3 and ASC can

colocalise with actin upon sterile inflammasome activation (Burger et al., 2016; Waite et al., 2009), although polymerised F-actin appears to supress pyroptotic IL-1β maturation (Burger et al., 2016). Additionally, caspase-11 modulates actin polymerisation to promote cell migration (Li et al., 2007), facilitates phagolysosomal fusion (Akhter et al., 2012) and enhances bacterial clearance (Caution et al., 2015). Indeed, NLRP3, ASC and caspase-11 can complex with the actin remodelling protein Flightless I to promote cortical co-localisation of actin in HeLa and COS cells, partially inhibiting caspase-1 and -11 in doing so (Burger et al., 2016; Li et al., 2008). Moreover, the caspase-recruitment domain (CARD) in caspase-11 can bind actin-related proteins Aip1 and WD40 (Li et al., 2007) as well as its traditional target, LPS. Competition for the caspase-11 CARD domain between LPS and actin-regulatory proteins may preclude simultaneous binding. Delineating the mechanism by which Tir signalling enhances non-canonical inflammasome activation may therefore represent a novel paradigm in the way inflammasome components respond to actin.

It is important for both the host and the bacterium to strike a balance between immune activation and tissue preservation. This is exemplified in so-called hyperactive immune cells, wherein GSDMD pore formation is limited so that cells remain viable enough to use the pore as a conduit for pro-inflammatory cytokine secretion (Evavold et al., 2017; Heilig et al., 2018). This is key, as prolonged cytokine secretion from live cells can aid clearance of infection both by promoting immune cell recruitment and priming T-helper type I (T_H1) cells, whereas cells that have died from pyroptosis, releasing a large burst of pro-inflammatory cytokines, are poor T_H1 stimulators and instead contribute to localised tissue damage (Evavold and Kagan, 2018). In addition to the dampening of pyroptosis by F-actin seen in human macrophages (Burger et al., 2016), mouse macrophages specifically excise GSDMD-damaged membranes to repair themselves (Rühl et al., 2018). Similarly, bacteria must limit cytokine secretion to evade elimination by immune cells. E69 already employs a roster of effectors that theoretically inhibit pyroptotic signalling in macrophages (Sanchez-Garrido *et al.,* under revision): NleF to limit caspase-4 cleavage (Pallett et al., 2017); a group of effectors to limit phagocytosis (§4.1), and NleA to prevent NLRP3 activation (Yen et al., 2015). However, despite these effectors, the activation of NLRP3 by Tir-dependent actin polymerisation prevails (Goddard et al., 2019). A further restraint on pyroptosis is EspZ, as demonstrated herein. EspZ renders cells refractory to effector translocation, in a manner dependent on its insertion into the host membrane

(Berger et al., 2012). By deleting all known non-Tir effectors in EPEC 1 and 2 (Cepeda-Molero et al., 2017), we can conclude that EspZ specifically limits Tir translocation in the context of E69-driven pyroptosis.

EPEC isolates differ in their ability to induce pathology, and this is reflected in their ability to induce cell death, as shown with E69, B171 and E11 in this work. E11 is notorious for its high infection rate (Viljanen et al., 1990), but despite whole-genome sequencing efforts, the secret behind E11's success remains elusive (Hazen and Rasko, 2019). One defining factor of E11 is the expression of EspT, (Bulgin et al., 2009b), but it is unknown whether EspT-induced membrane ruffling or phagocytosis plays a role in the infection of phagocytic cells. Although it is conceivable that an isolate with two independent mechanisms of entry would more efficiently present LPS to caspase-4, neither deletion of EspT from E11 or exogenous expression of EspT from E69 support this hypothesis.

It has previously been argued that necroptotic cell death is simply a molecular back-up option for when apoptotic cell death fails, although the number of A/E effectors that specifically inhibit necroptosis suggests the host necroptotic response is detrimental to pathogen survival (Pearson and Murphy, 2017; Peltzer and Walczak, 2019). We have previously demonstrated T3SS-dependent E69-driven necroptosis, confirmed by inhibition of RIPK1 and caspase-8 by Nec1 and zVAD respectively, knockdown of host necroptotic factors MLKL and RIPK3 and deletion of E69 EscF (P. Goddard et al., unpublished). While this was successfully recapitulated, the variability between infections with the in-house repertoire of effector deletion mutants hampered identification of the responsible effector protein, if indeed there is only one effector involved. NleG was the most promising candidate from initial screening. The NleG family of effectors are E3 ubiquitin ligases (Wu et al., 2010), of which there can be over a dozen NleG-like proteins encoded in a single A/E isolate. Conveniently, E69 only encodes one NleG, whose target during infection has yet to be identified. Several aspects of the necroptotic pathway are regulated by ubiquitination (Berghe et al., 2014; Silke et al., 2015). For example, RIPK1 is continually ubiquitylated by cellular inhibitor of apoptosis 1/2 (cIAP1/2) in the presence of caspase-8, leading to pro-inflammatory signalling. Conversely, cIAPs themselves can also be ubiquitylated for degradation, leading to necroptosis (Choi et al., 2019; Feoktistova et al., 2011; Tenev et al., 2011). Depending on the target of NleG, it is conceivable that a ubiquitin-ligase

deficient E69 infection could promote activation of the necroptotic pathway, however the phenotype reported in this work was neither reproducible nor able to be genetically complemented.

Currently, deletion of single effectors was insufficient for a significant change in necroptosis. This was initially surprising, given the theoretical impact of effectors on necroptotic signalling pathways. For example, inhibition of caspase-8 by NleF (Pallett et al., 2014) should predispose TNF-stimulate cells towards necrosome formation. However, it is more likely that multiple effectors in concert may be responsible for the necroptotic death observed. This has previously been demonstrated in non-myeloid HT-29 cells: EspL can degrade RIPK1 and RIPK3 (Pearson et al., 2017), and NleB can inhibit TRADD activation by GlcNacylating the TRADD death domain, but only an *espL/nleB* double mutant impacts necroptosis (Pearson et al., 2013; Scott et al., 2017). Additionally, a Δ*espZ* mutant approached significance in the effector screen; loss of EspZ during infection should result in uncontrolled effector translocation (Berger et al., 2012), therefore the presence of EspZ during WT infection may negatively regulate anti-necroptotic effector delivery. Finally, other E69-encoded virulence factors could contribute to necroptosis. EspC is a non-LEE-encoded serine protease that gains entry to host cells via the Type III translocon pore (Vidal and Navarro-García, 2008). Upon entry, EspC is able to induce an instrinsic apoptosis-like form of cell death by directly cleaving caspase-3 (Serapio-Palacios and Navarro-Garcia, 2016). Whether or not EspC could also target other caspases, such as caspase-8, remains untested. Nevertheless, together these observations highlight the importance of effector synergy during infection.

Chapter 5

Conclusions and Future Perspectives

5 Conclusions and future perspectives

The A/E family of pathogens are an important causative agent of infectious diarrhoea in humans, and their success is determined by the translocation of T3SS effector proteins. Dozens of families of effector proteins have been identified in a range of bacterial species with T3SSs, all of which with subtle adaptations that underpin the success of their associated bacterium. The A/E pathogens in particular translocate effectors that largely manipulate three key aspects of mammalian biology: the inflammatory response, maintenance of cytoskeletal structure and programmed cell death ((Shenoy et al., 2018); §1). The identification and investigation of three previously uncharacterised effector proteins in this study, NleN, NleO and EspS, contributes to our understanding of the latter two processes during infection.

The integrity and morphology of the actin cytoskeleton is a long-standing target of bacterial effectors (Navarro-Garcia et al., 2013). The elucidation of the *C. rodentium* GI11-encoded effector NleO as a Rac1-targeting putative cysteine protease is a surprising addition to the cytoskeleton-subverting arsenal, as it is not a WxxxE effector (Alto et al., 2006), and it exhibits no sequence or structural homology to any characterised T3 effector protein. Despite this, it is ubiquitous in human pathogenic *E. coli* isolates, warranting a more extensive investigation into its sequence prevalence and contribution to human disease severity. This is currently being undertaken in collaboration with the Sanger Centre (Cambridge, UK). Intriguingly, NleO cleaves Rac1 at an exclusive, yet undefined, site. The delineation and significance of this cleavage site is also under investigation in collaboration with the functional proteomics division at the Institute of Cancer Research (London, UK). The structural predictions of NleO guided the identification of its putative catalytic Cys residue, which is necessary for Rac1 cleavage. However, the second suggested catalytic residue, His20, requires further study. Confirmation of the tertiary structure of NleO is currently being pursued in collaboration with the Diamond Institute (Oxford, UK). The revelation of the presumably unique catalytic mechanism for NleO-induced Rac1 cleavage will be an exciting addition to the catalogue of Rho-family targeting effectors (Aktories, 2011; Bulgin et al., 2010; Orchard and Alto, 2012).

The induction of cell rounding by bacterial toxins is by no means unique (Arbeloa et al., 2011; Dong et al., 2010; Morita-Ishihara et al., 2013; Sheahan and Fullner Satchell, 2007). However, the extent of cell rounding induced by NleO is particularly interesting as it results in both the loss of cytoskeletal ultrastructures but also visually resembles actin blebs. Actin blebs are largely facilitated through RhoA-ROCK signalling (Ikenouchi and Aoki, 2017), but whether NleO specifically targets Rac1, or a conserved cleavage site in other Rho-family GTPases is currently unknown.

The inactivation of Rho GTPases by bacterial toxins has previously been reported to incite PYRIN inflammasome activation in monocytes (Schnappauf et al., 2019). PYRIN detects Rho inactivation through the depletion of the RhoA effectors PKN1 and 2, which normally phosphorylate PYRIN to maintain its inactivity through binding of the inhibitory 14-3-3 adaptor (Gao et al., 2016; Park et al., 2016). With the exception of YopT discussed in §3, examples of PYRIN inflammasome activation are currently limited to RhoA inactivation by covalent modification (Chung et al., 2016; Medici et al., 2019; Ratner et al., 2016; Xu et al., 2014). As such, if Rac1 cleavage is detected, it could proceed via a unique mechanism. As this cell rounding phenomenon was observed in HeLas, which are epithelial cells that do not express PYRIN under the conditions used in this study, investigation of the immunological consequences of Rac1 cleavage in another cell line may provide an insight into the role of NleO *in vivo*.

The subversion of actin dynamics by A/E pathogens is chiefly attributed to the key effector protein Tir (Lai et al., 2013), whose actin-polymerising ability was recently demonstrated to illicit NLRP3-dependent pyroptosis (Goddard et al., 2019). The toxicity of Tir can be partially quelled by EspZ, which limits Tir translocation (Berger et al., 2012), although other candidate effectors explored in §4 (EspT and TccP) did not appear to contribute as straightforwardly. This underscores the complexity of effector synergy and highlights the importance of investigating the function of effectors in the correct host and bacterial genetic background. Nevertheless, the functional relationship between actin perturbations and cell death resonates here too. It is conceivable that actin perturbations alone are sufficient to alert cytosolic sentinels. This was recently shown to be the case for the NLRC4 inflammasome during *S.* Typhimurium infection

(Kufer et al., 2019; Man et al., 2014), but the technical challenge of separating Tir localisation and signalling from the presence of LPS continues to preclude this line of investigation.

During the investigation of Tir and EspS toxicity, it was noted that expression of the T3SS during infection was sufficient to cause a significant level of lytic cell death. Many effectors are implicated in the molecular modulation of apoptosis (Santos and Finlay, 2015; Wong Fok Lung et al., 2014), but the bona fide execution of apoptosis of *C. rodentium*-infected cells in culture has yet to be demonstrated. For example, it is reported that 5 h of *C. rodentium* infection causes 50% HeLa detachment (Hemrajani et al., 2010). True apoptosis, however, is defined as the activation of the executioner caspases-3/7 and 9, the subsequent cleavage of cellular proteins and the characteristic rounding and blebbing of cells (Galluzzi et al., 2018). This study delineated a form of caspase-independent *C. rodentium*-induced cell death in epithelial-like HeLa cells that had yet to be formally reported, after which no caspase-9 cleavage or PARP cleavage is detected. Consistently, there is no significant difference in the relative number of apoptotic cells in the colons of uninfected or infected C57Bl/6 mice. The synergistic action of pro- and anti-apoptotic effectors could explain why individual effector mutations do not perturb caspase-9 or PARP. Alternatively, as these proteins are among the last to be cleaved in apoptotic cascades, probing an upstream process that is unique to the intrinsic or extrinsic apoptotic pathways may reveal a subtler subversion by *C. rodentium*. As HeLa cells do not express RIPK3, this form of cell death is not caspase-independent necroptosis (He et al., 2009; Sai et al., 2019). Whatever the mode of cell death might be, the corresponding increase in PI uptake could be simply mediated by the lytic nature of the EspB/D T3SS pore (Ide et al., 2001; Litvak et al., 2017), as may also be the case for Tir-independent pyroptosis induced by EPEC 0 in THP1s demonstrated in this study and in others (Baumann et al., 2018).

Continuing the theme of cell death, investigation of a second novel family of A/E effectors, EspS, revealed its wide-spread distribution across the several enteric pathogens. Like NleO, EspS resembles a cysteine protease (Calder et al., 2014), but its toxicity is not conserved among EspS family members. EspS localises to the mitochondria where its *C. rodentium* representative is able to interact with the mitochondrial anti-apoptotic protein TRIAP1, though this does not directly impact apoptosis or lipid membrane composition in HeLa cells or murine IECs isolated after *in* vivo infection. The putative association of EspS with lipids rendered its overexpression

or purification unfeasible. To circumvent this issue, solubilisation conditions were identified that would allow the pulldown of tagged EspS and its host interacting partners during mammalian cell infection. Not only could this enable the confirmation of TRIAP1 as a target protein, it could also reveal other host interactors, providing key insights into EspS function. Additionally, conditions under which EspS could be overexpressed in mammalian cells were identified. Harnessing this technique on a larger scale could facilitate the $EspS_{CR}$ purification and crystallisation. Given that other effectors such as NleG remained uncharacterised until their structures were solved (Wu et al., 2010), this may be the only way to probe the biochemical function of EspS *in vitro*. However, caution must be taken with this approach, as structural resemblance to eukaryotic proteins or fellow effectors has previously misled the investigative efforts into other effector proteins (Germane et al., 2008). Nevertheless, EspS clearly plays a synergistic role with other anti-proliferative effectors *in vivo*, as its deletion from the *C. rodentium* genome increases intestinal pathology in a murine infection model (Connolly et al., 2018).

Effector proteins exhibit fascinating diversity and specificity. Consequently, their study is warranted not only by their importance in bacterial pathogenesis. Effectors often demonstrate first-in-class functions, the characterisation of which broadens our understanding of protein biochemistry. Additionally, as effectors have witnessed the complexity of eukaryotic signalling cascades for considerably longer than modern researchers, they offer a unique insight into the breadth of capability of the mammalian cell. As such, effector biology is a continuing source of revelation and revelry.

References

Aasland, R., Abrams, C., Ampe, C., Ball, L.J., Bedford, M.T., Cesareni, G., Gimona, M., Hurley, J.H., Jarchau, T., Lehto, V.P., et al. (2002). Normalization of nomenclature for peptide motifs as ligands of modular protein domains. FEBS Lett. *513*, 141–144.

Abe, H., Tatsuno, I., Tobe, T., Okutani, A., and Sasakawa, C. (2002). Bicarbonate ion stimulates the expression of locus of enterocyte effacement-encoded genes in enterohemorrhagic Escherichia coli O157:H7. Infect. Immun. *70*, 3500–3509.

Abe, H., Miyahara, A., Oshima, T., Tashiro, K., Ogura, Y., Kuhara, S., Ogasawara, N., Hayashi, T., and Tobe, T. (2008). Global regulation by horizontally transferred regulators establishes the pathogenicity of Escherichia coli. DNA Res. *15*, 13–23.

Abreu, A.G., and Barbosa, A.S. (2017). How Escherichia coli circumvent complement-mediated killing. Front. Immunol. *8*, 1–6.

Adams, C., Cazzanelli, G., Rasul, S., Hitchinson, B., Hu, Y., Coombes, R.C., Raguz, S., and Yagüe, E. (2015). Apoptosis inhibitor TRIAP1 is a novel effector of drug resistance. Oncol. Rep. *34*, 415–422.

Adu-Bobie, J., Frankel, G., Bain, C., Goncalves, A.G., Trabulsi, L.R., Douce, G., Knutton, S., and Dougan, G. (1998). Detection of intimins α, β, γ, and δ, four intimin derivatives expressed by attaching and effacing microbial pathogens. J. Clin. Microbiol. *36*, 662–668.

Agatep, R., Kirkpatrick, R.D., Parchaliuk, D.L., Woods, R.A., and Gietz, R.D. (1998). Transformation of Saccharomyces cerevisiae by the lithium acetate/single-stranded carrier DNA/polyethylene glycol protocol. Tech. Tips Online *3*, 133–137.

Akhter, A., Caution, K., Abu Khweek, A., Tazi, M., Abdulrahman, B.A., Abdelaziz, D.H.A., Voss, O.H., Doseff, A.I., Hassan, H., Azad, A.K., et al. (2012). Caspase-11 Promotes the Fusion of Phagosomes Harboring Pathogenic Bacteria with Lysosomes by Modulating Actin Polymerization. Immunity *37*, 35–47.

Aktories, K. (2011). Bacterial protein toxins that modify host regulatory GTPases. Nat. Rev. Microbiol. *9*, 487–498.

Aktories, K., Lang, A.E., Schwan, C., and Mannherz, H.G. (2011). Actin as target for modification by bacterial protein toxins. FEBS J. *278*, 4526–4543.

Allen-Vercoe, E., Toh, M.C.W., Waddell, B., Ho, H., and DeVinney, R. (2005). A carboxy-terminal domain of Tir from enterohemorrhagic Escherichia coli O157:H7 (EHEC O157:H7) required for efficient type III secretion. FEMS Microbiol. Lett. *243*, 355–364.

Allen-Vercoe, E., Waddell, B., Toh, M.C.W., and DeVinney, R. (2006). Amino acid residues within enterohemorrhagic Escherichia coli O157:H7 Tir involved in phosphorylation, α-actinin recruitment, and Nck-independent pedestal formation. Infect. Immun. *74*, 6196–6205.

Alto, N.M., Shao, F., Lazar, C.S., Brost, R.L., Chua, G., Mattoo, S., McMahon, S.A., Ghosh, P., Hughes, T.R., Boone, C., et al. (2006). Identification of a bacterial type III effector family with G protein mimicry functions. Cell *124*, 133–145.

Alto, N.M., Weflen, A.W., Rardin, M.J., Yarar, D., Lazar, C.S., Tonikian, R., Koller, A., Taylor, S.S., Boone, C., Sidhu, S.S., et al. (2007). The type III effector EspF coordinates membrane trafficking by the spatiotemporal activation of two eukaryotic signaling pathways. J. Cell Biol. *178*, 1265–1278.

Ambrosi, C., Pompili, M., Scribano, D., Limongi, D., Petrucca, A., Cannavacciuolo, S., Schippa, S., Zagaglia, C., Grossi, M., and Nicoletti, M. (2015). The Shigella flexneri OspB effector: an early immunomodulator. Int. J. Med. Microbiol. *305*, 75–84.

Arbeloa, A., Bulgin, R.R., Mackenzie, G., Shaw, R.K., Pallen, M.J., Crepin, V.F., Berger, C.N., and Frankel, G. (2008). Subversion of actin dynamics by EspM effectors of attaching and effacing bacterial pathogens. Cell. Microbiol. *10*, 1429–1441.

Arbeloa, A., Blanco, M., Moreira, F.C., Bulgin, R., López, C., Dahbi, G., Blanco, J.E., Mora, A., Alonso, M.P., Mamani, R.C., et al. (2009). Distribution of espM and espT among enteropathogenic and enterohaemorrhagic Escherichia coli. J. Med. Microbiol. *58*, 988–995.

Arbeloa, A., Garnett, J., Lillington, J., Bulgin, R.R., Berger, C.N., Lea, S.M., Matthews, S., and Frankel, G.

(2010). EspM2 is a RhoA guanine nucleotide exchange factor. Cell. Microbiol. *12*, 654–664.
Arbeloa, A., Oates, C. V., Marchès, O., Hartland, E.L., and Frankel, G. (2011). Enteropathogenic and enterohemorrhagic Escherichia coli type III secretion effector EspV induces radical morphological changes in eukaryotic cells. Infect. Immun. *79*, 1067–1076.
Arnold, R., Brandmaier, S., Kleine, F., Tischler, P., Heinz, E., Behrens, S., Niinikoski, A., Mewes, H.-W., Horn, M., and Rattei, T. (2009). Sequence-Based Prediction of Type III Secreted Proteins. PLoS Pathog. *5*, e1000376.
Barthold, S.W., Coleman, G.L., Bhatt, P.N., Osbaldiston, G.W., and Jonas, A.M. (1976). The etiology of transmissible murine colonic hyperplasia. Lab. Anim. Sci. *26*, 889–894.
Baruch, K., Gur-Arie, L., Nadler, C., Koby, S., Yerushalmi, G., Ben-Neriah, Y., Yogev, O., Shaulian, E., Guttman, C., Zarivach, R., et al. (2011). Metalloprotease type III effectors that specifically cleave JNK and NF-κB. EMBO J. *30*, 221–231.
Baumann, D., Salia, H., Greune, L., Norkowski, S., Körner, B., Uckeley, Z.M., Frankel, G., Guenot, M., Rüter, C., and Schmidt, M.A. (2018). Multitalented EspB of enteropathogenic Escherichia coli (EPEC) enters cells autonomously and induces programmed cell death in human monocytic THP-1 cells. Int. J. Med. Microbiol. *308*, 387–404.
Belyy, A., Santecchia, I., Renault, L., Bourigault, B., Ladant, D., and Mechold, U. (2018). The extreme C terminus of the Pseudomonas aeruginosa effector ExoY is crucial for binding to its eukaryotic activator, F-actin. J. Biol. Chem. *293*, 19785–19796.
Berger, C.N., Crepin, V.F., Jepson, M.A., Arbeloa, A., and Frankel, G. (2009). The mechanisms used by enteropathogenic Escherichia coli to control filopodia dynamics. Cell. Microbiol. *11*, 309–322.
Berger, C.N., Crepin, V.F., Baruch, K., Mousnier, A., Rosenshine, I., and Frankel, G. (2012). EspZ of Enteropathogenic and Enterohemorrhagic Escherichia coli Regulates Type III Secretion System Protein Translocation. MBio *3*, 1–12.
Berger, C.N., Crepin, V.F., Roumeliotis, T.I., Wright, J.C., Carson, D., Pevsner-Fischer, M., Furniss, R.C.D., Dougan, G., Dori-Bachash, M., Yu, L., et al. (2017). Citrobacter rodentium Subverts ATP Flux and Cholesterol Homeostasis in Intestinal Epithelial Cells In Vivo. Cell Metab. *26*, 738-752.e6.
Berger, C.N., Crepin, V.F., Roumeliotis, T.I., Wright, J.C., Serafini, N., Pevsner-Fischer, M., Yu, L., Elinav, E., Di Santo, J.P., Choudhary, J.S., et al. (2018). The Citrobacter rodentium type III secretion system effector EspO affects mucosal damage repair and antimicrobial responses. PLoS Pathog. *14*, 1–23.
Berghe, T. Vanden, Linkermann, A., Jouan-Lanhouet, S., Walczak, H., and Vandenabeele, P. (2014). Regulated necrosis: the expanding network of non-apoptotic cell death pathways. Nat. Rev. Mol. Cell Biol. *15*, 135–147.
Bhat, M.I., Sowmya, K., Kapila, S., and Kapila, R. (2019). Escherichia coli K12: An evolving opportunistic commensal gut microbe distorts barrier integrity in human intestinal cells. Microb. Pathog. *133*, 103545.
Biemans-Oldehinkel, E., Sal-Man, N., Deng, W., Foster, L.J., and Finlay, B.B. (2011). Quantitative proteomic analysis reveals formation of an EscL-EscQ-EscN type III complex in enteropathogenic Escherichia coli. J. Bacteriol. *193*, 5514–5519.
Blasche, S., Mörtl, M., Steuber, H., Siszler, G., Nisa, S., Schwarz, F., Lavrik, I., Gronewold, T.M.A., Maskos, K., Donnenberg, M.S., et al. (2013). The E. coli effector protein NleF is a caspase inhibitor. PLoS One *8*, e58937.
Blasche, S., Arens, S., Ceol, A., Siszler, G., Schmid, M.A., Häuser, R., Schwarz, F., Wuchty, S., Aloy, P., Uetz, P., et al. (2014). The EHEC-host interactome reveals novel targets for the translocated intimin receptor. Sci. Rep. *4*, 22–26.
Blount, Z.D. (2015). The unexhausted potential of E. coli. Elife *4*, 1–12.
Bommarius, B., Maxwell, D., Swimm, A., Leung, S., Corbett, A., Bornmann, W., and Kalman, D. (2007). Enteropathogenic Escherichia coli Tir is an SH2/3 ligand that recruits and activates tyrosine kinases required for pedestal formation. Mol. Microbiol. *63*, 1748–1768.
Brachmann, C.B., Davies, A., Cost, G.J., Caputo, E., Li, J., Hieter, P., and Boeke, J.D. (1998). Designer deletion strains derived from Saccharomyces cerevisiae S288C: A useful set of strains and plasmids for PCR-mediated gene disruption and other applications. Yeast *14*, 115–132.

Brinkmann, V. (2004). Neutrophil Extracellular Traps Kill Bacteria. Science (80-.). *303*, 1532–1535.
Vander Broek, C.W., Zainal Abidin, N., and Stevens, J.M. (2017). BipC, a predicted Burkholderia pseudomallei type 3 secretion system translocator protein with actin binding activity. Front. Cell. Infect. Microbiol. *7*, 1–10.
Broz, P., and Monack, D.M. (2013). Newly described pattern recognition receptors team up against intracellular pathogens. Nat. Rev. Immunol. *13*, 551–565.
Brunder, W., Schmidt, H., and Karch, H. (1997). EspP, a novel extracellular serine protease of enterohaemorrhagic Escherichia coli O157:H7 cleaves human coagulation factor V. Mol. Microbiol. *24*, 767–778.
Brunet, A., Bonni, A., Zigmond, M.J., Lin, M.Z., Juo, P., Hu, L.S., Anderson, M.J., Arden, K.C., Blenis, J., and Greenberg, M.E. (1999). Akt promotes cell survival by phosphorylating and inhibiting a forkhead transcription factor. Cell *96*, 857–868.
Buchholz, U., Bernard, H., Werber, D., Böhmer, M.M., Remschmidt, C., Wilking, H., Deleré, Y., an der Heiden, M., Adlhoch, C., Dreesman, J., et al. (2011). German Outbreak of Escherichia coli O104:H4 Associated with Sprouts. N. Engl. J. Med. *365*, 1763–1770.
Buchrieser, C., Glaser, P., Rusniok, C., Nedjari, H., D'Hauteville, H., Kunst, F., Sansonetti, P., and Parsot, C. (2000). The virulence plasmid pWR100 and the repertoire of proteins secreted by the type III secretion apparatus of Shigella flexneri. Mol. Microbiol. *38*, 760–771.
Bulgin, R., Arbeloa, A., Goulding, D., Dougan, G., Crepin, V.F., Raymond, B., and Frankel, G. (2009a). The T3SS effector EspT defines a new category of invasive enteropathogenic E. coli (EPEC) which form intracellular actin pedestals. PLoS Pathog. *5*, e1000683.
Bulgin, R., Raymond, B., Garnett, J.A., Frankel, G., Crepin, V.F., Berger, C.N., and Arbeloa, A. (2010). Bacterial guanine nucleotide exchange factors SopE-Like and WxxxE effectors. Infect. Immun. *78*, 1417–1425.
Bulgin, R.R., Arbeloa, A., Chung, J.C.S., and Frankel, G. (2009b). EspT triggers formation of lamellipodia and membrane ruffles through activation of Rac-1 and Cdc42. Cell. Microbiol. *11*, 217–229.
Burger, D., Fickentscher, C., De Moerloose, P., and Brandt, K.J. (2016). F-actin dampens NLRP3 inflammasome activity via Flightless-I and LRRFIP2. Sci. Rep. *6*, 1–12.
Burnaevskiy, N., Fox, T.G., Plymire, D.A., Ertelt, J.M., Weigele, B.A., Selyunin, A.S., Way, S.S., Patrie, S.M., and Alto, N.M. (2013). Proteolytic elimination of N-myristoyl modifications by the Shigella virulence factor IpaJ. Nature *496*, 106–109.
Burstein, D., Zusman, T., Degtyar, E., Viner, R., Segal, G., and Pupko, T. (2009). Genome-Scale Identification of Legionella pneumophila Effectors Using a Machine Learning Approach. PLoS Pathog. *5*, e1000508.
Burstein, D., Satanower, S., Simovitch, M., Belnik, Y., Zehavi, M., Yerushalmi, G., and Ben-aroya, S. (2015). Novel Type III Effectors in Pseudomonas aeruginosa. Mol. Biol. *6*, 2–7.
Buss, C., Müller, D., Rüter, C., Heusipp, G., and Schmidt, M.A. (2009). Identification and characterization of Ibe, a novel type III effector protein of A/E pathogens targeting human IQGAP1. Cell. Microbiol. *11*, 661–677.
Cai, Z., Jitkaew, S., Zhao, J., Chiang, H.C., Choksi, S., Liu, J., Ward, Y., Wu, L.G., and Liu, Z.G. (2014). Plasma membrane translocation of trimerized MLKL protein is required for TNF-induced necroptosis. Nat. Cell Biol. *16*, 55–65.
Calder, T., Kinch, L.N., Fernandez, J., Salomon, D., Grishin, N. V., and Orth, K. (2014). Vibrio type III effector VPA1380 is related to the cysteine protease domain of large bacterial toxins. PLoS One *9*, 1–8.
Campellone, K.G., Rankin, S., Pawson, T., Kirschner, M.W., Tipper, D.J., and Leong, J.M. (2004a). Clustering of Nck by a 12-residue Tir phosphopeptide is sufficient to trigger localized actin assembly. J. Cell Biol. *164*, 407–416.
Campellone, K.G., Robbins, D., and Leong, J.M. (2004b). EspFU is a translocated EHEC effector that interacts with Tir and N-WASP and promotes Nck-independent actin assembly. Dev. Cell *7*, 217–228.
Carlson-Banning, K.M., and Sperandio, V. (2018). Enterohemorrhagic Escherichia coli outwits hosts through sensing small molecules. Curr. Opin. Microbiol. *41*, 83–88.
Carson, D., Barry, R., Hopkins, E.G.D., Roumeliotis, T.I., García-Weber, D., Mullineaux-Sanders, C., Elinav,

E., Arrieumerlou, C., Choudhary, J.S., and Frankel, G. (2019). Citrobacter rodentium induces rapid and unique metabolic and inflammatory responses in mice suffering from severe disease. Cell. Microbiol. 1–17.
Caution, K., Gavrilin, M.A., Tazi, M., Kanneganti, A., Layman, D., Hoque, S., Krause, K., and Amer, A.O. (2015). Caspase-11 and caspase-1 differentially modulate actin polymerization via RhoA and Slingshot proteins to promote bacterial clearance. Sci. Rep. *5*, 1–13.
Celli, J., Olivier, M., and Finlay, B.B. (2001). Enteropathogenic Escherichia coli mediates antiphagocytosis through the inhibition of PI 3-kinase-dependent pathways. EMBO J. *20*, 1245–1258.
Cepeda-Molero, M., Berger, C.N., Walsham, A.D.S., Ellis, S.J., Wemyss-Holden, S., Schüller, S., Frankel, G., and Fernández, L.Á. (2017). Attaching and effacing (A/E) lesion formation by enteropathogenic E. coli on human intestinal mucosa is dependent on non-LEE effectors. PLOS Pathog. *13*, e1006706.
Chardin, P., Boquet, P., Madaule, P., Popoff, M.R., Rubin, E.J., and Gill, D.M. (1989). The mammalian G protein rhoC is ADP-ribosylated by Clostridium botulinum exoenzyme C3 and affects actin microfilaments in Vero cells. EMBO J. *8*, 1087–1092.
Charpentier, X., and Oswald, E. (2004). Identification of the Secretion and Translocation Domain of the Enteropathogenic and Enterohemorrhagic. J. Bacteriol. *186*, 5486–5495.
Chen, X., Li, W., Ren, J., Huang, D., He, W.T., Song, Y., Yang, C., Li, W., Zheng, X., Chen, P., et al. (2014). Translocation of mixed lineage kinase domain-like protein to plasma membrane leads to necrotic cell death. Cell Res. *24*, 105–121.
Cheng, Y.L., Song, L.Q., Huang, Y.M., Xiong, Y.W., Zhang, X.A., Sun, H., Zhu, X.P., Meng, G.X., Xu, J.G., and Ren, Z.H. (2015). Effect of enterohaemorrhagic Escherichia coli O157: H7-specific enterohaemolysin on interleukin-1β production differs between human and mouse macrophages due to the different sensitivity of NLRP3 activation. Immunology *145*, 258–267.
Cherfils, J., and Zeghouf, M. (2013). Regulation of small GTPases by GEFs, GAPs, and GDIs. Physiol. Rev. *93*, 269–309.
Choi, M.E., Price, D.R., Ryter, S.W., and Choi, A.M.K. (2019). Necroptosis: a crucial pathogenic mediator of human disease. JCI Insight *4*.
Chung, L.K., Park, Y.H., Zheng, Y., Brodsky, I.E., Hearing, P., Kastner, D.L., Chae, J.J., and Bliska, J.B. (2016). The Yersinia Virulence Factor YopM Hijacks Host Kinases to Inhibit Type III Effector-Triggered Activation of the Pyrin Inflammasome. Cell Host Microbe *20*, 296–306.
Clements, A., Smollett, K., Lee, S.F., Hartland, E.L., Lowe, M., and Frankel, G. (2011). EspG of enteropathogenic and enterohemorrhagic E. coli binds the Golgi matrix protein GM130 and disrupts the Golgi structure and function. Cell. Microbiol. *13*, 1429–1439.
Clements, A., Young, J.C., Constantinou, N., and Frankel, G. (2012). Infection strategies of enteric pathogenic Escherichia coli. Gut Microbes *3*, 71–87.
Collins, J.W., Keeney, K.M., Crepin, V.F., Rathinam, V.A.K., Fitzgerald, K.A., Finlay, B.B., and Frankel, G. (2014). Citrobacter rodentium: infection, inflammation and the microbiota. Nat. Rev. Microbiol. *12*, 612–623.
Connolly, J.P.R., Brett Finlay, B., and Roe, A.J. (2015). From ingestion to colonization: The influence of the host environment on regulation of the LEE encoded type III secretion system in enterohaemorrhagic Escherichia coli. Front. Microbiol. *6*, 1–15.
Connolly, J.P.R., Slater, S.L., O'Boyle, N., Goldstone, R.J., Crepin, V.F., Ruano-Gallego, D., Herzyk, P., Smith, D.G.E., Douce, G.R., Frankel, G., et al. (2018). Host-associated niche metabolism controls enteric infection through fine-tuning the regulation of type 3 secretion. Nat. Commun. *9*, 4187.
Cookson, B.T., and Brennan, M.A. (2001). Pro-inflammatory programmed cell death. Trends Microbiol. *9*, 113–114.
Coombes, B.K., Wickham, M.E., Brown, N.F., Lemire, S., Bossi, L., Hsiao, W.W.L., Brinkman, F.S.L., and Finlay, B.B. (2005). Genetic and molecular analysis of GogB, a phage-encoded type III-secreted substrate in Salmonella enterica serovar typhimurium with autonomous expression from its associated phage. J. Mol. Biol. *348*, 817–830.
Coombes, B.K., Wickham, M.E., Mascarenhas, M., Gruenheid, S., Finlay, B.B., and Karmali, M.A. (2008). Molecular analysis as an aid to assess the public health risk of non-O157 shiga toxin-producing

Escherichia coli strains. Appl. Environ. Microbiol. *74*, 2153–2160.
Creasey, E.A., Delahay, R.M., Daniell, S.J., and Frankel, G. (2003a). Yeast two-hybrid system survey of interactions between LEE-encoded proteins of enteropathogenic Escherichia coli. Microbiology *149*, 2093–2106.
Creasey, E.A., Friedberg, D., Shaw, R.K., Umanski, T., Knutton, S., Rosenshine, I., and Frankel, G. (2003b). CesAB is an enteropathogenic Escherichia coli chaperone for the type-III translocator proteins EspA and EspB. Microbiology *149*, 3639–3647.
Crepin, V., Shaw, R., Abe, C., Knutton, S., and Frankel, G. (2005). Polarity of enteropathogenic Escherichia coli EspA filament assembly and protein secretion. J. Bacteriol. *187*, 2881–2889.
Crepin, V.F., Girard, F., Schüller, S., Phillips, A.D., Mousnier, A., and Frankel, G. (2010). Dissecting the role of the Tir:Nck and Tir:IRTKS/IRSp53 signalling pathways in vivo. Mol. Microbiol. *75*, 308–323.
Crepin, V.F., Collins, J.W., Habibzay, M., and Frankel, G. (2016). Citrobacter rodentium mouse model of bacterial infection. Nat. Protoc. *11*, 1851–1876.
Creuzburg, K., Heeren, S., Lis, C.M., Kranz, M., Hensel, M., and Schmidt, H. (2011). Genetic background and mobility of variants of the gene nleA in attaching and effacing Escherichia coli. Appl. Environ. Microbiol. *77*, 8705–8713.
Croxen, M.A., and Finlay, B.B. (2010). Molecular mechanisms of Escherichia coli pathogenicity. Nat. Rev. Microbiol. *8*, 26–38.
Cui, J., Yao, Q., Li, S., Ding, X., Lu, Q., Mao, H., Liu, L., Zheng, N., Chen, S., and Shao, F. (2010). Glutamine Deamidation and Dysfunction of Ubiquitin/NEDD8 Induced by a Bacterial Effector Family. Science (80-.). *329*, 1215–1218.
Dahan, S., Knutton, S., Shaw, R.K., Crepin, V.F., Dougan, G., and Frankel, G. (2004). Transcriptome of Enterohemorrhagic Escherichia coli O157 Adhering to Eukaryotic Plasma Membranes. Infect. Immun. *72*, 5452–5459.
Dahan, S., Wiles, S., La Ragione, R.M., Best, A., Woodward, M.J., Stevens, M.P., Shaw, R.K., Chong, Y., Knutton, S., Phillips, A., et al. (2005). EspJ is a prophage-carried type III effector protein of attaching and effacing pathogens that modulates infection dynamics. Infect. Immun. *73*, 679–686.
Dautin, N. (2010). Serine Protease Autotransporters of Enterobacteriaceae (SPATEs): Biogenesis and Function. Toxins (Basel). *2*, 1179–1206.
Dean, P., and Kenny, B. (2004). Intestinal barrier dysfunction by enteropathogenic Escherichia coli is mediated by two effector molecules and a bacterial surface protein. Mol. Microbiol. *54*, 665–675.
Dean, P., Maresca, M., Schüller, S., Phillips, A.D., and Kenny, B. (2006). Potent diarrheagenic mechanism mediated by the cooperative action of three enteropathogenic Escherichia coli-injected effector proteins. Proc. Natl. Acad. Sci. U. S. A. *103*, 1876–1881.
Dean, P., Scott, J.A., Knox, A.A., Quitard, S., Watkins, N.J., and Kenny, B. (2010). The enteropathogenic E. coli effector EspF targets and disrupts the nucleolus by a process regulated by mitochondrial dysfunction. PLoS Pathog. *6*.
Degterev, A., Huang, Z., Boyce, M., Li, Y., Jagtap, P., Mizushima, N., Cuny, G.D., Mitchison, T.J., Moskowitz, M.A., and Yuan, J. (2005). Chemical inhibitor of nonapoptotic cell death with therapeutic potential for ischemic brain injury. Nat. Chem. Biol. *1*, 112–119.
Delannoy, S., Beutin, L., and Fach, P. (2013). Discrimination of enterohemorrhagic Escherichia coli (EHEC) from Non-EHEC strains based on detection of various combinations of Type III effector genes. J. Clin. Microbiol. *51*, 3257–3262.
Deng, W., Vallance, B.A., Li, Y., Puente, J.L., and Finlay, B.B. (2003). Citrobacter rodentium translocated intimin receptor (Tir) is an essential virulence factor needed for actin condensation, intestinal colonization and colonic hyperplasia in mice. Mol. Microbiol. *48*, 95–115.
Deng, W., Puente, J.L., Gruenheid, S., Li, Y., Vallance, B.A., Vázquez, A., Barba, J., Ibarra, J.A., O'Donnell, P., Metalnikov, P., et al. (2004). Dissecting virulence: Systematic and functional analyses of a pathogenicity island. Proc. Natl. Acad. Sci. U. S. A. *101*, 3597–3602.
Deng, W., De Hoog, C.L., Yu, H.B., Li, Y., Croxen, M.A., Thomas, N.A., Puente, J.L., Foster, L.J., and Finlay, B.B. (2010). A comprehensive proteomic analysis of the type III secretome of Citrobacter rodentium. J. Biol. Chem. *285*, 6790–6800.

Deng, W., Yu, H.B., de Hoog, C.L., Stoynov, N., Li, Y., Foster, L.J., and Finlay, B.B. (2012). Quantitative Proteomic Analysis of Type III Secretome of Enteropathogenic Escherichia coli Reveals an Expanded Effector Repertoire for Attaching/Effacing Bacterial Pathogens. Mol. Cell. Proteomics *11*, 692–709.
Deng, W., Yu, H.B., Li, Y., and Finlay, B.B. (2015). SepD/SepL-dependent secretion signals of the type III secretion system translocator proteins in enteropathogenic Escherichia coli. J. Bacteriol. *197*, 1263–1275.
Dereeper, A., Guignon, V., Blanc, G., Audic, S., Buffet, S., Chevenet, F., Dufayard, J.F., Guindon, S., Lefort, V., Lescot, M., et al. (2008). Phylogeny.fr: robust phylogenetic analysis for the non-specialist. Nucleic Acids Res. *36*, 465–469.
Dhanasekaran, D.N., and Premkumar Reddy, E. (2017). JNK-signaling: A multiplexing hub in programmed cell death. Genes Cancer *8*, 682–694.
Dhuriya, Y.K., and Sharma, D. (2018). Necroptosis: A regulated inflammatory mode of cell death. J. Neuroinflammation *15*, 1–9.
Diepold, A., and Armitage, J.P. (2015). Type III secretion systems: the bacterial flagellum and the injectisome. Philos. Trans. R. Soc. B Biol. Sci. *370*, 20150020.
Diepold, A., Wiesand, U., and Cornelis, G.R. (2011). The assembly of the export apparatus (YscR,S,T,U,V) of the Yersinia type III secretion apparatus occurs independently of other structural components and involves the formation of an YscV oligomer. Mol. Microbiol. *82*, 502–514.
Ding, J., Wang, K., Liu, W., She, Y., Sun, Q., Shi, J., Sun, H., Wang, D.C., and Shao, F. (2016). Pore-forming activity and structural autoinhibition of the gasdermin family. Nature *535*, 111–116.
Ding, J., Pan, X., Du, L., Yao, Q., Xue, J., Yao, H., Wang, D.-C., Li, S., and Shao, F. (2019). Structural and Functional Insights into Host Death Domains Inactivation by the Bacterial Arginine GlcNAcyltransferase Effector. Mol. Cell 1–14.
Dondelinger, Y., Declercq, W., Montessuit, S., Roelandt, R., Goncalves, A., Bruggeman, I., Hulpiau, P., Weber, K., Sehon, C.A., Marquis, R.W., et al. (2014). MLKL Compromises Plasma Membrane Integrity by Binding to Phosphatidylinositol Phosphates. Cell Rep. *7*, 971–981.
Dondelinger, Y., Delanghe, T., Priem, D., Wynosky-Dolfi, M.A., Sorobetea, D., Rojas-Rivera, D., Giansanti, P., Roelandt, R., Gropengiesser, J., Ruckdeschel, K., et al. (2019). Serine 25 phosphorylation inhibits RIPK1 kinase-dependent cell death in models of infection and inflammation. Nat. Commun. *10*, 1729.
Dong, N., Liu, L., and Shao, F. (2010). A bacterial effector targets host DH-PH domain RhoGEFs and antagonizes macrophage phagocytosis. EMBO J. *29*, 1363–1376.
Dong, N., Zhu, Y., Lu, Q., Hu, L., Zheng, Y., and Shao, F. (2012). Structurally distinct bacterial TBC-like GAPs link Arf GTPase to Rab1 inactivation to counteract host defenses. Cell *150*, 1029–1041.
Donnenberg, M.S., Yu, J., and Kaper, J.B. (1993a). A second chromosomal gene necessary for intimate attachment of enteropathogenic Escherichia coli to epithelial cells. J. Bacteriol. *175*, 4670–4680.
Donnenberg, M.S., Tacket, C.O., James, S.P., Losonsky, G., Nataro, J.P., Wasserman, S.S., Kaper, J.B., and Levine, M.M. (1993b). Role of the eaeA gene in experimental enteropathogenic Escherichia coli infection. J. Clin. Invest. *92*, 1412–1417.
Donnenberg, M.S., Hazen, T.H., Farag, T.H., Panchalingam, S., Antonio, M., Hossain, A., Mandomando, I., Ochieng, J.B., Ramamurthy, T., Tamboura, B., et al. (2015). Bacterial Factors Associated with Lethal Outcome of Enteropathogenic Escherichia coli Infection: Genomic Case-Control Studies. PLoS Negl. Trop. Dis. *9*, e0003791.
Dziva, F., van Diemen, P.M., Stevens, M.P., Smith, A.J., and Wallis, T.S. (2004). Identification of Escherichia coli O157:H7 genes influencing colonization of the bovine gastrointestinal tract using signature-tagged mutagenesis. Microbiology *150*, 3631–3645.
Elliott, S.J., Krejany, E.O., Mellies, J.L., Robins-Browne, R.M., Sasakawa, C., and Kaper, J.B. (2001). EspG, a novel type III system-secreted protein from enteropathogenic Escherichia coli with similarities to virA of Shigella flexneri. Infect. Immun. *69*, 4027–4033.
Elliott, S.J., O'Connell, C.B., Koutsouris, A., Brinkley, C., Donnenberg, M.S., Hecht, G., and Kaper, J.B. (2002). A gene from the locus of enterocyte effacement that is required for enteropathogenic Escherichia coli to increase tight-junction permeability encodes a chaperone for EspF. Infect. Immun. *70*, 2271–2277.

Evavold, C.L., and Kagan, J.C. (2018). How Inflammasomes Inform Adaptive Immunity. J. Mol. Biol. *430*, 217–237.
Evavold, C.L., Ruan, J., Tan, Y., Xia, S., Wu, H., and Kagan, J.C. (2017). The Pore-Forming Protein Gasdermin D Regulates Interleukin-1 Secretion from Living Macrophages. Immunity *48*, 35-44.e6.
Farfán, M.J., Toro, C.S., Barry, E.M., and Nataro, J.P. (2011). Shigella enterotoxin-2 is a type III effector that participates in Shigella -induced interleukin 8 secretion by epithelial cells. FEMS Immunol. Med. Microbiol. *61*, 332–339.
Felix, R.S., Colleoni, G.W.B., Caballero, O.L., Yamamoto, M., Almeida, M.S.S., Andrade, V.C.C., Chauffaille, M. de L.L.F., Silva, W.A. da, Begnami, M.D., Soares, F.A., et al. (2009). SAGE analysis highlights the importance of p53csv, ddx5, mapkapk2 and ranbp2 to multiple myeloma tumorigenesis. Cancer Lett. *278*, 41–48.
Feoktistova, M., Geserick, P., Kellert, B., Dimitrova, D.P., Langlais, C., Hupe, M., Cain, K., MacFarlane, M., Häcker, G., and Leverkus, M. (2011). CIAPs Block Ripoptosome Formation, a RIP1/Caspase-8 Containing Intracellular Cell Death Complex Differentially Regulated by cFLIP Isoforms. Mol. Cell *43*, 449–463.
Feuerbacher, L.A., and Hardwidge, P.R. (2014). Influence of NleH effector expression, host genetics, and inflammation on Citrobacter rodentium colonization of mice. Microbes Infect. *16*, 429–433.
Fields, S., and Song, O. (1989). A novel genetic system to detect protein-protein interactions. Nature *340*, 245–246.
Figurski, D.H., and Helinski, D.R. (1979). Replication of an origin-containing derivative of plasmid RK2 dependent on a plasmid function provided in trans. Proc. Natl. Acad. Sci. *76*, 1648–1652.
Fook-Alves, V.L., de Oliveira, M.B., Zanatta, D.B., Strauss, B.E., and Colleoni, G.W.B. (2016). TP53 Regulated Inhibitor of Apoptosis 1 (TRIAP1) stable silencing increases late apoptosis by upregulation of caspase 9 and APAF1 in RPMI8226 multiple myeloma cell line. Biochim. Biophys. Acta - Mol. Basis Dis. *1862*, 1105–1110.
Frankel, G., and Phillips, A.D. (2008). Attaching effacing Escherichia coli and paradigms of Tir-triggered actin polymerization: Getting off the pedestal. Cell. Microbiol. *10*, 549–556.
Frankel, G., Candy, D.C.A., Fabiani, E., Adu-Bobie, J., Gil, S., Novakova, M., Phillips, A.D., and Dougan, G. (1995). Molecular characterization of a carboxy-terminal eukaryotic-cell-binding domain of intimin from enteropathogenic Escherichia coli. Infect. Immun. *63*, 4323–4328.
Fukazawa, A., Alonso, C., Kurachi, K., Gupta, S., Lesser, C.F., McCormick, B.A., and Reinecker, H.C. (2008). GEF-H1 mediated control of NOD1 dependent NF-κB activation by Shigella effectors. PLoS Pathog. *4*, 19–24.
Furniss, R.C.D., and Clements, A. (2017). Regulation of the Locus of Enterocyte Effacement in Attaching and Effacing Pathogens. J. Bacteriol. JB.00336-17.
Furniss, R.C.D., Slater, S., Frankel, G., and Clements, A. (2016). Enterohaemorrhagic E. coli modulates an ARF6:Rab35 signaling axis to prevent recycling endosome maturation during infection. J. Mol. Biol. *428*, 12–19.
Galluzzi, L., Vitale, I., Aaronson, S.A., Abrams, J.M., Adam, D., Agostinis, P., Alnemri, E.S., Altucci, L., Amelio, I., Andrews, D.W., et al. (2018). Molecular mechanisms of cell death: Recommendations of the Nomenclature Committee on Cell Death 2018. Cell Death Differ. *25*, 486–541.
Gao, W., Yang, J., Liu, W., Wang, Y., and Shao, F. (2016). Site-specific phosphorylation and microtubule dynamics control Pyrin inflammasome activation. Proc. Natl. Acad. Sci. U. S. A. *113*, E4857–E4866.
Gao, X., Wan, F., Mateo, K., Callegari, E., Wang, D., Deng, W., Puente, J., Li, F., Chaussee, M.S., Finlay, B.B., et al. (2009). Bacterial Effector Binding to Ribosomal Protein S3 Subverts NF-κB Function. PLoS Pathog. *5*, e1000708.
Gao, X., Wang, X., Pham, T.H., Feuerbacher, L.A., Lubos, M.-L., Huang, M., Olsen, R., Mushegian, A., Slawson, C., and Hardwidge, P.R. (2013). NleB, a Bacterial Effector with Glycosyltransferase Activity, Targets GAPDH Function to Inhibit NF-κB Activation. Cell Host Microbe *13*, 87–99.
García-Angulo, V.A., Deng, W., Thomas, N.A., Finlay, B.B., and Puente, J.L. (2008). Regulation of expression and secretion of NleH, a new non-locus of enterocyte effacement-encoded effector in Citrobacter rodentium. J. Bacteriol. *190*, 2388–2399.

García-Angulo, V.A., Martínez-Santos, V.I., Villaseñor, T., Santana, F.J., Huerta-Saquero, A., Martínez, L.C., Jiménez, R., Lara-Ochoa, C., Téllez-Sosa, J., Bustamante, V.H., et al. (2012). A distinct regulatory sequence is essential for the expression of a subset of nle genes in attaching and effacing Escherichia coli. J. Bacteriol. *194*, 5589–5603.
García-Gómez, E., Espinosa, N., de la Mora, J., Dreyfus, G., and González-Pedrajo, B. (2011). The muramidase EtgA from enteropathogenic Escherichia coli is required for efficient type III secretion. Microbiology *157*, 1145–1160.
Garmendia, J., and Frankel, G. (2005). Operon structure and gene expression of the espJ-tccP locus of enterohaemorrhagic Escherichia coli O157:H7. FEMS Microbiol. Lett. *247*, 137–145.
Garmendia, J., Phillips, A.D., Carlier, M.-F., Chong, Y., Schüller, S., Marches, O., Dahan, S., Oswald, E., Shaw, R.K., Knutton, S., et al. (2004). TccP is an enterohaemorrhagic Escherichia coli O157:H7 type III effector protein that couples Tir to the actin-cytoskeleton. Cell. Microbiol. *6*, 1167–1183.
Garmendia, J., Ren, Z., Tennant, S., Viera, M.A.M., Chong, Y., Whale, A., Azzopardi, K., Dahan, S., Sircili, M.P., Franzolin, M.R., et al. (2005). Distribution of tccP in clinical enterohemorrhagic and enteropathogenic Escherichia coli isolates. J. Clin. Microbiol. *43*, 5715–5720.
Garmendia, J., Carlier, M.F., Egile, C., Didry, D., and Frankel, G. (2006). Characterization of TccP-mediated N-WASP activation during enterohaemorrhagic Escherichia coli infection. Cell. Microbiol. *8*, 1444–1455.
Gawthorne, J.A., Audry, L., McQuitty, C., Dean, P., Christie, J.M., Enninga, J., and Roe, A.J. (2016). Visualizing the translocation and localization of bacterial type III effector proteins by using a genetically encoded reporter system. Appl. Environ. Microbiol. *82*, 2700–2708.
Gaytán, M.O., Martínez-Santos, V.I., Soto, E., and González-Pedrajo, B. (2016). Type Three Secretion System in Attaching and Effacing Pathogens. Front. Cell. Infect. Microbiol. *6*, 129.
Germane, K.L., and Spiller, B.W. (2011). Structural and functional studies indicate that the EPEC effector, EspG, directly binds p21-activated kinase. Biochemistry *50*, 917–919.
Germane, K.L., Ohi, R., Goldberg, M.B., and Spiller, B.W. (2008). Structural and functional studies indicate that Shigella VirA is not a protease and does not directly destabilize microtubules. Biochemistry *47*, 10241–10243.
Gill, R.K., Borthakur, A., Hodges, K., Turner, J.R., Clayburgh, D.R., Saksena, S., Zaheer, A., Ramaswamy, K., Hecht, G., and Dudeja, P.K. (2007). Mechanism underlying inhibition of intestinal apical Cl-/OH- exchange following infection with enteropathogenic E. coli. J. Clin. Invest. *117*, 428–437.
Glotfelty, L.G., Zahs, A., Hodges, K., Shan, K., Alto, N.M., and Hecht, G.A. (2014). Enteropathogenic E. coli effectors EspG1/G2 disrupt microtubules, contribute to tight junction perturbation and inhibit restoration. Cell. Microbiol. *16*, 1767–1783.
Goddard, P.J., Sanchez-Garrido, J., Slater, S.L., Kalyan, M., Ruano-Gallego, D., Marchès, O., Fernández, L.Á., Frankel, G., and Shenoy, A.R. (2019). Enteropathogenic Escherichia coli Stimulates Effector-Driven Rapid Caspase-4 Activation in Human Macrophages. Cell Rep. *27*, 1008-1017.e6.
Gomes, T.A.T., Elias, W.P., Scaletsky, I.C.A., Guth, B.E.C., Rodrigues, J.F., Piazza, R.M.F., Ferreira, L.C.S., and Martinez, M.B. (2016). Diarrheagenic Escherichia coli. Brazilian J. Microbiol. *47 Suppl 1*, 3–30.
Goosney, D.L., Celli, J., Kenny, B., and Finlay, B.B. (1999). Enteropathogenic Escherichia coli inhibits phagocytosis. Infect. Immun. *67*, 490–495.
Grishin, A.M., Cherney, M., Anderson, D.H., Phanse, S., Babu, M., and Cygler, M. (2014). NleH Defines a new family of bacterial effector kinases. Structure *22*, 250–259.
Gruenheid, S., Sekirov, I., Thomas, N.A., Deng, W., O'Donnell, P., Goode, D., Li, Y., Frey, E.A., Brown, N.F., Metalnikov, P., et al. (2004). Identification and characterization of NleA, a non-LEE-encoded type III translocated virulence factor of enterohaemorrhagic Escherichia coli O157:H7. Mol. Microbiol. *51*, 1233–1249.
Guttman, J.A., Kazemi, P., Lin, A.E., Vogl, A.W., and Finlay, B.B. (2007). Desmosomes are unaltered during infections by attaching and effacing pathogens. Anat. Rec. *290*, 199–205.
Haiko, J., and Westerlund-Wikström, B. (2013). The role of the bacterial flagellum in adhesion and virulence. Biology (Basel). *2*, 1242–1267.
Halavaty, A.S., Anderson, S.M., Wawrzak, Z., Kudritska, M., Skarina, T., Anderson, W.F., and Savchenko,

A. (2014). Type III effector NleH2 from Escherichia coli O157:H7 str. Sakai features an atypical protein kinase domain. Biochemistry *53*, 2433–2435.
Hannemann, S., and Galán, J.E. (2017). Salmonella enterica serovar-specific transcriptional reprogramming of infected cells. PLoS Pathog. *13*, 1–17.
Hayward, R.D., Hume, P.J., Humphreys, D., Phillips, N., Smith, K., and Koronakis, V. (2009). Clustering transfers the translocated Escherichia coli receptor into lipid rafts to stimulate reversible activation of c-Fyn. Cell. Microbiol. *11*, 433–441.
Hazen, T.H., and Rasko, D.A. (2019). The complete genome of the atypical enteropathogenic Escherichia coli archetype isolate E110019 highlights a role for plasmids in dissemination of the type III secreted effector ESPT. Infect. Immun. *87*, 1–10.
Hazen, T.H., Sahl, J.W., Fraser, C.M., Donnenberg, M.S., Scheutz, F., and Rasko, D. a (2013). Refining the pathovar paradigm via phylogenomics of the attaching and effacing Escherichia coli. Proc. Natl. Acad. Sci. U. S. A. *110*, 12810–12815.
Hazen, T.H., Donnenberg, M.S., Panchalingam, S., Antonio, M., Hossain, A., Mandomando, I., Ochieng, J.B., Ramamurthy, T., Tamboura, B., Qureshi, S., et al. (2016). Genomic diversity of EPEC associated with clinical presentations of differing severity. Nat. Microbiol. *1*, 15014.
He, S., Wang, L., Miao, L., Wang, T., Du, F., Zhao, L., and Wang, X. (2009). Receptor Interacting Protein Kinase-3 Determines Cellular Necrotic Response to TNF-α. Cell *137*, 1100–1111.
Heilig, R., Dick, M.S., Sborgi, L., Meunier, E., Hiller, S., and Broz, P. (2018). The Gasdermin-D pore acts as a conduit for IL-1β secretion in mice. Eur. J. Immunol. *48*, 584–592.
Hemrajani, C., Marchès, O., Wiles, S., Girard, F., Dennis, A., Dziva, F., Best, A., Phillips, A.D., Berger, C.N., Mousnier, A., et al. (2008). Role of NleH, a type III secreted effector from attaching and effacing pathogens, in colonization of the bovine, ovine, and murine gut. Infect. Immun. *76*, 4804–4813.
Hemrajani, C., Berger, C.N., Robinson, K.S., Marches, O., Mousnier, A., and Frankel, G. (2010). NleH effectors interact with Bax inhibitor-1 to block apoptosis during enteropathogenic Escherichia coli infection. Proc. Natl. Acad. Sci. *107*.
Herrero, M., De Lorenzo, V., and Timmis, K.N. (1990). Transposon vectors containing non-antibiotic resistance selection markers for cloning and stable chromosomal insertion of foreign genes in gram-negative bacteria. J. Bacteriol. *172*, 6557–6567.
Herring, C.D., Glasner, J.D., and Blattner, F.R. (2003). Gene replacement without selection: Regulated suppression of amber mutations in Escherichia coli. Gene *311*, 153–163.
Herrmann, C., Ahmadian, M.R., Hofmann, F., and Just, I. (1998). Functional Consequences of Monoglucosylation of Ha-Ras at Effector Domain Amino Acid Threonine 35. J. Biol. Chem. *273*, 16134–16139.
Herzer, P.J., Inouye, S., Inouye, M., and Whittam, T.S. (1990). Phylogenetic distribution of branched RNA-linked multicopy single-stranded DNA among natural isolates of Escherichia coli. J. Bacteriol. *172*, 6175–6181.
Higgins, L.M., Frankel, G., Douce, G., Dougan, G., and MacDonald, T.T. (1999). Citrobacter rodentium infection in mice elicits a mucosal Th1 cytokine response and lesions similar to those in murine inflammatory bowel disease. Infect. Immun. *67*, 3031–3039.
Hiyoshi, H., Kodama, T., Saito, K., Gotoh, K., Matsuda, S., Akeda, Y., Honda, T., and Iida, T. (2011). VopV, an F-actin-binding type III secretion effector, is required for vibrio parahaemolyticus-induced enterotoxicity. Cell Host Microbe *10*, 401–409.
Hobbs, C.K., Porter, V.L., Stow, M.L.S., Siame, B.A., Tsang, H.H., and Leung, K.Y. (2016). Computational approach to predict species-specific type III secretion system (T3SS) effectors using single and multiple genomes. BMC Genomics *17*, 1–11.
Hodges, K., Alto, N.M., Ramaswamy, K., Dudeja, P.K., and Hecht, G. (2008). The enteropathogenic Escherichia coli effector protein EspF decreases sodium hydrogen exchanger 3 activity. Cell. Microbiol. *10*, 1735–1745.
Hodgson, A., Wier, E.M., Fu, K., Sun, X., Yu, H., Zheng, W., Sham, H.P., Johnson, K., Bailey, S., Vallance, B.A., et al. (2015). Metalloprotease NleC Suppresses Host NF-κB/Inflammatory Responses by Cleaving p65 and Interfering with the p65/RPS3 Interaction. PLoS Pathog. *11*, 1–23.

Hohmann, and Dehghani (2019). The Cytoskeleton—A Complex Interacting Meshwork. Cells *8*, 362.
Holmes, A., Mühlen, S., Roe, A.J., and Dean, P. (2010). The EspF effector, a bacterial pathogen's swiss army knife. Infect. Immun. *78*, 4445–4453.
Holze, C., Michaudel, C., MacKowiak, C., Haas, D.A., Benda, C., Hubel, P., Pennemann, F.L., Schnepf, D., Wettmarshausen, J., Braun, M., et al. (2018). Oxeiptosis, a ROS-induced caspase-independent apoptosis-like cell-death pathway article. Nat. Immunol. *19*, 130–140.
Hopkins, E.G.D., Roumeliotis, T.I., Mullineaux-Sanders, C., Choudhary, J.S., and Frankel, G. (2019). Intestinal Epithelial Cells and the Microbiome Undergo Swift Reprogramming at the Inception of Colonic Citrobacter rodentium Infection. MBio *10*, 1–19.
Hovis, K.M., Mojica, S., McDermott, J.E., Pedersen, L., Simhi, C., Rank, R.G., Myers, G.S.A., Ravel, J., Hsia, R., and Bavoil, P.M. (2013). Genus-optimized strategy for the identification of chlamydial type III secretion substrates. Pathog. Dis. *69*, 213–222.
Hsu, Y., Jubelin, G., Taieb, F., Nougayrède, J.-P., Oswald, E., and Stebbins, C.E. (2008). Structure of the Cyclomodulin Cif from Pathogenic Escherichia coli. J. Mol. Biol. *384*, 465–477.
Hu, J., Worrall, L.J., and Strynadka, N.C. (2020). Towards capture of dynamic assembly and action of the T3SS at near atomic resolution. Curr. Opin. Struct. Biol. *61*, 71–78.
Huang, D., Zheng, X., Wang, Z., Chen, X., He, W., Zhang, Y., Xu, J.-G., Zhao, H., Shi, W., Wang, X., et al. (2016). The MLKL Channel in Necroptosis Is an Octamer Formed by Tetramers in a Dyadic Process. Mol. Cell. Biol. *37*, 1–17.
Huang, Z., Sutton, S.E., Wallenfang, A.J., Orchard, R.C., Wu, X., Feng, Y., Chai, J., and Alto, N.M. (2009). Structural insights into host GTPase isoform selection by a family of bacterial GEF mimics. Nat. Struct. Mol. Biol. *16*, 853–860.
Hume, P.J., Singh, V., Davidson, A.C., and Koronakis, V. (2017). Swiss army pathogen: The Salmonella entry toolkit. Front. Cell. Infect. Microbiol. *7*, 1–13.
Humphreys, D., Singh, V., and Koronakis, V. (2016). Inhibition of WAVE Regulatory Complex Activation by a Bacterial Virulence Effector Counteracts Pathogen Phagocytosis. Cell Rep. *17*, 697–707.
Ide, T., Laarmann, S., Greune, L., Schillers, H., Oberleithner, H., and Schmidt, M.A. (2001). Characterization of translocation pores inserted into plasma membranes by type III-secreted Esp proteins of enteropathogenic Escherichia coli. Cell. Microbiol. *3*, 669–679.
Iguchi, A., Thomson, N.R., Ogura, Y., Saunders, D., Ooka, T., Henderson, I.R., Harris, D., Asadulghani, M., Kurokawa, K., Dean, P., et al. (2009). Complete genome sequence and comparative genome analysis of enteropathogenic Escherichia coli O127:H6 strain E2348/69. J. Bacteriol. *91*, 347–354.
Iizumi, Y., Sagara, H., Kabe, Y., Azuma, M., Kume, K., Ogawa, M., Nagai, T., Gillespie, P.G., Sasakawa, C., and Handa, H. (2007). The Enteropathogenic E. coli Effector EspB Facilitates Microvillus Effacing and Antiphagocytosis by Inhibiting Myosin Function. Cell Host Microbe *2*, 383–392.
Ikenouchi, J., and Aoki, K. (2017). Membrane bleb: A seesaw game of two small GTPases. Small GTPases *8*, 85–89.
Izoré, T., Job, V., and Dessen, A. (2011). Biogenesis, regulation, and targeting of the type III secretion system. Structure *19*, 603–612.
Jacquemet, G., Hamidi, H., and Ivaska, J. (2015). Filopodia in cell adhesion, 3D migration and cancer cell invasion. Curr. Opin. Cell Biol. *36*, 23–31.
Jennings, E., Esposito, D., Rittinger, K., and Thurston, T.L.M. (2018). Structure-function analyses of the bacterial zinc metalloprotease effector protein GtgA uncover key residues required for deactivating NF-κB. J. Biol. Chem. *293*, 15316–15329.
Jepson, M.A., Pellegrin, S., Peto, L., Banbury, D.N., Leard, A.D., Mellor, H., and Kenny, B. (2003). Synergistic roles for the Map and Tir effector molecules in mediating uptake of enteropathogenic Escherichia coli (EPEC) into non-phagocytic cells. Cell. Microbiol. *5*, 773–783.
Jerse, A.E., and Kaper, J.B. (1991). The eae gene of enteropathogenic Escherichia coli encodes a 94-kilodalton membrane protein, the expression of which is influenced by the EAF plasmid. Infect. Immun. *59*, 4302–4309.
Julien, O., and Wells, J.A. (2017). Caspases and their substrates. Cell Death Differ. *24*, 1380–1389.
Kailasan Vanaja, S., Rathinam, V.A.K., Atianand, M.K., Kalantari, P., Skehan, B., Fitzgerald, K.A., and

Leong, J.M. (2014). Bacterial RNA:DNA hybrids are activators of the NLRP3 inflammasome. Proc. Natl. Acad. Sci. *111*, 7765–7770.
Kanack, K.J., Crawford, J.A., Tatsuno, I., Karmali, M.A., and Kaper, J.B. (2005). SepZ/EspZ is secreted and translocated into HeLa cells by the enteropathogenic Escherichia coli type III secretion system. Infect. Immun. *73*, 4327–4337.
Kaper, J.B., Nataro, J.P., and Mobley, H.L. (2004). Pathogenic Escherichia coli. Nat. Rev. Microbiol. *2*, 123–140.
Kawasaki, T., and Kawai, T. (2014). Toll-like receptor signaling pathways. Front. Immunol. *5*, 1–8.
Kayagaki, N., Warming, S., Lamkanfi, M., Walle, L. Vande, Louie, S., Dong, J., Newton, K., Qu, Y., Liu, J., Heldens, S., et al. (2011). Non-canonical inflammasome activation targets caspase-11. Nature *479*, 117–121.
Kayagaki, N., Stowe, I.B., Lee, B.L., O'Rourke, K., Anderson, K., Warming, S., Cuellar, T., Haley, B., Roose-Girma, M., Phung, Q.T., et al. (2015). Caspase-11 cleaves gasdermin D for non-canonical inflammasome signalling. Nature *526*, 666–671.
Kelley, L.A., Mezulis, S., Yates, C.M., Wass, M.N., and Sternberg, M.J.E. (2015). The Phyre2 web portal for protein modeling, prediction and analysis. Nat. Protoc. *10*, 845–858.
Kelly, M., Hart, E., Mundy, R., Marchès, O., Wiles, S., Badea, L., Luck, S., Tauschek, M., Frankel, G., Robins-Browne, R.M., et al. (2006). Essential role of the type III secretion system effector NleB in colonization of mice by Citrobacter rodentium. Infect. Immun. *74*, 2328–2337.
Kenny, B., and Jepson, M. (2000). Targeting of an enteropathogenic Escherichia coli (EPEC) effector protein to host mitochondria. Cell. Microbiol. *2*, 579–590.
Kenny, B., and Warawa, J. (2001). Enteropathogenic Escherichia coli (EPEC) Tir receptor molecule does not undergo full modification when introduced into host cells by EPEC-independent mechanisms. Infect. Immun. *69*, 1444–1453.
Kenny, B., DeVinney, R., Stein, M., Reinscheid, D.J., Frey, E.A., and Finlay, B.B. (1997). Enteropathogenic E. coli (EPEC) transfers its receptor for intimate adherence into mammalian cells. Cell *91*, 511–520.
Kenny, B., Ellis, S., Leard, A.D., Warawa, J., Mellor, H., and Jepson, M.A. (2002). Co-ordinate regulation of distinct host cell signalling pathways by multifunctional enteropathogenic Escherichia coli effector molecules. Mol. Microbiol. *44*, 1095–1107.
Kerr, J.F.R., Wyllie, A.H., and Currie, A.R. (1972). Apoptosis: A Basic Biological Phenomenon with Wideranging Implications in Tissue Kinetics. Br. J. Cancer *26*, 239–257.
Ketteler, J., Panic, A., Reis, H., Wittka, A., Maier, P., Herskind, C., Yagüe, E., Jendrossek, V., and Klein, D. (2019). Progression-Related Loss of Stromal Caveolin 1 Levels Mediates Radiation Resistance in Prostate Carcinoma via the Apoptosis Inhibitor TRIAP1. J. Clin. Med. *8*, 348.
Kim, D.W., Lenzen, G., Page, A.L., Legrain, P., Sansonetti, P.J., and Parsot, C. (2005). The Shigella flexneri effector OspG interferes with innate immune responses by targeting ubiquitin-conjugating enzymes. Proc. Natl. Acad. Sci. U. S. A. *102*, 14046–14051.
Kim, J., Thanabalasuriar, A., Chaworth-Musters, T., Fromme, J.C., Frey, E.A., Lario, P.I.I., Metalnikov, P., Rizg, K., Thomas, N.A., Lee, S.F., et al. (2007). The Bacterial Virulence Factor NleA Inhibits Cellular Protein Secretion by Disrupting Mammalian COPII Function. Cell Host Microbe *2*, 160–171.
Kim, M., Ogawa, M., Fujita, Y., Yoshikawa, Y., Nagai, T., Koyama, T., Nagai, S., Lange, A., Fässler, R., and Sasakawa, C. (2009). Bacteria hijack integrin-linked kinase to stabilize focal adhesions and block cell detachment. Nature *459*, 578–582.
Kralicek, S.E., Nguyen, M., Rhee, K.J., Tapia, R., and Hecht, G. (2018). EPEC NleH1 is significantly more effective in reversing colitis and reducing mortality than NleH2 via differential effects on host signaling pathways. Lab. Investig. *98*, 477–488.
Krause, M., and Gautreau, A. (2014). Steering cell migration: lamellipodium dynamics and the regulation of directional persistence. Nat. Rev. Mol. Cell Biol. *15*, 577–590.
Krause, M., Barth, H., and Schmidt, H. (2018). Toxins of Locus of Enterocyte Effacement-Negative Shiga Toxin-Producing Escherichia coli. Toxins (Basel). *10*, 241.
Kresse, A.U., Beltrametti, F., Muller, A., Ebel, F., and Guzman, C.A. (2000). Characterization of SepL of enterohemorrhagic Escherichia coli. J. Bacteriol. *182*, 6490–6498.

Kufer, T.A., Creagh, E.M., and Bryant, C.E. (2019). Guardians of the Cell: Effector-Triggered Immunity Steers Mammalian Immune Defense. Trends Immunol. *40*, 939–951.
Kurushima, J., Nagai, A., Nagamatsu, K., and Abe, A. (2010). EspJ effector in enterohemorrhagic E. coli translocates into host mitochondria via an atypical mitochondrial targeting signal. Microbiol. Immunol. *54*, 371–379.
Lacey, C.A., and Miao, E.A. (2019). Programmed Cell Death in the Evolutionary Race against Bacterial Virulence Factors. Cold Spring Harb. Perspect. Biol. a036459.
Lacher, D.W., Steinsland, H., Blank, T.E., Donnenberg, M.S., and Whittam, T.S. (2007). Molecular evolution of typical enteropathogenic Escherichia coli: Clonal analysis by multilocus sequence typing and virulence gene allelic profiling. J. Bacteriol. *189*, 342–350.
Lai, Y.S., Rosenshine, I., Leong, J.M., and Frankel, G. (2013). Intimate host attachment: enteropathogenic and enterohaemorrhagic Escherichia coli. Cell. Microbiol. *15*, 1796–1808.
Lara-Tejero, M., and Galán, J.E. (2019). The Injectisome, a Complex Nanomachine for Protein Injection into Mammalian Cells. EcoSal Plus *8*, 1–12.
Lara-Tejero, M., Kato, J., Wagner, S., Liu, X., and Galán, J.E. (2011). A sorting platform determines the order of protein secretion in bacterial type III systems. Science *331*, 1188–1191.
Larzábal, M., Marques Da Silva, W., Riviere, N., and Cataldi, Á. (2018). Novel Effector Protein EspY3 of Type III Secretion System from Enterohemorrhagic Escherichia coli Is Localized in Actin Pedestals. Microorganisms *6*, 112.
Law, R.J., Gur-Arie, L., Rosenshine, I., and Brett Finlay, B. (2013). In vitro and in vivo model systems for studying enteropathogenic Escherichia coli infections. Cold Spring Harb. Perspect. Med. *3*, a009977.
Law, R.J., Law, H.T., Scurll, J.M., Scholz, R., Santos, A.S., Shames, S.R., Deng, W., Croxen, M.A., Li, Y., de Hoog, C.L., et al. (2016). Quantitative Mass Spectrometry Identifies Novel Host Binding Partners for Pathogenic Escherichia coli Type III Secretion System Effectors. J. Proteome Res. *15*, 1613–1622.
Lee, M.-S., Oh, T.-K., Kim, M.H., Kwon, H., Lee, E.-Y., Kim, D.-J., Park, J.-H., and Tesh, V.L. (2015). Shiga toxins activate the NLRP3 inflammasome pathway to promote both production of the proinflammatory cytokine interleukin-1β and apoptotic cell death. Infect. Immun. *84*, 172–186.
Lee, S.F., Kelly, M., Mcalister, A., Luck, S.N., Garcia, E.L., Hall, R.A., Robins-Browne, R.M., Frankel, G., and Hartland, E.L. (2008). A C-terminal class I PDZ binding motif of EspI/NleA modulates the virulence of attaching and effacing Escherichia coli and Citrobacter rodentium. Cell. Microbiol. *10*, 499–513.
Levine, M.M., Bergquist, E.J., Nalin, D.R., Waterman, D.H., Hornick, R.B., Young, C.R., and Sotman, S. (1978). Escherichia coli strains that cause diarrhoea but do not produce heat-labile or heat-stable enterotoxins and are non-invasive. Lancet *1*, 1119–1122.
Leyton, D.L., Sloan, J., Hill, R.E., Doughty, S., and Hartland, E.L. (2003). Transfer Region of pO113 from Enterohemorrhagic Escherichia coli: Similarity with R64 and Identification of a Novel Plasmid-Encoded Autotransporter, EpeA. Infect. Immun. *71*, 6307–6319.
Li, J., Brieher, W.M., Scimone, M.L., Kang, S.J., Zhu, H., Yin, H., von Andrian, U.H., Mitchison, T., and Yuan, J. (2007). Caspase-11 regulates cell migration by promoting Aip1-Cofilin-mediated actin depolymerization. Nat. Cell Biol. *9*, 276–286.
Li, J., Yin, H.L., and Yuan, J. (2008). Flightless-I regulates proinflammatory caspases by selectively modulating intracellular localization and caspase activity. J. Cell Biol. *181*, 321–333.
Li, M., Rosenshine, I., Yu, H.B., Nadler, C., Mills, E., Hew, C.L., and Leung, K.Y. (2006). Identification and characterization of NleI, a new non-LEE-encoded effector of enteropathogenic Escherichia coli (EPEC). Microbes Infect. *8*, 2890–2898.
Li, S., Zhang, L., Yao, Q., Li, L., Dong, N., Rong, J., Gao, W., Ding, X., Sun, L., Chen, X., et al. (2013). Pathogen blocks host death receptor signalling by arginine GlcNAcylation of death domains. Nature *501*, 242–246.
Li, W., Liu, Y., Sheng, X., Yin, P., Hu, F., Liu, Y., Chen, C., Li, Q., Yan, C., and Wang, J. (2014). Structure and mechanism of a type III secretion protease, NleC. Acta Crystallogr. Sect. D Biol. Crystallogr. *70*, 40–47.
Li, Y., Tang, X., He, Q., Yang, X., Ren, X., Wen, X., Zhang, J., Wang, Y., Liu, N., and Ma, J. (2016). Overexpression of Mitochondria Mediator Gene TRIAP1 by miR-320b Loss Is Associated with Progression in Nasopharyngeal Carcinoma. PLoS Genet. *12*, 1–22.

Lieberman, J., Wu, H., and Kagan, J.C. (2019). Gasdermin D activity in inflammation and host defense. Sci. Immunol. *4*, 1–9.
Lifshitz, Z., Burstein, D., Schwartz, K., Shuman, H.A., Pupko, T., and Segal, G. (2014). Identification of novel Coxiella burnetii Icm/Dot effectors and genetic analysis of their involvement in modulating a mitogen-activated protein kinase pathway. Infect. Immun. *82*, 3740–3752.
Lin, D.Y.W., Diao, J., and Chen, J. (2012). Crystal structures of two bacterial HECT-like E3 ligases in complex with a human E2 reveal atomic details of pathogen-host interactions. Proc. Natl. Acad. Sci. U. S. A. *109*, 1925–1930.
Lin, Y., Devin, A., Rodriguez, Y., and Liu, Z.G. (1999). Cleavage of the death domain kinase RIP by Caspase-8 prompts TNF-induced apoptosis. Genes Dev. *13*, 2514–2526.
Litvak, Y., Sharon, S., Hyams, M., Zhang, L., Kobi, S., Katsowich, N., Dishon, S., Nussbaum, G., Dong, N., Shao, F., et al. (2017). Epithelial cells detect functional type III secretion system of enteropathogenic Escherichia coli through a novel NF-κB signaling pathway. PLoS Pathog. *13*, e1006472.
Liu, P., Qi, X., Bian, C.E., Yang, F.A.N., and Lin, X. (2017a). MicroRNA-18a inhibits ovarian cancer growth via directly targeting TRIAP1 and IPMK. Oncol. Lett. 1–8.
Liu, T., Zhang, L., Joo, D., and Sun, S.-C. (2017b). NF-κB signaling in inflammation. Signal Transduct. Target. Ther. *2*, 17023.
Liu, Y., Shoji-Kawata, S., Sumpter, R.M., Wei, Y., Ginet, V., Zhang, L., Posner, B., Tran, K.A., Green, D.R., Xavier, R.J., et al. (2013). Autosis is a Na+,K+-ATPase-regulated form of cell death triggered by autophagy-inducing peptides, starvation, and hypoxia-ischemia. Proc. Natl. Acad. Sci. U. S. A. *110*, 20364–20371.
Liu, Z., Zaki, M.H., Vogel, P., Gurung, P., Finlay, B.B., Deng, W., Lamkanfi, M., and Kanneganti, T.D. (2012). Role of inflammasomes in host defense against citrobacter rodentium infection. J. Biol. Chem. *287*, 16955–16964.
Lobstein, J., Emrich, C.A., Jeans, C., Faulkner, M., Riggs, P., and Berkmen, M. (2012). SHuffle, a novel Escherichia coli protein expression strain capable of correctly folding disulfide bonded proteins in its cytoplasm. Microb. Cell Fact. *11*, 56.
Lommel, S., Benesch, S., Rottner, K., Franz, T., Wehland, J., and Kühn, R. (2001). Actin pedestal formation by enteropathogenic Escherichia coli and intracellular motility of Shigella flexneri are abolished in N-WASP-defective cells. EMBO Rep. *2*, 850–857.
Loukiadis, E., Nobe, R., Herold, S., Tramuta, C., Ogura, Y., Ooka, T., Morabito, S., Kérourédan, M., Brugère, H., Schmidt, H., et al. (2008). Distribution, functional expression, and genetic organization of Cif, a phage-encoded type III-secreted effector from enteropathogenic and enterohemorrhagic Escherichia coli. J. Bacteriol. *190*, 275–285.
Lu, R., Herrera, B.B., Eshleman, H.D., Fu, Y., Bloom, A., Li, Z., Sacks, D.B., and Goldberg, M.B. (2015). Shigella Effector OspB Activates mTORC1 in a Manner That Depends on IQGAP1 and Promotes Cell Proliferation. PLoS Pathog. *11*, 1–21.
Luo, Y., Frey, E.A., Pfuetzner, R.A., Creaght, A.L., Knoechel, D.G., Haynes, C.A., Finlay, B.B., and Strynadka, N.C.J. (2000). Crystal structure of enteropathogenic Escherichia coli intimin-receptor complex. Nature *405*, 1073–1077.
Luo, Y., Hua, T., You, X., Lou, J., Yang, X., and Tang, N. (2019). Effects of miR-107 on the Chemo-drug sensitivity of breast cancer cells. Open Med. *14*, 59–65.
Luperchio, S.A., Newman, J. V., Dangler, C.A., Schrenzel, M.D., Brenner, D.J., Steigerwalt, A.G., and Schauer, D.B. (2000). Citrobacter rodentium, the causative agent of transmissible murine colonic hyperplasia, exhibits clonality: Synonymy of C. rodentium and mouse-pathogenic Escherichia coli. J. Clin. Microbiol. *38*, 4343–4350.
Ma, C., Wickham, M.E., Guttman, J.A., Deng, W., Walker, J., Madsen, K.L., Jacobson, K., Vogl, W.A., Finlay, B.B., and Vallance, B.A. (2006). Citrobacter rodentium infection causes both mitochondrial dysfunction and intestinal epithelial barrier disruption in vivo: Role of mitochondrial associated protein (Map). Cell. Microbiol. *8*, 1669–1686.
Madeira, F., Park, Y.M., Lee, J., Buso, N., Gur, T., Madhusoodanan, N., Basutkar, P., Tivey, A.R.N., Potter, S.C., Finn, R.D., et al. (2019). The EMBL-EBI search and sequence analysis tools APIs in 2019. Nucleic

Acids Res. *47*, W636–W641.
Maekawa, M., Ishizaki, T., Boku, S., Watanabe, N., Fujita, A., Iwamatsu, A., Obinata, T., Ohashi, K., Mizuno, K., and Narumiya, S. (1999). Signaling from Rho to the actin cytoskeleton through protein kinases ROCK and LIM-kinase. Science (80-.). *285*, 895–898.
Man, S.M., Ekpenyong, A., Tourlomousis, P., Achouri, S., Cammarota, E., Hughes, K., Rizzo, A., Ng, G., Wright, J.A., Cicuta, P., et al. (2014). Actin polymerization as a key innate immune effector mechanism to control Salmonella infection. Proc. Natl. Acad. Sci. *111*, 17588–17593.
Marchès, O., Ledger, T.N., Boury, M., Ohara, M., Tu, X., Goffaux, F., Mainil, J., Rosenshine, I., Sugai, M., De Rycke, J., et al. (2003). Enteropathogenic and enterohaemorrhagic Escherichia coli deliver a novel effector called Cif, which blocks cell cycle G2/M transition. Mol. Microbiol. *50*, 1553–1567.
Marchès, O., Wiles, S., Dziva, F., La Ragione, R.M., Schüller, S., Best, A., Phillips, A.D., Hartland, E.L., Woodward, M.J., Stevens, M.P., et al. (2005). Characterization of two non-locus of enterocyte effacement-encoded type III-translocated effectors, NleC and NleD, in attaching and effacing pathogens. Infect. Immun. *73*, 8411–8417.
Marchès, O., Covarelli, V., Dahan, S., Cougoule, C., Bhatta, P., Frankel, G., and Caron, E. (2008). EspJ of enteropathogenic and enterohaemorrhagic Escherichia coli inhibits opsono-phagocytosis. Cell. Microbiol. *10*, 1104–1115.
Martinez, E., Schroeder, G.N., Berger, C.N., Lee, S.F., Robinson, K.S., Badea, L., Simpson, N., Hall, R.A., Hartland, E.L., Crepin, V.F., et al. (2010). Binding to Na+/H+ exchanger regulatory factor 2 (NHERF2) affects trafficking and function of the enteropathogenic Escherichia coli type III secretion system effectors Map, EspI and NleH. Cell. Microbiol. *12*, 1718–1731.
Martins, F.H., Nepomuceno, R., Piazza, R.M.F., and Elias, W.P. (2017). Phylogenetic distribution of tir-cytoskeleton coupling protein (tccP and tccP2) genes in atypical enteropathogenic Escherichia coli. FEMS Microbiol. Lett. *364*, 1–7.
Matsuzawa, T., Kuwae, A., Yoshida, S., Sasakawa, C., and Abe, A. (2004). Enteropathogenic Escherichia coli activates the RhoA signaling pathway via the stimulation of GEF-H1. EMBO J. *23*, 3570–3582.
Matsuzawa, T., Kuwae, A., and Abe, A. (2005). Enteropathogenic Escherichia coli Type III Effectors EspG and EspG2 Alter Epithelial Paracellular Permeability. Infect. Immun. *73*, 6283–6289.
McCormack, R.M., Lyapichev, K., Olsson, M.L., Podack, E.R., and Munson, G.P. (2015a). Enteric pathogens deploy cell cycle inhibiting factors to block the bactericidal activity of Perforin-2. Elife *4*, 1–22.
McCormack, R.M., de Armas, L.R., Shiratsuchi, M., Fiorentino, D.G., Olsson, M.L., Lichtenheld, M.G., Morales, A., Lyapichev, K., Gonzalez, L.E., Strbo, N., et al. (2015b). Perforin-2 is essential for intracellular defense of parenchymal cells and phagocytes against pathogenic bacteria. Elife *4*, 1–29.
McDaniel, T.K., and Kaper, J.B. (1997). A cloned pathogenicity island from enteropathogenic Escherichia coli confers the attaching and effacing phenotype on E. coli K-12. Mol. Microbiol. *23*, 399–407.
McDaniel, T.K., Jarvis, K.G., Donnenberg, M.S., and Kaper, J.B. (1995). A genetic locus of enterocyte effacement conserved among diverse enterobacterial pathogens. Proc. Natl. Acad. Sci. U. S. A. *92*, 1664–1668.
McDermott, J.E., Corrigan, A., Peterson, E., Oehmen, C., Niemann, G., Cambronne, E.D., Sharp, D., Adkins, J.N., Samudrala, R., and Heffron, F. (2011). Minireview: Computational prediction of type III and IV secreted effectors in gram-negative bacteria. Infect. Immun. *79*, 23–32.
McDowell, M.A., Byrne, A.M.P., Mylona, E., Johnson, R., Sagfors, A., Crepin, V.F., Lea, S., and Frankel, G. (2019). The S. Typhi effector StoD is an E3/E4 ubiquitin ligase which binds K48- And K63-linked diubiquitin. Life Sci. Alliance *2*, 1–13.
McNamara, B.P., and Donnenberg, M.S. (1998). A novel proline-rich protein, EspF, is secreted from enteropathogenic Escherichia coli via the type III export pathway. FEMS Microbiol. Lett. *166*, 71–78.
Medici, N.P., Rashid, M., and Bliska, J.B. (2019). Characterization of pyrin dephosphorylation and inflammasome activation in macrophages as triggered by the Yersinia effectors YopE and YopT. Infect. Immun. *87*, 1–13.
Mellies, J.L., Navarro-Garcia, F., Okeke, I., Frederickson, J., Nataro, J.P., and Kaper, J.B. (2001). espC

pathogenicity island of enteropathogenic Escherichia coli encodes an enterotoxin. Infect. Immun. *69*, 315–324.
Melton-Celsa, A.R. (2014). Shiga Toxin (Stx) Classification, Structure, and Function. Microbiol. Spectr. *2*, 1–13.
Miao, E.A., Leaf, I.A., Treuting, P.M., Mao, D.P., Dors, M., Sarkar, A., Warren, S.E., Wewers, M.D., and Aderem, A. (2010a). Caspase-1-induced pyroptosis is an innate immune effector mechanism against intracellular bacteria. Nat. Immunol. *11*, 1136–1142.
Miao, E.A., Mao, D.P., Yudkovsky, N., Bonneau, R., Lorang, C.G., Warren, S.E., Leaf, I.A., and Aderem, A. (2010b). Innate immune detection of the type III secretion apparatus through the NLRC4 inflammasome. Proc Natl Acad Sci U S A *107*, 3076–3080.
Miliara, X., Garnett, J.A., Tatsuta, T., Abid Ali, F., Baldie, H., Pérez-Dorado, I., Simpson, P., Yague, E., Langer, T., and Matthews, S. (2015). Structural insight into the TRIAP1/PRELI-like domain family of mitochondrial phospholipid transfer complexes. EMBO Rep. *16*, 824–835.
Miliara, X., Tatsuta, T., Berry, J.L., Rouse, S.L., Solak, K., Chorev, D.S., Wu, D., Robinson, C. V., Matthews, S., and Langer, T. (2019). Structural determinants of lipid specificity within Ups/PRELI lipid transfer proteins. Nat. Commun. *10*, 1–15.
Mills, E., Baruch, K., Charpentier, X., Kobi, S., and Rosenshine, I. (2008). Real-time analysis of effector translocation by the type III secretion system of enteropathogenic Escherichia coli. Cell Host Microbe *3*, 104–113.
Milon, A., Oswald, E., and De Rycke, J. (1999). Rabbit EPEC: A model for the study of enteropathogenic Escherichia coli. Vet. Res. *30*, 203–219.
Ming, M., Ying, M., and Ling, M. (2019). miRNA-125a-5p inhibits hepatocellular carcinoma cell proliferation and induces apoptosis by targeting TP53 regulated inhibitor of apoptosis 1 and Bcl-2-like-2 protein. Exp. Ther. Med. 1196–1202.
Miyahara, A., Nakanishi, N., Ooka, T., Hayashi, T., Sugimoto, N., and Tobe, T. (2009). Enterohemorrhagic Escherichia coli effector EspL2 induces actin microfilament aggregation through annexin 2 activation. Cell. Microbiol. *11*, 337–350.
Miyake, M., Sakane, S., Kobayashi, C., Hanajima-Ozawa, M., Fukui, A., Kamitani, S., and Horiguchi, Y. (2008). A colorimetric assay for studying effector secretion through the bacterial type III secretion system. FEMS Microbiol. Lett. *278*, 36–42.
Morampudi, V., Graef, F.A., Stahl, M., Dalwadi, U., Conlin, V.S., Huang, T., Vallance, B.A., Yu, H.B., and Jacobson, K. (2017). Tricellular Tight Junction Protein Tricellulin Is Targeted by the Enteropathogenic Escherichia coli Effector EspG1, Leading to Epithelial Barrier Disruption. Infect. Immun. *85*, 1–20.
Morikawa, H., Kim, M., Mimuro, H., Punginelli, C., Koyama, T., Nagai, S., Miyawaki, A., Iwai, K., and Sasakawa, C. (2010). The bacterial effector Cif interferes with SCF ubiquitin ligase function by inhibiting deneddylation of Cullin1. Biochem. Biophys. Res. Commun. *401*, 268–274.
Morita-Ishihara, T., Miura, M., Iyoda, S., Izumiya, H., Watanabe, H., Ohnishi, M., and Terajima, J. (2013). EspO1-2 Regulates EspM2-Mediated RhoA Activity to Stabilize Formation of Focal Adhesions in Enterohemorrhagic Escherichia coli-Infected Host Cells. PLoS One *8*.
Mostowy, S., and Shenoy, A.R. (2015). The cytoskeleton in cell-autonomous immunity: Structural determinants of host defence. Nat. Rev. Immunol. *15*, 559–573.
Mühlen, S., Ruchaud-Sparagano, M.H., and Kenny, B. (2011). Proteasome-independent degradation of canonical NFκB complex components by the NleC protein of pathogenic Escherichia coli. J. Biol. Chem. *286*, 5100–5107.
Mullineaux-Sanders, C., Sanchez-Garrido, J., Hopkins, E.G.D., Shenoy, A.R., Barry, R., and Frankel, G. (2019). Citrobacter rodentium–host–microbiota interactions: immunity, bioenergetics and metabolism. Nat. Rev. Microbiol. *17*, 701–715.
Mulvihill, E., Sborgi, L., Mari, S.A., Pfreundschuh, M., Hiller, S., and Müller, D.J. (2018). Mechanism of membrane pore formation by human gasdermin-D. EMBO J. *37*, e98321.
Mundy, R., Petrovska, L., Smollett, K., Simpson, N., Wilson, R.K., Yu, J., Tu, X., Rosenshine, I., Clare, S., Dougan, G., et al. (2004a). Identification of a Novel Citrobacter rodentium Type III Secreted Protein, EspI, and Roles of This and Other Secreted Proteins in Infection. Infect. Immun. *72*, 2288–2302.

Mundy, R., Jenkins, C., Yu, J., Smith, H., and Frankel, G. (2004b). Distribution of espI among clinical enterohaemorrhagic and enteropathogenic Escherichia coli isolates. J. Med. Microbiol. *53*, 1145–1149.
Mundy, R., MacDonald, T.T., Dougan, G., Frankel, G., and Wiles, S. (2005). Citrobacter rodentium of mice and man. Cell. Microbiol. *7*, 1697–1706.
Nadler, C., Baruch, K., Kobi, S., Mills, E., Haviv, G., Farago, M., Alkalay, I., Bartfeld, S., Meyer, T.F., Ben-Neriah, Y., et al. (2010). The Type III Secretion Effector NleE Inhibits NF-κB Activation. PLoS Pathog. *6*, e1000743.
Nagai, T., Abe, A., and Sasakawa, C. (2005). Targeting of enteropathogenic Escherichia coli EspF to host mitochondria is essential for bacterial pathogenesis: Critical role of the 16th leucine residue in EspF. J. Biol. Chem. *280*, 2998–3011.
Napetschnig, J., and Wu, H. (2013). Molecular basis of NF-κB signaling. Annu. Rev. Biophys. *42*, 443–468.
Narumiya, S., and Thumkeo, D. (2018). Rho signaling research: history, current status and future directions. FEBS Lett. *592*, 1763–1776.
Nataro, J.P., and Kaper, J.B. (1998). Diarrheagenic Escherichia coli. Clin. Microbiol. Rev. *11*, 142–201.
Navarro-Garcia, F., Serapio-Palacios, A., Ugalde-Silva, P., Tapia-Pastrana, G., and Chavez-Dueñas, L. (2013). Actin cytoskeleton manipulation by effector proteins secreted by diarrheagenic escherichia coli pathotypes. Biomed Res. Int. *2013*.
Newton, H.J., Pearson, J.S., Badea, L., Kelly, M., Lucas, M., Holloway, G., Wagstaff, K.M., Dunstone, M.A., Sloan, J., Whisstock, J.C., et al. (2010). The type III effectors NleE and NleB from enteropathogenic E. coli and OspZ from Shigella block nuclear translocation of NF-kappaB p65. PLoS Pathog. *6*, e1000898.
Nguyen, Y., and Sperandio, V. (2012). Enterohemorrhagic E. coli (EHEC) pathogenesis. Front. Cell. Infect. Microbiol. *2*, 1–7.
Nieto-Pelegrin, E., Kenny, B., and Martinez-Quiles, N. (2014). Nck adaptors, besides promoting N-WASP mediated actin-nucleation activity at pedestals, influence the cellular levels of Enteropathogenic Escherichia coli Tir effector. Cell Adhes. Migr. *8*, 404–417.
Nissan, G., Gershovits, M., Morozov, M., Chalupowicz, L., Sessa, G., Manulis-Sasson, S., Barash, I., and Pupko, T. (2018). Revealing the inventory of type III effectors in Pantoea agglomerans gall-forming pathovars using draft genome sequences and a machine-learning approach. Mol. Plant Pathol. *19*, 381–392.
Nordlander, S., Pott, J., and Maloy, K.J. (2014). NLRC4 expression in intestinal epithelial cells mediates protection against an enteric pathogen. Mucosal Immunol. *7*, 775–785.
Nougayrède, J.P., and Donnenberg, M.S. (2004). Enteropathogenic Escherichia coli EspF is targeted to mitochondria and is required to initiate the mitochondrial death pathway. Cell. Microbiol. *6*, 1097–1111.
Nougayrède, J.P., Boury, M., Tasca, C., Marchès, O., Milon, A., Oswald, E., and De Rycke, J. (2001). Type III secretion-dependent cell cycle block caused in HeLa cells by enteropathogenic Escherichia coli O103. Infect. Immun. *69*, 6785–6795.
Nougayrède, J.P., Foster, G.H., and Donnenberg, M.S. (2007). Enteropathogenic Escherichia coli effector EspF interacts with host protein Abcf2. Cell. Microbiol. *9*, 680–693.
O'Boyle, N., Connolly, J.P.R., and Roe, A.J. (2018). Tracking elusive cargo: Illuminating spatio-temporal Type 3 effector protein dynamics using reporters. Cell. Microbiol. *20*, 1–9.
Ogino, T., Ohno, R., Sekiya, K., Kuwae, A., Matsuzawa, T., Nonaka, T., Fukuda, H., Imajoh-ohmi, S., and Abe, A. (2006). Assembly of the Type III Secretion Apparatus of Enteropathogenic Escherichia coli. J. Bacteriol. *188*, 2801–2811.
Ogura, Y., Ooka, T., Whale, A., Garmendia, J., Beutin, L., Tennant, S., Krause, G., Morabito, S., Chinen, I., Tobe, T., et al. (2007). TccP2 of O157:H7 and non-O157 enterohemorrhagic Escherichia coli (EHEC): Challenging the dogma of EHEC-induced actin polymerization. Infect. Immun. *75*, 604–612.
Ogura, Y., Abe, H., Katsura, K., Kurokawa, K., Asadulghani, M., Iguchi, A., Ooka, T., Nakayama, K., Yamashita, A., Hattori, M., et al. (2008). Systematic identification and sequence analysis of the genomic islands of the enteropathogenic Escherichia coli strain B171-8 by the combined use of whole-genome PCR scanning and fosmid mapping. J. Bacteriol. *190*, 6948–6960.

Ooka, T., Vieira, M.A.M., Ogura, Y., Beutin, L., La Ragione, R., Van Diemen, P.M., Stevens, M.P., Aktan, I., Cawthraw, S., Best, A., et al. (2007). Characterization of tccP2 carried by atypical enteropathogenic Escherichia coli. FEMS Microbiol. Lett. *271*, 126–135.
Ooka, T., Ogura, Y., Katsura, K., Seto, K., Kobayashi, H., Kawano, K., Tokuoka, E., Furukawa, M., Harada, S., Yoshino, S., et al. (2015). Defining the genome features of Escherichia albertii, an emerging enteropathogen closely related to Escherichia coli. Genome Biol. Evol. *7*, 3170–3179.
Orchard, R.C., and Alto, N.M. (2012). Mimicking GEFs: A common theme for bacterial pathogens. Cell. Microbiol. *14*, 10–18.
Orton, D.J., Arsenault, D.J., Thomas, N.A., and Doucette, A.A. (2013). GELFrEE fractionation combined with mass spectrometry for proteome analysis of secreted toxins from Enteropathogenic Escherichia coli (EPEC). Mol. Cell. Probes *27*, 200–207.
Overholtzer, M., Mailleux, A.A., Mouneimne, G., Normand, G., Schnitt, S.J., King, R.W., Cibas, E.S., and Brugge, J.S. (2007). A Nonapoptotic Cell Death Process, Entosis, that Occurs by Cell-in-Cell Invasion. Cell *131*, 966–979.
Pacheco, A.R., and Sperandio, V. (2012). Shiga toxin in enterohemorrhagic E.coli: regulation and novel anti-virulence strategies. Front. Cell. Infect. Microbiol. *2*, 81.
Pal, R.R., Baidya, A.K., Mamou, G., Bhattacharya, S., Socol, Y., Kobi, S., Katsowich, N., Ben-Yehuda, S., and Rosenshine, I. (2019). Pathogenic E. coli Extracts Nutrients from Infected Host Cells Utilizing Injectisome Components. Cell *177*, 683-696.e18.
Pallett, M.A., Berger, C.N., Pearson, J.S., Hartland, E.L., and Frankel, G. (2014). The type III secretion effector NleF of enteropathogenic Escherichia coli activates NF-κB early during infection. Infect. Immun. *82*, 4878–4888.
Pallett, M.A., Crepin, V.F., Serafini, N., Habibzay, M., Kotik, O., Sanchez-Garrido, J., Di Santo, J.P., Shenoy, A.R., Berger, C.N., and Frankel, G. (2017). Bacterial virulence factor inhibits caspase-4/11 activation in intestinal epithelial cells. Mucosal Immunol. *10*, 602–612.
Palmela, C., Chevarin, C., Xu, Z., Torres, J., Sevrin, G., Hirten, R., Barnich, N., Ng, S.C., and Colombel, J.F. (2018). Adherent-invasive Escherichia coli in inflammatory bowel disease. Gut *67*, 574–587.
Papatheodorou, P., Domańska, G., Öxle, M., Mathieu, J., Selchow, O., Kenny, B., and Rassow, J. (2006). The enteropathogenic Escherichia coli (EPEC) map effector is imported into the mitochondrial matrix by the TOM/Hsp70 system and alters organelle morphology. Cell. Microbiol. *8*, 677–689.
Park, H.H., Lo, Y.-C., Lin, S.-C., Wang, L., Yang, J.K., and Wu, H. (2007). The Death Domain Superfamily in Intracellular Signaling of Apoptosis and Inflammation. Annu. Rev. Immunol. *25*, 561–586.
Park, Y.H., Wood, G., Kastner, D.L., and Chae, J.J. (2016). Pyrin inflammasome activation and RhoA signaling in the autoinflammatory diseases FMF and HIDS. Nat. Immunol. *17*, 914–921.
Patel, J.C., and Galán, J.E. (2005). Manipulation of the host actin cytoskeleton by Salmonella - All in the name of entry. Curr. Opin. Microbiol. *8*, 10–15.
Pearson, J.S., and Murphy, J.M. (2017). Down the rabbit hole: Is necroptosis truly an innate response to infection? Cell. Microbiol. *19*, 1–5.
Pearson, J.S., Giogha, C., Ong, S.Y., Kennedy, C.L., Kelly, M., Robinson, K.S., Lung, T.W.F., Mansell, A., Riedmaier, P., Oates, C.V.L., et al. (2013). A type III effector antagonizes death receptor signalling during bacterial gut infection. Nature *501*, 247–251.
Pearson, J.S., Giogha, C., Muhlen, S., Nachbur, U., Pham, C.L., Zhang, Y., Hildebrand, J.M., Oates, C. V, Lung, T.W., Ingle, D., et al. (2017). EspL is a bacterial cysteine protease effector that cleaves RHIM proteins to block necroptosis and inflammation. Nat Microbiol *2*, 16258.
Peltzer, N., and Walczak, H. (2019). Cell Death and Inflammation – A Vital but Dangerous Liaison. Trends Immunol. *40*, 387–402.
Peralta-Ramírez, J., Hernandez, M., Manning-Cela, R., Luna-Muñoz, J., Garcia-Tovar, C., Nougayréde, J.P., Oswald, E., and Navarro-Garcia, F. (2008). EspF interacts with nucleation-promoting factors to recruit junctional proteins into pedestals for pedestal maturation and disruption of paracellular permeability. Infect. Immun. *76*, 3854–3868.
Petty, N.K., Bulgin, R., Crepin, V.F., Cerdeño-Tárraga, A.M., Schroeder, G.N., Quail, M.A., Lennard, N., Corton, C., Barron, A., Clark, L., et al. (2010). The Citrobacter rodentium genome sequence reveals

convergent evolution with human pathogenic Escherichia coli. J. Bacteriol. *192*, 525–538.
Petty, N.K., Feltwell, T., Pickard, D., Clare, S., Toribio, A.L., Fookes, M., Roberts, K., Monson, R., Nair, S., Kingsley, R.A., et al. (2011). Citrobacter rodentium is an unstable pathogen showing evidence of significant genomic flux. PLoS Pathog. *7*.
Pham, T.H., Gao, X., Tsai, K., Olsen, R., Wan, F., and Hardwidge, P.R. (2012). Functional Differences and Interactions between the Escherichia coli Type III Secretion System Effectors NleH1 and NleH2. Infect. Immun. *80*, 2133–2140.
Piscatelli, H., Kotkar, S.A., McBee, M.E., Muthupalani, S., Schauer, D.B., Mandrell, R.E., Leong, J.M., and Zhou, D. (2011). The EHEC Type III Effector NleL Is an E3 Ubiquitin Ligase That Modulates Pedestal Formation. PLoS One *6*, e19331.
Platenkamp, A., and Mellies, J.L. (2018). Environment Controls LEE Regulation in Enteropathogenic Escherichia coli. Front. Microbiol. *9*, 1–15.
Platnich, J.M., Chung, H., Lau, A., Sandall, C.F., Bondzi-Simpson, A., Chen, H.-M., Komada, T., Trotman-Grant, A.C., Brandelli, J.R., Chun, J., et al. (2018). Shiga Toxin/Lipopolysaccharide Activates Caspase-4 and Gasdermin D to Trigger Mitochondrial Reactive Oxygen Species Upstream of the NLRP3 Inflammasome. Cell Rep. *25*, 1525-1536.e7.
Plotnikov, A., Zehorai, E., Procaccia, S., and Seger, R. (2011). The MAPK cascades: Signaling components, nuclear roles and mechanisms of nuclear translocation. Biochim. Biophys. Acta - Mol. Cell Res. *1813*, 1619–1633.
Pollard, D.J., Young, J.C., Covarelli, V., Herrera-León, S., Connor, T.R., Fookes, M., Walker, D., Echeita, A., Thomson, N.R., Berger, C.N., et al. (2016). The Type III Secretion System Effector SeoC of Salmonella enterica subsp. salamae and S. enterica subsp. arizonae ADP-Ribosylates Src and Inhibits Opsonophagocytosis. Infect. Immun. *84*, 3618–3628.
Pollard, D.J., Berger, C.N., So, E.C., Yu, L., Hadavizadeh, K., Jennings, P., Tate, E.W., Choudhary, J.S., and Frankel, G. (2018). Broad-spectrum regulation of nonreceptor tyrosine kinases by the bacterial ADP-ribosyltransferase Espj. MBio *9*, 1–16.
Pollock, G.L., Oates, C.V.L., Giogha, C., Wong Fok Lung, T., Ong, S.Y., Pearson, J.S., and Hartland, E.L. (2017). Distinct Roles of the Antiapoptotic Effectors NleB and NleF from Enteropathogenic Escherichia coli. Infect. Immun. *85*, e01071-16.
Popa, C., Coll, N.S., Valls, M., and Sessa, G. (2016). Yeast as a Heterologous Model System to Uncover Type III Effector Function. PLoS Pathog. *12*, 1–17.
Potting, C., Tatsuta, T., König, T., Haag, M., Wai, T., Aaltonen, M.J., and Langer, T. (2013). TRIAP1/PRELI complexes prevent apoptosis by mediating intramitochondrial transport of phosphatidic acid. Cell Metab. *18*, 287–295.
El Qaidi, S., Chen, K., Halim, A., Siukstaite, L., Rueter, C., Hurtado-Guerrero, R., Clausen, H., and Hardwidge, P.R. (2017). NleB/SseK effectors from Citrobacter rodentium , Escherichia coli , and Salmonella enterica display distinct differences in host substrate specificity. J. Biol. Chem. *292*, 11423–11430.
El Qaidi, S., Zhu, C., McDonald, P., Roy, A., Maity, P.K., Rane, D., Perera, C., and Hardwidge, P.R. (2018). High-Throughput Screening for Bacterial Glycosyltransferase Inhibitors. Front. Cell. Infect. Microbiol. *8*, 1–8.
Quarato, G., Guy, C.S., Grace, C.R., Llambi, F., Nourse, A., Rodriguez, D.A., Wakefield, R., Frase, S., Moldoveanu, T., and Green, D.R. (2016). Sequential Engagement of Distinct MLKL Phosphatidylinositol-Binding Sites Executes Necroptosis. Mol. Cell *61*, 589–601.
Quitard, S., Dean, P., Maresca, M., and Kenny, B. (2006). The enteropathogenic Escherichia coli EspF effector molecule inhibits PI-3 kinase-mediated uptake independently of mitochondrial targeting. Cell. Microbiol. *8*, 972–981.
Radics, J., Königsmaier, L., and Marlovits, T.C. (2014). Structure of a pathogenic type 3 secretion system in action. Nat. Struct. Mol. Biol. *21*, 82–87.
Ramachandran, R.P., Vences-Catalán, F., Wiseman, D., Zlotkin-Rivkin, E., Shteyer, E., Melamed-Book, N., Rosenshine, I., Levy, S., and Aroeti, B. (2018). EspH Suppresses Erk by Spatial Segregation from CD81 Tetraspanin Microdomains. Infect. Immun. *86*, 1–16.

Rathinam, V.A.K., Vanaja, S.K., Waggoner, L., Sokolovska, A., Becker, C., Stuart, L.M., Leong, J.M., and Fitzgerald, K.A. (2012). TRIF licenses caspase-11-dependent NLRP3 inflammasome activation by gram-negative bacteria. Cell *150*, 606–619.
Ratner, D., Orning, M.P.A., Proulx, M.K., Wang, D., Gavrilin, M.A., Wewers, M.D., Alnemri, E.S., Johnson, P.F., Lee, B., Mecsas, J., et al. (2016). The Yersinia pestis Effector YopM Inhibits Pyrin Inflammasome Activation. PLOS Pathog. *12*, e1006035.
Raymond, B., Crepin, V.F., Collins, J.W., and Frankel, G. (2011). The WxxxE effector EspT triggers expression of immune mediators in an Erk/JNK and NF-κB-dependent manner. Cell. Microbiol. *13*, 1881–1893.
Reddick, L.E., and Alto, N.M. (2014). Bacteria fighting back: How pathogens target and subvert the host innate immune system. Mol. Cell *54*, 321–328.
Rendón, M.A., Saldaña, Z., Erdem, A.L., Monteiro-Neto, V., Vázquez, A., Kaper, J.B., Puente, J.L., and Girón, J.A. (2007). Commensal and pathogenic Escherichia coli use a common pilus adherence factor for epithelial cell colonization. Proc. Natl. Acad. Sci. U. S. A. *104*, 10637–10642.
Reubold, T.F., and Eschenburg, S. (2012). A molecular view on signal transduction by the apoptosome. Cell. Signal. *24*, 1420–1425.
Riley, L.W., Junio, L.N., Libaek, L.B., and Schoolnik, G.K. (1987). Plasmid-encoded expression of lipopolysaccharide O-antigenic polysaccharide in enteropathogenic Escherichia coli. Infect. Immun. *55*, 2052–2056.
Ritchie, J.M., and Waldor, M.K. (2005). The Locus of Enterocyte Effacement-Encoded Effector Proteins All Promote Enterohemorrhagic Escherichia coli Pathogenicity in Infant Rabbits. Infect. Immun. *73*, 1466–1474.
Robinson, K.S., Mousnier, A., Hemrajani, C., Fairweather, N., Berger, C.N., and Frankel, G. (2010). The enteropathogenic Escherichia coli effector NleH inhibits apoptosis induced by Clostridium difficile toxin B. Microbiology *156*, 1815–1823.
Rodríguez-Escudero, I., Hardwidge, P.R., Nombela, C., Cid, V.J., Finlay, B.B., and Molina, M. (2005). Enteropathogenic Escherichia coli type III effectors alter cytoskeletal function and signalling in Saccharomyces cerevisiae. Microbiology *151*, 2933–2945.
Rodriguez, D.A., Weinlich, R., Brown, S., Guy, C., Fitzgerald, P., Dillon, C.P., Oberst, A., Quarato, G., Low, J., Cripps, J.G., et al. (2016). Characterization of RIPK3-mediated phosphorylation of the activation loop of MLKL during necroptosis. Cell Death Differ. *23*, 76–88.
Roe, A.J., Tysall, L., Dransfield, T., Wang, D., Fraser-Pitt, D., Mahajan, A., Constandinou, C., Inglis, N., Downing, A., Talbot, R., et al. (2007). Analysis of the expression, regulation and export of NleA-E in Escherichia coli O157:H7. Microbiology *153*, 1350–1360.
Romo-Castillo, M., Andrade, A., Espinosa, N., Feria, J.M., Soto, E., Díaz-Guerrero, M., and González-Pedrajo, B. (2014). EscO, a functional and structural analog of the flagellar fliJ protein, is a positive regulator of EscN ATPase activity of the enteropathogenic Escherichia coli injectisome. J. Bacteriol. *196*, 2227–2241.
Rosenshine, I., Donnenberg, M.S., Kaper, J.B., and Finlay, B.B. (1992). Signal transduction between enteropathogenic Escherichia coli (EPEC) and epithelial cells: EPEC induces tyrosine phosphorylation of host cell proteins to initiate cytoskeletal rearrangement and bacterial uptake. Trends Cell Biol. *2*, 362.
Ross, N.T., and Miller, B.L. (2007). Characterization of the binding surface of the translocated intimin receptor, an essential protein for EPEC and EHEC cell adhesion. Protein Sci. *16*, 2677–2683.
Rottner, K., Faix, J., Bogdan, S., Linder, S., and Kerkhoff, E. (2017). Actin assembly mechanisms at a glance. J. Cell Sci. *130*, 3427–3435.
Roxas, J.L., Wilbur, J.S., Zhang, X., Martinez, G., Vedantam, G., and Viswanathan, V.K. (2012). The Enteropathogenic Escherichia coli-Secreted Protein EspZ Inhibits Host Cell Apoptosis. Infect. Immun. *80*, 3850–3857.
Roxas, J.L., Monasky, R.C., Roxas, B.A.P., Agellon, A.B., Mansoor, A., Kaper, J.B., Vedantam, G., and Viswanathan, V.K. (2018). Enteropathogenic Escherichia coli EspH-Mediated Rho GTPase Inhibition Results in Desmosomal Perturbations. Cell. Mol. Gastroenterol. Hepatol. *6*, 163–180.
Roy, A., Kucukural, A., and Zhang, Y. (2011). I-TASSER: a unified platform for automated protein

structure and function prediction. Nat Protoc *5*, 725–738.
Royan, S. V., Jones, R.M., Koutsouris, A., Roxas, J.L., Falzari, K., Weflen, A.W., Kim, A., Bellmeyer, A., Turner, J.R., Neish, A.S., et al. (2010). Enteropathogenic E. coli non-LEE encoded effectors NleH1 and NleH2 attenuate NF-κB activation. Mol. Microbiol. *78*, 1232–1245.
Ruano-Gallego, D., Álvarez, B., and Fernández, L.Á. (2015). Engineering the Controlled Assembly of Filamentous Injectisomes in E. coli K-12 for Protein Translocation into Mammalian Cells. ACS Synth. Biol. *4*, 1030–1041.
Ruchaud-Sparagano, M.H., Mühlen, S., Dean, P., and Kenny, B. (2011). The enteropathogenic E. coli (EPEC) Tir effector inhibits NF-κB activity by targeting TNFα receptor-associated factors. PLoS Pathog. *7*.
Rühl, S., Shkarina, K., Demarco, B., Heilig, R., Santos, J.C., and Broz, P. (2018). ESCRT-dependent membrane repair negatively regulates pyroptosis downstream of GSDMD activation. Science (80-.). *362*, 956–960.
Runte, C.S., Jain, U., Getz, L.J., Secord, S., Kuwae, A., Abe, A., LeBlanc, J.J., Stadnyk, A.W., Kaper, J.B., Hansen, A.M., et al. (2018). Tandem tyrosine phosphosites in the Enteropathogenic Escherichia coli chaperone CesT are required for differential type III effector translocation and virulence. Mol. Microbiol. *108*, 536–550.
Russo, T.A., and Johnson, J.R. (2000). Proposal for a New Inclusive Designation for Extraintestinal Pathogenic Isolates of Escherichia coli: ExPEC. J. Infect. Dis. *181*, 1753–1754.
Sai, K., Parsons, C., House, J.S., Kathariou, S., and Ninomiya-Tsuji, J. (2019). Necroptosis mediators RIPK3 and MLKL suppress intracellular Listeria replication independently of host cell killing. J. Cell Biol. *218*, 1994–2005.
Saldaña, Z., Erdem, A.L., Schüller, S., Okeke, I.N., Lucas, M., Sivananthan, A., Phillips, A.D., Kaper, J.B., Puente, J.L., and Girón, J.A. (2009). The Escherichia coli common pilus and the bundle-forming pilus act in concert during the formation of localized adherence by enteropathogenic E. coli. J. Bacteriol. *191*, 3451–3461.
Samba-louaka, A., Nougayrède, J.P., Watrin, C., Jubelin, G., Oswald, E., and Taieb, F. (2008). Bacterial cyclomodulin Cif blocks the host cell cycle by stabilizing the cyclin-dependent kinase inhibitors p21 waf1 and p27 kip1. Cell. Microbiol. *10*, 2496–2508.
Samba-Louaka, A., Nougayrède, J.P., Watrin, C., Oswald, E., and Taieb, F. (2009). The enteropathogenic Escherichia coli effector Cif induces delayed apoptosis in epithelial cells. Infect. Immun. *77*, 5471–5477.
Sampaio, S.C.F., Moreira, F.C., Liberatore, A.M.A., Vieira, M.A.M., Knobl, T., Romão, F.T., Hernandes, R.T., Ferreira, C.S.A., Ferreira, A.P., Felipe-Silva, A., et al. (2014). Analysis of the virulence of an atypical enteropathogenic escherichia coli strain in vitro and in vivo and the influence of type three secretion system. Biomed Res. Int. *2014*.
Samudrala, R., Heffron, F., and McDermott, J.E. (2009). Accurate Prediction of Secreted Substrates and Identification of a Conserved Putative Secretion Signal for Type III Secretion Systems. PLoS Pathog. *5*, e1000375.
Sandu, P., Crepin, V.F., Drechsler, H., McAinsh, A.D., Frankel, G., and Berger, C.N. (2017). The Enterohemorrhagic Escherichia coli Effector EspW Triggers Actin Remodeling in a Rac1-Dependent Manner. Infect. Immun. *85*, e00244-17.
Santos, A.S., and Finlay, B.B. (2015). Bringing down the host: Enteropathogenic and enterohaemorrhagic Escherichia coli effector-mediated subversion of host innate immune pathways. Cell. Microbiol. *17*, 318–332.
Santos, F.F., Yamamoto, D., Abe, C.M., Bryant, J.A., Hernandes, R.T., Kitamura, F.C., Castro, F.S., Valiatti, T.B., Piazza, R.M.F., Elias, W.P., et al. (2019). The Type III Secretion System (T3SS)-Translocon of Atypical Enteropathogenic Escherichia coli (aEPEC) Can Mediate Adherence. Front. Microbiol. *10*, 1–13.
Schauer, D.B., Zabel, B.A., Pedraza, I.F., O'Hara, C.M., Steigerwalt, A.G., and Brenner, D.J. (1995). Genetic and biochemical characterization of Citrobacter rodentium sp. nov. J.Clin.Microbiol. *33*, 2064–2068.
Schnappauf, O., Chae, J.J., Kastner, D.L., and Aksentijevich, I. (2019). The Pyrin Inflammasome in Health and Disease. Front. Immunol. *10*, 1745.
Scholzen, T., and Gerdes, J. (2000). The Ki-67 protein: From the known and the unknown. J. Cell.

Physiol. *182*, 311–322.
Schroder, K., and Tschopp, J. (2010). The Inflammasomes. Cell *140*, 821–832.
Schwidder, M., Heinisch, L., and Schmidt, H. (2019). Genetics, Toxicity, and Distribution of Enterohemorrhagic Escherichia coli Hemolysin. Toxins (Basel). *11*, 502.
Scott, N.E., Giogha, C., Pollock, G.L., Kennedy, C.L., Webb, A.I., Williamson, N.A., Pearson, J.S., and Hartland, E.L. (2017). The bacterial arginine glycosyltransferase effector NleB preferentially modifies Fas-associated death domain protein (FADD). J. Biol. Chem. *292*, 17337–17350.
Sekiya, K., Ohishi, M., Ogino, T., Tamano, K., Sasakawa, C., and Abe, a (2001). Supermolecular structure of the enteropathogenic Escherichia coli type III secretion system and its direct interaction with the EspA-sheath-like structure. Proc. Natl. Acad. Sci. U. S. A. *98*, 11638–11643.
Sells, M.A., Knaus, U.G., Bagrodia, S., Ambrose, D.M., Bokoch, G.M., and Chernoff, J. (1997). Human p21-activated kinase (Pak1) regulates actin organization in mammalian cells. Curr. Biol. *7*, 202–210.
Selyunin, A.S., and Alto, N.M. (2011). Activation of PAK by a bacteria type III effector EspG reveals alternative mechanisms of GTPase pathway regulation. Small GTPases *4*, 217–221.
Selyunin, A.S., Sutton, S.E., Weigele, B.A., Reddick, L.E., Orchard, R.C., Bresson, S.M., Tomchick, D.R., and Alto, N.M. (2011). The assembly of a GTPase-kinase signalling complex by a bacterial catalytic scaffold. Nature *469*, 107–111.
Selyunin, A.S., Reddick, L.E., Weigele, B. a, and Alto, N.M. (2014). Selective protection of an ARF1-GTP signaling axis by a bacterial scaffold induces bidirectional trafficking arrest. Cell Rep. *6*, 878–891.
Serapio-Palacios, A., and Navarro-Garcia, F. (2016). EspC, an autotransporter protein secreted by enteropathogenic Escherichia coli, causes apoptosis and necrosis through caspase and calpain activation, including direct procaspase-3 cleavage. MBio *7*, 1–18.
Sham, H.P., Shames, S.R., Croxen, M.A., Ma, C., Chan, J.M., Khan, M.A., Wickham, M.E., Deng, W., Finlay, B.B., and Vallance, B.A. (2011). Attaching and effacing bacterial effector NleC suppresses epithelial inflammatory responses by inhibiting NF-κB and p38 mitogen-activated protein kinase activation. Infect. Immun. *79*, 3552–3562.
Shames, S.R., Deng, W., Guttman, J.A., de Hoog, C.L., Li, Y., Hardwidge, P.R., Sham, H.P., Vallance, B.A., Foster, L.J., and Finlay, B.B. (2010). The pathogenic E. coli type III effector EspZ interacts with host CD98 and facilitates host cell prosurvival signalling. Cell. Microbiol. *12*, 1322–1339.
Shames, S.R., Bhavsar, A.P., Croxen, M.A., Law, R.J., Mak, S.H.C., Deng, W., Li, Y., Bidshari, R., de Hoog, C.L., Foster, L.J., et al. (2011a). The pathogenic Escherichia coli type III secreted protease NleC degrades the host acetyltransferase p300. Cell. Microbiol. *13*, 1542–1557.
Shames, S.R., Croxen, M.A., Deng, W., and Finlay, B.B. (2011b). The type III system-secreted effector EspZ localizes to host mitochondria and interacts with the translocase of inner mitochondrial membrane 17b. Infect. Immun. *79*, 4784–4790.
Shao, F., Merritt, P.M., Bao, Z., Innes, R.W., and Dixon, J.E. (2002). A Yersinia effector and a Pseudomonas avirulence protein define a family of cysteine proteases functioning in bacterial pathogenesis. Cell *109*, 575–588.
Shao, F., Vacratsis, P.O., Bao, Z., Bowers, K.E., Fierke, C.A., and Dixon, J.E. (2003). Biochemical characterization of the Yersinia YopT protease: cleavage site and recognition elements in Rho GTPases. Proc. Natl. Acad. Sci. U. S. A. *100*, 904–909.
Shaw, R.K., Cleary, J., Murphy, M.S., Frankel, G., and Knutton, S. (2005). Interaction of Enteropathogenic Escherichia coli with Human Intestinal Mucosa: Role of Effector Proteins in Brush Border Remodeling and Formation of Attaching and Effacing Lesions. Infect. Immun. *73*, 1243–1251.
Sheahan, K.L., and Fullner Satchell, K.J. (2007). Inactivation of small Rho GTPases by the multifunctional RTX toxin from Vibrio cholerae. Cell. Microbiol. *9*, 1324–1335.
Shen, H., Lu, S., Dong, L., Xue, Y., Yao, C., Tong, C., Wang, C., and Shu, X. (2018). hsa-miR-320d and hsa-miR-582, miRNA Biomarkers of Aortic Dissection, Regulate Apoptosis of Vascular Smooth Muscle Cells. J. Cardiovasc. Pharmacol. *71*, 275–282.
Sheng, X., You, Q., Zhu, H., Chang, Z., Li, Q., Wang, H., Wang, C., Wang, H., Hui, L., Du, C., et al. (2017). Bacterial effector NleL promotes enterohemorrhagic E. coli-induced attaching and effacing lesions by ubiquitylating and inactivating JNK. PLoS Pathog. *13*, 1–28.

Shenoy, A.R., Furniss, R.C.D., Goddard, P.J., and Clements, A. (2018). Modulation of host cell processes by T3SS effectors. Curr. Top. Microbiol. Immunol. *416*, 73–115.
Shi, J., Zhao, Y., Wang, Y., Gao, W., Ding, J., Li, P., Hu, L., and Shao, F. (2014). Inflammatory caspases are innate immune receptors for intracellular LPS. Nature *514*, 187–192.
Shi, J., Zhao, Y., Wang, K., Shi, X., Wang, Y., Huang, H., Zhuang, Y., Cai, T., Wang, F., and Shao, F. (2015). Cleavage of GSDMD by inflammatory caspases determines pyroptotic cell death. Nature *526*, 660–665.
Sievers, F., Wilm, A., Dineen, D., Gibson, T.J., Karplus, K., Li, W., Lopez, R., McWilliam, H., Remmert, M., Soding, J., et al. (2014). Fast, scalable generation of high-quality protein multiple sequence alignments using Clustal Omega. Mol. Syst. Biol. *7*, 539–539.
Silke, J., Rickard, J.A., and Gerlic, M. (2015). The diverse role of RIP kinases in necroptosis and inflammation. Nat. Immunol. *16*, 689–697.
Simovitch, M., Sason, H., Cohen, S., Zahavi, E.E., Melamed-Book, N., Weiss, A., Aroeti, B., and Rosenshine, I. (2010). EspM inhibits pedestal formation by enterohaemorrhagic Escherichia coli and enteropathogenic E. coli and disrupts the architecture of a polarized epithelial monolayer. Cell. Microbiol. *12*, 489–505.
Simpson, N., Shaw, R., Crepin, V.F., Mundy, R., FitzGerald, A.J., Cummings, N., Straatman-Iwanowska, A., Connerton, I., Knutton, S., and Frankel, G. (2006). The enteropathogenic Escherichia coli type III secretion system effector Map binds EBP50/NHERF1: Implication for cell signalling and diarrhoea. Mol. Microbiol. *60*, 349–363.
Singh, A.P., Sharma, S., Pagarware, K., Siraji, R.A., Ansari, I., Mandal, A., Walling, P., and Aijaz, S. (2018). Enteropathogenic E. Coli effectors EspF and Map independently disrupt tight junctions through distinct mechanisms involving transcriptional and post-transcriptional regulation. Sci. Rep. *8*, 1–17.
Singh, V., Davidson, A.C., Hume, P.J., Humphreys, D., and Koronakis, V. (2019a). Arf GTPase interplay with Rho GTPases in regulation of the actin cytoskeleton. Small GTPases *10*, 411–418.
Singh, V., Davidson, A., Hume, P.J., and Koronakis, V. (2019b). Pathogenic Escherichia coli Hijacks GTPase-Activated p21-Activated Kinase for Actin Pedestal Formation. MBio *10*, 688–694.
Sit, S.-T., and Manser, E. (2011). Rho GTPases and their role in organizing the actin cytoskeleton. J. Cell Sci. *124*, 679–683.
Siu, M.K., Abou-Kheir, W., Yin, J.J., Chang, Y.-S., Barrett, B., Suau, F., Casey, O., Chen, W.-Y., Fang, L., Hynes, P., et al. (2014). Loss of EGFR signaling regulated miR-203 promotes prostate cancer bone metastasis and tyrosine kinase inhibitors resistance. Oncotarget *5*, 3770–3784.
Slater, S.L., Sågfors, A.M., Pollard, D.J., Ruano-Gallego, D., and Frankel, G. (2018). The Type III Secretion System of Pathogenic Escherichia coli. In Current Topics in Microbiology and Immunology, (Springer Berlin Heidelberg), pp. 51–72.
Smith, K., Humphreys, D., Hume, P.J., and Koronakis, V. (2010). Enteropathogenic Escherichia coli Recruits the Cellular Inositol Phosphatase SHIP2 to Regulate Actin-Pedestal Formation. Cell Host Microbe *7*, 13–24.
Soledad-Cadona, J., Bustamante, A.V., González, J., and Mariel-Sanso, A. (2018). Pathogenicity islands distribution in non-O157 shiga toxin-producing Escherichia coli (STEC). Genes (Basel). *9*, 3–13.
Song, T., Li, K., Zhou, W., Zhou, J., Jin, Y., Dai, H., Xu, T., Hu, M., Ren, H., Yue, J., et al. (2017). A Type III Effector NleF from EHEC Inhibits Epithelial Inflammatory Cell Death by Targeting Caspase-4. Biomed Res. Int. *2017*.
Sontag, R.L., Nakayasu, E.S., Brown, R.N., Niemann, G.S., Sydor, M.A., Sanchez, O., Ansong, C., Lu, S., Choi, H., Valleau, D., et al. (2016). Identification of Novel Host Interactors of Effectors Secreted by Salmonella and Citrobacter. MSystems *1*, e00032-15.
Stevens, M.P., and Frankel, G.M. (2014). The Locus of Enterocyte Effacement and Associated Virulence Factors of Enterohemorrhagic Escherichia coli. Microbiol. Spectr. *2*, 1–25.
Stockwell, B.R., Friedmann Angeli, J.P., Bayir, H., Bush, A.I., Conrad, M., Dixon, S.J., Fulda, S., Gascón, S., Hatzios, S.K., Kagan, V.E., et al. (2017). Ferroptosis: A Regulated Cell Death Nexus Linking Metabolism, Redox Biology, and Disease. Cell *171*, 273–285.
Strasser, A., Jost, P.J., and Nagata, S. (2009). The Many Roles of FAS Receptor Signaling in the Immune System. Immunity *30*, 180–192.

Strauch, E., Hammerl, J.A., Konietzny, A., Schneiker-Bekel, S., Arnold, W., Goesmann, A., Pühler, A., and Beutin, L. (2008). Bacteriophage 2851 is a prototype phage for dissemination of the Shiga toxin variant gene 2c in Escherichia coli O157:H7. Infect. Immun. *76*, 5466–5477.
Swimm, A., Bommarius, B., Li, Y., Cheng, D., Reeves, P., Sherman, M., Veach, D., Bornmann, W., and Kalman, D. (2004). Enteropathogenic Escherichia coli use redundant tyrosine kinases to form actin pedestals. Mol. Biol. Cell *15*, 3520–3529.
Taieb, F., Nougayrède, J.P., Watrin, C., Samba-Louaka, A., and Oswald, E. (2006). Escherichia coli cyclomodulin Cif induces G2 arrest of the host cell cycle without activation of the DNA-damage checkpoint-signalling pathway. Cell. Microbiol. *8*, 1910–1921.
Takeuchi, O., and Akira, S. (2010). Pattern Recognition Receptors and Inflammation. Cell *140*, 805–820.
Tang, D., Kang, R., Berghe, T. Vanden, Vandenabeele, P., and Kroemer, G. (2019). The molecular machinery of regulated cell death. Cell Res.
Tapia, R., Kralicek, S.E., and Hecht, G.A. (2017). EPEC effector EspF promotes Crumbs3 endocytosis and disrupts epithelial cell polarity. Cell. Microbiol. *19*, 1–14.
Tatsuta, T., and Langer, T. (2017). Intramitochondrial phospholipid trafficking. Biochim. Biophys. Acta - Mol. Cell Biol. Lipids *1862*, 81–89.
Teixeira, N.B., Rojas, T.C.G., Da Silveira, W.D., Matheus-Guimarães, C., Silva, N.P., and Scaletsky, I.C.A. (2015). Genetic analysis of enteropathogenic Escherichia coli (EPEC) adherence factor (EAF) plasmid reveals a new deletion within the EAF probe sequence among O119 typical EPEC strains. BMC Microbiol. *15*.
Tenev, T., Bianchi, K., Darding, M., Broemer, M., Langlais, C., Wallberg, F., Zachariou, A., Lopez, J., MacFarlane, M., Cain, K., et al. (2011). The Ripoptosome, a Signaling Platform that Assembles in Response to Genotoxic Stress and Loss of IAPs. Mol. Cell *43*, 432–448.
Teper, D., Burstein, D., Salomon, D., Gershovitz, M., Pupko, T., and Sessa, G. (2016). Identification of novel Xanthomonas euvesicatoria type III effector proteins by a machine-learning approach. Mol. Plant Pathol. *17*, 398–411.
Terlizzi, M.E., Gribaudo, G., and Maffei, M.E. (2017). UroPathogenic Escherichia coli (UPEC) infections: Virulence factors, bladder responses, antibiotic, and non-antibiotic antimicrobial strategies. Front. Microbiol. *8*.
Thanabalasuriar, A., Koutsouris, A., Hecht, G., and Gruenheid, S. (2010). The bacterial virulence factor NleA's involvement in intestinal tight junction disruption during enteropathogenic E. coli infection is independent of its putative PDZ binding domain. Gut Microbes *1*, 114–118.
Thanabalasuriar, A., Bergeron, J., Gillingham, A., Mimee, M., Thomassin, J.L., Strynadka, N., Kim, J., and Gruenheid, S. (2012). Sec24 interaction is essential for localization and virulence-associated function of the bacterial effector protein NleA. Cell. Microbiol. *14*, 1206–1218.
Thomassin, J., He, X., and Thomas, N.A. (2011). Role of EscU auto-cleavage in promoting type III effector translocation into host cells by enteropathogenic Escherichia coli Role of EscU auto-cleavage in promoting type III effector translocation into host cells by enteropathogenic Escherichia coli. BMC Microbiol. *11*, 205.
Thumkeo, D., Watanabe, S., and Narumiya, S. (2013). Physiological roles of rho and rho effectors in mammals. Eur. J. Cell Biol. *92*, 303–315.
Tobe, T., Beatson, S.A., Taniguchi, H., Abe, H., Bailey, C.M., Fivian, A., Younis, R., Matthews, S., Marches, O., Frankel, G., et al. (2006). An extensive repertoire of type III secretion effectors in Escherichia coli O157 and the role of lambdoid phages in their dissemination. Proc. Natl. Acad. Sci. U. S. A. *103*, 14941–14946.
Tomson, F.L., Viswanathan, V.K., Kanack, K.J., Kanteti, R.P., Straub, K. V., Menet, M., Kaper, J.B., and Hecht, G. (2005). Enteropathogenic Escherichia coli EspG disrupts microtubules and in conjunction with Orf3 enhances perturbation of the tight junction barrier. Mol. Microbiol. *56*, 447–464.
Tu, X., Nisan, I., Yona, C., Hanski, E., and Rosenshine, I. (2003). EspH, a new cytoskeleton-modulating effector of enterohaemorrhagic and enteropathogenic Escherichia coli. Mol. Microbiol. *47*, 595–606.
Turco, M.M., and Sousa, M.C. (2014). The structure and specificity of the type III secretion system effector NleC suggest a DNA mimicry mechanism of substrate recognition. Biochemistry *53*, 5131–

5139.
Vallance, B.A., Deng, W., Knodler, L.A., and Finlay, B.B. (2002). Mice lacking T and B lymphocytes develop transient colitis and crypt hyperplasia yet suffer impaired bacterial clearance during Citrobacter rodentium infection. Infect. Immun. *70*, 2070–2081.
Valleau, D., Little, D.J., Borek, D., Skarina, T., Quaile, A.T., Leo, R. Di, Houliston, S., Lemak, A., Arrowsmith, C.H., Coombes, B.K., et al. (2018). Functional diversification of the NleG effector family in enterohemorrhagic Escherichia coli. Proc. Natl. Acad. Sci. U. S. A. *115*, 10004–10009.
Vidal, J.E., and Navarro-García, F. (2008). EspC translocation into epithelial cells by enteropathogenic Escherichia coli requires a concerted participation of type V and III secretion systems. Cell. Microbiol. *10*, 1975–1986.
Viljanen, M.K., Peltola, T., Kuistila, M., Huovinen, P., Junnila, S., Olkkonen, L., and Jarvinen, H. (1990). Outbreak of diarrhoea due to Escherichia coli 0111:B4 in schoolchildren and adults: association of Vi antigen-like reactivity. Lancet *336*, 831–834.
Vinatzer, B.A., Jelenska, J., and Greenberg, J.T. (2005). Bioinformatics correctly identifies many type III secretion substrates in the plant pathogen Pseudomonas syringae and the biocontrol isolate P. fluorescens SBW25. Mol. Plant-Microbe Interact. *18*, 877–888.
Vingadassalom, D., Kazlauskas, A., Skehan, B., Cheng, H.-C., Magoun, L., Robbins, D., Rosen, M.K., Saksela, K., and Leong, J.M. (2009). Insulin receptor tyrosine kinase substrate links the E. coli O157:H7 actin assembly effectors Tir and EspFU during pedestal formation. Proc. Natl. Acad. Sci. *106*, 6754–6759.
Vingadassalom, D., Campellone, K.G., Brady, M.J., Skehan, B., Battle, S.E., Robbins, D., Kapoor, A., Hecht, G., Snapper, S.B., and Leong, J.M. (2010). Enterohemorrhagic E. coli Requires N-WASP for Efficient Type III Translocation but Not for EspFU-Mediated Actin Pedestal Formation. PLoS Pathog. *6*, e1001056.
Vlisidou, I., Marchés, O., Dziva, F., Mundy, R., Frankel, G., and Stevens, M.P. (2006). Identification and characterization of EspK, a type III secreted effector protein of enterohaemorrhagic Escherichia coli O157:H7. FEMS Microbiol. Lett. *263*, 32–40.
Wagner, S., Königsmaier, L., Lara-Tejero, M., Lefebre, M., Marlovits, T.C., and Galán, J.E. (2010). Organization and coordinated assembly of the type III secretion export apparatus. Proc. Natl. Acad. Sci. U. S. A. *107*, 17745–17750.
Waite, A.L., Schaner, P., Hu, C., Richards, N., Balci-Peynircioglu, B., Hong, A., Fox, M., and Gumucio, D.L. (2009). Pyrin and ASC Co-Localize to Cellular Sites that Are Rich in Polymerizing Actin. Exp. Biol. Med. *234*, 40–52.
Wan, F., Weaver, A., Gao, X., Bern, M., Hardwidge, P.R., and Lenardo, M.J. (2011). IKKβ 2 phosphorylation regulates RPS3 nuclear translocation and NF-κ B function during infection with Escherichia coli strain O157:H7. Nat. Immunol. *12*, 335–344.
Wang, D., Roe, A.J., McAteer, S., Shipston, M.J., and Gally, D.L. (2008). Hierarchal type III secretion of translocators and effectors from Escherichia coli O157:H7 requires the carboxy terminus of SepL that binds to Tir. Mol. Microbiol. *69*, 1499–1512.
Wang, H., Sun, L., Su, L., Rizo, J., Liu, L., Wang, L.F., Wang, F.S., and Wang, X. (2014a). Mixed Lineage Kinase Domain-like Protein MLKL Causes Necrotic Membrane Disruption upon Phosphorylation by RIP3. Mol. Cell *54*, 133–146.
Wang, X., Parashar, K., Sitaram, A., and Bliska, J.B. (2014b). The GAP activity of type III effector YopE triggers killing of Yersinia in macrophages. PLoS Pathog. *10*, e1004346.
Wang, X., Du, Y., Hua, Y., Fu, M., Niu, C., Zhang, B., Zhao, W., Zhang, Q., and Wan, C. (2017). The EspF N-Terminal of Enterohemorrhagic Escherichia coli O157:H7 EDL933w Imparts Stronger Toxicity Effects on HT-29 Cells than the C-Terminal. Front. Cell. Infect. Microbiol. *7*, 1–12.
Wang, Y., Dawson, V.L., and Dawson, T.M. (2009). Poly(ADP-ribose) signals to mitochondrial AIF: A key event in parthanatos. Exp. Neurol. *218*, 193–202.
Watanabe, Y., Tamura, Y., Kawano, S., and Endo, T. (2015). Structural and mechanistic insights into phospholipid transfer by Ups1–Mdm35 in mitochondria. Nat. Commun. *6*, 7922.
Waterhouse, A.M., Procter, J.B., Martin, D.M.A., Clamp, M., and Barton, G.J. (2009). Jalview Version 2-A multiple sequence alignment editor and analysis workbench. Bioinformatics *25*, 1189–1191.

Weflen, A.W., Alto, N.M., Viswanathan, V.K., and Hecht, G. (2010). E. coli secreted protein F promotes EPEC invasion of intestinal epithelial cells via an SNX9-dependent mechanism. Cell. Microbiol. *12*, 919–929.
Weiss, S.M., Ladwein, M., Schmidt, D., Ehinger, J., Lommel, S., Städing, K., Beutling, U., Disanza, A., Frank, R., Jänsch, L., et al. (2009). IRSp53 Links the Enterohemorrhagic E. coli Effectors Tir and EspFU for Actin Pedestal Formation. Cell Host Microbe *5*, 244–258.
Whale, A.D., Hernandes, R.T., Ooka, T., Beutin, L., Schuller, S., Garmendia, J., Crowther, L., Vieira, M.A.M., Ogura, Y., Krause, G., et al. (2007). TccP2-mediated subversion of actin dynamics by EPEC 2 - a distinct evolutionary lineage of enteropathogenic Escherichia coli. Microbiology *153*, 1743–1755.
WHO (2018). WHO | WHO estimates of the global burden of foodborne diseases.
Wickham, M.E., Lupp, C., Mascarenhas, M., Vázquez, A., Coombes, B.K., Brown, N.F., Coburn, B.A., Deng, W., Puente, J.L., Karmali, M.A., et al. (2006). Bacterial Genetic Determinants of Non-O157 STEC Outbreaks and Hemolytic-Uremic Syndrome after Infection. J. Infect. Dis. *194*, 819–827.
Wickham, M.E., Lupp, C., Vázquez, A., Mascarenhas, M., Coburn, B., Coombes, B.K., Karmali, M.A., Puente, J.L., Deng, W., and Brett Finlay, B. (2007). Citrobacter rodentium virulence in mice associates with bacterial load and the type III effector NleE. Microbes Infect. *9*, 400–407.
Wilbur, J.S., Byrd, W., Ramamurthy, S., Ledvina, H.E., Khirfan, K., Riggs, M.W., Boedeker, E.C., Vedantam, G., and Viswanathan, V.K. (2015). The Secreted Effector Protein EspZ Is Essential for Virulence of Rabbit Enteropathogenic Escherichia coli. Infect. Immun. *83*, 1139–1149.
Wilson, R.K., Shaw, R.K., Daniell, S., Knutton, S., and Frankel, G. (2001). Role of EscF, a putative needle complex protein, in the type III protein translocation system of enteropathogenic Escherichia coli. Cell Microbiol *3*, 753–762.
Wong, A.R.C., Raymond, B., Collins, J.W., Crepin, V.F., and Frankel, G. (2012a). The enteropathogenic E. coli effector EspH promotes actin pedestal formation and elongation via WASP-interacting protein (WIP). Cell. Microbiol. *14*, 1051–1070.
Wong, A.R.C., Clements, A., Raymond, B., Crepin, V.F., and Frankel, G. (2012b). The Interplay between the Escherichia coli Rho Guanine Nucleotide Exchange Factor Effectors and the Mammalian RhoGEF Inhibitor. MBio *3*, 1–10.
Wong Fok Lung, T., Pearson, J.S., Schuelein, R., and Hartland, E.L. (2014). The cell death response to enteropathogenic Escherichia coli infection. Cell. Microbiol. *16*, 1736–1745.
Wu, B., Skarina, T., Yee, A., Jobin, M.C., Dileo, R., Semesi, A., Fares, C., Lemak, A., Coombes, B.K., Arrowsmith, C.H., et al. (2010). NleG type 3 effectors from enterohaemorrhagic Escherichia coli are U-Box E3 ubiquitin ligases. PLoS Pathog. *6*.
Wu, C., Lu, W., Zhang, Y., Zhang, G., Shi, X., Hisada, Y., Grover, S.P., Zhang, X., Li, L., Xiang, B., et al. (2019). Inflammasome Activation Triggers Blood Clotting and Host Death through Pyroptosis. Immunity *50*, 1401-1411.e4.
Xu, H., Yang, J., Gao, W., Li, L., Li, P., Zhang, L., Gong, Y.N., Peng, X., Xi, J.J., Chen, S., et al. (2014). Innate immune sensing of bacterial modifications of Rho GTPases by the Pyrin inflammasome. Nature *513*, 237–241.
Xue, L., Tang, B., Chen, W., and Luo, J. (2019). DeepT3: Deep convolutional neural networks accurately identify Gram-negative bacterial type III secreted effectors using the N-Terminal sequence. Bioinformatics *35*, 2051–2057.
Yan, D., Wang, X., Luo, L., Cao, X., and Ge, B. (2012). Inhibition of TLR signaling by a bacterial protein containing immunoreceptor tyrosine-based inhibitory motifs. Nat. Immunol. *13*, 1063–1071.
Yang, J., Tauschek, M., Hart, E., Hartland, E.L., and Robins-Browne, R.M. (2010). Virulence regulation in *Citrobacter rodentium*: the art of timing. Microb. Biotechnol. *3*, 259–268.
Yang, J., Zhao, Y., and Shao, F. (2015). Non-canonical activation of inflammatory caspases by cytosolic LPS in innate immunity. Curr. Opin. Immunol. *32*, 78–83.
Yao, Q., Cui, J., Zhu, Y., Wang, G., Hu, L., Long, C., Cao, R., Liu, X., Huang, N., Chen, S., et al. (2009). A bacterial type III effector family uses the papain-like hydrolytic activity to arrest the host cell cycle. Proc. Natl. Acad. Sci. U. S. A. *106*, 3716–3721.
Yao, Q., Zhang, L., Wan, X., Chen, J., Hu, L., Ding, X., Li, L., Karar, J., Peng, H., Chen, S., et al. (2014).

Structure and Specificity of the Bacterial Cysteine Methyltransferase Effector NleE Suggests a Novel Substrate in Human DNA Repair Pathway. PLoS Pathog. *10*.
Yap, S. V, Koontz, J.M., and Kontrogianni-Konstantopoulos, A. (2011). HAX-1: A family of apoptotic regulators in health and disease. J. Cell. Physiol. *226*, 2752–2761.
Yen, H., Ooka, T., Iguchi, A., Hayashi, T., Sugimoto, N., and Tobe, T. (2010). Nlec, a type III secretion protease, compromises NF-kB activation by targeting p65/rela. PLoS Pathog. *6*.
Yen, H., Sugimoto, N., and Tobe, T. (2015). Enteropathogenic Escherichia coli Uses NleA to Inhibit NLRP3 Inflammasome Activation. PLoS Pathog. *11*, 1–23.
Yen, H., Karino, M., and Tobe, T. (2016). Modulation of the Inflammasome Signaling Pathway by Enteropathogenic and Enterohemorrhagic Escherichia coli. Front. Cell. Infect. Microbiol. *6*, 89.
Yerushalmi, G., Litvak, Y., Gur-Arie, L., and Rosenshine, I. (2014). Dynamics of expression and maturation of the type III secretion system of enteropathogenic Escherichia coli. J. Bacteriol. *196*, 2798–2806.
Yip, C.K., Finlay, B.B., and Strynadka, N.C.J. (2005). Structural characterization of a type III secretion system filament protein in complex with its chaperone. Nat. Struct. Mol. Biol. *12*, 75–81.
Yoshida, S., Katayama, E., Kuwae, A., Mimuro, H., and Suzuki, T. (2002). Shigella deliver an effector protein to trigger host microtubule destabilization, which promotes Rac1 activity and efficient bacterial internalization. EMBO J. *21*.
Yoshida, S., Handa, Y., Suzuki, T., Ogawa, M., Suzuki, M., Tamai, A., Abe, A., Katayama, E., and Sasakawa, C. (2006). Microtubule-Severing Activity of Shigella Is Pivotal for Intercellular Spreading. Science (80-.). *314*, 985–989.
Young, J.C., Clements, A., Lang, A.E., Garnett, J. a., Munera, D., Arbeloa, A., Pearson, J., Hartland, E.L., Matthews, S.J., Mousnier, A., et al. (2014). The Escherichia coli effector EspJ blocks Src kinase activity via amidation and ADP ribosylation. Nat. Commun. *5*, 5887.
Zeng, Z., Surewaard, B.G.J., Wong, C.H.Y., Guettler, C., Petri, B., Burkhard, R., Wyss, M., Le Moual, H., Devinney, R., Thompson, G.C., et al. (2018). Sex-hormone-driven innate antibodies protect females and infants against EPEC infection. Nat. Immunol. *19*, 1100–1111.
Zhang, T.-M. (2019). TRIAP1 Inhibition Activates the Cytochrome c/Apaf-1/Caspase-9 Signaling Pathway to Enhance Human Ovarian Cancer Sensitivity to Cisplatin. Chemotherapy *64*, 119–128.
Zhang, Y., and Skolnick, J. (2005). TM-align: A protein structure alignment algorithm based on the TM-score. Nucleic Acids Res. *33*, 2302–2309.
Zhang, J., Cong, R., Zhao, K., Wang, Y., Song, N., and Gu, M. (2019). High TRIAP1 expression in penile carcinoma is associated with high risk of recurrence and poor survival. Ann. Transl. Med. *7*, 330–330.
Zhang, Q., Lenardo, M.J., and Baltimore, D. (2017). 30 Years of NF-κB: A Blossoming of Relevance to Human Pathobiology. Cell *168*, 37–57.
Zhang, X., McDaniel, A.D., Wolf, L.E., Keusch, G.T., Waldor, M.K., and Acheson, D.W.K. (2000). Quinolone Antibiotics Induce Shiga Toxin–Encoding Bacteriophages, Toxin Production, and Death in Mice. J. Infect. Dis. *181*, 664–670.
Zhang, Y., Higashide, W.M., McCormick, B.A., Chen, J., and Zhou, D. (2006). The inflammation-associated Salmonella SopA is a HECT-like E3 ubiquitin ligase. Mol. Microbiol. *62*, 786–793.
Zhang, Y., Mühlen, S., Oates, C. V., Pearson, J.S., and Hartland, E.L. (2016). Identification of a distinct substrate-binding domain in the bacterial cysteine methyltransferase effectors NleE and OspZ. J. Biol. Chem. *291*, 20149–20162.
Zhao, S., Zhou, Y., Wang, C., Yang, Y., Wu, X., Wei, Y., Zhu, L., Zhao, W., Zhang, Q., and Wan, C. (2013). The N-Terminal Domain of EspF Induces Host Cell Apoptosis after Infection with Enterohaemorrhagic Escherichia coli O157:H7. PLoS One *8*.
Zhao, Y., Yang, J., Shi, J., Gong, Y.-N., Lu, Q., Xu, H., Liu, L., and Shao, F. (2011). The NLRC4 inflammasome receptors for bacterial flagellin and type III secretion apparatus. Nature *477*, 596–600.
Zhou, M., Ding, X., Ma, F., Xu, Y., Zhang, J., Zhu, G., and Lu, Y. (2019). Long polar fimbriae contribute to pathogenic Escherichia coli infection to host cells. Appl. Microbiol. Biotechnol. *103*, 7317–7324.
Zhou, Y., Huang, C., Yin, L., Wan, M., Wang, X., Li, L., Liu, Y., Wang, Z., Fu, P., Zhang, N., et al. (2017). Nϵ-Fatty acylation of Rho GTPases by a MARTX toxin effector. Science (80-.). *358*, 528–531.